CHARACTERIZING THE BINDING SITE OF GPVI INHIBITORS FOR THE DEVELOPMENT OF NOVEL ANTI-PLATELET AGENTS

By

Foteini-Nafsika Damaskinaki





A thesis submitted to the University of Nottingham and the University of Birmingham for the dual degree of

DOCTOR OF PHILOSOPHY

Faculty of Science
School of Pharmacy
University of Nottingham, UK

Institute of Cardiovascular Sciences
College of Medical and Dental Sciences
University of Birmingham, UK

July 2022

UNIVERSITY OF
BIRMINGHAM

University of Birmingham Research Archive

e-theses repository

This unpublished thesis/dissertation is copyright of the author and/or third parties. The intellectual property rights of the author or third parties in respect of this work are as defined by The Copyright Designs and Patents Act 1988 or as modified by any successor legislation.

Any use made of information contained in this thesis/dissertation must be in accordance with that legislation and must be properly acknowledged. Further distribution or reproduction in any format is prohibited without the permission of the copyright holder.

Abstract

Ischemic cardiovascular and cerebrovascular diseases are two of the major disorders responsible for deaths and morbidity globally. Blood platelets play an important role in prevention of excessive bleeding and wound healing and their dysregulation can have a great impact in the former pathologies. Current antiplatelet therapies have an intrinsic bleeding risk which can even result to life-threatening bleeding. The platelet collagen receptor GPVI has emerged as a promising target for long-term prevention of both arterial thrombosis and inflammation-driven thrombosis with a lower bleeding risk and a minimal effect on haemostasis. Due to the decreased bioavailability of current anti-GPVI biological agents, formulating oral medication against GPVI. However, the nature of GPVI extracellular domain structure and multiple sites of interaction within GPVI are limiting the development of small molecule inhibitors. The aim of this thesis is to develop and characterise selective small molecule inhibitors and nanobody GPVI ligands in order to map the binding sites within GPVI to aid future design of inhibitors. The methodological approach included the use of a structural-based virtual screening, with subsequent testing, and a combination of mutation studies with protein crystallography of GPVI in complex with potent nanobody (Nb) ligands. Although compound **22** showed promising results on collagen-induced aggregation, fluorescence-based assays ruled out this molecule as a selective GPVI inhibitor. The crystal structure of a new potent anti-GPVI nanobody, Nb35, in complex with the extracellular domain of GPVI was resolved, revealing an overlapping binding site and similar binding coordinates with that of Nb2. Mutation studies revealed GPVI residue R46 as a residue important for the inhibitory function of Nb2, Nb21 and Nb35 on collagen signalling while R60 is important for the interaction with Nb21 but not Nb2 and Nb35. These findings are highly applicable in the future design of screening strategies for potent small molecule GPVI inhibitors.

Publications arising from this thesis

Damaskinaki F.N., Moran L.A., Garcia A., Kellam B. & Watson S.P. (2021). Overcoming challenges in developing small molecule inhibitors for GPVI and CLEC-2, Platelets, 32:6, 744-752,doi: 10.1080/09537104.2020.1863939.

Damaskinaki FN., Jooss N., Martin E., Clark J., Thomas M., Poulter N., Emsley J., Kellam B., Watson S.P., Slater A. (Accepted/In press: 07 Nov 2022) Characterizing the binding of GPVI with nanobody 35 reveals a novel monomeric structure of GPVI where the conformation of D1+D2 is independent of dimerization. J Thromb Heamost.

Publications aided by the present work

Clark, J.C, **Damaskinaki F.N**., Cheung H., Slater A. & Watson S.P. (2021) Structure-function relationship of the platelet glycoprotein VI (GPVI) receptor: does it matter if it is a dimer or monomer?, Platelets, 32:6, 724-732, DOI: 10.1080/09537104.2021.1887469.

Kardeby C., **Damaskinaki F.N**., Sun Y. & Watson S.P. (2021) Is the endogenous ligand for PEAR1 a proteoglycan: clues from the sea, Platelets, 32:6, 779-785, DOI: 10.1080/09537104.2020.1863938.

Dedication

This thesis is dedicated to the most important people in my life, my family, my boyfriend and my best friend. My mum, Maria, my dad Stelios and my brother Manos have always been by my side and I could never ask for a better family. Despite all of them being thousands of kilometres away, I have never felt so close to you. Not everyone is lucky enough to have such a supportive and vibrant family. You have supported me in my most difficult moments, waited for me in every arrival gate, shouted the loudest in all my accomplishments, taught me not be afraid of living and made me who I am today. My brother, in particular, is and will be my partner in crime, one of my best friends and the one that makes me laugh the most. Your intelligence, authenticity and matureness has always inspired everyone around and I know that you are going achieve anything you set your mind to. Juan, my boyfriend has been with me throughout this whole PhD and I couldn't ask for a better partner. You are one of my biggest inspirations, my passion, my love, my biggest fan, the most intelligent and fierce human and the light of my life. You are the most amazing human I have and will ever meet. I would like to dedicate this work to my best friend and my other big inspiration, Eleana. Your courage towards anything life throws at you and your friendship have helped me go through this, even when an ocean and 5 hours difference were between us. Finally, I would like to dedicate this to some people that are not in this world anymore. My grandmothers, Foteini and Nafsika, my grandfather Michalis, my uncles George and Petros and my auntie Maria. Each and every one of you, are always in my heart.

Acknowledgements

I would now like to thank and show my appreciation to everyone who has supported me over the past few years, being in the lab or outside of it. Obviously, my first honourable mention are my supervisors, Steve Watson & Barrie Kellam. I can't thank them enough for giving me the opportunity to do this PhD, the support they have given me for 3 whole years. Even throughout the pandemic, caused by the Covid-19 outburst, communication was carried out as it normally has. I would also like to thank COMPARE for providing the financial support throughout my PhD, both my scientific and personal expenses, including conferences, transportation and accommodation, while being part of a great scientific community.

The people from the Nottingham and the Birmingham platelet group have supported me in every aspect of the PhD. I have made true and long-lasting friendships and there are people I will miss dearly.

I first need to thank Alex, Jo and Lourdes from the University of Birmingham for being my mentors and teachers during this PhD. Alex has achieved the impossible, by officially converting a chemist to a biologist. His presence in the lab has been most invaluable and I will never forget our disturbing and funny conversations. Thanks to him, being in Birmingham was the best decision I ever took. I am sure he will be a great father to his little girl. Jo is the most methodical person I have ever met and has managed me to make an organised human being. She is the definition of what we call in my country "a calm power", a quiet but strong person. Lourdes is a wizard of biological assays, my Spanish teacher and the person that knew how to put a smile in my face. I couldn't forget the help of Amanda for her invaluable help in giving me thorough and very helpful feedback for my Thesis and for being one of the people that I looked forward to see in the lab. All of these people have been supporting me both inside the laboratory and personally. I wouldn't be able to have anything without you. I also need to thank Professor Dirk-Peter Horton for offering his support and valuable feedback on my assessments and the project itself. I would like to thank Beata, Lourdes and Ying in Birmingham for keeping the equipment and reagents of the lab in a top state; to the point that you would think they are magicians. I also would like to thank Gayle, Sharmaine, Christine and Sally for all the administration help throughout my PhD. The amount of bureaucracy that these ladies have to go through, plus keeping up the COMPARE and Platelet group journal clubs and latest updates and opportunities up to date. Thank you Jack, Jack and Eddie for making Recepticons a team of great scientists. Evie requires a special mention because she is my favourite COMPARE person and a beautiful mind. Luis, my friend and co-author, and Hilaire made my days in the yellow bubble much brighter. Martina and Gina have been great friends and colleagues and I wish them all the best. Thank you also Eleyna, Natalie, Tom, Harry, Emma and everyone else in the Platelet group for being great people to work with. I will always remember the laughs we experienced together. Oh, I forgot to thank the golden camel for giving me a push when I needed it.

At the University of Nottingham, I would like to thank Nick for being my chemistry lab mentor throughout all these years. Nick is my favourite and most knowledgeable chemist, with the biggest heart I have ever met. I am grateful to call you a friend and I can never repay you for the support I had from you and your family. Thank you as well Sara for your support and company within and outside the lab. I could never figure out how you were on 3 external company projects, had a life and still had time to help everyone. Professors Jonas Emsley, Charlie Laughton and my internal supervisors, Shailesh Mistry have been made many elements of my PhD possible and I am truly thankful to be able to work with you. Thank you Ian for training me in all the Unix and HPC elements and for making my experience so user friendly (a very rare talent these days). I also need to thank the amazing Lubna, our D floor master how kindly provided me with the plates of molecules from my screenings and for my experiments. Also thank you Steve Vernon, who can solve literally any technical problem. It's like he doesn't know what a problem means. I cannot forget to mention Lee, our safety officer and NMR master who is ironically into extreme sports and

has broken multiple bones. Jane made a lot of the administrative work within the C-floor possible and tolerated a lot of our nonsense. I would also like to thank Mark for his support and for being the first person who showed me what a nanobody is. From the C floor family I want to thank my dear friend and my favourite artist, biggest hugger and travel buddy, Bianca. Thank you C35 lab Akeel, Christophe, Divneet, and also Scot, Rui Ling, Eleonora, Emmanuel, Kev, Ryan, Jack, Mat, Louise, Chris, Chaolong and everyone else in C floor for making me feel like part of a family all these years.

Outside the lab, I have already thanked my family, boyfriend and my best friend, so now it's time for the invisible heroes. Being away from home you realise how people show their brightest colours during the most difficult times. Special thanks to my study buddies, Maria and Marianna, who made studying fun, even when it seemed impossible. Marianna is my sanctuary when I most needed it and my most precious childhood friend. She is one of my role models and I inspire to be like her one day. Writing with Maria, a person who wrote another thesis alongside me, and for always being willing to offer a drink and a laugh afterwards, was one of the most important things anyone could have done for me. I couldn't have done it without these two. My dear friends from Greece Katerina, Ioanna, Maria, Dimitri, Irene and Chatzo, thank you for being on the other end of the phone, even at 6am Greece time, making me laugh and listening to my whining but mostly for eliminating all the distances. My friends around the world that I met during my master's Daniela, Ade, Gytis, Alonso, Rubal and Muyi. You have proven me that true friendship has no borders or boundaries. My three guys all happen to be great scientists as well and I can't wait to see their development within their field. My relatives and family friends have shown their love repeatedly. So thank you Niko, Michali, Giota, Andreas, Zoe, Ioanna, Maria, Kallia and my lovely little nieces Iro, Zenia, Efi, Zoe and Anna. You have watched over me and my family since I was born and made sure you send me big (like really, really big) packages full of my favourite stuff from home. I would also like thank the Petra Mare hotel staff for always checking on me since I was little and always welcoming me back with the biggest hugs (which are now elbow shakes for obvious reasons). Finally, I would like to thank my boyfriend's family for welcoming me, even though they speak zero English, and asking me every day (literally) how I am and if I am wearing a jacket.

Table of Contents

CHAPTER 1: GENERAL INTRODUCTION 1

1.1 CARDIOVASCULAR DISEASE 2

1.2 PLATELET PHYSIOLOGY & FUNCTIONS 3

1.2.1 Platelet structure & formation 3

1.2.2 Platelet functions 5

1.3 PLATELET RECEPTORS 8

1.3.1 Immunoreceptor tyrosine-based activation motif (ITAM) receptors 9

1.3.2 G protein-coupled receptors (GPCRs) 10

1.4 GLYCOPROTEIN VI (GPVI) 12

1.4.1 The role of GPVI in haemostasis and thrombosis 12

1.4.2 GPVI signalling 13

1.4.3 GPVI structure 15

1.4.4 GPVI ligand binding sites 18

1.4.5 GPVI clustering & functional significance in ligand binding 24

1.5 OTHER GPVI LIGAND INTERACTIONS 26

1.5.1 Fibrin & fibrinogen 27

1.5.2 Snake venom toxins 28

1.5.3 Other endogenous & exogenous ligands 29

1.6 GPVI INHIBITORS 30

1.6.1 GPVI inhibitors in the clinic 30

1.6.2 Small molecule inhibitors 31

1.6.3 Nanobodies 33

1.7 AIMS & OBJECTIVES 35

CHAPTER 2: MATERIALS AND METHODS 37

2.1. VIRTUAL DOCKING STUDIES 38

2.1.1 Ligand structure preparation 38

2.1.2 Protein structure preparation 38

2.1.3 Structure-based pharmacophore development 38

2.1.4 Site selection & Grid generation 39

2.1.5 Virtual ligand docking 39

2.1.6 Compound selection for screening 39

2.2. SYNTHESIS OF SMALL MOLECULE CONTROLS FOR AGGREGATION STUDIES 40

2.2.1. General procedure and characterization 40

2.2.2 Synthesis 41

2.3. BIOLOGICAL METHODS 43

2.3.1. Materials and Antibodies 43

2.3.2. Expression, labelling & purification of nanobodies 44

2.3.3. GPVI expression & purification 49

2.3.4. Mutagenesis & expression of GPVI mutants 50

2.3.5. Competition ELISA 51

2.3.6. NFAT luciferase reporter assay 52

2.3.7. Preparation of human platelets 53

2.3.8. Aggregation assay 53

2.3.9. Flow cytometry 54

2.3.10. Crystallisation of GPVI-nanobody complex 56

2.3.11. Statistical analysis 59

2.3.12. Appendix 60

CHAPTER 3: *IN SILICO* INVESTIGATION FOR SMALL MOLECULE LIGANDS FOR GPVI 64

3.1 INTRODUCTION 65

3.2 AIMS 68

3.3 RESULTS 68

3.3.1 Target and binding site selection 68

3.3.2 Structure-based pharmacophore generation & in silico screening 72

3.3.3 Synthesis of positive and negative controls for aggregation studies 81

3.3.4 Aggregation assays for compound selection 83

3.3.5 Competition enzyme-linked immunosorbent assay (ELISA): 22, O1 and O2 binding to monomeric or dimeric recombinant GPVI 95

3.3.6 Effect of 22, O1 & O2 on NFAT signalling 97

3.4 DISCUSSION 100

CHAPTER 4: MAPPING THE BINDING SITES OF NANOBODIES ON GPVI .. 104

4.1 INTRODUCTION 105

4.2 AIMS 109

4.3 RESULTS 109

4.3.1 Crystallisation of GPVI in complex with nanobodies 21 and 35 109

4.3.2 Probing the Nb21 binding site through mutations studies 120

4.3.3 Flow cytometry for nanobody binding 129

4.3.4 Flow cytometry for nanobody displacement in human platelets 132

4.3.5 Outsourced data for the binding of Nb21 and Nb35 on GPVI 144

4.4 DISCUSSION 146

CHAPTER 5: GENERAL DISCUSSION 150

5.1 DRUG DISCOVERY AND DEVELOPMENT: FROM SMALL MOLECULES TO NEW MEDICINES 151

5.2 SUMMARY OF RESULTS 152

5.3 *IN SILICO* INVESTIGATION FOR SMALL MOLECULE LIGANDS FOR GPVI 153

5.4 MAPPING THE BINDING SITES OF NANOBODIES ON GPVI 154

5.5 FURTHER DISCUSSION 157

5.6 FUTURE OF GPVI INHIBITORS 160

5.7 FINAL CONCLUSIONS 161

REFERENCES 162

Table of figures

Figure 1.1. Major components & structure of a platelet. 4

Figure 1.2. General scheme for platelet activation cascade. 6

Figure 1.3. Main stages of thrombus formation. 7

Figure 1.4. GPVI signalling. 14

Figure 1.5. Ribbon representation of the structure of GPVI. 16

Figure 1.6. X-ray structure of collagen fibre. 19

Figure 1.7. Previously predicted binding site of CRP. 21

Figure 1.8. CRP binding site. 23

Figure 1.9. Fibrinogen conversion to fibrin and polymerization of fibrin strands. 27

Figure 1.10. Small molecules developed as GPVI inhibitors reported in literature. 32

Figure 1.11. Schematic representation of antibody fragments and nanobodies. 34

Figure 3.1. Generated collagen and CRP binding sites for this project. 71

Figure 3.2. Pharmacophore structure-based model aligned with (top) collagen and (bottom) CRP pocket within GPVI. 73

Figure 3.3.General scheme for altered synthesis for 6b (Bhunia et al., 2017). 82

Figure 3.4. Compound 6_0 & 6b inhibition of collagen and thrombin-induced platelet aggregation.....83

Figure 3.5. Inhibition of collagen-induced platelet aggregation by the 30 compounds selected for screening.....86

Figure 3.6. Structure and aggregation assay of top seven compounds with inhibition properties against collagen-induced aggregation.....87

Figure 3.7. Top docking poses of the inhibitors within their corresponding binding pockets. 89

Figure 3.8. Chemical structures of compounds O1 and O1. 91

Figure 3.9. Summary data of light transition aggregation assays. 93

Figure 3.10. Average aggregation data and standard deviation values corresponding to the platelet aggregation experiments using 22, O1 & O2.....94

Figure 3.11. Competition ELISA of dimeric and monomeric GPVI binding to GPVI with collagen and 22, O1 & O2. 96

Figure 3.12. Effect of 22, O1 & O2 on collagen signalling. 98

Figure 3.13. Expression of different GPVI DNA quantities in DT40 cells. 99

Figure 4.1. Binding interface of Nb2 to the surface of GPVI. 1088

Figure 4.2. Sequence alignment between the inhibitory nanobodies Nb2, Nb21 & Nb35. 110

Figure 4.3. Gel filtration of nanobody complexes for crystallisation studies. 112

Figure 4.4. Protein crystal of Nb35-GPVI NQ complex used for x-ray diffraction. 114

Figure 4.5. Protein crystal of Nb21-GPVI NQ complex.....114

Figure 4.6. Binding interface of Nb35 to the surface of GPVI. 116

Figure 4.7. Comparison between the Nb2 and Nb35 binding site. 118

Figure 4.8. Overlay of the GPVI amino acids that are included in nanobody binding and the ones included in the small molecule binding site. 119

Figure 4.9. Residue R38, R46, R60 & R67 location within the D1 GPVI domain. 121

Figure 4.10. NFAT signal optimization based on DNA transfection efficiency.....122

Figure 4.11. Expression of WT GPVI from different DNA quantities in DT40 cells. 123

Figure 4.12. NFAT signal optimization based on agonist concentration.....124

Figure 4.13. Effect of R38A, R46A, R60A & R67A GPVI mutations to GPVI signalling. 125

Figure 4.14. Expression of GPVI mutant constructs in DT40 cells.....126

Figure 4.15. Effect of R46A & R60A GPVI mutations to inhibition efficacy of Nb2, Nb21 & Nb35 towards GPVI signalling.....128

Figure 4.16. Effect of R38A, R46A, R60A and R67A GPVI mutations to the binding of His-tagged Nb2, Nb21 and Nb35. 131

Figure 4.17. Saturation assay of A647-Nb21 in washed platelets. 134

Figure 4.18. Displacement assay of A647-Nb21 in washed platelets by Nb21. 136

Figure 4.19. Saturation curve of A-647 Nb2 and A647-Nb35 in washed platelets. 137

Figure 4.20. Displacement assay of His-tagged Nb21 in washed platelets by Nb2 and Nb35. 139

Figure 4.21. Saturation assay of His-tagged Nb21 in washed platelets. 141

Figure 4.22. Displacement assay of His-Nb21 and Nb21 in washed platelets. 143

Figure 4.23. Results of competition ELISA for Nb21 and Nb35 displacement by Nb2...144

Figure 4.24. SPR analysis for Nb35 binding on monomeric and dimeric extracellular GPVI. 145

List of tables

Table 2.1. Reagents and Antibodies.....43

Table 2.2. Nanobody Parameters generated from ExPASy ProtParam tool. 44

Table 2.3. Sequence of primers used for the generation of GPVI point mutations. 51

Table 2.4. Nanobody, recombinant GPVI mutant and complex parameters generated from ExPASy ProtParam tool.....56

Table 2.5. Crystallographic data collection and refinement statistics.....58

Table 2.6. Protein sequence of nanobody constructs. 60

Table 2.7. Protein sequence of recombinant GPVI constructs.....60

Table 2.8. DNA and protein sequence of recombinant GPVI mutant constructs for NFAT assay......61

Table 2.9. Protein sequence of full-length GPVI construct used for NFAT assays.....63

Table 3.1. Small molecule inhibitors against GPVI reported in literature.....67

Table 3.2. Top scorers from the collagen pocket virtual screen.. 75

Table 3.3. Top scorers from the CRP pocket virtual screen. 78

Abbreviations

ACD	Acid-citrate-dextrose
ADAM	Alpha disintegrin and metalloproteinase domain-containing protein
ADP	Adenosine diphosphate
AMP	Adenosine monophosphate
ATP	Adenosine triphosphate
A647	Alexa Fluor™ 647
BSA	Bovine serum albumin
BRET	Bioluminescence resonance energy transfer
cAMP	Cyclic adenosine monophosphate
CDR	Complementarity-determining regions
cGMP	Cyclic guanosine monophosphate
CLEC-2	C-type lectin-like receptor 2
CRP	Collagen-related-peptide
CVD	Cardiovascular disease
DAG	1,2-diacylglycerol
DAPT	Dual-antiplatelet therapy
DMEM	Dulbecco's modified eagle medium
DNA	Deoxyribonucleic acid
DTS	Dense tubular system
dSTORM	Direct stochastic optical reconstruction microscopy
DVT	Deep vein thrombosis
ECM	Extracellular matrix
EDTA	Ethylenediaminetetraacetic acid
ELISA	Enzyme-linked immunosorbent assay
EMMPRIN	Extracellular Matrix Metalloproteinase Inducer
Et_3N	Triethylamine
Fab	Antigen-binding fragment
Fc	Fragment crystallisable

FC	Flow cytometry
FcRγ-chain	Fc receptor γ-chain
ΔG	Gibbs free energy change
GDP	Guanosine diphosphate
GMP	Guanosine monophosphate
GP	Glycoprotein
GPCR	G protein-coupled receptor
GPIb	Glycoprotein Ib
GPIIb/IIIa	Glycoprotein IIb/IIIa
GPVI	Glycoprotein VI
GPVI NQ	Glycoprotein VI N-72 glycosylation mutant
GTP	Guanosine triphosphate
ΔH	Enthalpy change
HEPES	4-(2-Hydroxyethyl)-1-piperazineethanesulfonic acid
HIT	Heparin-induced thrombocytopenia
HPLC-MS	High performance liquid chromatography mass spectrometry
HRP	Horseradish peroxidase
Ig	Immunoglobulin
Indo	Indomethacin
IP3	Inositol 1,4,5-trisphosphate
IP3-R	Inositol trisphosphate receptor
IRAG	IP3-R-associated cGMP kinase substrate
ISTH	International Society on Thrombosis and Haemostasis
ITAM	Immunoreceptor tyrosine-based activation motif
ITP	Thrombocytopenic purpura
J	Coupling constant
K_D	Equilibrium dissociation constant
LAIR-1	Leukocyte Associated Immunoglobulin-Like Receptor 1
LAT	Linker of activated T cells
LPS	Lipopolysaccharide

LTA	Light transmission assay
mAb	Monoclonal antibody
MCCC	Managed chemical compound collection
MCS	Multiple cloning site
MES	2-(*N*-morpholino)ethanesulfonic acid
Nb	Nanobody
NEM	*N*-Ethylmaleimide
NFAT	Nuclear factor of activated T cells
NMR	Nuclear magnetic resonance
OCS	Open canalicular system
PAR	Protease-activated receptor
PBP	Platelet basic protein
PBS	Phosphate-buffered saline
PDB	Protein Data Bank
PDEs	Phosphodiesterases
PEG	Polyethylene glycol
PF4	Platelet factor 4
PGI_2	Prostaglandin I_2 (prostacyclin)
PI3 kinase	Phosphoinositide 3 kinase
PIP2	Phosphatidylinositol 4,5-bisphosphate
PIP3	Phosphatidylinositol 3,4,5-trisphosphate
PKA	Protein kinase A
PKC	Protein kinase C
PLC	Phospholipase C
PLCγ2	Phospholipase C γ2
PMA	Phorbol 12-myristate-13-acetate
PRP	Platelet rich plasma
PRR	Pattern recognition receptor
PS	Phosphatidylserine
R_f	Retention factor

RCF	Relative centrifugal force
RGD	Arginine-glycine-aspartic acid amino acid sequence
RhoA	Ras homology family member A
RNA	Ribonucleic acid
RPMI	Roswell park memorial institute
R_t	Retention time
SAR study	Structure activity relationship study
ΔS	Entropy change
SDS	Sodium dodecyl sulphate
SEM	Standard error of the mean
SH2	Src homology 2
SH3	Src homology 3
SHP	SH2-domain containing protein-tyrosine phosphatases
Syk	Spleen tyrosine kinase
TBS-T	Tris-buffered saline, Tween-20
TP	Thromboxane receptor
TRAP	Thrombin receptor-activating peptide
Tris	tris(hydroxymethyl)aminomethane
TLC	Thin-layer chromatography
TxA2	Thromboxane A_2
TxB2	Thromboxane B_2
VEGF	Vascular endothelial growth factor
V_HH	Variable heavy chain domain
VITT	Vaccine-induced immune thrombotic thrombocytopenia
VWF	von Willebrand factor

Word count: 30,255

Chapter 1

General Introduction

1.1 Cardiovascular disease

Cardiovascular disease (CVD) is an umbrella term used to describe a group of conditions that affect the heart or circulation, including high blood pressure, coronary heart disease, stroke and vascular dementia. It accounts for 25% of all deaths in the UK (British Heart Foundation, 2021 Factsheet). It is estimated that 32% of people in the world died from CVDs in 2019, of which 85% were due to heart attack and stroke (WHO, 2021). Heart attack, angina or stroke can manifest through heart conditions that affect heart muscles, valves and abnormal rhythms (arrhythmias). However, the underlying cause for many of these is atherosclerosis where the coronary or cerebral vessels are narrowed or blocked due to a blood clot (known as thrombosis). There are several additional forms of thrombosis including venous thrombosis which is driven by inflammation in the vessel wall.

When a plaque in a diseased arterial vessel ruptures, it exposes its interior collagen-rich contents to the blood triggering formation of a blood clot, which can result in a blockage of the blood supply. Arterial thrombi are rich in platelets (Alkarithi *et al.*, 2021); plaque rupture triggers platelets to aggregate at the site of ruptured spot, forming thrombi and ultimately blocking the blood vessel. Thrombi can also embolise creating blockages in downstream arterial or venous vessels. The most serious of these are venous thrombosis as this can lead to pulmonary embolism (Koupenova *et al.*, 2016) and ischaemic stroke.

Since platelets are major drivers of thrombosis in the arterial circulation, antiplatelet drugs are usually administered for treatment of both acute thrombotic episodes and in longer-term prevention. Current prophylactic antiplatelet therapy is the dual-antiplatelet therapy (DAPT) with low dose acetyl salicylic acid (aspirin) which is combined with ADP-receptor ($P2Y_{12}$) antagonists (clodipogrel, prasugrel, ticagrelor) for high-risk individuals (McFadyen *et al.*, 2018). GPIIb/IIIa inhibitors (e.g. abciximab, eptifibatide, tirofiban) are also used in an acute thrombotic episode (McFadyen *et al.*, 2018). However, patients on antiplatelet agents can still experience adverse effects. In particular, excessive bleeding poses a problem with all of these strategies, varying from nuisance bleeding, causes lower compliance, to life-threatening bleeding in a sub-population of patients, notably the elderly (Kalyanasundaram and Lincoff, 2011). Clodipogrel and aspirin may cause excess bleeding, with an incidence of 2-3% of gastrointestinal spontaneous bleeding (Alli *et al.*, 2011), 1-2% of bleeding in sites that have undergone puncture or surgery (Mehta *et al.*, 2001) while the risk of major bleeding can increase from about 2-fold with DAPT than with aspirin alone or more than 2.5-fold when

aspirin is combined with warfarin (Chan and Weitz, 2019). Ticagrelor administration can increase the prevalence of major bleeding, including fatal intracranial bleeding (Vogel *et al.*, 2022). Prasugrel is the most potent of the $P2Y_{12}$ inhibitors, but it is contraindicated to patients with a history of SP-induced myocardial infraction and patients over 75 years old, with clodipogrel being administered instead (Vogel *et al.*, 2022). Even Glycoprotein IIb/IIIa inhibitors (abciximab, tirofiban, eptifibatide), that act on the final pathway of platelet aggregation, have shown an increase of major bleeding and are currently reserved for no-reflow after percutaneous coronary intervention and thrombotic complications (Levine *et al.*, 2011).

It is becoming apparent that with the intrinsic risks of these medications, making current medication more potent is not the solution. Hence, there is a medical need for new antiplatelet agents that have minimal effects on the mechanism responsible for cessation of bleeding, haemostasis. For the past few years, several promising new antiplatelet have undergone phase I and IIa clinical trials, including platelet glycoprotein VI (GPVI) inhibitors in the anticipation that they will cause less bleeding side effects. This anticipation derives from the recognition that haemostasis and thrombosis can be successfully targeted using selective antithrombotic therapies (Plow *et al.*, 2018).

1.2 Platelet physiology & functions

1.2.1 Platelet structure & formation

The shape of resting platelets is discoidal and the typical diameter is 2-3 μm, with a thickness of 0.5 μm and an average cell volume of 6-10 fl (Thon and Italiano, 2012; Gremmel *et al.*, 2016). Their life-span in the circulation in human is up to 10 days (Daly, 2011; Ware *et al.*, 2013; Grozovsky *et al.*, 2015; Pluthero and Kahr, 2018). Platelets lack a nucleus but they do contain other organelles including mitochondria, endoplasmic reticulum and secretory granules (Figure 1.1) (Machlus and Italiano, 2013, 2019). α Granules contain more than 300 proteins, which are released upon platelet activation at the site of vessel injury (Coppinger *et al.*, 2004; Wijten *et al.*, 2013). The protein component of platelets is obtained from much larger progenitor polynucleated cells, megakaryocytes, which reside in the bone marrow. Platelets are shed into the circulation from megakaryocyte endings that extend directly to blood vessels, called proplatelets (Machlus and Italiano, 2013 and 2019).

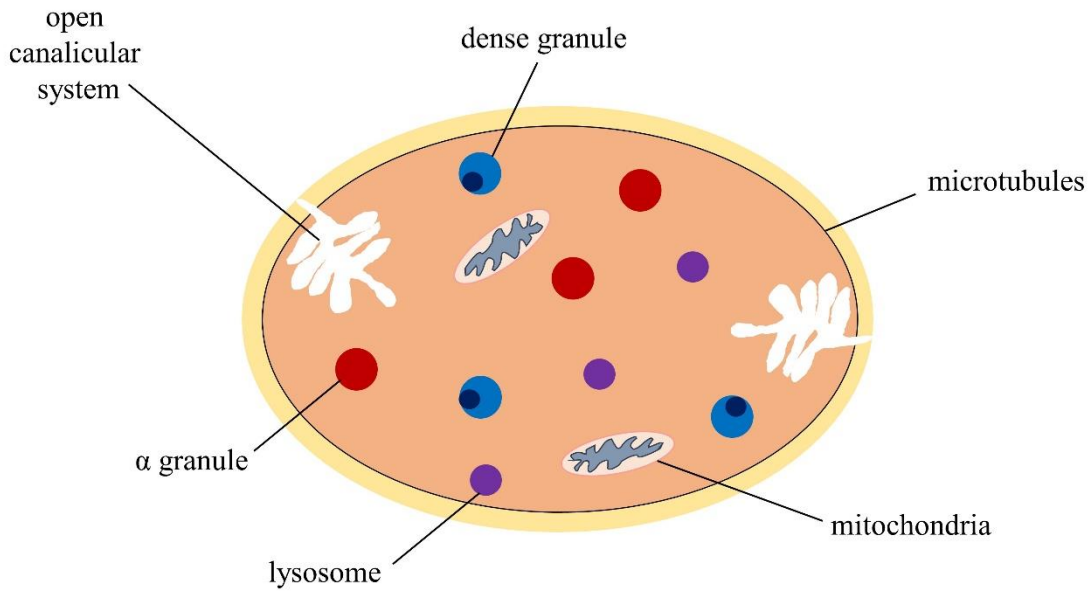


Figure 1.1. Major components & structure of a platelet. *The surface is connected to an open canalicular system which is important for exchange with the extracellular environment during platelet secretion, and microtubules, for shape maintenance or change. Amongst the major cellular components of platelets are dense granules, alpha granules, lysosomes and mitochondria.*

1.2.2 Platelet functions

1.2.2.1 Platelets in haemostasis

Resting platelets are ordinarily prevented from activation through suppression mechanisms, including the release of nitric oxide (NO) and prostacyclin (PGI_2) from endothelial cells (Jin *et al.*, 2005). Upon injury, endothelial cells expose von Willebrand Factor (VWF), a blood glycoprotein, which binds to collagen fibres in the extracellular matrix (ECM) and acts as a tethering site for circulating platelets through binding to the receptor complex GPIb-IX-V (Figure 1.2). This interaction is vital for platelet capture under high shear conditions, but does not mediate firm adhesion due to a rapid rate of dissociation (Andrews and Berndt, 2013). This deceleration facilitates the binding of exposed collagen to the platelet receptor GPVI, which induces mobilization of internally stored calcium (Watson *et al.*, 2010; Nieswandt *et al.*, 2011a; Dütting *et al.*, 2012). Consequent calcium mobilisation induces morphologic and cytoskeletal changes, secretion of platelet granular content and transition to a spheroidal shape with extended pseudopods to reinforce platelet tethering (Li *et al.*, 2010; Hartwig, 2013; Sharda and Flaumenhaft, 2018). GPVI activation also converts integrin receptors α2β1 (GPIa/IIa) and αIIbβ3 (GPIIb/IIIa) from their low to high affinity states to enhance platelet binding to collagen and to other platelets via fibrinogen and VWF respectively (Nieswandt & Watson, 2003; Nieswandt *et al.*, 2011). ADP, released from dense granules, and thromboxane A_2 (TxA_2) which is generated *de novo,* are two of the most important activation-feedback agents for platelet recruitment for thrombus growth (Offermanns, 2006; Clemetson, 2012; Periayah *et al.*, 2017). While GPVI is critical for initial platelet activation on contact with immobilised collagen *in vitro* (Watson *et al.*, 2010), in the vessel wall *in vivo* this role is shared with newly generated thrombin and release of ADP from damaged cells (Watson *et al*., 2015).

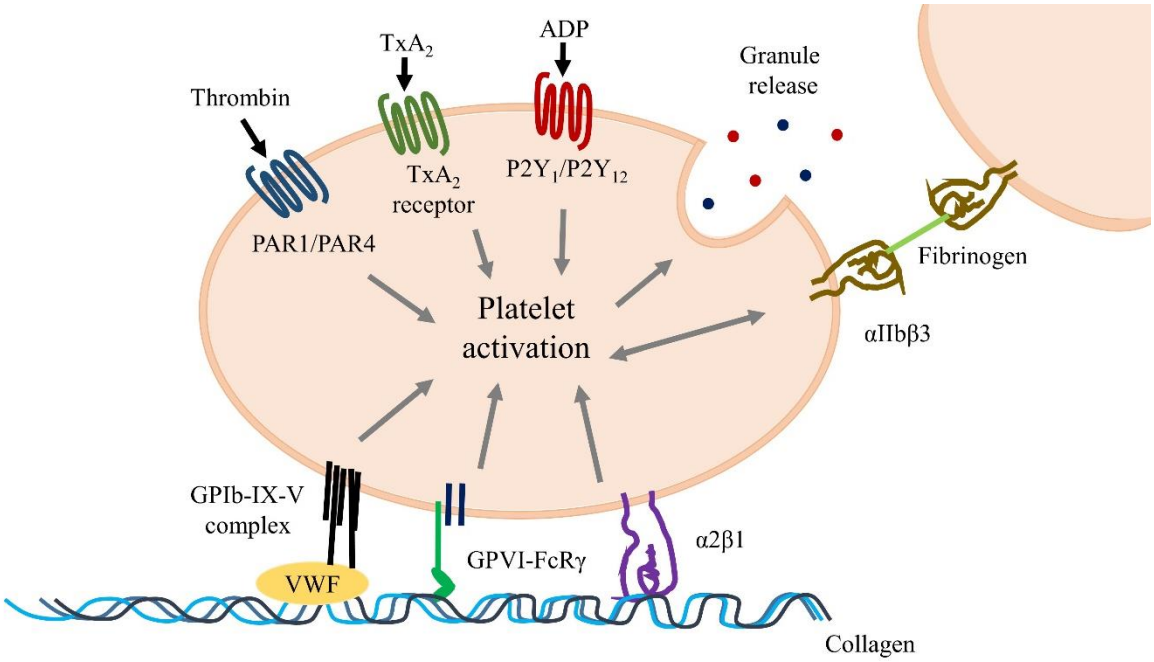


Figure 1.2. General scheme platelet activation cascade. *Resting platelets bind to VWF, tethered to exposed collagen, through the GPIb-IX-V receptor complex, but does not establish a firm adhesion. GPVI-mediated activation then occurs through collagen binding. GPVI activation leads to α2β1 and αIIbβ3 activation by converting them from a low to high affinity state. ADP from granules is released while TxA_2 is generated de novo. These agents facilitate further recruitment of aggregation factors and thrombin. Fibrinogen is ligated to αIIbβ3 for further activation of platelets and stronger adhesion. Thrombin enzymatically converts fibrinogen to fibrin creating a fibrin mesh with activated platelets, which strengthens the thrombus through clot retraction.*

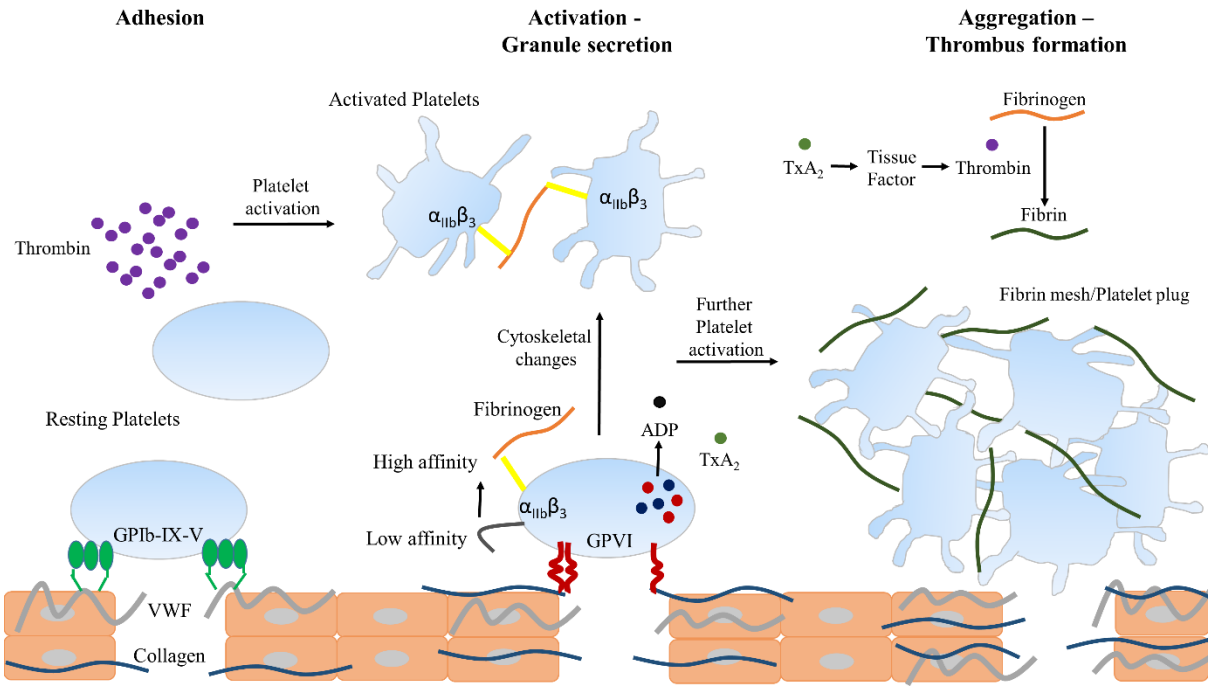


Figure 1.3. Main stages of thrombus formation. *(Left) Following a vascular trauma, platelets are initially exposed to VWF and the soluble agonist thrombin, which leads to platelet tethering to the damaged endothelium and platelet activation, respectively. (Centre) Firm platelet adhesion to the site of injury is then mediated by engagement of GPVI and integrin α2β1 with exposed collagen fibres. Integrin receptor αIIbβ3 interactions with fibrinogen, fibrin and VWF, are also critical for platelet aggregation and stabilisation. These interactions lead to morphological platelet changes, spreading and activation. Platelet activation also induces granulation secretion of α-and dense granules to secrete secondary mediators and soluble agonists, such as ADP and* TxA_2*. The latter further recruit and activate circulating platelets. (Right) Platelet aggregation and platelet plug formation is supported by in situ thrombin generation, which in turn converts fibrinogen to fibrin to form a fibrin network, which is a key step for the formation of a platelet plug generation and finally a stable thrombus.*

The presence of tissue factor in the vessel supports the formation of thrombin (Figure 1.3). Thrombin, in turn, activates platelet protease-activated receptors and converts fibrinogen to insoluble strands of fibrin, giving the blood clot its impenetrable properties through the creation of a thick mesh of fibrin fibres (Estevez and Du, 2017; Periayah *et al.*, 2017; Weisel and Litvinov, 2017).

1.2.2.2 The role of platelets beyond haemostasis

Platelets have been found to participate in a plethora of other critical functions including the prevention of vascular leakage during inflammation, known as inflammatory haemostasis or vascular integrity (Ho-Tin-Noé *et al.*, 2011; Deppermann, 2018; Rayes *et al*., 2019). During inflammation and immune cell diapedesis, stored platelet contents such as chemokines and cytokines and platelet receptors including those on intracellular granules (e.g. P-selectin) have been shown to promote and sustain inflammation (Smyth *et al.*, 2009; Cerletti *et al.*, 2012; Ware *et al.*, 2013; Golebiewska and Poole, 2015; Deppermann, 2018b; Margraf and Zarbock, 2019). Red and white blood cells can leak from the blood vessels, creating micro tears that single platelets are capable of sealing while supporting leukocyte recruitment, which demonstrates both vasoprotective and inflammation-promoting functions of platelets (Gros *et al.*, 2015; Ho-Tin-Noé *et al.*, 2018; Rayes *et al.*, 2019). This is deficient in patients with a low platelet count (known as thrombocytopenia) leading to bleeding at sites of inflammatory challenge (Goerge *et al.*, 2008; Ho-Tin-Noé *et al*., 2011). The low platelet count can also lead to severe bleeding as seen in patients with immune thrombocytopenia (ITP), as well as in patients with the inherited platelet disorders Bernard-Soulier Syndrome (BSS) and Glanzmann's Thrombasthaenia (Cohen *et al.*, 2000; Stevens and Meyer, 2002). Platelet granules contain pro-angiogenic factors that promote angiogenesis and support the formation of lymphatic vessels including in cancer (Labelle and Hynes, 2012; Ware *et al.*, 2013; Golebiewska and Poole, 2015; Rayes *et al.*, 2019).

1.3 Platelet receptors

Upon activation, the network of platelet receptors work synergistically with the downstream signalling pathways of each individual receptor merging into a common pathway to cause aggregation (GPIIbIIIa activation) and granule secretion, resulting in multiple positive feedback loops (Kauskot and Hoylaerts, 2012; Saboor *et al.*, 2013).

1.3.1 Immunoreceptor tyrosine-based activation motif (ITAM) receptors

An immunoreceptor tyrosine-based activation motif (ITAM) is a conserved amino acid sequence found in the cytoplasmic domain of immunoreceptors (Figure 1.4) containing two YxxL motifs separated by 6-12 amino acid residues. This is indicated as Yxx(L/I)x6-12Yxx(L/I), with x being any amino acid (Boulaftali *et al.*, 2014). There are two platelet receptor chains that contain this motif; the Fc receptor γ chain (FcRγ) and the low affinity immune receptor FcγRIIA (which is only found in primates) with GPVI associating with FcRγ in the membrane (Isakov, 1997; Bergmeier and Stefanini, 2013). Upon ligand binding, platelet ITAM receptors activate their signalling cascade through dimerization or higher order clustering leading to phosphorylation of the ITAM by Src family kinases. The signalling cascade then involves a plethora of adapter proteins, tyrosine kinases and enzymes such as linker for activation of T-cells (LAT), Bruton's tyrosine kinase (Btk) and phospholipase Cγ2 (PLCγ2) with the ultimate step being Ca^{2+} mobilization (Boulaftali *et al.*, 2014; Estevez and Du, 2017). ITAM receptor signalling is illustrated in detail in Section 1.3.2.

GPVI is a receptor solely expressed in megakaryocytes and platelets and it belongs to the immunoglobulin (Ig)-like superfamily of receptors, being the main collagen signalling receptor (Nieswandt & Watson, 2003). With around 3000-4000 copies per platelet in humans it is the most highly expressed ITAM receptor on platelets (Best *et al.*, 2003; Nieswandt & Watson, 2003; Burkhart *et al.*, 2012).

CLEC-2 is a C-type lectin-like receptor type II transmembrane receptor with a hemi-ITAM, representing 50% of an ITAM. CLEC-2 is expressed in platelets, megakaryocytes and a sub-population of myeloid cells (Lowe *et al.*, 2015), with the major endogenous ligand being podoplanin (Astarita *et al.*, 2012; Pan and Xia, 2015). Heme, a hemoglobin precursor released from damaged red blood cells, has also been found to activate CLEC-2 in mice and human platelets (Bourne *et al.*, 2021). CLEC-2 has a minor or negligible role in haemostasis in human but supports pathological thrombus formation at sites of inflammation (Hughes *et al*., 2010; Suzuki-Inoue *et al*., 2018; Rayes *et al.*, 2019; Bourne *et al.*, 2021).

FcγRIIA, also named CD32A, is a low affinity receptor for the Fc IgG domain in humans (Clemetson and Clemetson, 2013; Qiao *et al.*, 2015; Anania *et al.*, 2019). FcγRIIA is implicated in immune diseases and thrombosis as seen in patients with heparin-induced thrombocytopenia (HIT) or vaccine-induced immune thrombotic thrombocytopenia (VITT), which are caused by

pathological immunoglobulin G (IgG) antibodies against platelet factor 4 (PF4), inducing platelet activation upon binding and cross-linking FcγRIIA (Greinacher, Selleng and Warkentin, 2017; Greinacher *et al.*, 2021; Schultz *et al.*, 2021; Scully *et al.*, 2021).

1.3.2 G protein-coupled receptors (GPCRs)

G protein-coupled receptors (GPCRs) are a large family of seven-transmembrane receptors and is one of the major agonist receptor families in on platelets. They play a crucial role on platelet activation and thrombus growth by major soluble platelet agonists (Figure 1.4). These include ADP , TxA_2 and thrombin (Woulfe, 2005; Offermanns, 2006).

Thrombin signals through PAR receptors, giving rise to an increase in intracellular Ca^{2+} and activation of protein kinase C, leading to rapid cytoskeletal shape changes in platelets and powerful activation (Clemetson and Clemetson, 2013; Estevez and Du, 2017; Heuberger and Schuepbach, 2019). Thrombin activates PAR1 by binding to its amino-terminal exodomain to cleave a and reveal a new receptor amino terminus that serves as a tethered peptide ligand through intramolecular binding to the receptor core and initiate signaling (Voss *et al.*, 2007).

The purinergic receptors $P2Y_1$ and $P2Y_{12}$ are the major GPCRs to mediate ADP platelet responses (Clemetson and Clemetson, 2013; Estevez and Du, 2017; Koupenova and Ravid, 2018). Granule secretion following Ca^{2+} mobilisation leads to ADP release. ADP binding to $P2Y_1$ leads to rapid shape change and reversible aggregation, while $P2Y_{12}$ activation induces sustained platelet aggregation without a shape change (Woulfe, 2005; Hechler and Gachet, 2011; Estevez and Du, 2017; Koupenova and Ravid, 2018).

Another activation-enhancing pathway is through the feedback mediator TxA_2, an eicosanoid with potent pro-thrombotic and vasoconstriction properties, that binds to the thromboxane-prostanoid receptors TPα and TPβ, which are important for vasoconstriction, shape change, granule secretion and aggregation in platelets (Hayes *et al.*, 1999; Offermanns, 2006; Clemetson and Clemetson, 2013; Estevez and Du, 2017).

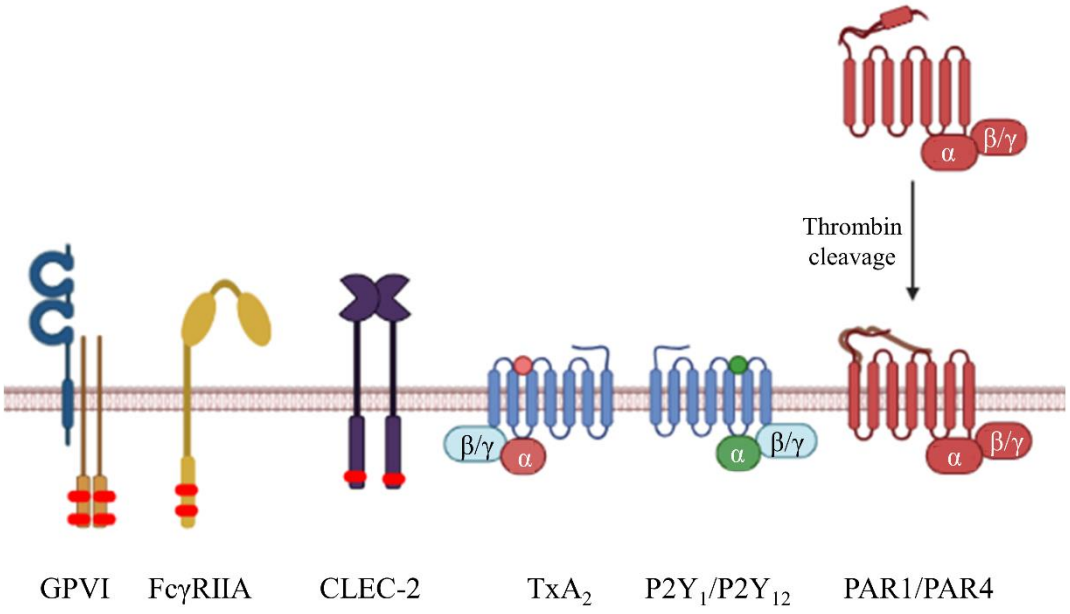


Figure 1.4. General structure of platelet receptors and ITAM receptors. *GPVI, FcRIIA and CLEC-2 receptor belong to the ITAM receptor family, while TxA_2, $P2Y_1/P2Y_{12}$ and PAR1/PAR4 comprise members of the GPCR family. GPCRs are comprised of a seven-transmembrane helix core with an extracellular N-terminus and an intracellular C-terminus. GPCRs are associated with heterotrimeric G proteins, containing α and β/γ subunits, which in turn are their principal signal transmission mechanism. Although receptor TxA_2 and $P2Y_1/P2Y_{12}$ rely on endogenous ligand binding, including TxA_2 and ADP respectively, to initiate their biological cascade, PAR1 and PAR4 rely on enzymatic thrombin cleavage of a specific portion of the extracellular N-terminus which creates a new N-terminus that acts as a tethered ligand for the receptor. Immunoreceptor tyrosine-based activation motif (ITAM) containing receptors, including GPVI and FcγRIIA, contain two YxxL groups, separated by 6 to 12 amino acid. CLEC-2 contains only one separate chain and it is typically named as a hemITAM. Fc receptor signaling is dependent on one or more ITAM motifs in their cytosolic chains where conserved tyrosine residues are phosphorylated upon receptor cross-linking to initiate an ITAM-related signalling cascade.*

1.4 Glycoprotein VI (GPVI)

1.4.1 The role of GPVI in haemostasis and thrombosis

GPVI plays a critical role in collagen-related signalling in platelets, an observation which came from GPVI deficient patients who exhibited mildly extended bleeding times and whose platelets were unable to adhere specifically to collagen fibrils (Sugiyama *et al.*, 1987; Moroi *et al.*, 1989). The loss of GPVI in the first identified patients was due to auto-antibodies and was associated with a profound thrombocytopenia that contributed to or indeed was responsible for the bleeding diathesis. A steady number of patients with GPVI-deficient platelets and immune thrombocytopenia, and an even smaller number with congenital disorders, including several patients homozygous for the same mutation in Chile which prevents GPVI expression (see below) were further reported, with most of these patients having a mild bleeding disorder and platelets that fail to aggregate to collagen (Nurden *et al.*, 2004; Kojima *et al.*, 2006; Arthur *et al.*, 2007a; Matus *et al.*, 2013; Nurden and Nurden, 2014). The latter phenotype was successfully reproduced in mouse models, where mice had their functional GPVI levels depleted by injection of anti-GPVI antibodies to generate a "GPVI knockout-like" phenotype, or by disruption of the GPVI gene (so-called GPVI knockout mice) (Nieswandt *et al.*, 2001; Schulte *et al.*, 2003). Platelets from these mice showed no adherence nor aggregation in response to collagen and the mice were protected from thrombus formation and long-term thrombotic protection (Nieswandt *et al.*, 2001). The tail-bleeding times of these mice were also mildly prolonged. These findings suggest that GPVI plays a minor role in haemostasis in mice (Nieswandt *et al.*, 2001; Schulte *et al.*, 2003).

This may also be the case in humans as the only patients with a severe bleeding phenotype also have a marked reduction in platelet count. Indeed, the most convincing evidence that GPVI does not play an important role in haemostasis is the observation from GPVI deficient patients residing in Chile who only show mild bleeding symptoms, which appear to resolve in adulthood (Matus *et al.*, 2013; Nagy *et al.*, 2020). The patients in these studies all have a homozygous adenine insertion in exon 6 of *GPVI* (c.711_712insA) that introduces a stop codon prior to the transmembrane domain and thereby translates into a truncated, non-functional cytosolic protein. This protein contains the extracellular domain of GPVI without the transmembrane domain and is visible in western blot as a band of ≈49kDa, as opposed to the wild type band of 62kDa. Interestingly, heterozygous individuals for this mutation do not exhibit any excess

bleeding and have a normal response to collagen and the snake venom toxin convulxin (Matus *et al.*, 2013).

On the other hand, GPVI seems to play a major role in pathological thrombus formation in the arterial circulation. In mouse models of thrombosis, GPVI-depleted platelets failed to adhere and aggregate on damaged subendothelium preventing arterial thrombus formation (Nieswandt *et al.*, 2001; Bender *et al.*, 2011; Eckly *et al.*, 2011). Emerging evidence for a role in venous thrombosis has also been shown by the presence of a variant in the *GP6* gene, rs1613662, which is associated with a higher risk for venous thromboembolism (El-Galaly *et al.*, 2013). In addition, GPVI has been shown to contribute to platelet aggregation induced by fibrin and fibrinogen (Alshehri *et al.*, 2015; Mammadova-Bach *et al.*, 2015; Mangin *et al.*, 2018), and this may support its role in thrombus formation in combination with integrin αIIbβ3 (Perrella *et al.*, 2021).

1.4.2 GPVI signalling

Upon collagen binding, crosslinking of adjacent GPVI receptors initiates tyrosine phosphorylation of the ITAM conserved motif within the non-covalently associated FcRγ-chain homodimer (Zheng *et al.*, 2001; Bori-Sanz *et al.*, 2003) by the Src family kinases Fyn and Lyn (Figure 1.5) (Suzuki-Inoue *et al.*, 2002). Subsequently, the tyrosine kinase Syk is recruited and activated through its tandem SH2 domain, which phosphorylates the linker of activated T cells (LAT) adaptor. This acts as a tethering site for SH2 domain containing leukocyte protein of 76 kDa (SLP-76) and other signal transduction proteins, such as phospholipase Cγ2 (PLCγ2) and phosphoinositide-3 kinase (PI3K) (Nieswandt and Watson, 2003; Hughes *et al.*, 2008). These effectors initiate integrin signalling, Ca^{2+} mobilization, cytoskeletal re-organization and degranulation, which are pivotal for platelet activation and further aggregation (Boulaftali *et al.*, 2014). Downregulation of activated GPVI is mediated through metalloprotease ADAM10-induced shedding of the receptor ectodomain (Gardiner *et al.*, 2007; Bender *et al.*, 2010).

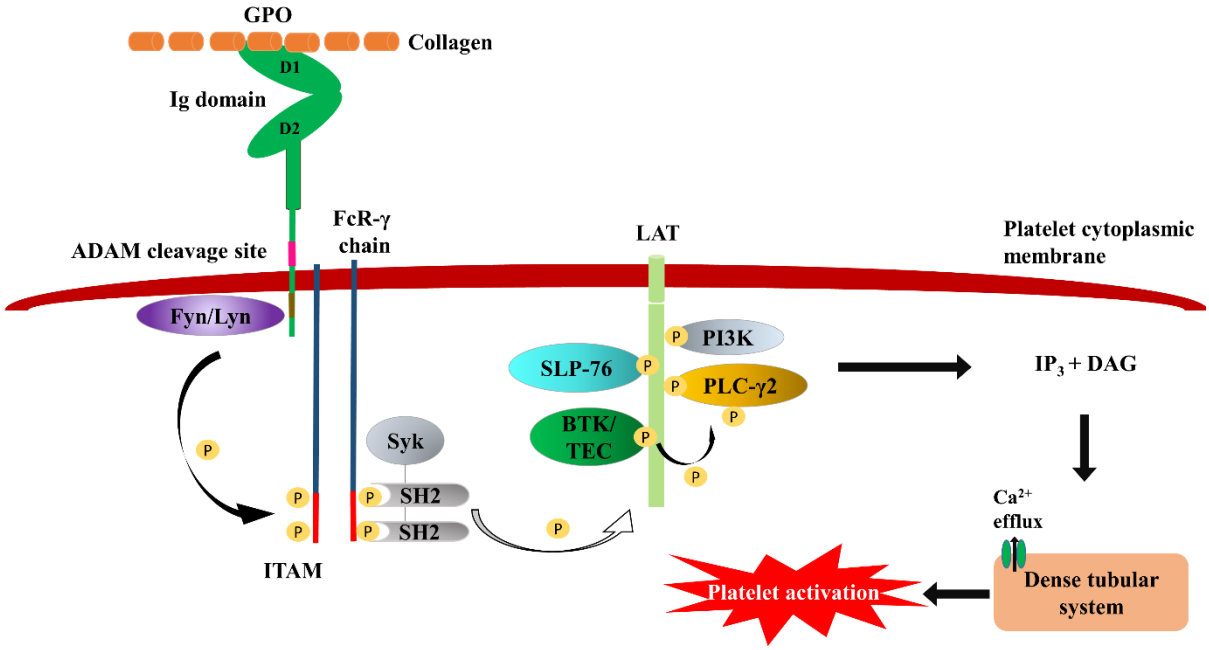


Figure 1.5. GPVI signalling. *Exposed collagen from endothelial cells is tethered to the GPVI ectodomain through the D1 immunoglobulin domain. Oligomerisation of GPVI lead to the phosphorylation of the FcR γ-chain-ITAM motifs. The phosphorylated ITAM motif then initiates a Syk-dependent signalling cascade causing the formation of a LAT (linker of activated T cells)-regulated signalling scaffold and subsequent PLCγ2 recruitment and activation. Downregulation of activated GPVI is through metalloprotease ADAM10-mediated shedding.*

1.4.3 GPVI structure

The leukocyte receptor complex (LRC) on human chromosome 19 encodes two collagen receptors: leukocyte-associated immunoglobulin (Ig)–like receptor-1 (LAIR-1) and glycoprotein VI (GPVI). Although they are structurally similar, their function and expression is very different (Brondij*k et al*., 2010).

The GPVI ectodomain is 62kDa, comprises two extracellular β sheet Ig domains (D1 and D2) and composed of 319 amino acids (Moroi and Jung, 2004). D1 and D2 are orientated so that they form an approximate 90° angle to each other with a buried D1-D2 interface surface area of 8.55-8.77 nm^2 (855-877 $Å^2$) (Horii *et al.*, 2006). Each Ig domain is comprised in total of two β sheets, from the ABE and A′GFCC′ strands, a short 3_{10} helix and 2 polyproline type II (PPII) helix stretches (Figure 1.6). The D1 surface also features a shallow groove of a hydrophobic nature which is surrounded by charged and polar residues including Lys41, Lys59, Arg60, and Arg166; the impact of these on collagen and collagen-related peptide (CRP) binding is discussed later (Horii *et al.*, 2006). The D2 domain is connected to a mucin-rich stalk region that contains multiple O-linked glycosylation sites (Moroi and Jung, 2004; Watson *et al.*, 2010). Arg272 within the transmembrane region of GPVI is linked with a FcR γ-chain homodimer through a salt bridge (Moroi and Jung, 2004). The cytosolic tail of GPVI contains a calmodulin (CaM) binding site and a proline-rich region which binds to the Src kinases, Lyn and Fyn (Figure 1.6). The penultimate residue (Cys338) in human GPVI has been reported to mediate disulfide-dependent GPVI dimerization after ligand binding (Arthur *et al.*, 2007), although the functional significance and extent of dimerization is not known. As mentioned above, the FcRγ-chain contains an ITAM motif, which is crucial for elucidating downstream signalling of the GPVI-FcRγ-chain-ITAM complex (Berlanga *et al*., 2000).

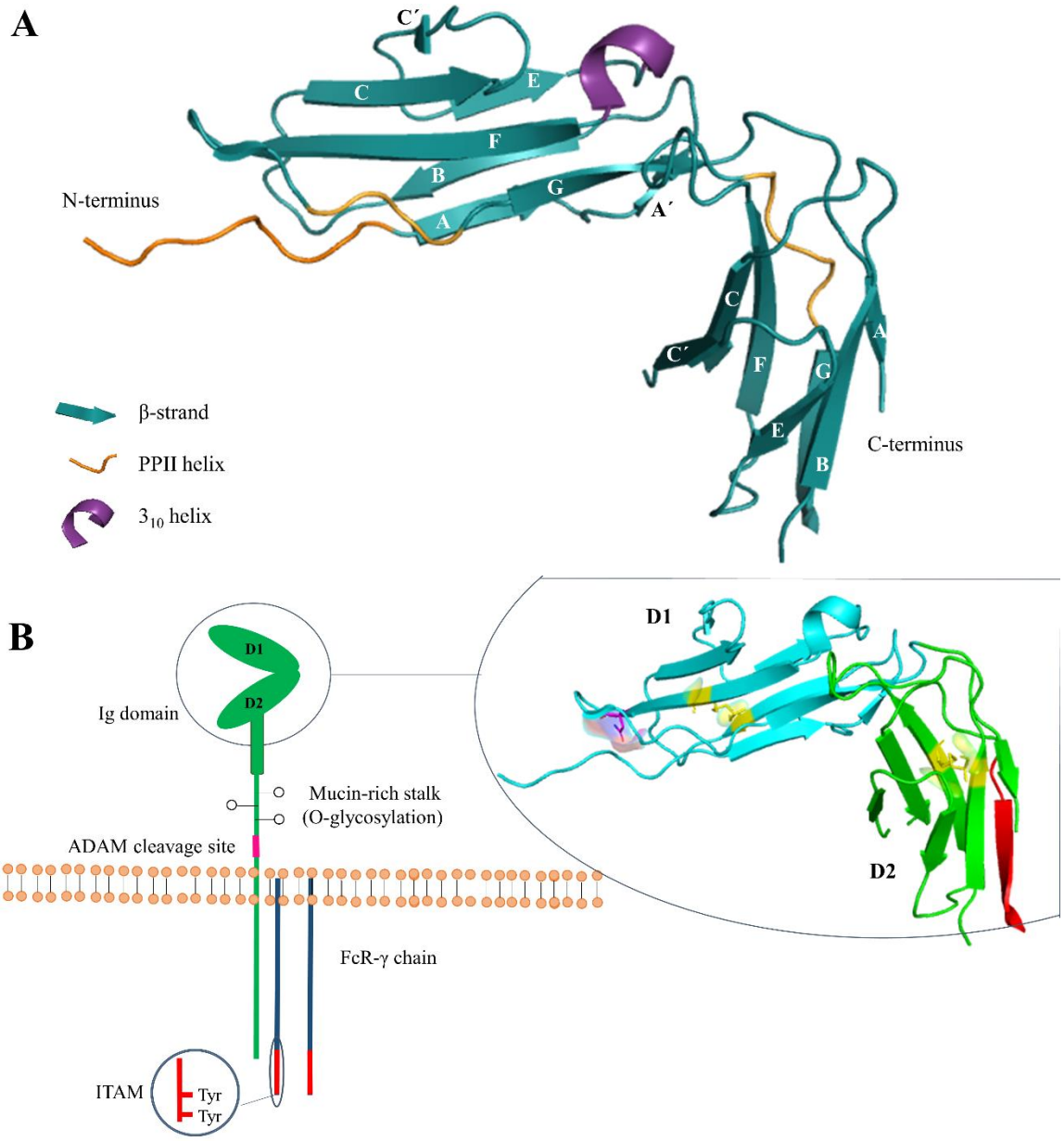


Figure 1.6. Ribbon representation of the structure of GPVI. (A) The secondary structure of the Ig domain of GPVI is annotated, from the ABE and A′GFCC′ strands, forming two β sheets (blue), a short 3_{10} helix (purple) and 2 polyproline type II (PPII) helix stretches (orange) (PDB: 2GI7). (B) Cartoon representation of GPVI receptor in the membrane. The Ig domain is connected to a mucin-rich stalk region with multiple O-linked glycosylation sites followed by an FcR γ-chain homodimer. The cytosolic tail of GPVI contains an ITAM motif at the end of each FcRγ-chain. An ADAM13 cleavage site is also featured right before the transmembrane domain. (Top right) The D1 and D2 domain are coloured as blue and green, respectively, while the N-glycosylation sites are shown in purple, the disulfide bonds in yellow and the dimer interface in red. The dimer interface corresponds to the G strands in the D2 domain, as indicated in (A) and is shown in red in the top right corner. Figures adapted from Horii *et al.*, 2006.

There is much evidence to suggest GPVI is present on the surface of platelets as a mixture of monomers, dimers and even higher order clusters and that the predominant form of GPVI in resting platelets is monomeric, with the population of dimeric GPVI increasing upon collagen or CRP binding shown both through the use of dimer-specific antibodies (Jung *et al.*, 2012; Loyau *et al.*, 2012) and the advanced imaging techniques of single molecule microscopy and fluorescence correlation spectroscopy (Berlanga *et al.*, 2007; Poulter *et al.*, 2017; Clark *et al.*, 2021). Monomeric and dimeric recombinant GPVI constructs are widely used in experimental studies, with the dimeric form being generated by fusing the extracellular domains of GPVI with the dimeric Fc domain of IgG (Moroi and Jung, 2004; Jung *et al.*, 2009; Jung *et al.*, 2012; Loyau *et al.*, 2012). However, there is a debate in literature on whether clustering in platelets is occurring due to a conformational change on GPVI or increased dimer formation and whether a unique epitope in the dimer is responsible for collagen binding, which is discussed in more detail in Section 1.4.5.

Slater et al. (2021) also showed a novel structure of a GPVI dimer, as demonstrated by an inhibitory nanobody crystallized with the ectodomain of GPVI. It revealed a hinge by the outward extension of the C-C` loop of GPVI within the domain swap that has not been described in detail before. The presence of this extended hinge loop seems to facilitate the formation of this unique conformation, where two D2 domain from GPVI monomer exchange structural elements and fold into a dimer (Slater et al., 2021). The loop forms a domain swap hinge by the C-C` loop that extends outwards, resulting in a unique folding with an adjacent D2 domain of another GPVI monomer. Evidence in support of the functional significance of this hinge was shown by its genetic deletion, where Nb2 binding was not affected, but collagen-induced GPVI signalling was abolished. The hinge was not included in the recent structure of the GPVI-CRP complex (PDB: 5OU8,9) (Feitsma et al., 2022) and while it was included in the structure that Horii et al. published, different crystallization conditions could affect the domain swap (Horii *et al.*, 2006), or the nanobody may be responsible for stabilising this conformation in the crystal. Since dimerization of recombinant GPVI ectodomain was not detected in solution (Horii *et al.*, 2006), the generation of a stable dimeric form would probably require more contact regions and therefore full length GPVI should be studied. Hence the domain swap GPVI conformation cannot be ruled out as a potential functional dimeric conformation.

1.4.4 GPVI ligand binding sites

Collagen is the most studied GPVI ligand and is crucial for studying and understanding how GPVI is activated. The most abundant collagen in blood vessel tissues are type I, III and IV (Gelse *et al.*, 2003), with GPVI primarily binding to type I and type III collagen (Barnes, Knight and Farndale, 1996; Jung *et al.*, 2008; Nieswandt and Watson, 2011). A collagen preparation, named "Horm" collagen, is the most common preparation for platelet studies and comprises a fibrils suspension of equine collagen, mostly type I and smaller amounts of type III, and other ECM proteins (Sorushanova *et al.*, 2019).

Collagen is a fibrous protein whose composition and structure can vary between different types of connective tissues in which it is present. Collagen has a unique quaternary structure consisting of three α-helix polypeptides that coil into an extended supercoiled right-handed triple helix (Figure 1.7). Each collagen chain is ~300 nm long and 1.5-nm in diameter (Boedtker and Doty, 1956; Shoulders and Raines, 2009) with just over 1000 amino acids (Bella, 2016). Hydrogen bonding creates a spiral network of intermolecular backbone NH – O=C interactions between adjacent polypeptides to hold the three helixes together. The bond angle of the C – N proline or hydroxyproline, although responsible for destabilization of single helices, also helps stabilise the final three-stranded collagen helix, which bestows collagen its characteristic structure (Kramer *et al.*, 1999; Shoulders and Raines, 2009).

Multiple collagen isoforms exist, with each different type having a polyproline II-like chain core and Gly as every third residue, a (Gly-X-Y)n repetition motif, that grants the characteristic properties of each type (Kramer *et al.*, 1999; Gelse *et al.*, 2003). The activation motif within collagen that activates GPVI is a glycine–proline–hydroxyproline (GPO) motif (Smethurst et al., 2007). This has also been investigated through the first reported selective GPVI agonist, CRP, which is based on a GPO repeat motif of 10 repetitions. CRP, cross-linked by lysine or cysteines, was reported to cause platelet aggregation independent of platelet receptor α2β1 (Morton *et al.*, 1995) by GPVI dimerization and oligomerisation and consequent phosphorylation of the FcR γ-chain-ITAMs (Kato-Takagaki *et al.*, 2009). Cross-linking is necessary for the high activity of CRP but is preparation dependent (Morton *et al.*, 1995; Achison *et al.*, 1996; Asselin *et al.*, 1997) and the final product a mixture of dimers, trimers and high order polymers. The activity of each batch of CRP is measured through bioassay.

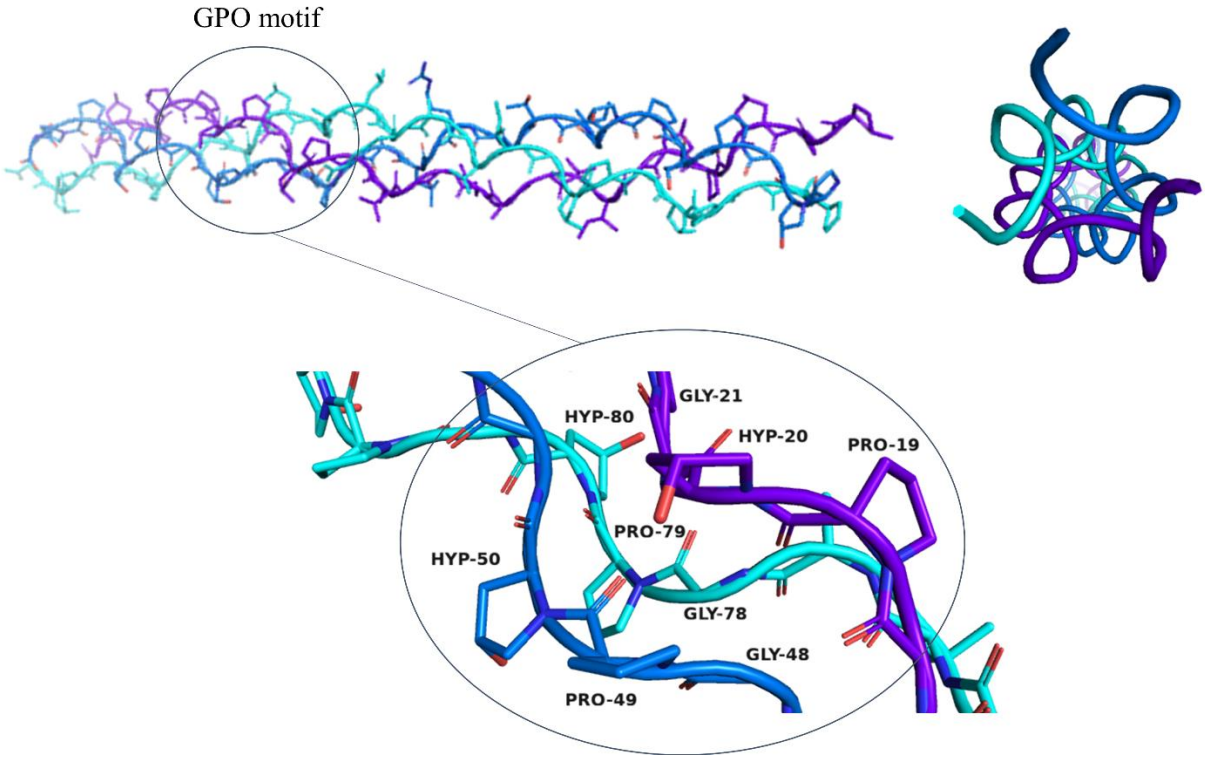


Figure 1.7. X-ray structure of collagen fibre. *(Top) Stick (left) and cartoon (right) representation of collagen consisting of three α helix peptides wrapped around in a super helix with a right-handed orientation. (Bottom) Enlarged view of the GPO repetition motif within a collagen strand. The glycine residues are hydrogen bonding though backbone interactions while proline and hydroxyproline are required for the formation of each helix and the superhelix. Proline (PRO), Glycine (GLY) and Hydroxyproline (HYP) residues highlighted. PDB: 1BKV.*

Mutation and homology studies on GPVI, as well as computational structural modelling, have been employed to investigate the binding sites of collagen on GPVI. These studies used recombinant human GPVI residues 1-185 from D1 and D2. Multiple amino acids from this construct were mutated to investigate their role in collagen, CRP and D1D2 specific antibody binding, while also employing molecular modelling (Lecut *et al.*, 2004; Smethurst *et al.*, 2004; O'Connor *et al.*, 2006). Smethust *et al* (2004) and O'Connor *et al* (2006) reported that mutation of residues Lys41, Lys59, Arg60 and Arg166 decreases collagen affinity. Mutation of residue Lys59 to the mouse equivalent (K59E), decreases affinity for both collagen and CRP, while the R60A and R166A mutations reduce collagen affinity but have no effect on CRP binding (Smethurst *et al.*, 2004; O'Connor *et al.*, 2006).

Lecut *et al* (2004) has reported additional amino acids in the D1 domain surface GPVI (Gly30, Val34 and Leu36) that greatly affect the interaction with collagen and CRP when mutated. It was observed that monoclonal antibodies raised against D1D2 had selective inhibitory properties on GPVI interaction with collagen, CRP or convulxin, despite the fact that these all competed for the collagen binding site. It was then concluded that the CRP binding site could either be an extension of the main collagen binding site, or a separate one that partially overlaps with the latter (Lecut *et al.*, 2004). After Horii *et al* (2006) revealed the crystal structure of the GPVI ectodomain, they used molecular modelling to dock CRP on the D1 domain. The model showed that the presence of a defined collagen binding groove within D1. This groove is formed by hydrophobic residues Leu53, Phe54, Pro56, Leu62, and Tyr66, and the aliphatic part of Lys41, polar residues Ser43, Ser44, Glu48, Glu50, Ser61 and basic residues Lys41, Arg46, Arg59, Arg166 around the D1 region (Figure 1.8). The cavity generated by these coordinates were later used for small molecule docking studies by other groups (Kato-Takagaki *et al.*, 2009; Bhunia *et al.*, 2017), including the present study.

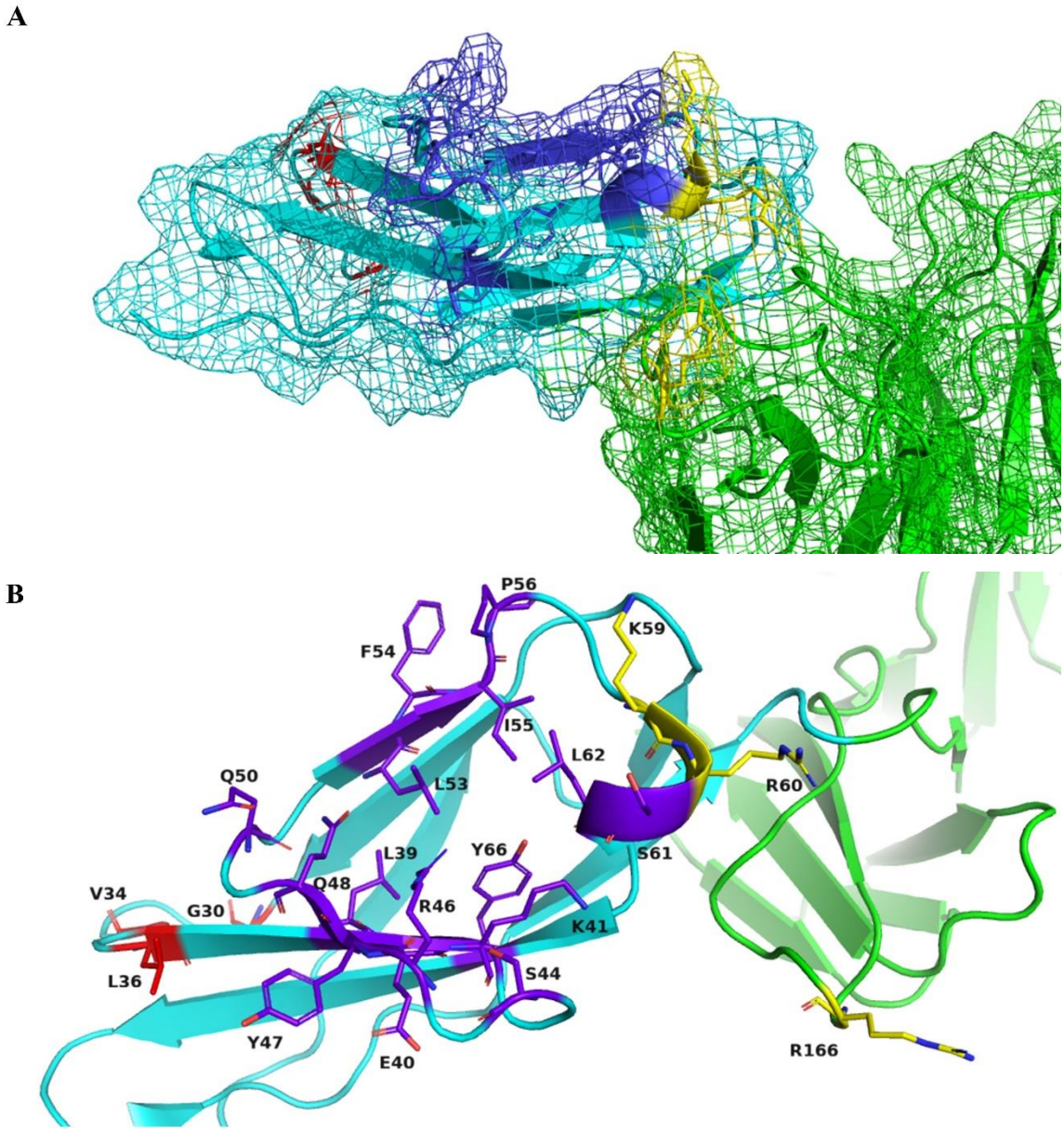


Figure 1.8. Previously predicted binding site of CRP. *View of the residues in D1 that interact with CRP in molecular docking experiments (Horii, et al. 2006). (A) Mesh surface and (B) stick annotation of the predicted binding residues for collagen or CRP. (A) A detached single monomer of GPVI twisted towards the top view of the receptor to highlight the literature reported amino acids. (B) Lys59, Arg60 and Arg166 residues in yellow (K59, R60 and R160) (Smethurst et al., 2004; O'Connor et al., 2006), and in Gly30, Val34 and Leu36 red (G30, V34 and L36) (Lecut et al., 2004) are important for collagen or CRP binding in mutation studies. Predicted collagen binding site residues Leu39-Lys41, Ser44, Arg46-Glu48, Glu50, Leu53-Pro56, Lys59, Leu62 and Tyr66 (L39-K41, S44, R46- Q48, Q50, L53- P56, K59, L62 and Y66) are highlighted.*

In addition to the unbound D1 and D2 structure, the structure of D1 and D2 in complex with synthetic CRP has been reported (Feitsma *et al.*, 2022) (PDB: 5OU8,9), and the CRP binding site has now been fully mapped (Figure 1.9) through the co-crystallisation of GPO-3 and GPO-5 repetition peptides with the GPVI D1 and D2 ectodomain. These data reveal that the CRP binding site is located in the D1 region. CRP sits within the D1 surface, towards the N-terminal, in an almost parallel manner to the D1D2 plane and perpendicular to the D1 plane (Figure 1.9). CRP directly interacts with Glu40, Arg67, Gln71 and Trp76, alongside Arg38. This suggests that a number of the residues identified in the mutation studies do not comprise the major CRP binding residues suggesting that the loss of binding may be due to a conformational change.

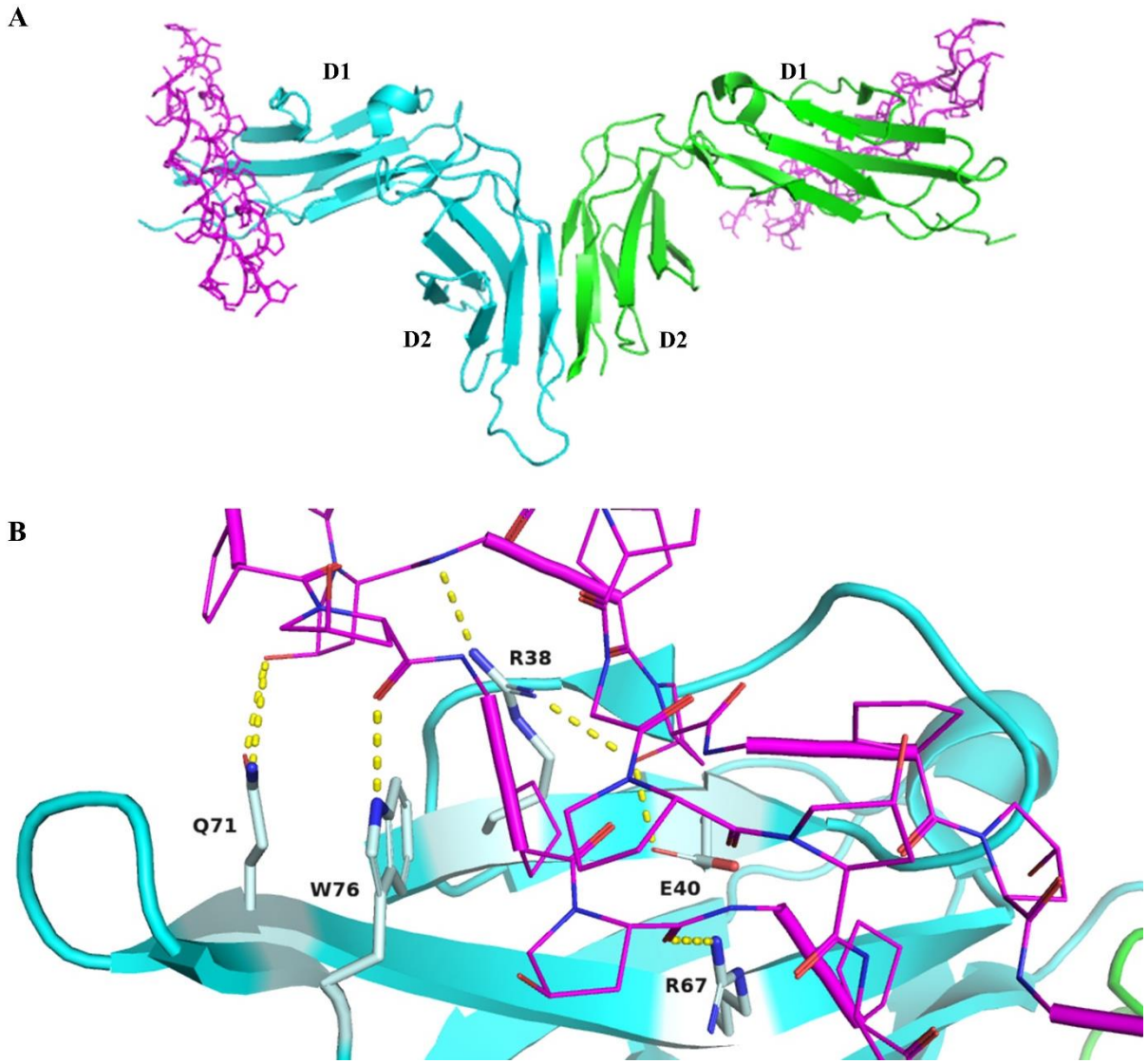


Figure 1.9. CRP binding site. *(A) Structure of GPVI extracellular domain (blue) bound to a GPO-3 peptide (purple). The dimeric crystal structure of GPVI ectodomain (PDB: 2GI7) and the CRP structure bound to a single GPVI monomer (PDB: 5OU8) were used for illustration purposes. (B) Close-up of the polar interactions between GPVI D1 domain and GPO-3. Amino acids Arg38, Glu40, Arg67, Gln71 and Trp76are highlighted (light blue). Backbone and side group interactions hydroxyproline residues of the GPO-3 are observed with the highlighted GPVI amino acids (PDB: 5OU8).*

In summary, these data place the GPVI binding sites in the D1 region of the GPVI ectodomain with many of the amino acids identified in the early mutagenesis studies now being recognised as distinct from the binding site for CRP. This suggests that these may represent allosteric binding sites which have the potential to be targeted for inhibition. The mapping of the CRP binding site reveals multiple points of contact with GPVI on a relatively flat surface, lacking a defined binding pocket. A large surface area of the receptor is easier to occupy and form a multi-interaction network by large protein ligands instead of small molecules that interact with a smaller area, as seen by the affinity of many small-molecule inhibitors that falls in the micro-molar range, including current GPVI inhibitors, thereby making it challenging to identify a small molecule inhibitor (Damaskinaki *et al.*, 2021).

1.4.5 GPVI clustering & functional significance in ligand binding

Although it is widely accepted that the predominant form of GPVI in resting platelets is monomeric and the population of GPVI dimers increases upon ligand binding, one of the biggest debates when investigating the activation mechanism of GPVI is how its structure relates to its function in platelets, including the actual conformation adopted in the membrane during resting and activated states for collagen binding, as discussed above.

Collagen has been reported to bind the dimeric form of GPVI more strongly than the monomeric form. This interaction was firstly observed through surface plasmon resonance (SPR), where the binding constant (K_D) for the soluble recombinant dimeric GPVI-Fc (GPVI-Fc_2) was approximately 576 nM whereas the monomer was too weak and could not be estimated (Miura *et al.*, 2002). In addition, unlike GPVI-Fc, monomeric GPVI was unable to inhibit collagen-induced platelet aggregation (Miura *et al.*, 2002). These results suggest that collagen shows high affinity for GPVI-Fc due to the existence of a dimer-unique epitope or through an increase in avidity. The former was supported by a study where the GPVI ectodomain was solved by X-ray crystallography (Horii *et al.*, 2006), and proposed a dimerization site within the D2 domain. However, even in high concentrations, recombinant monomeric GPVI failed to dimerise in solution, suggesting that dimerization may have been driven by the crystallisation conditions. Later on, dimer-specific antibodies, m-Fab-F (Jung *et al.*, 2009) 204-11 Fab (Jung *et al.*, 2012) and 9E18 (Loyau *et al.*, 2012) were developed and found to bind unique epitopes in GPVI, with mAb 204–11 inhibiting aggregation under flow, suggesting the functional significance of dimeric GPVI. m-Fab-F was not used for quantitation of the dimerization degree on platelets due to its low K_D= 408 nM. mAb 204-11 has also

recently been used to detect the presence of GPVI dimers in platelets of stroke patients using flow cytometry (Induruwa *et al.*, 2022). This study revealed that the binding of mAb 204-11 and P-selectin (a protein exposed on activated platelets and endothelial cells that facilitates cell adhesion) was significantly higher compared to resting platelets of healthy patients while a correlation between the binding of mAb 204-11 and P-selectin exposure after CRP-XL (cross-linked collagen-related peptide) addition was also found. Based on these results, the authors proposed that GPVI dimerisation primes in platelets of stroke patients (Induruwa *et al.*, 2022). However, it should be noted that the binding site of mAb 204-11 on this population of platelets has not been established leaving the possibility that it could be to an off-target site.

Berlanga *et al.* (2007) used C-terminal tagged GPVI constructs bioluminescence resonance energy transfer (BRET) to confirm dimerisation and possibly higher order oligomerisation of GPVI in transfected cell lines, either with or without the FcR γ-chain. A specific BRET signal was observed indicating the presence of dimers, with the level of dimerization in the presence of the FcRγ-chain being only marginally increased, meaning that dimerisation is not dependent on this associated chain (Berlanga *et al.*, 2007). This was also extended in a transfected cell line model where co-immunoprecipitation of GPVI tagged with myc- and flag-tagged was observed (Berlanga *et al.*, 2007). A similar conclusion was reached in platelets using a chemical cross-linker with both dimers and higher order oligomers observed (Berlanga et al., 2007). These observations suggested that GPVI is expressed as a dimer and/or higher clusters in a transfected cell line and in platelets although the stoichiometry of the interaction, and the presence of monomers, was not known.

A recent study by Clark *et al.* (2021) in transfected cell lines and washed platelets revealed that collagen binding and activation is not dependent on dimerization. This conclusion came from the fact that collagen binding and collagen-induced activation still occurs in a D2-deleted GPVI construct, which is predicted to be unable to form dimers. The authors used a Nanoluciferase (NanoLuc; Nluc) BRET technique (NanoBRET) in GPVI constructs where the D2 domain was removed and observed no BRET-specific signal upon D2 domain deletion while CRP-mediated stimulation on GPVI D2-deleted constructs also did not increase the BRET signal. To detect the presence of GPVI as a monomer and/or a dimer on resting cells, the authors used fluorescence correlation spectroscopy (FCS), a powerful technique for quantification of molecular dynamics, by measuring the molecular brightness of fluorescently tagged constructs' in the membrane. Then, photon counting histogram (PCH) analysis was used

to resolve the amplitude of the fluctuations in mean fluorescence intensity of a fluorescently tagged CD28-eGFP (dimer control), CD86-eGFP (monomer control), and GPVI-eGFP. An intermediate PCH signal was detected in GPVI-eGFP suggesting the presence of an equilibrium of monomers and dimers on the surface of the tested cell lines in the absence of an FcRγ chain (Clark *et al.*, 2021). This study concluded that collagen binds and activates GPVI regardless of D2-domain dimerisation with GPVI being present in the cell membrane predominantly as a mixture of monomers and dimers.

Another study using direct stochastic optical reconstruction microscopy (dSTRORM) and confocal microscopy techniques to detect clusters of GPVI dimers, utilising 204-11 Fab to identify the latter, focused on the exploration of the hypothesis on whether the formation of GPVI clusters results in an increase in avidity which facilitates platelet activation (Poulter *et al.*, 2017). GPVI dimer clustering upon platelet adhesion to collagen was observed (Poulter *et al.*, 2017). The high number of GPO motifs in collagen for GPVI binding was reported to promote the formation of large GPVI clusters on the plasma membrane. Both Horm collagen and collagen III generate higher GPVI cluster densities than collagen Toolkit peptide III-30 [a triple-helical peptide comprising the full collagen domain of human collagen III, (Raynal *et al.*, 2006)] or CRP suggesting a co-operative role for α2β1 (Poulter *et al.*, 2017). The findings of this study also supported that platelets can activate through clustering of GPVI dimers, given that clustering was measured using a dimer-specific antibody. The latter has also been supported by studies conducted on fibrinogen, but here an increase in affinity for the fused dimer over the monomer was attributed in an increase in avidity (Xu *et al.*, 2021). It has now been shown by other studies as well that collagen binds recombinant monomeric GPVI (Onselaer *et al.*, 2017; Zhang *et al.*, 2020) while x-ray crystallography data have placed the CRP binding site on the D1 domain of GPVI (Fei*tsma et al*., 2022). The latter seems to be the binding site for collagen as well, due to completion between the CRP and collagen (Clark *et al.*, 2021). Therefore, avidity in most likely the driving mechanism for the higher affinity of collagen for GPVI-Fc over monomeric GPVI.

1.5 Other GPVI ligand interactions

GPVI has also been shown to interact with other endogenous and exogenous ligands. This wide variety of ligands, as well as the presence of multiple binding sites within the GPVI ectodomain, gives an opportunity for the development of novel targeting and investigative strategies for GPVI.

1.5.1 Fibrin & fibrinogen

Fibrin is generated from soluble blood fibrinogen through cleavage by thrombin (Weisel and Litvinov, 2017). It is comprised of three globular regions, two D regions linked to a central E region, linked with two α helix peptides. Each E-region has two strands, A and B, near its centre which are linked to fibrinopeptides A (FpA) and B (FpB), respectively (Figure 1.10). After cleavage of those peptides through thrombin, A and B strands are revealed in the central region. When fibrin is cleaved by plasmin, it releases D-dimer which can then serve as an antagonist for fibrinogen and fibrin binding receptors, such as GPIIb/IIIa (Weisel and Litvinov, 2017).

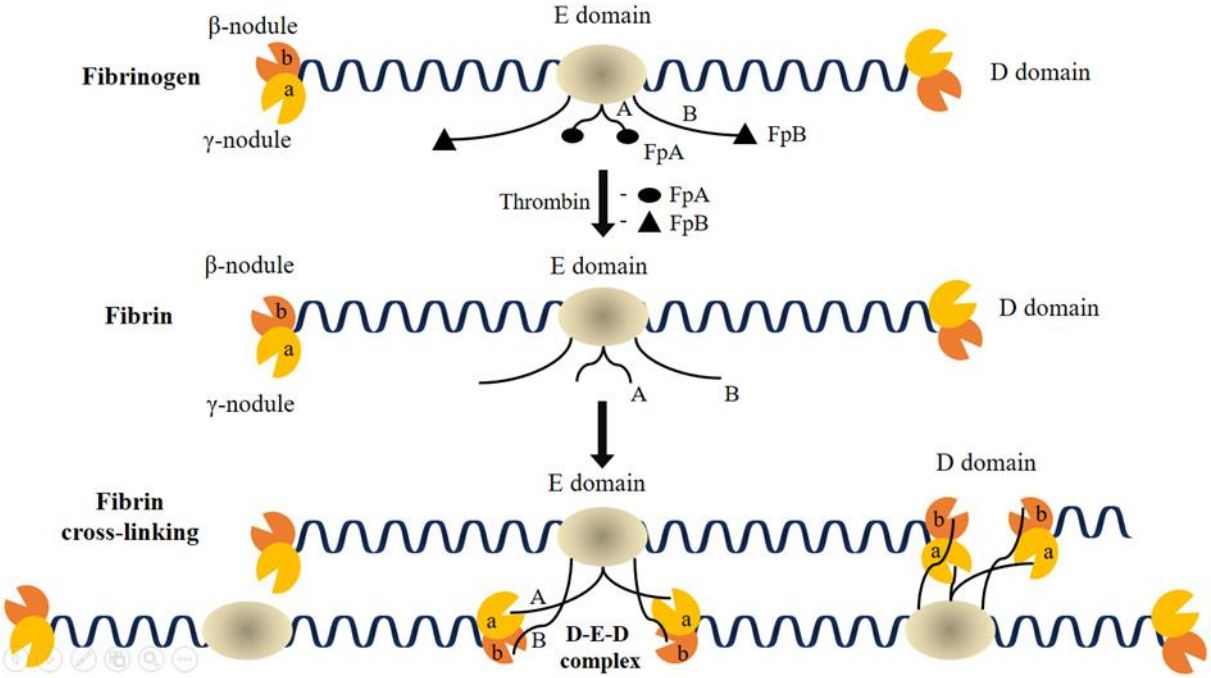


Figure 1.10. Fibrinogen conversion to fibrin and polymerization of fibrin strands. *Thrombin cleaves fibrinogen to create a fibrin monomer by removing fibrinopeptides FpA and FpB of the E domain from the N-termini of A and B knobs and exposing their ends. The exposed knobs can then interact with other fibrin monomers. This interaction is also known as a "knob-hole". The A and B knobs form these interactions with the complementary pockets 'a' and 'b' of the D domain of fibrinogen or fibrin generating a D-E-D complex and consequently a fibrin network. Figure adapted from Stamboroski et al., 2021.*

Fibrin and fibrinogen have been shown to activate GPVI (Mammadova-Bach *et al.*, 2015; Onselaer *et al.*, 2017) but there is controversy on whether this is through direct binding to monomeric (Mangin *et al.*, 2018) or dimeric GPVI (Induruwa *et al.*, 2018), or if there is any binding at all (Ebrahim *et al.*, 2018). A recent review collectively reported different data from research teams that studied the mode of GPVI binding to fibrin (Slater *et al.*, 2019). It indicated that fibrin can activate GPVI and that the disagreement within the data from different research teams studying the GPVI mode of binding for collagen, fibrin and their synthetic analogues was likely associated with the use of different forms of recombinant GPVI and experimental conditions.

Despite the above controversy, the experimental evidence for activation of the GPVI-FcR γ-chain by fibrin and fibrinogen is strong. GPVI deficient platelets fail to spread on fibrin and fibrinogen. In a 2018 study (Mangi*n et al*., 2018), immobilized fibrinogen was shown to activate human but not mouse GPVI while it was also shown that this interaction aids platelet aggregation under flow. Full spreading of human platelets from GPVI-deficient patients on immobilised fibrinogen was abolished while spreading of platelets from human-GPVI-transgenic mouse showed full spreading (Mangi*n et al*., 2018). In the same study, fibrinogen binding to human GPVI was confirmed by SPR in a human GPVI-transfected RBL-2H3 cell line. Fibrinogen, in particular, was recently found to bind dimeric GPVI with higher affinity than the monomeric form, with the αC-region of fibrinogen being the most important for high-affinity GPVI binding (Xu *et al.*, 2021). However, no self-assembly of GPVI was observed, suggesting that the increased affinity of fibrinogen for dimeric GPVI is more likely attributed to avidity than a unique dimeric GPVI conformation. In addition, similar binding profiles of GPVI to fibrin and fibrinogen variants were observed, suggesting that fibrin polymerization is not necessary for GPVI binding (Xu *et al.*, 2021).

1.5.2 Snake venom toxins

Snake venom toxins fall into two families, the C-type lectin-like and the metalloproteinase-disintegrins. Both toxin families include GPVI agonists, with the most characterized snake venom toxin being convulxin. Convulxin is commonly used to study the activation of GPVI due to its potency and absence of binding to a second collagen receptor on platelets, integrin α2β1 (Polgár *et al.*, 1997; Kato *et al.*, 2003; Lecut *et al.*, 2003; Lockyer *et al.*, 2006). Its binding site is distinct from that of collagen (Lecut *et al.*, 2004). However, other reports found convulxin to weakly bind GPIb (Du *et al.*, 2002a; Du *et al.*, 2002b; Kanaji *et al.*, 2003) and to

promote platelet cross-linking although the overall contribution to platelet activation appears minor (Clemetson, 2010).

Convulxin is a member of the C-type lectin-like venom toxins. It is a 72 kDa protein with a cyclic heterotetrameric form of α and β dimers subunits (α4β4)2, that are linked with a disulphide bridge between CysC81α and CysC77β. The convulxin dissociation constant (K_D) for GPVI binding is 0.8-3 nM and the proposed binding sites on GPVI lie on the D1 and D1/D2 interface (Murakami *et al.*, 2003; Batuwangala *et al.*, 2004; Horii *et al.*, 2009). The multimeric structure of convulxin has been previously proposed to cause clustering of GPVI (Polgár *et al.*, 1997), with convulxin binding up to eight GPVI monomers through the Ig domain, aiding the bridging of GPVI to other platelets (Horii *et al.*, 2009).

Other C-type lectin family proteins such as alboluxin, alboaggregin-A, ophioluxin, and stejnulxin also cause platelet aggregation and this is assumed to be through the Ig domains of GPVI, with alboagregin-A and alboluxin also occupying GPIbα (Du *et al.*, 2002a; Du *et al.*, 2002b; Andrews *et al.*, 2003; Lee *et al.*, 2003). On the other hand, the metalloproteinase, alborhagin, binds to GPVI through a partially overlapping, but distinct binding site to that of convulxin (Andrews *et al.*, 2001).

1.5.3 Other endogenous & exogenous ligands

Other endogenous ligands for GPVI include ECM proteins, laminin, fibronectin, vitronectin, adiponenctin, CD147 and amyloid Aβ40 (Montagu*e et al.*, 2021). The physiological significance of many of these interactions is still undetermined. Amongst the ECM proteins, laminin, a major protein of the basement membrane, is known to support adhesion of platelets through integrin α6β1 and GPVI, with α6β1 facilitating binding of laminin to GPVI (Inoue *et al.*, 2006; Ozaki *et al.*, 2009). Fibronectin has been reported to support the adhesion of platelets to intact atherosclerotic endothelium, and vitronectin to activated endothelial cells, both through an interaction with GPVI (Bültmann *et al.*, 2010; Schönberger *et al.*, 2012). The membrane protein extracellular matrix metalloproteinase inducer (EMMPRIN), also known as CD147 or basigin, mediates monocyte adhesion to immobilized platelets (Schulz *et al.*, 2011), while adiponectin and amyloid Aβ40 peptide have been shown to induce tyrosine-kinase dependent platelet aggregation through GPVI (Riba *et al.*, 2008; Elaskalani *et al.*, 2018; Donner *et al.*, 2020).

Many exogenous ligands have also been identified as GPVI agonists, including charged diesel exhaust particles, nanoparticles and sulphated polysaccharides (Alshehri, Montague, *et al.*, 2015; Flierl *et al.*, 2015). The charged nature of these ligands and, consequently, their potential for developing electrostatic interactions are likely to interact with positively charged amino acids (Alshehri, Montague, *et al.*, 2015; Montague *et al.*, 2021), within the more hydrophilic D1 region of GPVI, such as the lysine (K41 and K59) or asparagine (R60 and R61) residues (Alshehri, Montague, *et al.*, 2015).

Monoclonal antibodies (mAbs) are an established tool for studying the functional role of GPVI. Several have been shown to activate GPVI in mouse and human platelets. Two of the most studied mAbs are JAQ1 (Nieswandt *et al.*, 2001) and 1G5 (Al-Tamimi *et al.*, 2009). The cross-linked species of JAQ1 and 1G5 exhibit GPVI activation properties, but the monovalent antigen-binding fragments (Fabs), that contains one constant and one variable domain of each of the heavy and the light chain, fail to induce platelet aggregation, presumably due to a failure to induce crosslinking (Lecut *et al.*, 2004). Meanwhile, Fabs of the monoclonal antibodies 1G5 and 12A5, block collagen and CRP-induced platelet aggregation but not convulxin-induced aggregation, demonstrating the distinction between the convulxin and collagen/CRP binding sites (Al-Tamimi *et al.*, 2009).

1.6 GPVI inhibitors

As described above, clustering of GPVI is achieved through the presence of repeat sequences on a single ligand, as demonstrated by collagen, and current potent inhibitors for the study and therapeutic targeting of GPVI are antibodies and their fragments. Despite attempts to develop small molecule inhibitors, there has been no success in developing any with higher than micromolar level affinities or adequate specificity, as many have demonstrated off-target interaction with other platelet receptors. A possible explanation for this could be due to a disruption of the cell membrane, rather than blockade of ligand binding (Chen *et al.*, 2007; Chandasana *et al.*, 2015; Bhateria *et al.*, 2017; Onselaer *et al.*, 2019).

1.6.1 GPVI inhibitors in the clinic

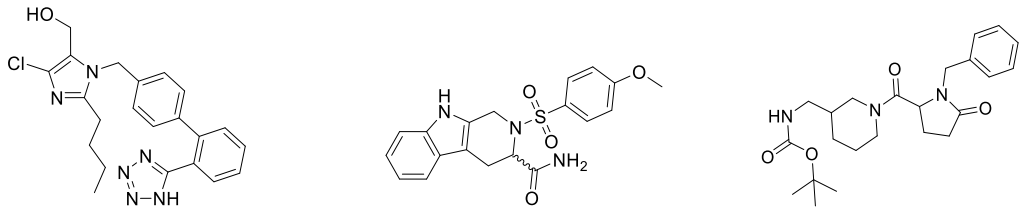
So far, the main targeting strategy in the clinic for GPVI involves protein inhibitors. Two GPVI-targeting agents have been developed to date and are currently undergoing phase II clinical trials. These are: revacept (Schüpke *et al.*, 2019), a GPVI-Fc fusion protein, and anti-GPVI Fab fragment, ACT017 (Voors-Pette *et al.*, 2019), now known as glenzocimab. Revacept

is a recombinant dimeric form of the extracellular part of GPVI fused to the Fc chain of human immunoglobulin G1 (IgG1). It competes with endogenous platelet GPVI for collagen binding. This agent entered phase II trials after the observation that it inhibited platelet aggregation on atherosclerotic plaque *ex vivo* under flow conditions, therefore, its effects could be beneficial in patients with atherosclerotic plaque rupture (Jamasbi *et al.*, 2015).

ACT017 is a humanized anti-mouse monoclonal antibody derivative of Fab 9O12 (Muzard *et al.*, 2009), a Fab commonly used for the inhibition of platelet aggregation and adhesion (Lecut *et al.*, 2003). ACT017 showed improved affinity and specificity for GPVI-Fc (K_D=4.1 nM), compared to Fab 9O12 (K_D=17 nM), measured through SPR, and inhibits GPVI-Fc binding to collagen (IC_{50}=28.54 nM) in an ELISA assay. Using molecular and homology modelling to generate the ectodomain of GPVI, the binding sites of 9012 and 10B12 were mapped to the D1 domain, which was also supported by binding assays, with 9O12 residing in an adjacent but not identical site to that of 10B12 (Lecu*t et al*., 2004). However, it has been reported in abstract form that structural characterisation of the co-crystal glenzocimab in complex with extracellular monomeric GPVI shows that the site of interaction of glenzocimab to be in the D2 domain of GPVI (Jandrot-Perrus, 2022). The mode of binding is described in more detail in Chapter 4.

1.6.2 Small molecule inhibitors

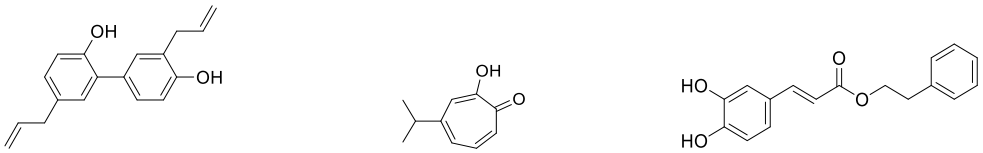
Several small molecule GPVI inhibitors have been reported (Figure 1.11). Such agents include the angiotensin II receptor antagonist losartan (Taylor *et al.*, 2014), and the natural bioactive compounds: honokiol (Lee *et al.*, 2017), hinokitiol (Lin *et al.*, 2013) and caffeic acid phenethyl ester (CAPE) (Chen *et al.*, 2007). All of these have shown inhibition of collagen-induced platelet aggregation. Losartan and honokiol have shown anti-platelet effects via multiple receptors, but their mechanism of action is not fully established (Onselaer *et al.*, 2019). A primary losartan metabolite analogue, S002-333 (Bhunia *et al.*, 2017), and a synthetic pyroglutamylpiperazine analogue, S007-867 (Misra *et al.*, 2018), have been demonstrated to have antithrombotic efficacy in *in vitro* and *in vivo* models.



Losartan
(IC_{50}=6μM)

S002-333
(IC_{50}=6μM)

S007-867
(IC_{50}= 6.7μM)



Caffeic acid phenethyl ester (CAPE)
(IC_{50}= 14μM)

Hinokitiol
(IC_{50}=~1μM)

Honokiol
(IC_{50}= 0.6μM)

Figure 1.11. Small molecules developed as GPVI inhibitors reported in literature. *Figure obtained from Damaskinaki et al., 2021.*

Losartan, found in a drug-repurposing virtual screening, is an angiotensin II receptor antagonist that acts as a non-competitive GPVI antagonist, with an IC_{50} of around 6 μM (Jiang *et al.*, 2015; Onselaer *et al.*, 2019) on collagen-induced platelet aggregation. Losartan has proven adequate specificity when it comes to inhibition of aggregation induced by collagen over other platelet agonists (10 μM ADP, 1 μM U46619 [a synthetic analogue of the endoperoxide prostaglandin PGH_2] where the IC_{50} for inhibition is > 22 μM) but the *in vitro* antiplatelet effect of losartan is not expected to reach efficacy administered as a therapeutic dose in patients (Jiang *et al.*, 2015). Honokiol has a reported IC_{50} of 0.6 μM against 1μg/mL of collagen (Lee *et al.*, 2017) against of collagen with no effect on ADP or thrombin at 5 μM, and blocks convulxin but not rhodocytin, a CLEC-2 agonist. CLEC-2 is often studied in parallel with GPVI within biological assays, to determine ligand specificity between platelet ITAM receptors. However, an order of magnitude greater IC_{50} value was reported in follow-up study against 1μg/mL of collagen of 4.6μM (Onselae*r et al.*, 2019). Hinokitiol (Collagen 1μg/mL [IC_{50}: ~ 1 μM]) (Lin *et al.*, 2013), S002-333 (Collagen 2 μg/mL [IC_{50}: 6.7 μM], CRP-XL 0.3 1μg/mL [IC_{50} = 53.5 μM]) (Bhunia *et al.*, 2017), 31a (Collagen 1μg/mL [IC_{50}: 6 μM]) (Anil Kumar *et al.*, 2014), also known as S007-867 (Misra *et al.*, 2018), caffeic acid phenethyl ester

(CAPE) (IC_{50}: 14 μM, collagen 2μg/mL) (Hsiao *et al.*, 2007) and Trowaglerix venom decapeptide Troα10 (IC_{50}: 30.42 μM, collagen 2μg/mL) (Chang *et al.*, 2017) are also agents that have been reported within the last decade with promising *in vivo* and *ex vivo* properties but all have low affinity which will render them as weak antagonists against a multimeric ligand.

1.6.3 Nanobodies

A nanobody is a single-domain antibody (sdAb) consisting of a single monomeric variable region derived from an antibody produced in camelids (Figure 1.12). Similarly to an antibody, it is able to selectively bind a specific antigen but has a molecular weight of 12–15kDa, making them much smaller than common antibodies (150–160kDa) and smaller than Fab fragments (~50kDa) and single-chain variable fragments (~25kDa) (Harmsen and De Haard, 2007). They were first engineered from heavy-chain antibodies found in camelids, called variable heavy chain domain (V_HH) fragments. V_HHs comprise of four conserved sequence stretches, called framework regions, that surround three hypervariable complementarity-determining regions (CDR), with the CDR3 region being the major antigen binding sequence (Muyldermans, 2013; Mitchell and Colwell, 2018a, 2018b).

Nanobodies can demonstrate equal specificity to antibodies, and in some cases a higher stability and diversity, and they are easily produced and cultured in large concentrations *in vitro* (Lipman *et al.*, 2005; Olafsen and Wu, 2010). Over the last two decades, there has been an increase in nanobody research and their pharmaceutical applications, including their potential use for fluorescent imaging (Beghein and Gettemans, 2017) and the treatment of acute coronary syndrome, cancer, Alzheimer's disease, and Covid-19 (Muyldermans, 2013; Steeland *et al.*, 2016; Jovčevska and Muyldermans, 2020; Yang and Shah, 2020; *J.* Xu *et al.*, 2021). Caplacizumab, a V_HH anti-VWF humanized nanobody, has recently entered the clinic for the treatment of patients with acquired thrombotic thrombocytopenic purpura (Scully *et al.*, 2019; Jovčevska and Muyldermans, 2020).

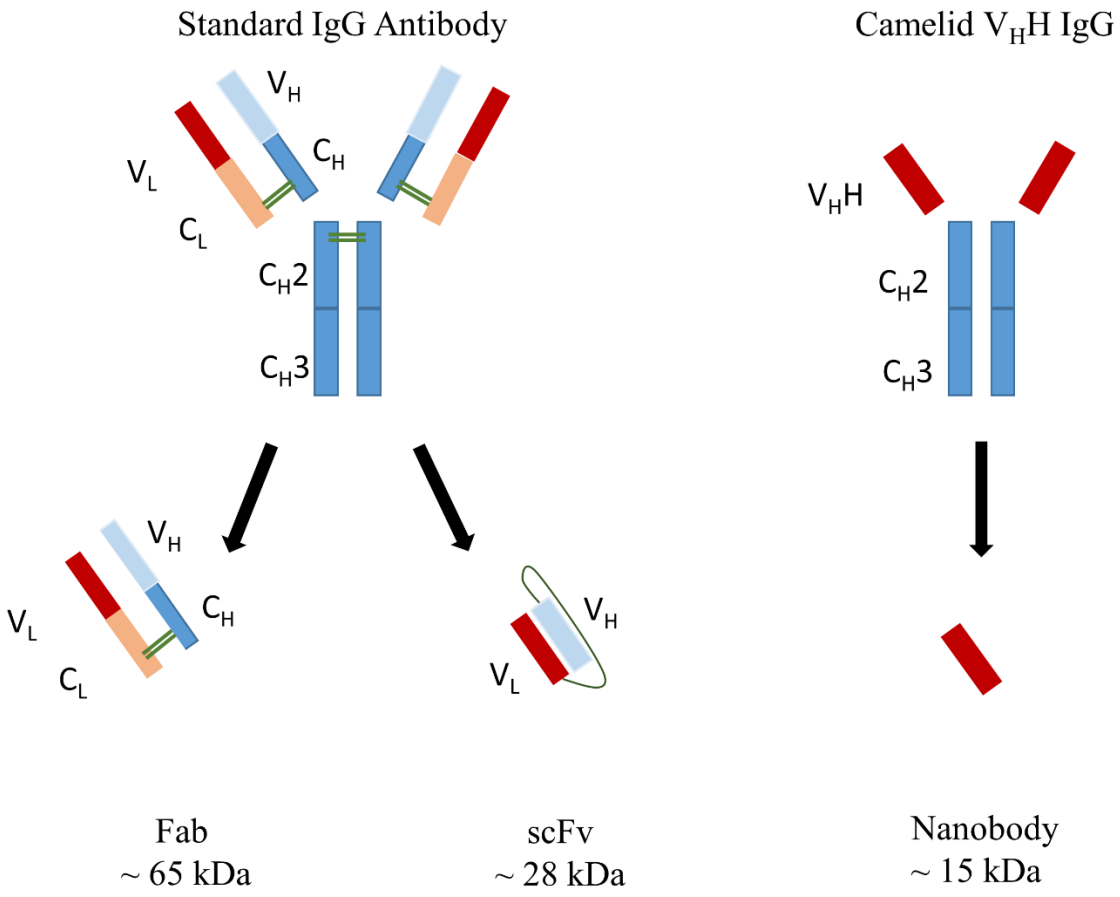


Figure 1.12. Schematic representation of antibody fragments and nanobodies. *Left: A standard IgG antibody (Ab) consists of a constant (C) and a variable (V) unit two heavy chains (V_H,C_H,C_{H2},C_{H3}) of two light chains (V_L,C_L). A region on an antibody that binds to antigens is a fragment antigen-binding (Fab) region while a single-chain variable fragment (scFv) is a fusion protein of the variable chains of V_H and V_L connected with a short peptide linker. Right: Camelids can naturally produce antibodies of a single variable domain of a heavy chain (V_HH) attached to a C_{H2} and C_{H3} core. Disulfide bonds between the different chains are shown in green.*

A recent study, where multiple nanobody inhibitors were raised against recombinant human GPVI, structurally characterized the interaction of the most potent nanobody in complex with GPVI (Slater *et al.*, 2021). This was the first published structure of GPVI bound to an exogenous ligand. The inhibitory nanobodies raised in this study are amongst the most potent GPVI inhibitors so far described and provide an excellent opportunity for the potential development of antithrombotic drugs and therapeutic agents for cardiovascular diseases. 54 nanobodies were raised against human GPVI from a VIB nanobody core, from 33 distinct families, categorized according to their CDR3 regions, for the identification of distinct binding epitopes within GPVI. Three of these nanobodies, Nb2, Nb21, and Nb35, showed the strongest inhibition of collagen-induced platelet aggregation. Nb2 had a K_D of 0.6 and 0.7 nM against recombinant monomeric and dimeric GPVI, respectively, as measured by SPR (Slater *et al.*, 2021). They also studied the effect of these nanobodies on collagen-induced GPVI signalling via a nuclear factor of activated T-cells (NFAT) reporter assay. A concentration of 100nM reduced collagen-induced signalling by more than 80% for nanobodies Nb2, Nb21 and Nb35, while also inhibiting platelet aggregation and thrombus formation of whole blood under flow conditions (Slater *et al.*, 2021).

1.7 Aims & Objectives

Despite the great progress that has been made in the clinic regarding GPVI inhibition, the efficacy and toxicity gap of small molecules as inhibitors, as well as the controversial data regarding the mechanism of GPVI oligomerization, impede their optimization. More insight is needed on the activation mechanism, the different mode of action of endogenous ligands and clarification of their binding modes. Anti-GPVI agents and endogenous ligands are a starting point to obtain more information on the exact mode of binding in order to understand how the structure and observed effects of such agents relate to platelet activation.

This project aimed to develop GPVI-specific ligands with highaffinity and explore the mode of binding of established potent ones, through the use of imaging and crystallography techniques. Characterizing the mode of action of these agents and mapping the site of interaction of these agents is of outmost importance for effective understanding of the mechanisms of GPVI inhibition and discovery of ligand binding grooves that can be used for future design of novel inhibitors. High-affinity and selective ligands were used in this study, to

overcome the targeting challenges that researchers have previously faced when developing small ligands for GPVI, including a lack of affinity, or sufficient binding surface in precursor molecules. The complex interactions between a protein ligand and a receptor can be difficult for a small molecule to mimic as the site of interaction may have relatively few binding features, cover a large surface area while a small molecule interaction may reduce but not block binding of an endogenous protein ligand. In order to counter the effects of avidity of big protein ligands a small molecule ligand should bind to a key site in the receptors with high affinity and have a slow off-rate.

Development of affinity small ligands was attempted by employing structural-based virtual screening and docking studies of an insourced compound library to identify potent novel small molecules ligands while potent inhibitory nanobodies were fluorescently labelled for competition studies and the identification of their binding site. In addition, to achieve structural characterization of the binding site of high-affinity GPVI ligands, co-crystallisation was attempted in this study using Nb21 and Nb35 (Slater *et al.*, 2021) to establish and monitor receptor-ligand binding effects, and aid future development of GPVI ligands and safer antiplatelet drugs.

In summary, the main aims of this thesis are:

1. Designing and testing novel small molecule ligands to specific regions of GPVI, using *in silico* modelling techniques.
2. Use newly developed GPVI-specific nanobodies, Nb21 and Nb35, to perform mutation studies to identify if these bind to sites on GPVI distinct to the known binding site of Nb2. This will identify potential novel binding sites on GPVI that could be used in structural studies to map new binding pockets, in order to aid anti-GPVI inhibitor development.
3. Co-crystallization of nanobodies with GPVI to identify key amino acids for the binding site of GPVI and the binding mode, including the degree of any binding site overlaps between these sites.

Chapter 2

Materials and Methods

2.1. Virtual Docking Studies

2.1.1 Ligand structure preparation

Docking studies were performed using Schrödinger Maestro 11.9 (Schrödinger Release 2018-1: Schrödinger, LLC, 2016, New York, NY) to dock a variety of literature ligands (Gaur *et al.*, 2006; Zhao *et al.*, 2006; Im *et al.*, 2009; Tsuchiya, 2011; Ono *et al.*, 2014; Taylor *et al.*, 2014; Yi *et al.*, 2014; Bhunia *et al.*, 2017) and Managed Chemical Compound Collection (MCCC), which currently comprises >85K entries Molecules that comply with Lipinski's rule of 5 and contain no reactive functional groups. Samples are stored as 10 mM DMSO stock solutions at optimum condition and purity of compounds is monitored via a dedicated LC-MS system. The MCCC library is located in the University of Nottingham. Communication with the management facility was made to obtain a virtual copy of the compound library (obtained in 2018, 84,665 in-stock compounds) for the purposes of this project. This library was provided following ligand preparation to obtain all possible ligand conformations while compound physicochemical properties were also provided.

2.1.2 Protein structure preparation

PDB files 2GI7 and 5OU7-9 were used for docking studies related to the collagen binding site and CRP binding site. Protein preparation wizard was used for protein preparation, including adding missing hydrogen atoms, remove water molecules and setting the physical condition of pH was at 7.4 ± 1.0 for atom typing.

2.1.3 Structure-based pharmacophore development

Binding site identification and verification for docking were conducted using SiteMap (Schrödinger, LLC, 2018-1, New York, NY). Structure-based pharmacophores were generated using the Receptor cavity option from The Develop Pharmacophore Model function was used through the Auto (E-pharmacophore) method, which utilises both ligand- and structure-based approaches to generate energetically optimized, structure-based pharmacophores for compound screening. [(Loving *et al*., 2009; Salam *et al*., 2009), Schrödinger, LLC, 2018-1, New York, NY]. This method is using the Glide XP scoring function to predict potential protein-ligand interactions, exclude receptor-based volumes and rank pharmacophore features based on ligand-binding potential. These features are extrapolated from inverse features from the receptor cavity to generate complementary receptor features at the receptor coordinates,

where a ligand feature has the potential to develop a favourable interaction with the receptor. For the purpose of this study, negative charges were set to be equal to hydrogen bond donors and positive charges with hydrogen bond acceptors, but aromatic rings were not equalized to hydrophobic groups. Equalisation is referred to the absence of distinction between two features. In this case, aromatic rings were always presented as a separate feature, even if it is functioning as a hydrophobic group

2.1.4 Site selection & Grid generation

For the collagen site cavity generation residues Leu39-Lys41, Ser44, Arg46-Glu48, Glu50, Leu53-Pro56, Lys59, Leu62 and Tyr66 were used while for CRP L36, R38, E40, Y47, D49, R67, Q71 and W76. The collagen binding site residues were extrapolated from literature (Kato-Takagaki *et al.*, 2009; Brondijk *et al.*, 2010; Bhunia *et al.*, 2017) while CRP residues were extrapolated manually using the CRP residues that interact with each GPVI chain from PDB file 5OU8. SiteMap was also used to identify drugable cavities and confirm the druggability of the collagen binding site cavity. The collagen cavity was included in the SiteMap results and was used for receptor docking grid generation. No restrictions or forced interactions were applied to the grids. The CRP binding site did not have a corresponding result in SiteMap and the residues were used for grid generation.

2.1.5 Virtual ligand docking

Glide [(Friesner *et al.*, 2004, 2006; Halgren *et al.*, 2004), Schrödinger Release 2018-1: Glide, Schrödinger, LLC, New York, NY, 2016] was used for ligand docking. Van der Waals radius scaling factor was set to 1.0 and partial charge cut off value was set to 0.25. The docking calculations were made in Standard Precision Mode (GlideScore SP). Glide scores were compared to literature compound losartan (Bhunia *et al*., 2017) as a reference. PDB file 5OU7 was used for the docking studies using the pockets that corresponded to the pharmacophore that corresponded to the most suitable pocket for docking (SiteMap score, docking scores, Pharmacophore merge using Hypothesis Alignment).

2.1.6 Compound selection for screening

Later, the generated models were used for screening of the MCCC compound library. Compound selection was firstly based on pharmacophore matching score (PhaseScreen Score) by comparing the generated pharmacophore features to the ones of each compound, monitoring their distances to each pharmacophore feature. The 1000 compounds with the highest

PhaseScreen Score from each pharmacophore were selected for ligand docking to each of the two pockets. 15 with the highest docking score from each pocket, using the Glide Score for ranking, were then selected for testing (30 in total) aggregation assay screening on human washed platelets.

2.2. Synthesis of small molecule controls for aggregation studies

2.2.1. General procedure and characterization

Reagents and anhydrous solvents were obtained from Sigma Aldrich, Alfa Aesar and Fisher Scientific and were used on reagent grade, unless stated otherwise. The three agents (**22, O1, O2**) were obtained from Enamine Ltd. (NCC-00036322, CAS No. 796122-84-4) and OTAVA chemicals Ltd. (MolPort-000-485-212, CAS No. 880398-56-1, MolPort-004-892-254, CAS No. 901654-94-2). Melting points were determined in open capillaries on an electrically heated melting point apparatus and are otherwise uncorrected. Thin-layer chromatography (TLC) was performed in Merck Silica gel 60 A F254 plates under UV light and standard TLC stains were used to visualise the silica gel plates. Retention factor (R_f) values in a given solvent system are reported to two decimal places. Column chromatography was used for compound purification via either a Thompson pump or normal phase Interchim Puriflash pre-packed cartridges consisting of 50 μM silica or a glass column using Merck Geduran silica gel 60 A (230-240 μm). Column size selected was generally 40-60 times the loading amount. Nuclear magnetic resonance spectra, proton (H-1) nuclear magnetic resonance (^{1}H-NMR) and carbon-13 nuclear magnetic resonance, (^{13}C-NMR), were obtained at room temperature using a Bruker AV400 (spectrometer operating at 400 MHz). All samples were prepared in deuterated solvent DMSO-*d6*. Chemical shifts (δ) were recorded in ppm and coupling constants (*J*) were recorded in Hz. The spectra were analysed using MestReNova12.0.1 software. Analytical HPLC was performed on a Shimadzu UFLCXR system coupled to an Applied Biosystems API2000. A Phenomenex Gemini-NX 3μm-110A C18, 50x2mm was used for HPLC-MS. The column was thermostated at 40°C before use while the flow rate was 0.5mL/min, running time was 5 min and injection volume was 5 μL. Sample concentration of compounds was 0.35 mmol·L^{-1} compound. UV detection was used at 220 (channel2) and 254nm (channel1). Gradient elution was performed with solvent A: 2.5% Formic Acid in deionised water; solvent B: 2.5% Formic Acid in MeCN. Pre-equilibration run for 1 min at 5% B; then method run was 5 to 98% solvent B in 2min, 98% B for 2min, 98 to 5% B in 0.5min then 5% for one min.

2.2.2 Synthesis

A racemic mixture of tryptophan was esterified with *in situ* production of HCl from $SOCl_2$ to yield the corresponding methyl ester, compound **1**. Pictet-Spengler reaction conditions were used to generate the cyclized tryptophan analogue, β carboline carboxylate **2.** . A sulphonamide addition to compound **2** was then conducted to yield ***compound* 2**. Compound **3** was then purified by column chromatography and converted to the corresponding non-substituted amide to produce racemic **4** (Bhunia *et al*., 2017).

2.2.2.1 DL-tryptophan methyl ester (2)

Thionyl chloride (0.85 mL, 11.65 mmol, 2.4 eq.) was dissolved in anhydrous MeOH (25 mL) at 0 °C. The solution was allowed to cool down to r.t. and *DL*-tryptophan (1.00 g, 4.90 mmol) was added. The solution was refluxed for 15-18 hours. The reaction was monitored through TLC analysis (eluent MeOH/EtOAc 1:10) and HPLC-MS. Solvent evaporation under vacuum yielded colourless crystals. The resulting crystals were diluted with water (10 mL) and recrystallized in aqueous Na_2CO_3 (10%). The precipitate was collected by filtration and the crude compounds were used directly for next steps without further purification..

Yield (53 %); mp 241°C; ^{1}H NMR (400 MHz, DMSO- d_6): δ 10.62 (s, 1H, -N**H** indole), 8.42 (br s, 2H, -N**H₂** amide), 7.55 (d, *J* = 7.88 Hz, 1H, -Ar**H** 4-indole), 7.41 (d, *J* = 8.1 Hz, 1H, -Ar**H** 7-indole), 7.23 (s, 1H, -Ar**H** 2-indole), 7.16 (ddd, *J* = 8.1, 7.0, 1.2 Hz, 1H, -Ar**H** 6-indole), 7.08 (ddd, *J* = 8.0, 7.1, 1.1 Hz, 1H, -Ar**H** 5-indole), 4.35 (dd, *J* = 7.3, 5.5 Hz, 1H,-SR-NH_2C**H**COOH), 3.81 (s, 3H,-C**H₃**), 3.52 – 3.35 (m, 2H,-diastereotopic indole-3-**CH_2**-); ^{13}C NMR (101 MHz, CD_3OD) δ 170.9, 138.4, 128.2, 125.6, 123.0, 120.34118.8, 112.7, 107.5, 54.7, 53.6, 27.6; LCMS *m/z* calc. for $C_{12}H_{14}N_2O_2$ [M^+]: 220, (HPLC-MS) R_t = 1.18 min, (TLC) R_f = 0.30.

2.2.2.2 (3*SR*)-Methyl 2,3,4,9-tetrahydro-*1H*-pyrido[3,4-*b*]indole-3-carboxylate (3)

To a solution of DL-tryptophan methyl ester hydrochloride **2** (0.200 g, 0.92 mmol) in dry methanol (5 mL), formaldehyde (36.5-38% w/v solution in water, 0.1 mL) was added. The reaction mixture was stirred for 15-18 hours at room temperature, concentrated under vacuum, and cooled at 0°C to give (*SR*)-Methyl 2,3,4,9-(3*SR*)-Methyl 2,3,4,9-tetrahydro-*1H*-pyrido[3,4-*b*]indole-3-carboxylate tetrahydro-*1H*-pyrido[3,4-*b*]indole-3-carboxylate hydrochloride **3**.

Yield (83 %); mp 199-201°C; ^{1}H NMR (400 MHz, DMSO-d_6) δ 10.29 (s, 1H, -N**H** indole), 7.48 (d, *J* = 7.8 Hz, 1H, -Ar**H** 4-indole), 7.37 (d, *J* = 8.1 Hz, 1H, -Ar**H** 7-indole), 7.11 (ddd, *J* = 8.2, 7.0, 1.2 Hz, 1H, -Ar**H** 6-indole), 7.02 (ddd, *J* = 8.0, 7.0, 1.0 Hz, 1H, -Ar**H** 5-indole), 4.64 (dd, *J* = 10.0, 5.4 Hz, 1H, - NHC**H**COOCH$_3$), 4.40 (s, 2H, indole-2-C**H$_2$**NH), 3.83 (s, 3H, -C**H**$_3$), 3.31 (dd, *J* = 15.9, 5.3 Hz, 1H, diastereotopic –C**H**$_2$CHCOO CH$_3$), 3.08 (ddt, *J* = 16.0, 10.0, 1.7 Hz, 1H, diastereotopic –C**H**$_2$CHCOO CH$_3$), -aliphatic R$_2$N**H** proton not seen; ^{13}C NMR (101 MHz, DMSO- d_6) δ 169.5, 136.7, 126.8, 126.2, 122.3, 119.6, 118.4, 111.9, 104.8, 54.2, 53.6, 40.7, 22.4. LCMS: *m/z* calc. for $C_{13}H_{14}N_2O_2$ [M$^+$]: 231, (HPLC-MS) R_t = 1.78 min, (TLC) R_f = 0.18.

2.2.2.3 (3*SR*)-Methyl-2-(4-methoxyphenylsulfonyl)-2,3,4,9-tetrahydro-*1H*-pyrido[3,4-*b*]indole-3-carboxylate (4)

The racemic (3*SR*)-2,3,4,9-tetrahydro-*1H*-pyrido[3,4-*b*]indole-3-carboxamide **3** (0.250 g, 1.09 mmol, 1 eq) in dry DMF (5 mL) was stirred followed by addition of dry triethylamine (0.146 mL, 1.64 mmol, 1.5 eq) and 4-methoxybenzenesulfonyl chloride (0.269 g, 1.31 mmol, 1.2 eq) at 0 °C. The reaction mixture was stirred for 6h at room temperature, and the completion of the reaction was monitored by TLC (eluent MeOH/EtOAc, 20:1) and HPLC-MS. Upon completion the reaction mixture was concentrated under vacuum and the residue was separated with silica column chromatography (eluent EtOAc/PET, 10:1) to get (3*SR*)-Methyl-2-(4-methoxyphenylsulfonyl)-2,3,4,9-tetrahydro-*1H*-pyrido[3,4-*b*]indole-3-carboxylate **4**.

Yield (73 %); mp 99-102°C; ^{1}H NMR (400 MHz, DMSO-d_6) δ 10.83 (s, 1H, -N**H** indole), 7.83 – 7.73 (m, 2H,-SO$_2$-Ar-2,5-**H**), 7.37 (d, *J* = 7.8 Hz, 1H, -Ar**H** 4-indole), 7.28 (d, *J* = 8.1 Hz, 1H, -Ar**H** 7-indole), 7.13 – 7.07 (m, 2H, (CH$_3$)$_3$O-Ar-3,4-**H**), 7.04 (ddd, *J* = 8.2, 7.1, 1.3 Hz, 1H, -Ar**H** 6-indole), 6.95 (ddd, *J* = 8.0, 7.0, 1.0 Hz, 1H, -Ar**H** 5-indole), 5.15 (dd, *J* = 6.7, 1.4 Hz, 1H,-SR- NHC**H**COOH), 4.72 – 4.63 (m, 1H, indole-2-C**H$_2$**NH), 4.50 – 4.39 (m, 1H, indole-2-C**H$_2$**NH), 3.81 (s, 3H, -COOC**H$_3$**), 3.42 (s, 3H,-OC**H$_3$**), 3.28 – 3.13 (m, 1H, diastereotopic –C**H**$_2$CHCOOH), 2.94 (dd, *J* = 15.8, 6.5 Hz, 1H, diastereotopic –C**H**$_2$CHCOOH); ^{13}C NMR (101 MHz, DMSO-d_6) δ 170.6, 162.6, 136.0, 130.5, 129.1, 128.8, 126.1, 121.2, 118.7, 117.7, 114.4, 111.1, 103.8, 55.7, 53.6, 52.3, 40.5, 23.9; LCMS *m/z* calc. for $C_{20}H_{20}N_2O_5S$ [M$^+$]:401, (HPLC-MS) R_t = 2.91 min, (TLC) R_f = 0.70.

2.2.2.4 (3*SR*)-2-(4-Methoxyphenylsulfonyl)-2,3,4,9-tetrahydro-*1H*-pyrido[3,4-*b*]indole-3-carboxamide (5)

The (3*SR*)-Methyl-2-(4-methoxyphenylsulfonyl)-2,3,4,9-tetrahydro-*1H*-pyrido[3,4-*b*] indole-3-carboxylate **4** (0.100 gr, 0.250 mmol) was taken in a dried sealed pressure tube, and to it was added freshly prepared MeOH/NH_3 (~7 N solution, 20mL, 3.7 eq), and the reaction mixture was stirred for 78 h at 35 °C. Completion of the reaction was monitored by TLC analysis (eluent MeOH/EtOAc, 20:1) and the solvent was removed under vacuum. The solid was then purified using column chromatography (eluent EtOAc/PET, 10:1) to get (3*SR*)-2-(4-Methoxyphenylsulfonyl)-2,3,4,9-tetrahydro-*1H*-pyrido[3,4-*b*]indole-3-carboxamide **5**.

Yield (72 %); mp 165-168°C; ^{1}H NMR (400 MHz, DMSO-d_6) δ 10.77 (s, 1H-N**H** indole), 7.77 – 7.65 (m, 2H,-SO_2-Ar-2,5-**H**), 7.42 (s, 1H, -amide –N**H**$_2$), 7.33 – 7.22 (m, 2H, -Ar**H** 5-indole), 7.04 (d, *J* = 8.9 Hz, 2H, -$(CH_3)_3$O-Ar-3,4-**H**), 7.07 – 6.97 (m, 1H, -Ar**H** 6-indole), 6.92 (td, *J* = 7.5, 7.0, 1.1 Hz, 1H, -Ar**H** 5-indole), 4.85 (dd, *J* = 6.8, 1.3 Hz, 1H, - NHC**H**$COOCH_3$), 4.70 (s, 2H, indole-2-C**H**$_2$NH), 3.78 (s, 3H,-OC**H**$_3$), 3.13 (d, *J* = 15.7 Hz, 1H,-diastereotopic –C**H**$_2$CHCOOCH), 2.68 (dd, *J* = 15.6, 6.9 Hz, 1H,-diastereotopic –C**H**$_2$CHCOOCH_3); ^{13}C NMR (101 MHz, DMSO-d_6) δ 171.6, 162.5, 135.9, 131.0, 129.3, 129.0, 126.3, 120.9, 118.5, 117.4, 114.4, 111.0, 103.9, 55.6, 53.60, 41.0, 23.5; LCMS calc. for $C_{19}H_{19}N_3O_4S$ [M^+] *m/z* : 386, (HPLC-MS) R_t= 2.65 min, (TLC) R_f = 0.41.

2.3. Biological methods

2.3.1. Materials and Antibodies

Table 2.1. Reagents and Antibodies

Reagent	Supplier	Use
Horm collagen	Nycomed, Munich, Germany	Aggregation assay: 3 μg/mL NFAT: 10 μg/mL, ELISA: 4 μg/mL
CRP-XL	CambCol Laboratories, Cambridge, UK	Aggregation assay: 10 μg/mL
PAR1-peptide (SFLLRN)	Severn Biotech, Kidderminster, UK	Aggregation assay: 1 U/mL

HY101 (Human anti-GPVI monoclonal antibody, raised in mice)	Invitrogen, ThermoFisher Scientific, Paisley, UK	FC: 1:400 (1.25 μg/ml)
Anti-6-His IgG Alexa Fluor 647 (monoclonal, raised in mice)	Invitrogen, ThermoFisher Scientific, Paisley, UK	FC: 1:400
Anti-mouse IgG Alexa Fluor 647 (polyclonal, raised in goat)	Invitrogen, ThermoFisher Scientific, Paisley, UK	FC: 1:400
Goat Anti- human IgG-Fc-HRP	Invitrogen, ThermoFisher Scientific, Paisley, UK	ELISA: 1:10,000
Anti-rabbit IgG HRP conjugate (polyclonal, raised in donkeys)	GE Healthcare Life Sciences, Illinois, USA	ELISA: 1:10,000
Alexa Fluor™ 647 Antibody Labeling Kit	Invitrogen, ThermoFisher Scientific, Paisley, UK	Nb labelling, 1 dye vial/reaction
pcDNA3.1 vector	Invitrogen, ThermoFisher Scientific, Paisley, UK	NFAT, mutation studies: 1μg
PEI	Polysciences, Pennsylvania, USA	Nb expression: 1mg/mL
ATP	Sigma, Merck Life Science UK Limited, Dorset, UK	NFAT: 0.1 M
Other	Sigma, Merck Life Science UK Limited, Dorset, UK	

2.3.2. Expression, labelling & purification of nanobodies

53 nanobodies belonging to 32 different structural families (categorised by CDR3 regions) specific to human GPVI were generated by VIB nanobody core (Brussels, Belgium) (Slater *et al.*, 2021) to create a conformation-specific reagent library for the distinction of different GPVI epitopes. A pMECS phagemid vector was used for cloning of the nanobody sequence. The vector (ampicillin resistance gene) contained a PelB signal sequence on the N-terminus with HA and His6 tags on the C-terminus. Adjacent to the His6 tag, a TAG stop codon (in TG1 cells, the stop codon is read as glutamine) and then a gene III of M13 phage. The nanobodies were expressed as fusion proteins with protein III of the phage, used by VIB nanobody core during nanobody extraction.

2.3.2.1 Preparation of LB agar plates with antibiotic

1 L of freshly prepared and autoclaved Lennox broth (LB) was heated with 7.5 g of agar until all reagents were fully melted. When the LB agar mixture was cooled off to room temperature (and still in a fully liquid state), ampicillin was added to a final concentration of 100 μg/mL (stock 100 mg/mL). 5mL of the final ampicillin/LB agar mixture was poured in sterile polystyrene size 100 mm × 15 mm plates and in sterile conditions. The ampicillin/LB plates were left to cool off in room temperature and were then stored in 4 °C.

2.3.2.2 Cell transformation & glycerol stock solutions for nanobodies

For the nanobodies used in Chapter 3 and 4, nanobody plasmids were transformed into chemically competent WK6 *E. coli* cells. The cells were incubated with the nanobody sequence-containing plasmid (obtained VIB nanobody core) on ice for 30 min. The cells were then subjected to heat shock at 42 °C for 45 sec and were incubated on ice for 5 min. All following experimental steps were conducted under sterile conditions. After adding 400 μL of autoclaved LB medium to the cells, the mix was incubated at 37 ^{o}C for 1 h with 180 rpm shaking. 100 μL of the cell mix was then plated onto ampicillin/LB agar plates and incubated at 37 ^{o}C for 15-18 hours. A distinct and single colony on the LB agar plates was picked using a pipette tip and transferred to a tube with LB supplemented with 100 μg/mL of ampicillin. The solution was incubated for 15-18 hours at 37 ^{o}C and shaking at 180 rpm. The following day, 1 mL of the bacterial culture was transferred under sterile conditions to a sterile tube. It was centrifuged at 2000 g for 10 min at 4 ^{o}C. The supernatant was removed and pellets were resuspended in 1 mL of LB + 8% glycerol. The glycerol stock was snap-frozen in a liquid nitrogen and stored immediately at -80 ^{o}C.

2.3.2.3 Pre-culture generation

20 mL of LB with 100 μg/mL of ampicillin were inoculated with the nanobody glycerol stock and incubated at 37 ^{o}C and shaking at 180 rpm for 15-18 hours.

2.3.2.4 Growth and induction

1 L of Terrific broth (TB) medium was made by dissolving 12 g Tryptone (Duchefa Biochemie) and 24 g yeast (Duchefa Biochemie) in 1 L distilled water followed by autoclaving. On the day of use, 2.3 g KH_2PO_4 and 16.4 g $K_2HPO_4.3H_20$ were diluted in 10 mL of autoclaved ddH_2O and filtered into the TB medium and the medium was supplemented with ampicillin to a final concentration of 100 μg/mL. 2mL of the bacterial pre-culture was added to the TB

medium and left to grow at 37 °C and shaking at 180rpm for 4-5 h until an OD_{600} of 0.5-0.6 was reached. Nanobody expression was induced by the addition of IPTG to a final concentration of 1 mM and were further incubated at 30 °C with shaking for 15-18 hours.

2.3.2.5 Extraction of nanobodies from periplasm of E. coli

The 15-18 hours induced culture was centrifuged for 20 min at 3000 g and 4 °C. After the centrifugation, the supernatant was removed and the left over culture was added on the top of the pellet and centrifuged for 20 min at 3000 g and 4 °C. A TES solution was freshly prepared by combining 0.2 M Tris pH 8.0, 0.5 mM EDTA and 0.5 M sucrose. The solution was further diluted 4 times in water to generate a diluted TES solution (TES/4). The cell pellet was fully re-suspended with 12 mL TES solution and was transferred in a falcon tube. The falcon tube was left with rotation for 1 h at 4 °C. 18mL TES/4 was added and incubated at 4 °C for 1 h with rotation. Next, samples were centrifuged for 30 min at 3000 g and 4 °C to collect the supernatants.

2.3.2.6 Purification

PD-10 gravity column containing 1 mL of HisPur NI-NTA Superflow Agarose beads (ThermoFisher Scientific) was washed 3 times in phosphate buffered saline (PBS) before being applied to the nanobody supernatant and incubated for 30 mins. The nickel agarose beads were collected using PD-10 gravity columns, which were washed with milliQ water, and further washed with 30-50 mL of PBS. The nanobodies were eluted with 1 mL PBSwith 0.5 M imidazole. The elute was then purified using a MabSelect 1mL affinity column, equilibrated in PBS and the samples were eluted using a gradient elution with increasing concentrations of 100mM Glycine pH=3.0 from 10% up to 100%.His-tag removal from nanobodies

Postdoctoral fellow, Dr Alexandre Slater (University of Birmingham, UK), from the Birmingham Platelet Group, has previously engineered nanobody constructs Nb2, 21 and 35 to contain a thrombin cleavage motif before the 6-His repeat sequence of the His-tags to generate non- tagged versions for structural studies.

The nanobodies were first incubated with 1 mL of nickel agarose, as described above, and were incubated on a roll rack room at temperature for 30 min. For the cleaving reaction, the purified nanobodies were dialyzed for buffer exchange to remove any phosphate containing groups, as the thrombin cleavage utilises calcium, which can be precipitated in the presence of phosphate ions (Guan and Dixon, 1991; Hakes and Dixon, 1992). For this reason, an exchange

with a Tris-NaCl buffer (20 mM Tris, 140 mM NaCl, pH 7.4) with 2.5 mM $CaCl_2$ was used. Following nickel agarose incubation, the beads were then washed with the thrombin cleavage buffer and were then then left with 1 mL of the cleavage buffer plus 0.1U/mL of thrombin for 15-18 hours at room temperature on a roll rack. The beads were then washed off with 3 mL of cleavage buffer to collect the cleaved nanobodies and the nickel beads were discarded. The nanobodies were then spin concentrated at 500 μL and purified using a gel filtration column (Superdex 200 Increase 10/300 GL, 24 mL) to yield the purified non-tagged nanobodies.

2.3.2.7 Nanobody direct labelling with Alexa Fluor-647 succinimidyl ester

For the flow cytometry studies for nanobody displacement in Chapter 4, His-tagged and non His-tagged nanobodies stock solutions were dialysed for 15-18 hours in PBS and then diluted to a final concentration of 1 mg/mL. The nanobody concentration was determined using Nanodrop Spectrophotometer ND-1000 and Protein A280 software. The molecular weight and extinction coefficient were calculated using ExPASy ProtParam (Table 2.2).

Table 2.2. Nanobody Parameters generated from ExPASy ProtParam tool. *The extinction coefficient is generated in Abs 0.1% (=1 g/l), assuming all pairs of Cys residues form cysteine disulfide bridge.* The extinction coefficient is also shown as M-1 cm-1 and generated at 280 nm measured in water. The nanobody concentration was obtained by adjusting the NanoDrop measurements based on the extinction coefficient of each nanobody. The extinction coefficients were generated by loading each nanobody sequence to the ExPASy Prot Param tool.*

Nanobody construct	Molecular Weight (Da)	Extinction Coefficient (g/L)	Extinction Coefficient (M-1 cm-1)*
His-tagged Nb2	15988.47	1.195	30,620
His-tagged Nb21	15934.41	1.791	28,545
His-tagged Nb35	16115.69	1.623	26,150
Nb2	15165.62	2.019	30,620
Nb21	15111.57	1.889	28,545
Nb35	15292.84	1.710	26,150

Alexa Fluor™ 647 Antibody Labeling Kit (Cat. No.: A20186) was used for labelling of both nanobodies. The reaction vials contained Alexa Fluor™ 647 carboxylic acid succinimidyl ester and the nanobody solutions (10 μg/mL), adjusted at pH=7.8 using a 1M sodium bicarbonate solution, were covered to avoid sun exposure and were left in a roll rack for 1 h. Then the reaction mixture was run through a 30,000 MWCO (molecular weight cut-off) size–exclusion resin column (PBS, pH 7.2, 2mM NaN_3) and the nanobody elute was collected through centrifugation at 1100 g for 5 min. Labelled nanobodies were further dialyzed in PBS to remove excess free dye. The final concentrations and degree of labelling (DOL) were measured and calculated, using the equations below, with Protein A280 software, using Proteins & Labels function as described in the labelling kit. The nanobodies were covered with aluminium foil and stored at -80 °C.

Calculation for the concentration of protein in the sample:

$$Protein\ concentration\ (M) = \frac{[\mathrm{A280} - (\mathrm{A647} \times 0.03)] \times dilution\ factor}{\varepsilon \times 10}$$

where the molar extinction coefficient (ε) in cm^{-1} M^{-1} at 280 nm of each nanobody was obtained by Expacy calculated parameters (.) using the absorbance at 280 nm (A280) and 647 nm (A647) measured. The value 0.03 is the correction factor for the contribution of Alexa Fluor® 647 to the absorbance at 280 nm. The nominal path length of NanoDrop® is 1mm, so for the protein concertation of calculation the ε of the protein was multiplied by 10.

Calculation for the degree of labelling (DOL):

$$\text{Moles dye per mole protein} = \frac{\text{A647} \times \text{dilution factor}}{239{,}000 \times 10 \times protein\ concentration\ (M)}$$

where ε_{dye}= 239,000 (in $cm^{-1}M^{-1}$) is the approximate molar extinction coefficient of Alexa Fluor™ 647. The nominal pathlength of NanoDrop® is 1 mm, so for the DOL calculation the ε_{dye} was multiplied by 10.

2.3.2.8 Purity Determination

A precast polyacrylamide gel (NuPAGE™ 4 to 12%, Bis-Tris, 1.0–1.5 mm, Mini Protein Gels, Invitrogen™, UK) was loaded with 10µL of samples with 5 µL of an SDS-containing bromophenol blue tracking dye buffer 2X (Gel Loading Dye, Blue, 6X, New England Biolabs™, UK) and 5 µL of nanobody, that were previously prepared, and an MS protein 1 kDa ladder (Color Prestained Protein Standard, Broad Range, 11–245 kDa, New England Biolabs™, UK). The samples were incubated at 95 °C for 5min before loading and the gel was ran at 160 V. Bands were visualized using a triphenylmethane protein staining (Coomassie brilliant blue G-250) dye.

2.3.2.9 Concentration determination

Measurement was conducted using Nanodrop Spectrophotometer ND-1000. Protein absorption at 280nm were measured using Proteins A280 software. 2 µL of each sample was measured 3 times. Molecular weight and Extinction coefficients were calculated using ExPasy ProtParam tool (), and nanodrop readings were corrected and converted to molar concentrations using these values. The nanobodies were then snap-frozen in a liquid nitrogen bath and stored immediumtely at -80 °C.

2.3.3. GPVI expression & purification

For the GPVI constructs used in Chapter 4, 150 mL of LB with 100 µg/mL of ampicillin (100mg/mL stock) were inoculated with the glycerol stock (stored in -80 ^{o}C) of the GPVI plasmid transformed into XL1blue cells. The mixture was incubated at 37 ^{o}C with shaking at 180 rpm for 15-18 hours. The plasmid was purified using Sigma_Plasmid_Maxiprep kit.

HEK293T cells were grown in Dulbecco's Modified Eagle Medium (DMEM) with 10% fetal bovine serum (heat-inactivated), 1% penicillin (100 µg/mL), 1% streptomycin (100 µg/mL) and 1% glutamine (4 mM) and were used for GPVI expression. Cells were grown at 37 ºC and 5% CO_2. 5 x 10^6 cells were seeded onto 15 cm dishes and left to grow for 15-18 hours. For each 15 cm plate, 12.5 µg DNA and 37.5 µL of 1 mg/mL PEI were diluted in 2.5 ml serum free medium and incubated for 20 mins at room temperature. This was then added drop-wise to the HEK cells and the medium was collected after day 3 post transfection and the cells were topped up with medium. A second collection was performed on day 6 post transfection. The filtered medium was then purified using a MabSelect 1 mL affinity column, equilibrated in PBS and the samples were eluted using a gradient elution with increasing concentrations of 100 mM Glycine, pH=3.0. Then the samples were run through an AKTA Pure, Superdex 200 Increase 10/300 GL 24 mL gel filtration column to yield the soluble GPVI is expressed as a dimeric Fc-tagged protein. For ELISA and, predominantly, crystallisation studies, the monomeric form of soluble GPVI is also used. The Fc tag is cleavable due to the presence of an FXa cleavage site, where cleavage yields two GPVI monomeric units and one Fc homodimer unit. In order to obtain the desired amount of monomeric GPVI, GPVI-Fc was cleaved for 15-18 hours with FXa 1 mg per 300µg of protein and 12.5 µL $CaCl_2$ per 1 mL of reaction solution. The reaction mixture was then run again down an S200 column to remove residual Fxa and Fc. The progress of each step and protein purity was monitored by SDS-PAGE gel. Determination of GPVI concentration was conducted as described in 2.3.2.9 using the data from . The final proteins were snap-frozen in a liquid nitrogen bath and then stored at -80 °C.

2.3.4. Mutagenesis & expression of GPVI mutants

Site-directed mutagenesis of full length human GPVI was performed using a Q5® Site-Directed Mutagenesis Kit from New England Biolabs. Alanine scanning mutagenesis in four amino acids within the wild type GPVI (WT GPVI) sequence was performed to identify protein positions that are important for nanobody binding. Alanine substitution is commonly used due to its chemically non-reactive nature and represents a deletion of an amino acid side chain at the β carbon. The WT GPVI cDNA was cloned into a mammalian expression vector previously in the lab. This cDNA was mixed with Q5 Hot Start High-Fidelity 2x Master Mix and each oligonucleotide primer pair corresponding to each alanine substitution mutant (Table 2.3). Exponential polymerase chain reaction (PCR) was used for DNA amplification and to the PCR product was then mixed with the 10x Kinase, Ligase, DpnI (KLD) enzyme mix and the 2x

KLD reaction buffer in the quantities specified by the manufacturers kit for 5 min. In this reaction, the KLD reaction, the DNA is phosphorylated, ligated and finally degraded through the DpnI. NEB-5-alpha competent *E. coli* cells were thawed and incubated with 5µL of the KLD reaction mix on ice for 30 min. They were then heat shocked at 42 °C for 30 sec and incubated on ice for 5 additional min. 950 µL of a SOC solution into the cell mix and were heated at 37 °C for 1 h with shaking. 100 µL of cells were then spread on a kanamycin/LB agar plate and further incubated for 15-18 hours at 37 °C.

Bacterial colonies were picked and grown in LB supplemented with kanamycin for 15-18 hours at 37 °C with shaking at 180 rpm. The DNA content was isolated and purified using GenElute™ Plasmid Miniprep Kit. The DNA was sequenced for correctness and for confirmation of the amino acid substitution mutation through outsourced sequencing services from EurofinsGenomics TubeSeq plasmid.

Table 2.3. Sequence of primers used for the generation of GPVI point mutations.

GPVI Mutant	**Forward primer**	**Reverse primer**
R38A	GGACCTGTACgccCTGGAGAAGCTGAGTTCCAGC	ACGCCCGGAGGTCCCTGG
R46A	GAGTTCCAGCgccTACCAGGATCAGGCAGTCC	AGCTTCTCCAGGCGGTAC
R60A	CGGCCATGAAgccAAGTCTGGCT	GGATGAAGAGGACTGCCT
R67A	CTGGACGCTAgccCTGCTCCTAC	CCAGACTTCTCTTCATGGC

The plasmids were also transformed into XL1-blue competent cells for glycerol stock storage at -80^{o}Ctransformation and glycerol stock as previously described in Section 2.3.2.

2.3.5. Competition ELISA

For the ELISA experiments for nanobody GPVI-specific conformation binding assay in Chapter 3, 96-well ELISA polystyrene plates (Clear Flat-Bottom Immuno Nonsterile 96-Well Plates, Invitrogen™, UK) were coated with 100 µL of 4 µg/mL Horm collagen (in PBS) for 15-18 hours at 4 °C. They were then wash 3 times with 200 µL 0.05 % Tween20 in PBS (PBS-T). The wells were blocked for 1 hour with 200 µL 3 % bovine serum albumin (BSA). 99 µL

of monomeric and dimeric GPVI (100 nM) diluted in block buffer (1 % BSA in PBS) was mixed with 1µL of compound ligand (**22**, **O1**, **O2**) in DMSO or 1 µL of His-tagged Nb2 in PBS, as a positive control, and then incubated with the wells for 1 h. 100 µL of anti 6 His-HRP or anti-IgG-Fc-HRP (1: 10,000 in block buffer), for monomeric and dimeric GPVI respectively, were added and left for 1 h. Next, 50 µL of TMB solution were added and after 15 min the reactions was stopped with 50 µL 1 M H_2SO_4 and the fluorescence was measured at 450 nm in a plate reader.

2.3.6. NFAT luciferase reporter assay

For the cell signalling experiments in Chapter 4, a nuclear factor of activated T cells (NFAT) reporter-luciferase assay was used to determine whether the GPVI mutants could signal upon nanobody binding. DT40 chicken B cells were grown in Roswell Park Memorial Institute (RPMI) 1640 medium supplemented with fertile 10% fetal bovine serum (heat-inactivated), 1% chicken serum, 1% penicillin (100 µg/mL), 1% streptomycin (100 µg/mL), 1% glutamine (4 mM) and 50 µM 2β-mercaptoethanol and were used for membrane expression of full length human GPVI with FcRγ chain. DT40 cells are non-adhesive haematopoietic cells that contain signalling proteins necessary for the GPVI- signalling cascade. $2x10^7$ cells were transfected in 400µL of serum-free RPMI by electroporation using a GenePulser II machine (Bio-Rad) at 350 V and 500 µF. For nanobody binding studies to GPVI, 2 µg of GPVI DNA, 2 µg human FcRγ-chain DNA and 15µg NFAT-luciferase reporter DNA were used for transfection. For the optimisation of GPVI receptor expression for the NFAT assay regarding the GPVI mutants' studies, mock-transfected DT40 cells with empty vector cDNA and 50 ng/mL of PMA plus 1 µM of ionomycin served as negative and positive controls respectively. After optimization of receptor expression, for GPVI mutants 1µg of DNA for human GPVI and FcRγ-chain were used. The transfected cells were added to complete RPMI medium in a 6-well plate and incubated for 15-18 hours at 37°C. The following day, cell counts were adjusted to $2x10^6$ cells/mL into 96-well plates in complete RPMI medium.

Horm Collagen and CRP were both used at a final concentration of 10 µg/mL. To determine basal signalling levels, RPMI medium was added to cells for basal samples. 25 µM, 175 µM or 250 µM of small compound added to the test wells prior to collagen or CRP addition for the determination of their inhibition potential towards signalling related to those two agonists. For mutation studies (Chapter 4), the final concentration of nanobodies Nb2, Nb21 and Nb35 was

100 nM in a total volume of 100 µL/well. 50 µL of each agonist was added to 50 µL of cells in a well of a 96-well plate with each condition performed in triplicates.

The cells were incubated for 6h at 37°C and then frozen at -80°C. For the NFAT assay, 11 µL of luciferase harvest buffer (1 M KH_2PO_4, 12.5% Triton X-100 and 1 M dithiothreitol, DTT) was added to each well and samples were left for 5 min at room temperature for cell lysis. 90 µL of the samples were then added to the wells of the opaque plate with 90 µL of luciferase assay buffer (1 M KH_2PO_4, 0.1 M $MgCl_2$, 0.1 M ATP in ddH_2O). Luciferase luminescence measurements were performed with a microplate luminometer (Berthold Technologies, Wildbad, Germany). The machine was primed with 1 mM of luciferin in ddH2O and luciferin was loaded in the wells (50 µL, counting time 10 sec per well).

2.3.7. Preparation of human platelets

13.5 mL of blood was drawn from healthy volunteers that had not taken medication that influence platelet function in the previous 14 days in accordance with the Declaration of Helsinki (local ethical review no: ERN_11-0175) (World Medical Association Declaration of Helsinki, 2013). Trisodium citrate 4% [w/v] was used as the anticoagulant in a ration of 1:10 trisodium citrate to blood. 10% of acid-citrate-dextrose (ACD; 85 mM trisodium citrate, 75 mM citric acid and 111 mM glucose) was added per blood volume. Platelet-rich plasma (PRP) was prepared by centrifugation at 200 *g* for 20 min at room temperature. The platelet-rich plasma (PRP) was isolated and further centrifuged at 1000 g for 10 min at room temperature in the presence of 5 µL PGI_2 (2.8 µM). The platelet poor plasma (PPP) was removed and the pellet, that contained the platelets, was re-suspended with 12.5 mL of Tyrode's buffer (145 mM NaCl, 2.9 mM KCl, 1 mM $MgCl_2$, 5 mM glucose, pH 7.3, °C) in the presence of 5 µL PGI_2 (0.28 µg) and 1.5 mL ACD and was further centrifuged at 1000g for 10min. Tyrode's buffer was removed and 3mL of Tyrode's were used to re-suspend the platelets. Using a Coulter Z_2 cell the suspension was diluted to a density of 2×10^8 platelets/mL with Tyrode's buffer. The platelets were rested for 20 min. Stimulation of platelets was performed in an aggregometer at 37 °C, with continuous stirring at 1200 rpm.

2.3.8. Aggregation assay

As a preliminary compound screening, set of literature compounds **4**, Bhunia, 2017 (Bhunia *et al.*, 2017) and **3**, WO2006070385A1 (Gaur *et al.*, 2006)) were synthesized as described above and used for aggregation assays in washed platelets. Two platelet activation agonists

(thrombin and collagen) were used as a control to measure the percentage of aggregation inhibition caused by the two compounds (Chapter 3). The compounds are insoluble in water and so they were dissolved in DMSO to generate stock solutions of 500 mM. Then the amount of stock needed to create a solution of 5mM was transferred in freshly prepared Tyrode's buffer and then from this solution a new solution of 1 mM was created. The 5 µL from each solution that were generated were used in 500 µL of washed platelets for the aggregation assay, so the final concentrations in the platelet tubes were 50 µM and 10 µM respectively. A turbidimetric method was applied to measure platelet aggregation, using a Chronolog Corporation aggregometer. Freshly prepared platelet rich plasma ($2x10^8$ platelets/mL, 500 µL) was prewarmed to 37 °C for 2 min in the warm well, then stirred for 1min in the stirrer (measuring) well and finally incubated with compound (10 µM and 50 µM) for 1 min or an isovolumetric solvent control (5 µL of DMSO) for 1 min before addition of the agonists (3 µg/mL Horm collagen or 0.1 units/mL thrombin). The reaction was allowed to proceed for at least 3 min, and the extent of aggregation was expressed as percentage of light transmission.

For the second screening an aggregation assay was used but instead of a Chronolog Corporation aggregometer, a Platelet Aggregation profiler, Model PAP-8E 2.1.0 was employed. For this assay the same procedure as the previously described was followed. The compounds that resulted from the docking studies were used. A final compound concentration of 10 µM was used in 400 µL of freshly prepared $2x10^8$ platelets/mL while the collagen final concentration was 3 µg/mL. To the platelet solution a final concentration of 10µM of each inhibitor from 4mM stock solutions was achieved to while dry DMSO (99.8%) was used as a control. A freshly prepared Tyrrode's buffer was used as blank the test wells.

2.3.9. Flow cytometry

For the flow cytometry experiments in Chapter 3 and 4, the samples were analysed on a BD accuri C6 flow cytometer (BD Biosciences, USA). Platelets were gated on cell size based on forward scatter (FSC) against side scatter (SSC) to exclude background noise and potential contamination by other blood components. 10,000 events per sample were set to logarithmic increase on both the light scatter and fluorescent channel. All samples were tested in the FL4 fluorescent channel. cSampler Software (BD Biosciences, USA) for data expression in MFI (arbitrary units). A positive % marker was set to determine the fluorescence attributed to the platelets or DT40 cells in combination with the corresponding fluorescent nanobody (Table

2.1) used in each experiment. In the case of the flow cytometry studies on platelets with labelled Alexa Fluor™ 647 nanobodies, only platelets were used for setting up the marker (Chapter 4).

2.3.9.1 Determination of transfection efficacy of different GPVI constructs

Flow cytometry was used to confirm membrane expression of GPVI constructs. The cells were adjusted to a concentration of $2x10^6$ cells/mL and were combined with a FACS block buffer (1% BSA, 2% normal goat serum [NGS] in PBS). After a PBS buffer wash, anti-human GPVI HY101 antibody (Table 2.1) was added to the cells for 30 min (1:400 stock dilution in block buffer) and samples were washed with PBS. Samples were then stained with anti-mouse Alexa Fluor™ 647 secondary antibody for 30 min (1:400 stock dilution in block buffer). All incubation were conducted on ice and covered from light. Samples were resuspended in 500 µL on PBS. Any buffers related to platelet treatment were kept in room temperature and centrifugation was avoided whenever possible.

Flow cytometry experiments were also conducted to check membrane expression levels of GPVI mutant constructs and to measure the difference in nanobody binding between the wild type and the mutant GPVI constructs. The transfected DT40 cells with mutant GPVI were prepared for transfection level check, as previously mentioned, using HY101 and then Alexa-Fluor™ 647 antibodies. For binding studies of nanobodies in the different GPVI mutants, nanobodies were used as the primary antibody (final concentration of 100nM in block buffer) and monoclonal Anti-6-His IgG Alexa Fluor ™ 647 was used a secondary nanobody (1:400 dilution in block buffer) with an incubation time of 30mins.

2.3.9.2 Flow cytometry of labelled nanobodies

For saturation and displacement experiments between different labelled nanobodies (Chapter 4) human platelets were used. 50 µL of platelets were incubated with 25µL FACS block (1% BSA 2%NGS PBS). For the detection of GPVI surface levels on platelets, after 10 min, 25 µL HY101 anti- GPVI antibody (1:400 dilution in block buffer). For the control platelet sample during flow cytometry displacement studies for Alexa-647 labelled nanobody, platelets were incubated with Alexa Fluor™ 467 (5 ng/mL) for 15 min and centrifuged at 1000 g for 10 min in the presence of 1 µL PGI_2 (0.28 µg) and were resuspended in Tyrrode's buffer. For the saturation curve and displacement studies of directly-labelled nanobodies with Alexa Fluor™ 647, 50 µL at 2x stock concentration were prepared to result 0.1 0.3, 1, 3, 10 and 30nM final nanobody concentrations.

For the saturation curve in His-tagged non-fluorescent nanobodies, 25 µL of His-tagged in block buffer at 2x stock concentration were prepared to result 0.1 0.3, 1, 3, 10, 30, 100 and 300 nM final nanobody concentrations were added in the solution instead. After 30 mins incubation 25 µL anti-mouse Alexa-647 secondary antibody (1:400 dilution in block buffer) were added and further incubated for 30 mins. For the displacement assay, platelets were incubated with 25 µL at 2x stock concentration to generate a final concentration of 100nM of His-tagged Nb21 and increasing concentrations of 25 µL Nb21 at 2x stock concentration to result on 1, 10, 100 and 1000 nM. 25 µL of an anti-His Alexa-647 secondary antibody (1:400) was used as a staining control and to detect the presence of His-Nb21 bound to platelets (control cells).

2.3.10. Crystallisation of GPVI-nanobody complex

Table 2.4. Nanobody, recombinant GPVI mutant and complex parameters generated from ExPASy ProtParam tool. *The extinction coefficient is generated in Abs 0.1% (=1 g/l), assuming all pairs of Cys residues form cysteine disulfide bridges. * The extinction coefficient is also shown as M^{-1} cm^{-1} and generated at 280 nm measured in water. The nanobody concentration was obtained by adjusting the NanoDrop measurements based on the extinction coefficient of each nanobody. The extinction coefficients were generated by loading each nanobody sequence to the ExPASy Prot Param tool.*

Name	Molecular Weight (Da)	Extinction Coefficient (M-1 cm-1)*	Extinction Coefficient (g/L)
GPVI NQ	21120.97	33140	1.569
GPVI NQ + Nb 21	42055.82	66405	1.579
GPVI NQ + Nb 35	36395.80	59290	1.629

2.3.10.1 Sample preparation for crystallization condition screening

Generation and purification of each nanobody and GPVI NQ was performed similarly to the procedures followed for wild-type GPVI, as described in Sections 2.3.2 and 2.3.3. After each individual purified protein was obtained, the proteins were mixed at a molar ratio of 1:1. Complexes of GPVI NQ with Nb21 and Nb35 were generated throughout this project. After 15 min of incubation, the sample was then spin concentrated to a volume of 500 µL and loaded onto the gel filtration column (Superdex 200 Increase 10/300 GL 24 mL). The gel filtration buffer was consistently 20 mM Tris, 140 mM NaCl, pH 7.4 in all protein complexes. All the

fractions obtained from gel filtration were checked with a Bolt™ 4 to 12%, Bis-Tris, 1.0 mm gel. These fractions were then joined and spin concentrated to 10 mg/mL.

2.3.10.2 Crystal plate set-up & optimization

The concentrations used for setting up crystal trays were 6 mg/mL for the GPVI NQ/Nb35 complex and 5 mg/mL for the GPVI NQ/Nb21. The prepared complex was centrifuged at x 1500 g for 5 mins prior to use. For loading the sitting drop technique was used. The volumes of the crystallisation buffer (no complex control) and complex sample was 0.22 µL of buffer and 0.22 µL protein or gel filtration buffer. The complex and screening buffer loading was performed through a Mosquito® Crystal apparatus. For the crystal buffer condition screening Morpheus®, Morpheus® II, Morpheus® III, Structure 1 & 2, ProPlex™, MemGold™, MemGoldMeso, MIDAS™, MIDASplus™ and JCSG Plus™ screening 96-well plates by Molecular Dimensions. The plates were sealed and placed in a 20 °C incubator. All crystallization and optimization procedures were conducted using the materials and the facilities in Jonas Emsley's laboratory. Crystals were obtained for GPVI NQ/Nb21 (0.1 M sodium cacodylate, 15% w/v PEG 4000 and pH=6.0) and GPVI NQ/Nb35 (1.6 M magnesium sulfate heptahydrate 0.1 M MES monohydrate, pH=6.5) complexes.

2.3.10.3 Crystal structure analysis

The GPVI NQ/Nb35 complex was fired using the I04 beamline. Diffraction data were generated and collected from the Diamond Light Source i24 Beamline. From Information System for Protein CrystallographY Beamlines (ISPyB), autoPROC and STARANSINO processing file were used to index the diffraction data. CCP4 software suite was used for structure determination. PHASER molecular replacement was performed using 2GI7 and a Nb35 homology model generated from SWISS-MODEL (Waterhouse *et al.*, 2018) (https://swissmodel.expasy.org) were used as templates. 2GI7 was split into two files corresponding to the D1 and D2 domain of extracellular GPVI. This was followed by model building in Crystallographic Object-Oriented Toolkit (COOT) and multiple rounds of refinement in Refinement of Macromolecular Structures (REFMAC).

Table 2.5. Crystallographic data collection and refinement statistics.

Data Collection	**Value**
Space group	H 3 2
Cell dimensions:	
a, b, c (Å)	122.51 122.51 181.11
α, β, γ (°)	90.00 90.00 120.00
Resolution (Å)	30.05 – 3.78
R_{merge}	0.075 (0.669)*
|/σ|	16.3 (1.9)*
Completeness (%)	98.8 (86.0)*
Redundancy	6.6 (5.1)*
Wavelength (Å)	0.9795 Å
Refinement:	
No. of reflections	5357
R_{work}/R_{free} (%)	0.235 / 0.314
No. atoms:	
Protein	2255
Ca^{2+}	
Water	
B-factors (Å^2):	
Protein	193.56
Metal	
Water	
RMS deviations:	
Bond lengths (Å)	0.0080
Bond angles (°)	1.825

aRmerge = Σh Σi| <Ih> - Ih,i|/Σh Σi Ih,I where I is the observed intensity and <Ih> is the average intensity of multiple observations from symmetry-related reflections calculated. bRwork = Sum(h) ||Fo|h - |Fc|h| / Sum(h)|Fo|h, where Fo and Fc are the observed and calculatedstructure factors, respectively. Rfree computed as in Rwork, but only for (5%) randomly selected reflections, which were omitted in refinement, calculated using REFMAC.

*Values in parentheses are for highest-resolution shell.

2.3.11.Statistical analysis

All statistical test and analysis are indicated in the figure legends. Results are shown as mean ± standard error of the mean (SEM) (unless stated otherwise) and the number of independent experiments is described in Figure legends. Data were processed using PRISM v8.4.3 (GraphPad, San Diego, CA). Statistical analysis in Chapters 3 and 4 was by one-way analysis of variance (ANOVA) with a Dunnet post-hoc test. For ELISA assays in Chapter 3, a two-way ANOVA test with a Dunnet post-hoc test where used. For NFAT assays, in Chapter 4 multiple *t* tests with a Holm-Sidak post-hoc test. Background luciferase signal from the mock-transfected DT40 control cells was subtracted from each sample value and then the luciferase activity data was normalised for PMA plus ionomycin values and are presented as a percentage of the positive control PMA plus ionomycin response. For the NFAT assay of the GPVI mutants for the monitoring of the effects of nanobodies in collagen-induced signalling (Figure 4.15), statistical analysis was by two-way ANOVA with a Tukey post-hoc test. Significance was set at $P \leq 0.05$.

2.3.12. Appendix

Table 2.6. Protein sequence of nanobody constructs. *The amino acid sequence of each nanobody construct are listed. Nanobodies were generated by Dr. Alexandre Slater in the lab of Prof. Steve P. Watson (Birmingham).*

Nanobody construct	Amino acid sequence
His-tagged Nb2	QVQLQESGGGLVQPGGSLRLSCAAAGFTFDYYAIAWFRQAPGKEREGVSCI SSSDGTTYYADSVKGRFTISKDNAKNTMYLQMNSLKPEDTAVYYCATSPL YSTNDRCISEDYDYWGQGTQVTVSSAAAYPYDVPDYGSHHHHHH
His-tagged Nb21	QVQLQESGGGLVQPGGSLRLSCAASGRTFTRSIMGWFHQAPGKEREFLAGI SWSGANTYYADSVRGRFTISRDNAKNTVSLQMNSLNPEDTAVYYCAADPS HPGSLISTRRSDYDSWGRGTQVTVSSAAAYPYDVPDYGSHHHHHH
His-tagged Nb35	QVQLQESGGGLVQAGGSLRLSCAASGVTFDSAAMAWFRQVPGKEREFVA VISTESGGRTDHADSVKGRFLISRDNARHMVYLQMNSLNPEDTAVYYCASS LLYCSASGCYANRDSYDYWGQGTQVTVSSAAAYPYDVPDYGSHHHHHH
Nb2	QVQLQESGGGLVQPGGSLRLSCAAAGFTFDYYAIAWFRQAPGKEREGVSCI SSSDGTTYYADSVKGRFTISKDNAKNTMYLQMNSLKPEDTAVYYCATSPL YSTNDRCISEDYDYWGQGTQVTVSSAAAYPYDVPDYGS
Nb21	QVQLQESGGGLVQPGGSLRLSCAASGRTFTRSIMGWFHQAPGKEREFLAGI SWSGANTYYADSVRGRFTISRDNAKNTVSLQMNSLNPEDTAVYYCAADPS HPGSLISTRRSDYDSWGRGTQVTVSSAAAYPYDVPDYGS
Nb35	QVQLQESGGGLVQAGGSLRLSCAASGVTFDSAAMAWFRQVPGKEREFVA VISTESGGRTDHADSVKGRFLISRDNARHMVYLQMNSLNPEDTAVYYCASS LLYCSASGCYANRDSYDYWGQGTQVTVSSAAAYPYDVPDYGS

Table 2.7. Protein sequence of recombinant GPVI constructs. *The amino acid sequence of each GPVI construct are listed. The N72-glycosylation mutant (NQ GPVI) is highlighted in magenta on the original GPVI structure (WT GPVI) for reference.*

GPVI construct	Amino acid sequence
Wild type GPVI (WT GPVI)	QSGPLPKPSLQALPSSLVPLEKPVTLRCQGPPGVDLYRLEKLSSSRYQDQAVLFIP AMKRSLAGRYRCSYQNGSLWSLPSDQLELVATGVFAKPSLSAQPGPAVSSGGD VTLQCQTRYGFDQFALYKEGDPAPYKNPERWYRASFPIITVTAAHSGTYRCYSF SSRDPYLWSAPSDPLELVVT
N72-glycosylation mutant (GPVI NQ)	DKLASSGPLPKPSLQALPSSLVPLEKPVTLRCQGPPGVDLYRLEKLSSSRYQDQA VLFIPAMKRSLAGRYRCSYQQGSLWSLPSDQLELVATGVFAKPSLSAQPGPAVS SGGDVTLQCQTRYGFDQFALYKEGDPAPYKNPERWYRASFPIITVTAAHSGTYR CYSFSSRDPYLWSAPSDPLELVVTGDPIEGR

Table 2.8. DNA and protein sequence of recombinant GPVI mutant constructs for NFAT assay. *The DNA and amino acid sequence of each GPVI construct are listed. The single point alanine mutations, (R38A, R46A, R60A, and R67A) are highlighted in yellow and each arginine equivalent is highlighted on the original GPVI structure (WT GPVI) for reference.*

GPVI construct	**DNA sequence**	**Amino acid sequence**
Wild type GPVI (WT GPVI)	atgtctccatccccgaccgccctcttctgtcttgggctgtgtctggggcgtgtgccagcgcagagtg gaccgctccccaagccctccctccaggctctgcccagctccctggtgcccctggagaagccagt gaccctccggtgccagggacctccgggcgtggacctgtaccgcctggagaagctgagttccag caggtaccaggatcaggcagtcctcttcatcccggccatgaagagaagtctggctggacgctacc gctgctcctaccagaacggaagcctctggtccctgcccagcgaccagctggagctcgttgccac gggagtttttgccaaaccctcgctctcagcccagcccggcccggcggtgtcgtcaggaggggac gtaaccctacagtgtcagactcggtatggctttgaccaatttgctctgtacaaggaaggggacccctg cgccctacaagaatcccgagagatggtaccgggctagtttccccatcatcacggtgaccgccgcc cacagcggaacctaccgatgctacagcttctccagcagggacccatacctgtggtcggccccca gcgacccccctggagcttgtggtcacaggaacctctgtgacccccagccggttaccaacagaacc accttcctcggtagcagaattctcagaagccaccgctgaactgaccgtctcattcacaaacaaagt cttcacaactgagacttctaggagtatcaccaccagtccaaaggagtcagactctccagctggtcc tgcccgccagtactacaccaagggcaacctggtccggatatgcctcggggctgtgatcctaataat cctggcggggtttctggcagaggactggcacagccggaggaagcgcctgcggcacaggggca gggctgtgcagaggccgcttccgcccctgccgcccctcccgcagacccggaaatcacacgggg gtcaggatggaggccgacaggatgttcacagccgcgggttatgttca	QSGPLPKPSLQALPSSLVPLEKPVTL RCQGPPGVDLYRLEKLSSSRYQDQA VLFIPAMKRSLAGRYRCSYQNGSL WSLPSDQLELVATGVFAKPSLSAQP GPAVSSGGDVTLQCQTRYGFDQFA LYKEGDPAPYKNPERWYRASFPIIT VTAAHSGTYRCYSFSSRDPYLWSAP SDPLELVVT
R38A	atgtctccatccccgaccgccctcttctgtcttgggctgtgtctggggcgtgtgccagcg cagagtggaccgctccccaagccctccctccaggctctgcccagctccctggtgcccc tggagaagccagtgaccctccggtgccagggacctccgggcgtggacctgtacgccc tggagaagctgagttccagcaggtaccaggatcaggcagtcctcttcatcccggccat gaagagaagtctggctggacgctaccgctgctcctaccagaacggaagcctctggtcc ctgcccagcgaccagctggagctcgttgccacgggagttttgccaaaccctcgctctc agcccagcccggcccggcggtgtcgtcaggaggggacgtaaccctacagtgtcaga ctcggtatggctttgaccaatttgctctgtacaaggaaggggaccctgcgccctacaag aatcccgagagatggtaccgggctagtttccccatcatcacggtgaccgccgcccaca gcggaacctaccgatgctacagcttctccagcagggacccatacctgtggtcggcccc cagcgacccccctggagcttgtggtcacaggaacctctgtgacccccagccggttacca acagaaccaccttcctcggtagcagaattctcagaagccaccgctgaactgaccgtctc attcacaaacaaagtcttcacaactgagacttctaggagtatcaccaccagtccaaagga gtcagactctccagctggtcctgcccgccagtactacaccaagggcaacctggtccgg atatgcctcggggctgtgatcctaataatcctggcggggtttctggcagaggactggca cagccggaggaagcgcctgcggcacaggggcagggctgtgcagaggccgcttccg cccctgccgcccctcccgcagacccggaaatcacacgggggtcaggatggaggccg acaggatgttcacagccgcgggttatgttca	QSGPLPKPSLQALPSSLVPLEKPVTL RCQGPPGVDLYALEKLSSSRYQDQA VLFIPAMKRSLAGRYRCSYQNGSL WSLPSDQLELVATGVFAKPSLSAQP GPAVSSGGDVTLQCQTRYGFDQFA LYKEGDPAPYKNPERWYRASFPIIT VTAAHSGTYRCYSFSSRDPYLWSAP SDPLELVVT
R46A	atgtctccatccccgaccgccctcttctgtcttgggctgtgtctggggcgtgtgccagcg cagagtggaccgctccccaagccctccctccaggctctgcccagctccctggtgcccc tggagaagccagtgaccctccggtgccagggacctccgggcgtggacctgtaccgcc tggagaagctgagttccagcgcctaccaggatcaggcagtcctcttcatcccggccatg aagagaagtctggctggacgctaccgctgctcctaccagaacggaagcctctggtccc tgcccagcgaccagctggagctcgttgccacgggagttttgccaaaccctcgctctca gcccagcccggcccggcggtgtcgtcaggaggggacgtaaccctacagtgtcagact	QSGPLPKPSLQALPSSLVPLEKPVTL RCQGPPGVDLYALEKLSSSAYQDQ AVLFIPAMKRSLAGRYRCSYQNGSL WSLPSDQLELVATGVFAKPSLSAQP GPAVSSGGDVTLQCQTRYGFDQFA LYKEGDPAPYKNPERWYRASFPIIT

	cggtatggctttgaccaatttgctctgtacaaggaaggggaccctgcgccctacaagaa tcccgagagatggtaccgggctagtttccccatcatcacggtgaccgccgcccacagc ggaacctaccgatgctacagcttctccagcagggacccatacctgtggtcggccccca gcgacccccctggagcttgtggtcacaggaacctctgtgacccccagccggttaccaac agaaccaccttcctcggtagcagaattctcagaagccaccgctgaactgaccgtctcatt cacaaacaaagtcttcacaactgagacttctaggagtatcaccaccagtccaaaggagt cagactctccagctggtcctgcccgccagtactacaccaagggcaacctggtccggat atgcctcggggctgtgatcctaataatcctggcggggtttctggcagaggactggcaca gccggaggaagcgcctgcggcacaggggcagggctgtgcagaggccgcttccgcc cctgccgcccctcccgcagacccggaaatcacacgggggtcaggatggaggccgac aggatgttcacagccgcgggttatgttca	VTAAHSGTYRCYSFSSRDPYLWSAP SDPLELVVT
R60A	atgtctccatccccgaccgccctcttctgtcttgggctgtgtctggggcgtgtgccagcg cagagtggaccgctccccaagccctccctccaggctctgcccagctccctggtgcccc tggagaagccagtgaccctccggtgccagggacctccgggcgtggacctgtacgccc tggagaagctgagttccagcaggtaccaggatcaggcagtcctcttcatcccggccat gaagccaagtctggctggacgctaccgctgctcctaccagaacggaagcctctggtcc ctgcccagcgaccagctggagctcgttgccacgggagtttttgccaaaccctcgctctc agcccagcccggcccggcggtgtcgtcaggaggggacgtaaccctacagtgtcaga ctcggtatggctttgaccaatttgctctgtacaaggaaggggaccctgcgccctacaag aatcccgagagatggtaccgggctagtttccccatcatcacggtgaccgccgcccaca gcggaacctaccgatgctacagcttctccagcagggacccatacctgtggtcggcccc cagcgacccccctggagcttgtggtcacaggaacctctgtgacccccagccggttacca acagaaccaccttcctcggtagcagaattctcagaagccaccgctgaactgaccgtctc attcacaaacaaagtcttcacaactgagacttctaggagtatcaccaccagtccaaagga gtcagactctccagctggtcctgcccgccagtactacaccaagggcaacctggtccgg atatgcctcggggctgtgatcctaataatcctggcggggtttctggcagaggactggca cagccggaggaagcgcctgcggcacaggggcagggctgtgcagaggccgcttccg cccctgccgcccctcccgcagacccggaaatcacacgggggtcaggatggaggccg acaggatgttcacagccgcgggttatgttca	QSGPLPKPSLQALPSSLVPLEKPVTL RCQGPPGVDLYALEKLSSSRYQDQA VLFIPAMKASLAGRYRCSYQNGSL WSLPSDQLELVATGVFAKPSLSAQP GPAVSSGGDVTLQCQTRYGFDQFA LYKEGDPAPYKNPERWYRASFPIIT VTAAHSGTYRCYSFSSRDPYLWSAP SDPLELVVT
R67A	atgtctccatccccgaccgccctcttctgtcttgggctgtgtctggggcgtgtgccagcg cagagtggaccgctccccaagccctccctccaggctctgcccagctccctggtgcccc tggagaagccagtgaccctccggtgccagggacctccgggcgtggacctgtaccgcc tggagaagctgagttccagcaggtaccaggatcaggcagtcctcttcatcccggccat gaagagaagtctggctggacgctagccctgctcctaccagaacggaagcctctggtcc ctgcccagcgaccagctggagctcgttgccacgggagtttttgccaaaccctcgctctc agcccagcccggcccggcggtgtcgtcaggaggggacgtaaccctacagtgtcaga ctcggtatggctttgaccaatttgctctgtacaaggaaggggaccctgcgccctacaag aatcccgagagatggtaccgggctagtttccccatcatcacggtgaccgccgcccaca gcggaacctaccgatgctacagcttctccagcagggacccatacctgtggtcggcccc cagcgacccccctggagcttgtggtcacaggaacctctgtgacccccagccggttacca acagaaccaccttcctcggtagcagaattctcagaagccaccgctgaactgaccgtctc attcacaaacaaagtcttcacaactgagacttctaggagtatcaccaccagtccaaagga gtcagactctccagctggtcctgcccgccagtactacaccaagggcaacctggtccgg atatgcctcggggctgtgatcctaataatcctggcggggtttctggcagaggactggca cagccggaggaagcgcctgcggcacaggggcagggctgtgcagaggccgcttccg cccctgccgcccctcccgcagacccggaaatcacacgggggtcaggatggaggccg acaggatgttcacagccgcgggttatgttca	QSGPLPKPSLQALPSSLVPLEKPVTL RCQGPPGVDLYALEKLSSSRYQDQA VLFIPAMKRSLAGRYACSYQNGSL WSLPSDQLELVATGVFAKPSLSAQP GPAVSSGGDVTLQCQTRYGFDQFA LYKEGDPAPYKNPERWYRASFPIIT VTAAHSGTYRCYSFSSRDPYLWSAP SDPLELVVT

Table 2.9. Protein sequence of full-length GPVI construct used for NFAT assays.

Construct	**Amino acid sequence**
Human GPVI-Fc (full plasmid)	MSPSPTALFCLGLCLGRVPAQSGPLPKPSLQAPSSLVPLEKPVTLRCQGPPGVDLYRLE KLSSSRYQDQAVLFIPAMKRSLAGRYRCSYQNGSLWSLPSDQLELVATGVFAKPSLS AQPGPAVSSGGDVTLQCQTRYGFDQFALYKEGDPAPYKNPERWYRASFPIITVTAAH SGTYRCYSFSSRDPYLWSAPSDPLELVVTGTSVTPSRLPTEPPSPVAEFSEATAELTVSF TNEVFTTETSRSITASPKESDSPAGPARQYYTKGNLVRICLGAVILIILAGFLAEDWHSR RKRLRHRGRAVQRPLP PLPPLPLTRK SNGGQDGGRQ DVHSRGLCS

Chapter 3

In silico investigation for small molecule ligands for GPVI

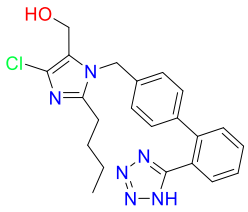
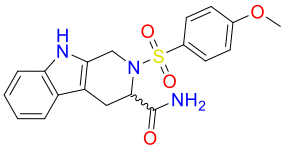
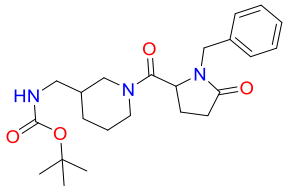
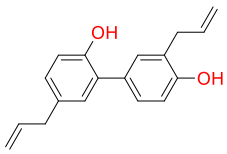
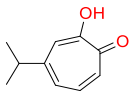
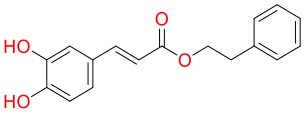
3.1 Introduction

Given the fact that current antiplatelet strategies and related biological targets affect biological cascades responsible for normal haemostasis, with their risk of bleeding being associated with increased treatment intensity and drug affinity, the clinical benefit to these therapies seems to have reached a limit. For the past few years several promising new antiplatelet agents have undergone Phase I clinical trials to introduce novel and safer antiplatelet agents in the clinic. These include protein disulfide-isomerases, phosphatidylinositol 3 kinase β (PI3Kβ) inhibitors and protease-activated receptor (PAR) inhibitors (McFadyen *et al.*, 2018). In particular, a PAR1 inhibitor has made it to the clinic under the name vorapaxar, while a PAR4 inhibitor (BMS-986141) has made it out of a phase II clinical trial, but vorapaxar use is limited due to excess bleeding and intracranial haemorrhage (Morrow *et al.*, 2012; Cheng *et al.*, 2015) while a second clinical trial for BMS-986141 study was not completed (NCT02671461) and more clinical studies are needed (Li *et al*., 2019). Two GPVI inhibitors have undergone Phase I and II trials, with a Phase III trial planned for the Fab glenzocimab in the next year. Both inhibitors are large protein based (known as biologics) which limits their biodistribution.

Despite the multimeric nature, high affinity and slow off-rates of GPVI-targeting antibodies and related biologics agents, their lack of oral bioavailability and high production cost limits their application in long-term prevention for patients at risk of thrombosis (Damaskinak*i et al*., 2021). Small molecules have low molecular weights, with their pharmacokinetics and pharmacodynamics being more easily studied or predicted than those of biologics (Zhao *et al*., 2012). This is most prevalent in the case of monoclonal antibodies that exhibit non-linear pharmacokinetics due to Fc-receptor mediated clearance (Garg and Balthasar, 2007). Unlike biologics, small molecules the physicochemical properties of a molecule can be more easily modulated to create drugs with lower metabolic targeting, higher volume of distribution and stability and oral bioavailability, which crucial for enhancing patient compliance (Zhao *et al*., 2012; Vargason *et al*., 2021). In addition, small molecule drugs have simpler characterisation, formulation, manufacturing and regulatory processes, making them more cost-effective (Makurvet, 2021; Vargason *et al*., 2021). However, the interactions between a protein ligand and a receptor can be difficult to mimic in a small molecule, as the site of interaction may have relatively few features and cover a large surface area. Therefore, small molecule ligands must bind to key receptor sites or allosteric pockets with high affinity with slow off-rate kinetics to

overcome the effects of avidity, while protein half-life, binding site surface area, target residue identification and characterisation and chemical group reactivity should be considered (Ran and Gestwicki, 2018). Several small-molecule GPVI inhibitors have been reported (Table 3.10). The most thoroughly studied of these is the angiotensin II receptor antagonist, losartan (Taylor *et al.*, 2014; Damaskinaki *et al.*, 2021). The binding site of losartan to GPVI has been investigated by 1H NMR NOESY overlap and docking studies alongside that of pep-10L; neither inhibitor have structural similarities to the GPO triplet motif found in collagen or CRP (Kato-Takagaki et al., 2009). Several natural bioactive compounds, namely honokiol (Lee *et al.*, 2017), hinokitiol (Lin *et al.*, 2013) and caffeic acid phenethyl ester (CAPE) have also been identified (Chen *et al.*, 2007). The binding of honokiol to GPVI has been studied (Damaskinaki *et al.*, 2021) using surface plasmon resonance (SPR) (Onselaer *et al.*, 2019). S002-333 (Bhunia *et al.*, 2017). A pyridoindole-based compound, and S007-867 (Misra *et al.*, 2018), a chiral 3-aminomethylpiperidine analogue, also block collagen-induced aggregation and have antithrombotic efficacy *in vivo*. All of the ligands display IC_{50} values in the micromolar range on platelet aggregation assays (Table 3.10). Moreover, losartan has been shown to inhibit other platelet receptors, notably those for thromboxane A_2 and CLEC-2 at similar or slightly higher concentrations (Onselaer *et al.*, 2019), which suggests that it may be having a generalized effect and off-target binding.

Table 3.10. Small molecule inhibitors against GPVI reported in literature. *This table includes the cell type, biological assay and agonist concentration used with the corresponding IC_{50} determined from each assay used in each study.*

Name	Structure	Biological assay	Aggregation inducer	IC_{50}
Losartan		LTA, washed platelets	Collagen (1µg/mL)	6.5µM (Jiang *et al.*, 2015)
S002-333		LTA in PRP	Collagen (2µg/mL)	6µM (Bhunia *et al.*, 2017)
S007-867		LTA, washed platelets	Collagen (1µg/mL)	6.7µM (Misra *et al.*, 2018)
CAPE		LTA, washed platelets	Collagen (2µg/mL)	14µM (Chen *et al.*, 2007)
Hinokitiol		LTA, washed platelets	Collagen (1µg/mL)	~1µM (Lin *et al.*, 2013)
Honokiol		LTA, washed platelets	Collagen (1µg/mL)	0.6µM (Lee *et al.*, 2017) 4.6 µM (Onselaer *et al.*, 2019)

3.2 Aims

As yet, molecular docking studies have only generated ligands within the micromolar affinity range due to the lack of potent agonists, ligands or inhibitors to serve as a starting point. The approach undertaken in this Chapter is to perform a virtual docking study for the determination of small molecule ligands for the different GPVI binding sites reported. As previously discussed, literature data indicates that the collagen and CRP binding sites are located in the D1 domain of the GPVI ectodomain (see Section 1.4.1). The best indication of a ligand binding site within the collagen binding interface is the one that was revealed by NMR overlap and docking studies using losartan and pep-10L (Kato-Takagaki *et al.*, 2009), and hence this binding site is included in the virtual docking studies. In addition, the CRP binding site has not been previously used for the identification of small molecule ligands as it has only recently been reported. With advances in molecular docking software, novel ligand chemotypes for GPVI can be revealed for the development of ligands with higher affinity and specificity. Functional studies are to be implemented in order to confirm binding and selectivity/off-target binding.

3.3 Results

3.3.1 Target and binding site selection

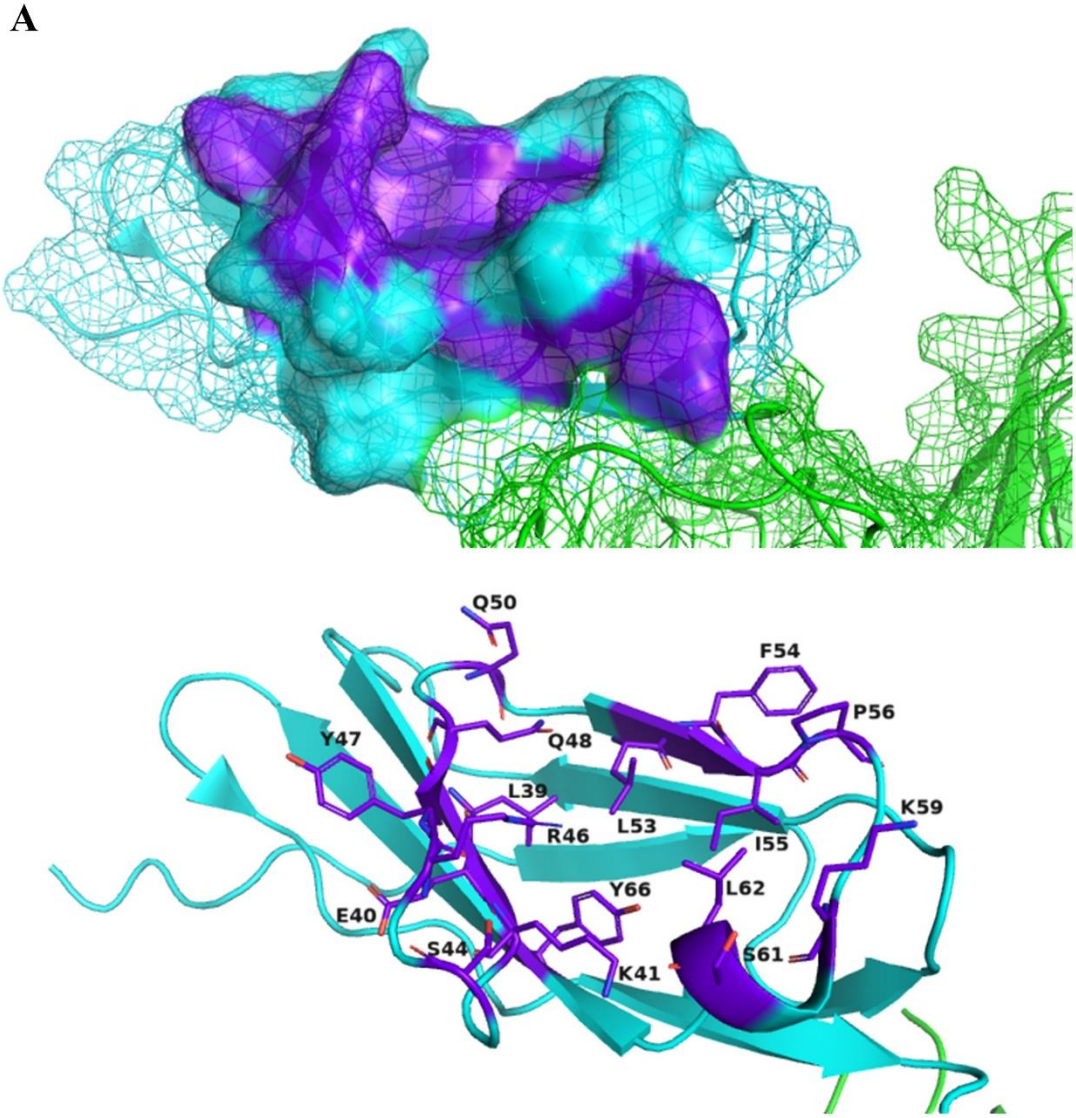
For the purpose of this study, the crystal structures of GPVI ectodomain (Horii *et al.*, 2006) and co-crystallized GPVI ectodomain with CRP (Feitsm*a et al*., 2022) were used (Protein Data Bank (PDB) ID: 2GI7, 5OU7-9). The main tool of investigation was 2GI7, since this structure includes extra amino acids in the D2 domain, including P102-2205 and P131-N136, which are included in the GPVI construct used in this study for biological assays and crystallisation (Chapter 4). For protein preparation, Protein Preparation Wizard was used [(Sastr*y et al*., 2013), Schrödinger Release 2018-1: Protein Preparation Wizard; Epik, Schrödinger, LLC, New York, NY, USA, 2016] to correct common problems such as missing hydrogen atoms, incomplete side chains and loops, ambiguous protonation states, flipped residues and missing disulfide bonds.

SiteMap (Schrödinger Release 2018-1: Schrödinger, LLC, 2016, New York, NY, USA), a binding site detection tool, was used to identify the pockets that could be docked by ligands

(druggability/ligandability) and score them according to their characteristics including Wan Der Vaals radii, metallic ion presence, electrostatic force region, protein amino acid properties, volume, and protein interior or surface regions and was used for the detection of candidate binding sites [(Halgren, 2007, 2009), Schrödinger Release 2018-1: SiteMap, Schrödinger, LLC, New York, NY, 2016]. The main function of this tool is the identification and categorisation of the different sub-regions of a binding site to allow for assessment of ligand complementarity. SiteMap can highlight these sub-regions where occupancy can be achieved by hydrophobic groups or by ligand moieties with the potential for polar interactions, such as hydrogen-bond acceptors or donors, charged side chain groups or molecule parts with metal-binding, halogen binding or π-π stacking functionality (Halgren, 2007, 2009). Recently, a combined virtual screening study for the identification of novel GPVI inhibitors also used SiteMap to predict and define the binding site of small molecules within GPVI (Olğaç *et al.*, 2022). The resulting pocket was compared to other literature findings related to the binding site of losartan and other GPVI inhibitors (Kato-Takagaki *et al.*, 2009; Ono *et al.*, 2010; Taylor *et al.*, 2014; Bhunia *et al.*, 2017). The binding site coordinates were then used for grid generation and virtual screening of the MolPort database, resulting to the identification of sixteen hits and two promising GPVI inhibitors (Olğaç *et al.*, 2022). SiteMap also detected and utilised the same pocket in the present study.

A group of pockets were chosen for docking, with one main pocket chosen for each of the aforementioned PDB files (Figure 3.13), one for small molecule binding region within the collagen binding site and one for CRP. They were both placed in the D1 region of GPVI. Residues Leu39-Lys41, Ser44, Arg46-Glu48, Leu53, Ile55, Lys59, Leu62, Asp63 and Tyr66 were included in a SiteMap result and were used for the collagen binding site Grid generation (Figure 3.13A). On the other hand, the CRP site, as suggested by crystallographic data, was not detected by SiteMap and the amino acids that interacted with CRP were manually selected (Leu36, Arg38, Glu40, Tyr47, Arg67, Ser69, Gln71 and Trp76) (Figure 3.13B). For the purpose of this study, the pockets that were generated are called the collagen pocket and the CRP pocket, each referring to the small molecule binding region within the collagen binding site and the CRP binding site respectively.

A



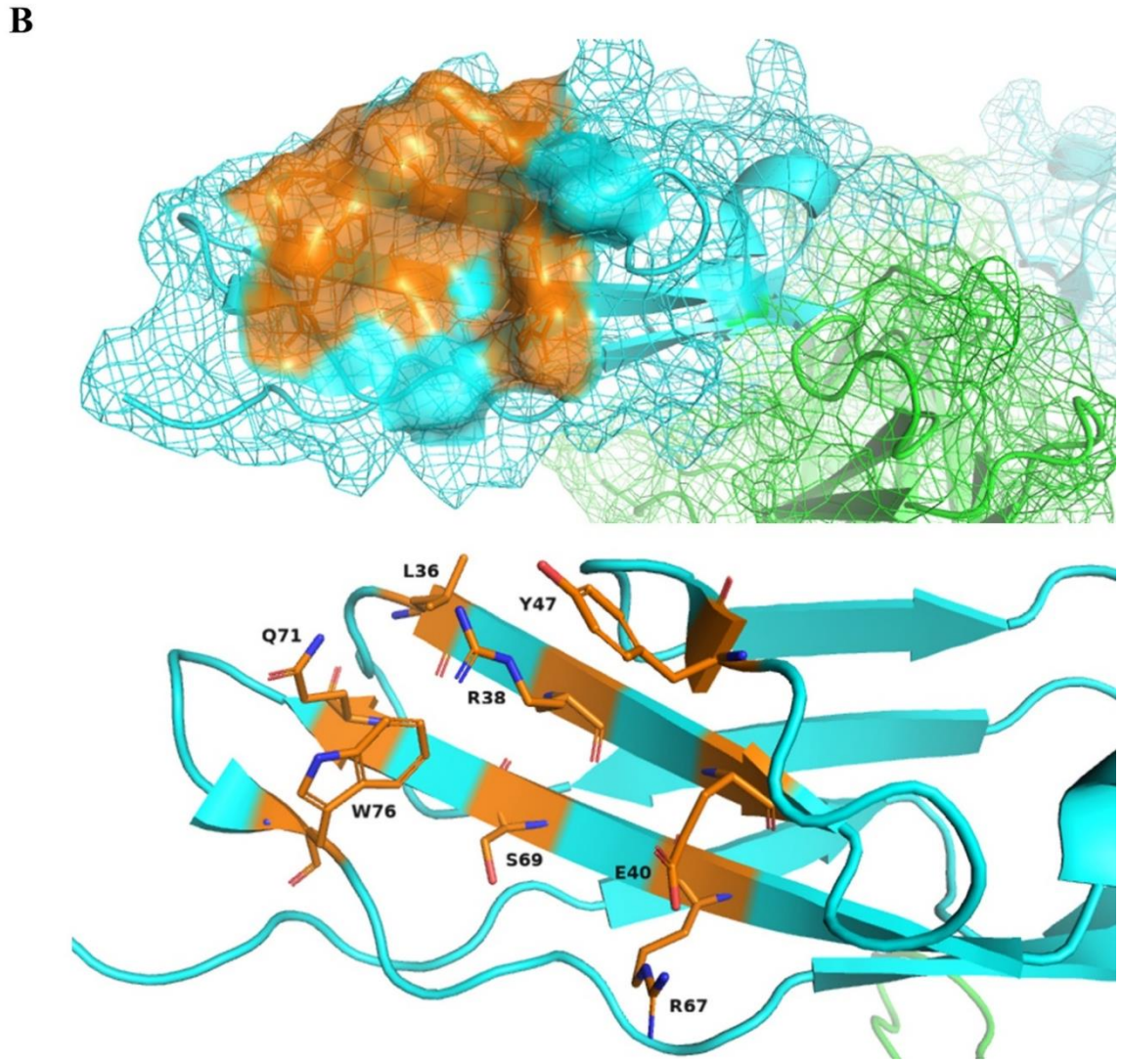


Figure 3.13. Generated collagen and CRP binding sites for this project. *View of the dimeric form of GPVI. The mesh surfaces are representing the binding sites generated in this study, collagen and CRP binding sites. The top image in each panel represents the surface area of the corresponding binding site while the bottom one is a cartoon representation with the amino acids implicated in binding being highlighted as labelled and coloured sticks. (A) Collagen binding site with residues Leu39-Lys41, Ser44, Arg46-Glu48, Leu53, Ile55, Lys59, Leu62, Asp63 and Tyr66 are highlighted in purple while the (B) CRP binding site with residues Leu36, Arg38, Glu40, Tyr47, Arg67, Ser69, Gln71 and Trp76 are highlighted in orange. PDB: 5OU7.*

3.3.2 Structure-based pharmacophore generation & *in silico* screening

A pharmacophore extrapolated from the receptor cavity and amino acids that are appropriate for interacting with novel ligands instead of a known ligand set of active compounds was a more appealing approach rather than developing a pharmacophore from a ligand-based one due to the low affinities that have been reported. This reverse engineering approach was used to generate a structure-based pharmacophore (Figure 3.) and screen a virtual copy of the MCCC compound library. For more information about the library, see Chapter 2. Each of the pockets present in the surface of each GPVI monomer in each PDB file were used for pharmacophore development. The generated pharmacophores from each pocket were used for screening the full MCCC ligand set against them.

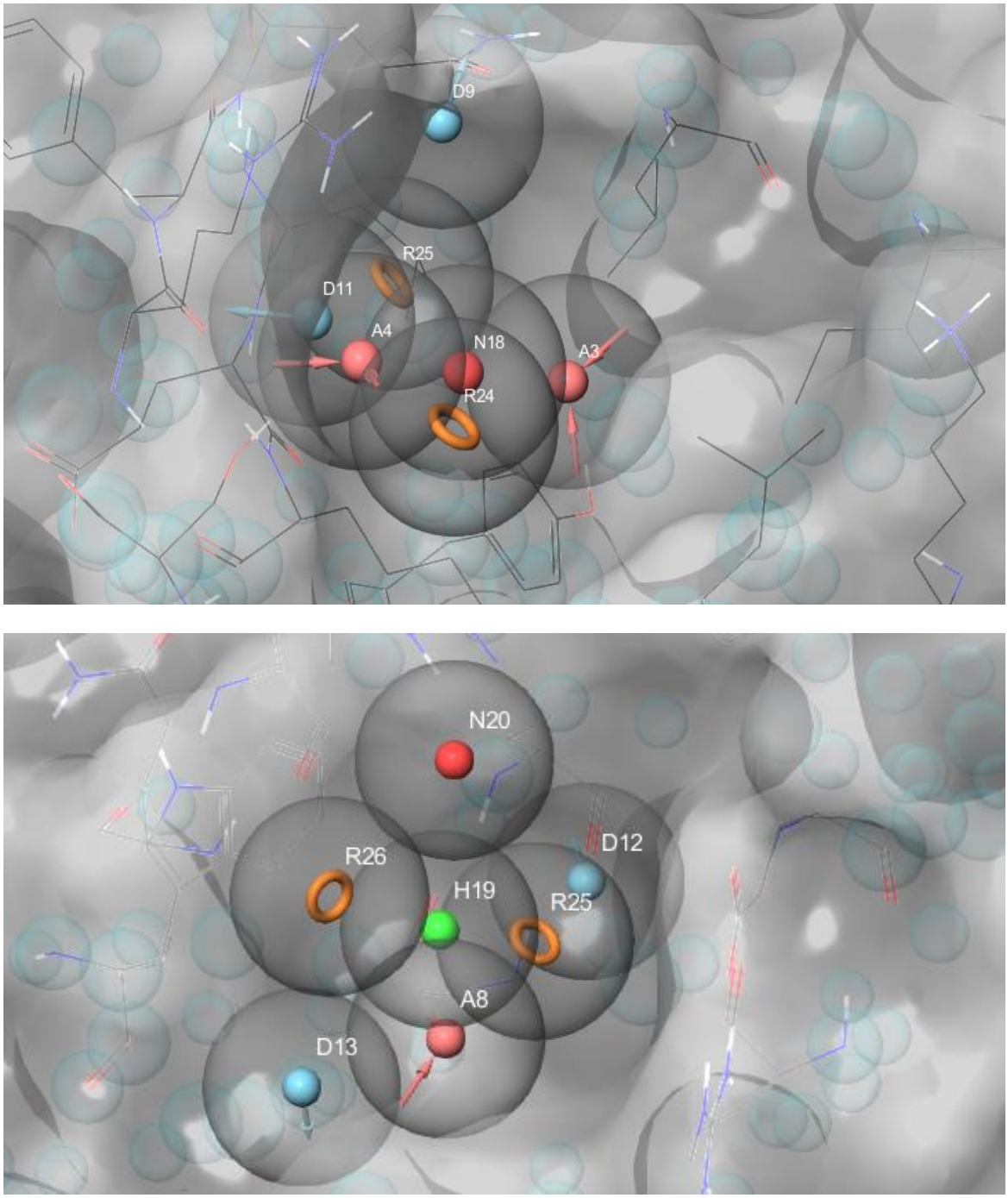
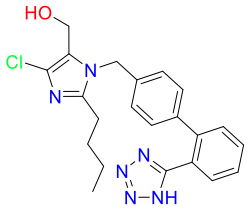
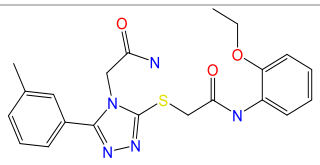
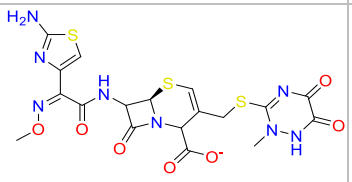
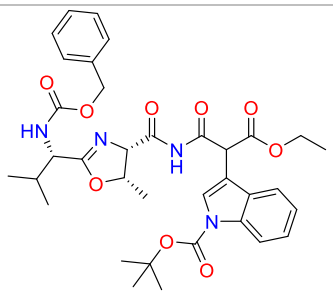
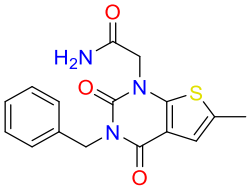
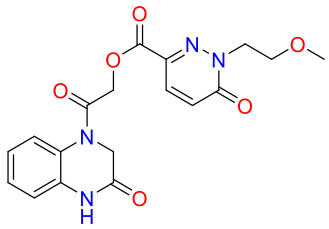
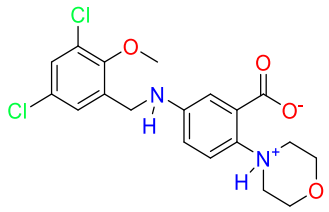
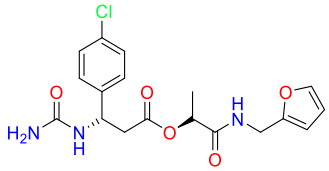
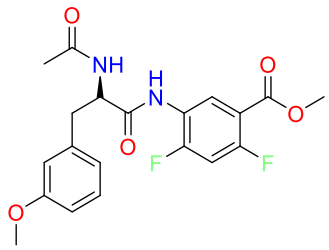
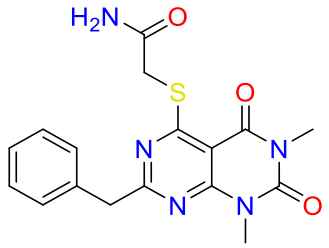
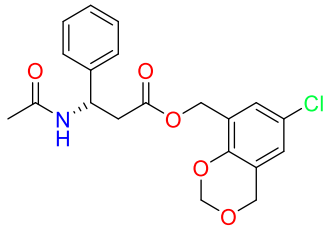
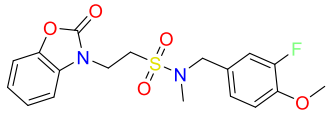


Figure 3.2. Pharmacophore structure-based model aligned with (top) collagen and (bottom) CRP pocket within GPVI. *The Auto (E-pharmacophore) method of the Develop Pharmacophore Model function (Schrödinger Suite, 2018-1) was used to develop each pharmacophore. Pocket druggability was confirmed sing SiteMap for the collagen pocket. Negative charges were equalized to hydrogen bond donors and positive charges with hydrogen bond acceptors, but aromatic rings were not equalized to hydrophobic groups. Top: Residues Leu39-Lys41, Ser44, Arg46-Gln48, Gln50, Leu53-Pro56, Lys59, Leu62 and Tyr66 were used for the generation of a pharmacophore for the collagen pocket. Bottom: Residues Leu36, Arg38, Glu40, Tyr47, Arg67, Ser69, Gln71 and Trp76 were used for the generation of a pharmacophore for the CRP pocket. The different shapes represent the pharmacophore elements that are optimal for binding in this pocket.* ***Red****: Negative charge,* ***Pink****: H-bond acceptor,* ***Blue****: H-bond donor,* ***Orange****: Aromatic ring. PDB: 2GI7.*

The top 1000 fits from each pharmacophore were selected for ligand docking to the two pockets. PDB file 5OU7 was used for the docking studies using the pockets that corresponded to the pharmacophore of the most suitable pocket for docking based on the SiteMap score, docking scores and Pharmacophore merge using Hypothesis Alignment. The docking score function (Glide) is a docking score mathematical function used to predict the binding affinity between the ligand and the receptor, after they have been docked (Friesner *et al.*, 2006). The docking score is using protein-ligand coulomb-vdW energy, lipophilic interactions, charged interactions and hydrogen bonding, rotatable bond penalties and water molecules' displacement by a ligand from lipophilic-rich protein amino acid regions to predict the ligand-receptor binding affinity as ΔG energy (Friesner *et al.*, 2006). Hence, the lower the score arithmetical value, the better the predicted complex affinity and the higher the docking score. The compounds from each pharmacophore were then docked on their corresponding pocket to identify the ones that have the potential to bind GPVI. 15 with the highest docking scores from the collagen (Table 3.2) and the CRP pockets (Table 3.3) were selected, giving 30 compounds in total for testing for the ability to inhibit aggregation of washed platelets.

Table 3.2. Top scorers from the collagen pocket virtual screen. *The chemical structures of the top fifteen selected hit compounds obtained following Glide function docking (Schrödinger Release 2018-1) using default settings and no docking restrictions. The E-pharmacophore entry of the collagen pocket generated during the pharmacophore screening was also used for grid generation and docking of 1000 compounds. The docking score as generated by Glide is given in free Gibb's energy kcal/mol. Losartan was used as a reference. The PhaseScreen score is also displayed to indicate pharmacophore compatibility with the resulting hit compounds. PDB: 2GI7.*

Compound No.	**Structure**	**Sample ID**	**DockingScore (kcal/mol)**	**PhaseScreen Score**
Losartan			-4.383	1.543
1		NCC-00016958	-5.834	0.348
2		NCC-00089733	-5.800	0.518
3		NCC-00000100	-5.737	0.535
4		NCC-00009159	-5.585	0.563

5		NCC-00036491	-5.448	0.358
6		NCC-00010447	-5.426	0.585
7		NCC-00027627	-5.363	0.370
8		NCC-00045022	-5.313	0.566
9		NCC-00076503	-5.306	0.583
10		NCC-00080036	-5.270	0.306
11		NCC-00019521	-5.230	0.397

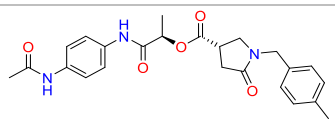
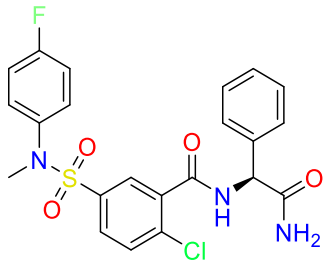
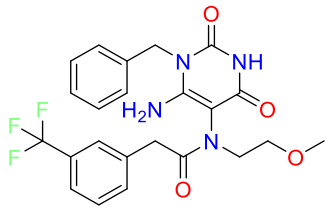
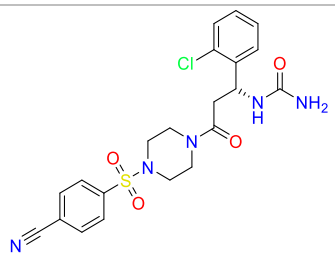
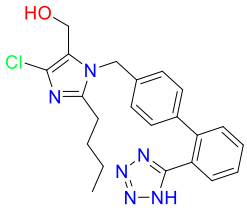
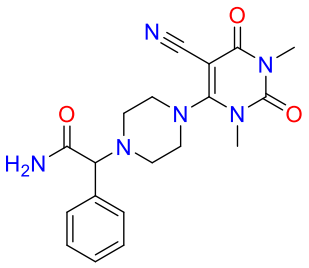
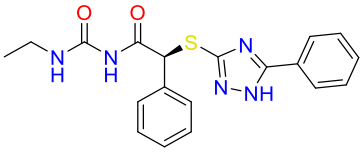
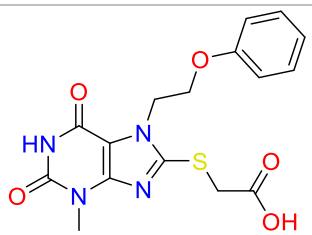
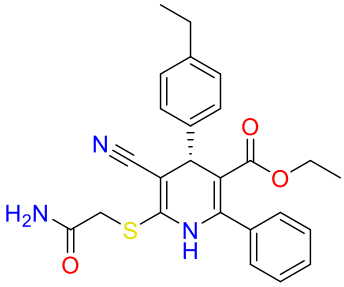
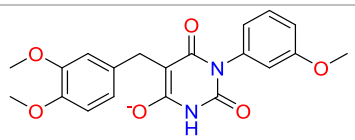
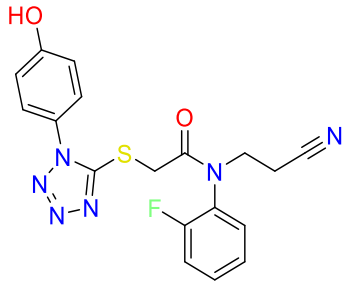
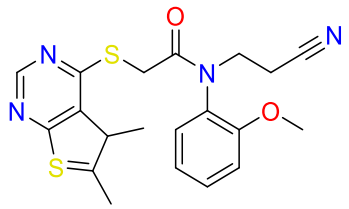
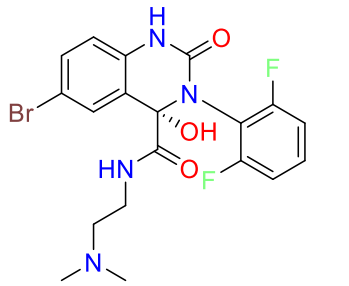
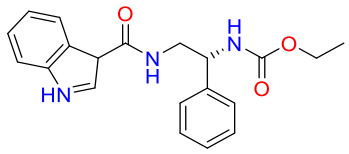
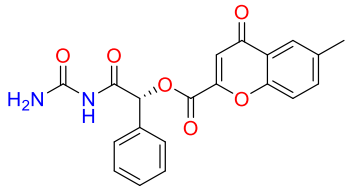
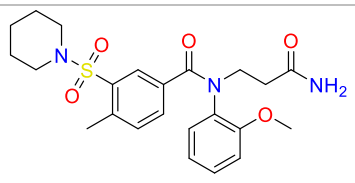
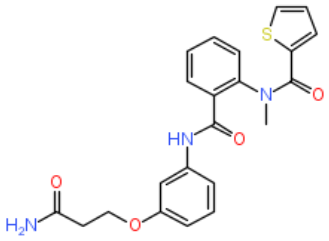
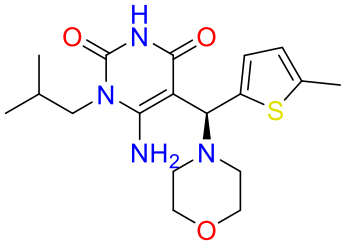
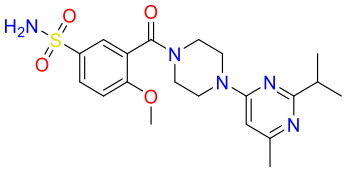
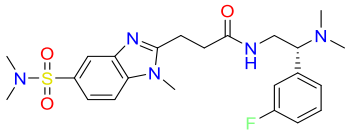
12		NCC-00087865	-5.205	0.372
13		NCC-00062664	-5.149	0.761
14		NCC-00062965	-5.126	0.564
15		NCC-00033183	-5.116	0.507

Table 3.3. Top scorers from the CRP pocket virtual screen. *The chemical structures of the top fifteen selected hit compounds obtained following Glide function docking (Schrödinger Release 2018-1) of 1000 compounds using default settings and no docking restrictions. The E-pharmacophore entry of the CRP pocket generated during the pharmacophore screening was also used for grid generation and docking. The docking score as generated by Glide is given in free Gibb's energy kcal/mol. The PhaseScreen score is also displayed to indicate pharmacophore compatibility with the resulting hit compounds. PDB: 2GI7.*

Compound No.	**Structure**	**Sample ID**	**Docking Score (kcal/mol)**	**PhaseScreen Score**
Losartan			-4.383	1.543
16		NCC-00050179	-6.366	1.045
17		NCC-00072385	-6.096	0.894
18		NCC-00073524	-5.928	0.998
19		NCC-00004174	-5.884	0.888

20		NCC-00004291	-5.845	0.932
21		NCC-00047324	-5.763	0.920
22		NCC-00036322	-5.758	0.903
23		NCC-00002867	-5.732	0.903
24		NCC-00049596	-5.724	0.882
25		NCC-00029275	-5.664	0.803
26		NCC-00087703	-5.603	0.910

27		NCC-00027910	-5.574	0.907
28		NCC-00047446	-5.565	0.587
29		NCC-00042902	-5.560	1.012
30		NCC-00080160	-5.513	0.587

3.3.3 Synthesis of positive and negative controls for aggregation studies

Compound "**6b**" (Bhunia *et al.,* 2017) was included in this study as a positive control of inhibition of aggregation in washed human platelets. Compounds (3SR)-Methyl-2-(4-methoxyphenylsulfonyl)-2,3,4,9-tetrahydro-1H-pyrido[3,4-b]indole-3-carboxylate (Patent No. WO1006070385A1, Gaur *et al.,* 2006) and "**6b**" (Bhunia *et al.,* 2017) were synthesised. For the purpose of this study, from here onwards compounds (3SR)-Methyl-2-(4-methoxyphenylsulfonyl)-2,3,4,9-tetrahydro-1H-pyrido[3,4-b]indole-3-carboxylate and "**6b**" will be referred as **4** and **5** respectively. These compounds were then tested in order to establish a positive and negative control respectively for the platelet aggregation assay for screening of the selected compounds. A structure-activity relationship (SAR) study for GPVI inhibitors has been reported (Bhunia *et al.*, 2017) from which racemic compound **5** showed greater inhibition of collagen-induced platelet aggregation to its enantiomers (Bhateria *et al.*, 2017; Bhunia *et al.*, 2017). It was hypothesized by the authors that this difference could be attributed to the presence of a second binding site in the GPVI interdomain region and that the two enantiomers work in synergy to achieve a higher inhibition effect on collagen-induced aggregation in platelets. The specificity of those ligands is higher for collagen (collagen 2 μg/mL, IC_{50} = 10.4 μM) over other GPVI agonists (CRP-XL 0.3 μg/mL, [IC_{50} = 53.5 μM], convulxin 10 ng/mL, [IC_{50} = 5.7 μM] respectively). In addition, it is the only SAR study to date for GPVI inhibitors supported by virtual docking studies, conformation of individual isomers and biological data. It was the racemic mixture **4** that was synthesized and tested, as it was the most active one (IC_{50}= 6.7 μM) in that study, even compared to the individual enantiomers, with 6c being more active (IC_{50}= 25.3 μM) than 6d (IC_{50}= 126.3 μM). An analogue previously described by the same group that did not demonstrate inhibition of collagen-induced aggregation, **4**, was used as a negative control. Both of the IC_{50} values for those compounds were obtained in platelet-rich plasma (PRP), where protein binding may have influenced the results, and so I evaluated their inhibition potential in human washed platelets.

The compounds were not commercially available and had to be synthesized. Although most of the synthetic procedure was extrapolated from the original source, it was not followed step-by-step (Figure 3.3), due to purification and synthetic liabilities. Initially, a racemic mixture of *DL*-tryptophan **1** was esterified to yield compound **2 [2a, DL-tryptophan methyl ester, (Bhunia et al., 2017)]**, by *in situ* production of hydrochloric acid from thionyl chloride. The cyclization step of the tryptophan methyl ester **3** to the corresponding tetrahydro pyrido-indole

compound **3** was conducted as stated in the original synthesis. However, the next steps were modified (Figure 3.3) and a sulphonyl chloride addition step was implemented instead to produce compound**4.** Then, ammonia in methanol under pressure was introduced to yield the final product **4** (Figure 3.3) [**6b**, (3SR)-2-(4-Methoxyphenylsulfonyl)-2,3,4,9-tetrahydro-1H-pyrido[3,4-b]indole-3-carboxamide, (Bhunia et al., 2017)]. Characterization was conducted using TLC, HPLC-MS, ^{1}H 400MHz and ^{13}C NMR101MHz. Purity of each reaction product was extrapolated from each ^{1}H NMR spectrum.

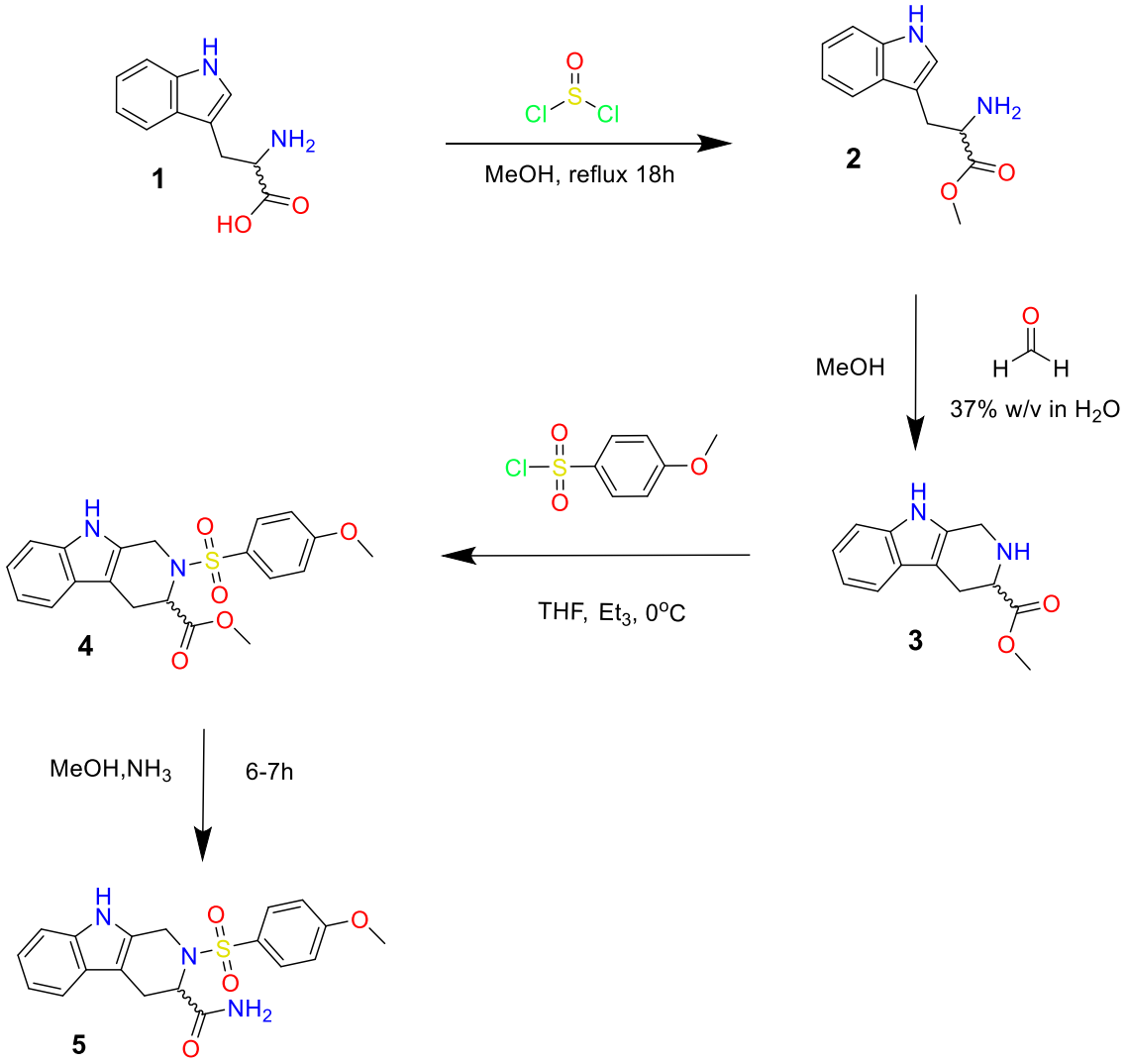


Figure 3.3. General scheme for altered synthetic procedure for 5 (Bhunia et al., 2017). *Reagents and conditions: (a) sulfurous dichloride, MeOH, reflux 16-18h, −10 to 30 °C; (b) 1. formaldehyde, 10:1 MeOH/H_2O, 37% w/v in H_2O 2. Saturated NaHCO3 solution; (c) 4-methoxybenzenesulfonyl chloride, THF, Et_3N, 0 °C; (d) NH_3 in MeOH, 6-7h. This route also generated the negative control used in this study from the WO1006070385A1 patent (**4**). Synthesis was adapted and modified from Bhunia et al. (2017).*

3.3.4 Aggregation assays for compound selection

For the purpose of this study, compounds were screened through a light transmission assay (LTA) using a PAP-8E 2.1.0 aggregometer. This assay relies on the turbidimetric method to measure platelet aggregation where minimal light transmission is represented by the non-aggregated platelets while maximum light transmission is achieved upon platelets aggregation. Platelet solutions with DMSO and subsequent addition of either collagen (3µg/mL) or thrombin receptor activating peptide (TRAP), a powerful platelet and PAR1 agonist, (0.1 units/mL) was used to establish agonist controls, while for the test solutions, compound **4** and **5** were added prior to agonist addition. The data indicated that no inhibition was observed after collagen or thrombin activation relative to the control. In contrast, both **4** and **5** slightly increased the light transmission signal at 10µM (Figure 3.4).

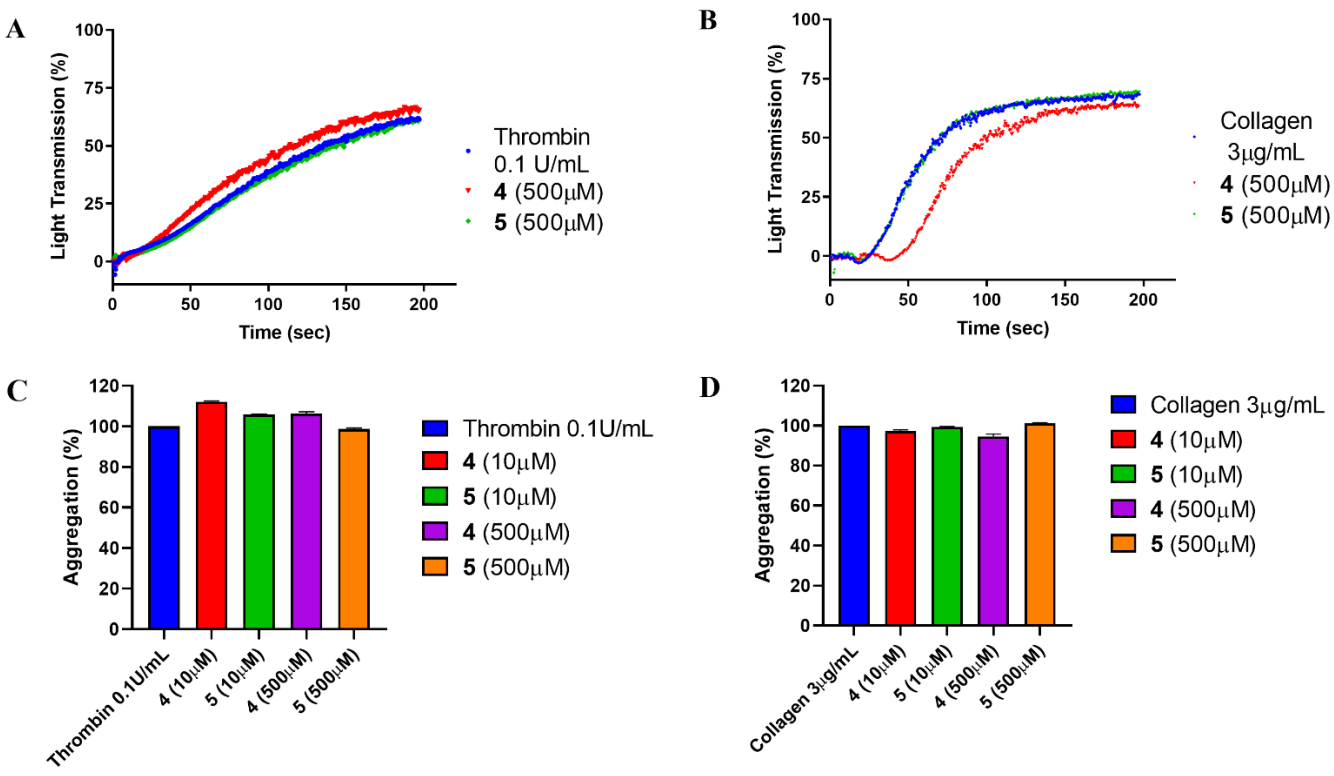
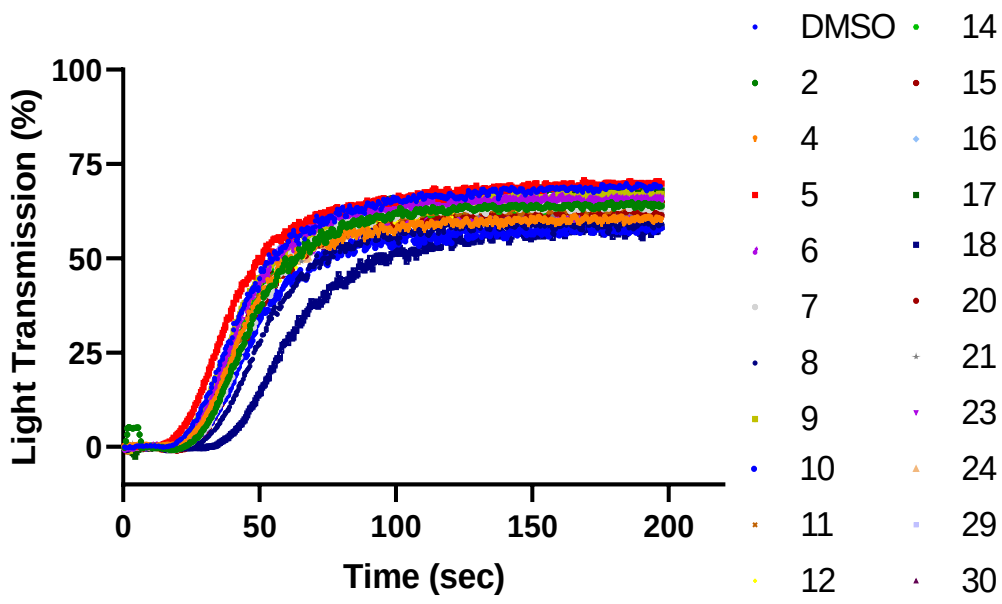


Figure 3.4. Compound 4 & 5 inhibition of collagen and thrombin-induced platelet aggregation. *Representative aggregation traces showing the effect of 10µM of compounds* ***4*** *&* ***5*** *of on (A) thrombin and (B) collagen-induced platelet aggregation in washed platelets in Tyrode's buffer. Percentage of aggregation effect of* ***4*** *&* ***5*** *in concentrations of 10µM and a high concentration of 500µM when incubated with platelets prior to addition of (C) 0.1units/mL of thrombin and (D) 3µg/mL of collagen. Aggregation was monitored by light transmission aggregometry at 37°C with constant stirring at 1200 rpm. The percentage of DMSO to washed platelets was 1/300. Data points were normalised to the corresponding agonist control of each donor to represent overall aggregation. Significance was measured using one-way ANOVA with a Dunnett post-hoc test where: P≤0.05. Data presented as mean±SEM from three different experiments performed in triplet (n=3).*

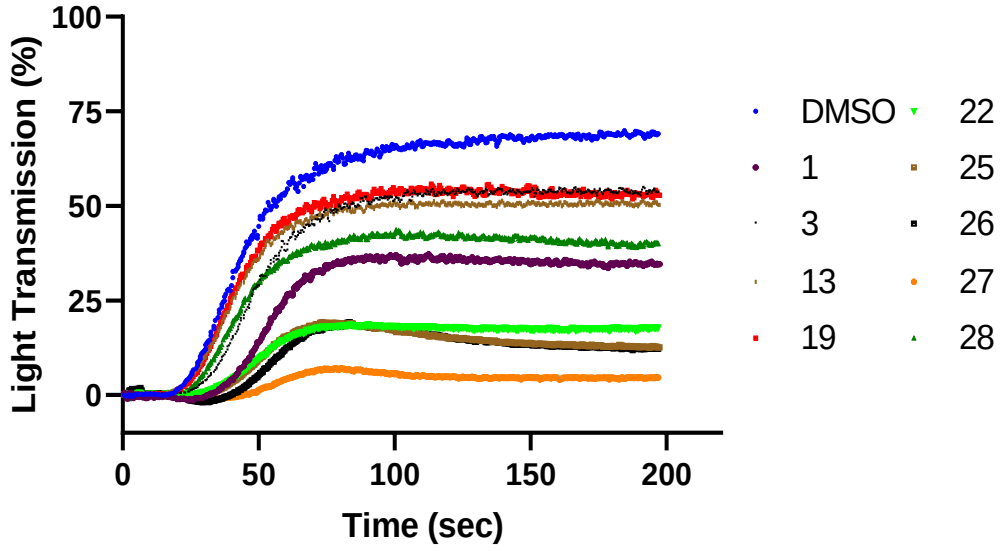
For screening purposes, 96-well plates of the compounds (Table 3.2 and Table 3.3) were generated by collecting them from the physical insourced MCCC library (BDI, School of Pharmacy, University of Nottingham, UK). The compounds were then tested against collagen-induced aggregation at a concentration of 10μM for their potential for platelet aggregation inhibition. The compound concentration remained constant in the next series of aggregation experiments. Although most compounds failed to inhibit collagen-induced platelet aggregation (Figure 3.5), four of them, **22**, **25**, **26** and **27**, lowered collagen-induced aggregation by more than 50% while another two, **28** and **1**, reduced it by more than 30%. Another one, **13**, which showed around 20% of signal reduction was also selected to ensure reproducibility. Five of them belong to the CRP group and two to the collagen group. Following the screening first-pass compound filtering, the seven compounds were tested again for reproducibility and account for experimental variation between blood donors.

A

i.


Light Transmission (%)
100
75
50
25
0
0
50
100
150
200
Time (sec)
DMSO
2
4
5
6
7
8
9
10
11
12
14
15
16
17
18
20
21
23
24
29
30

ii.


Light Transmission (%)
100
75
50
25
0
0
50
100
150
200
Time (sec)
DMSO
1
3
13
19
22
25
26
27
28

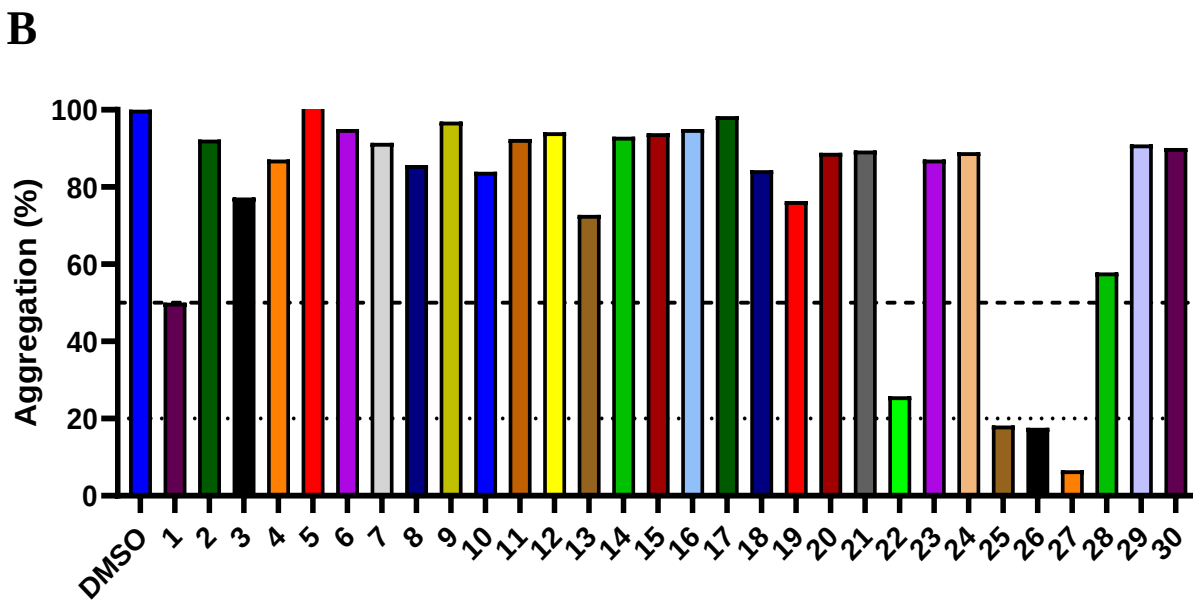
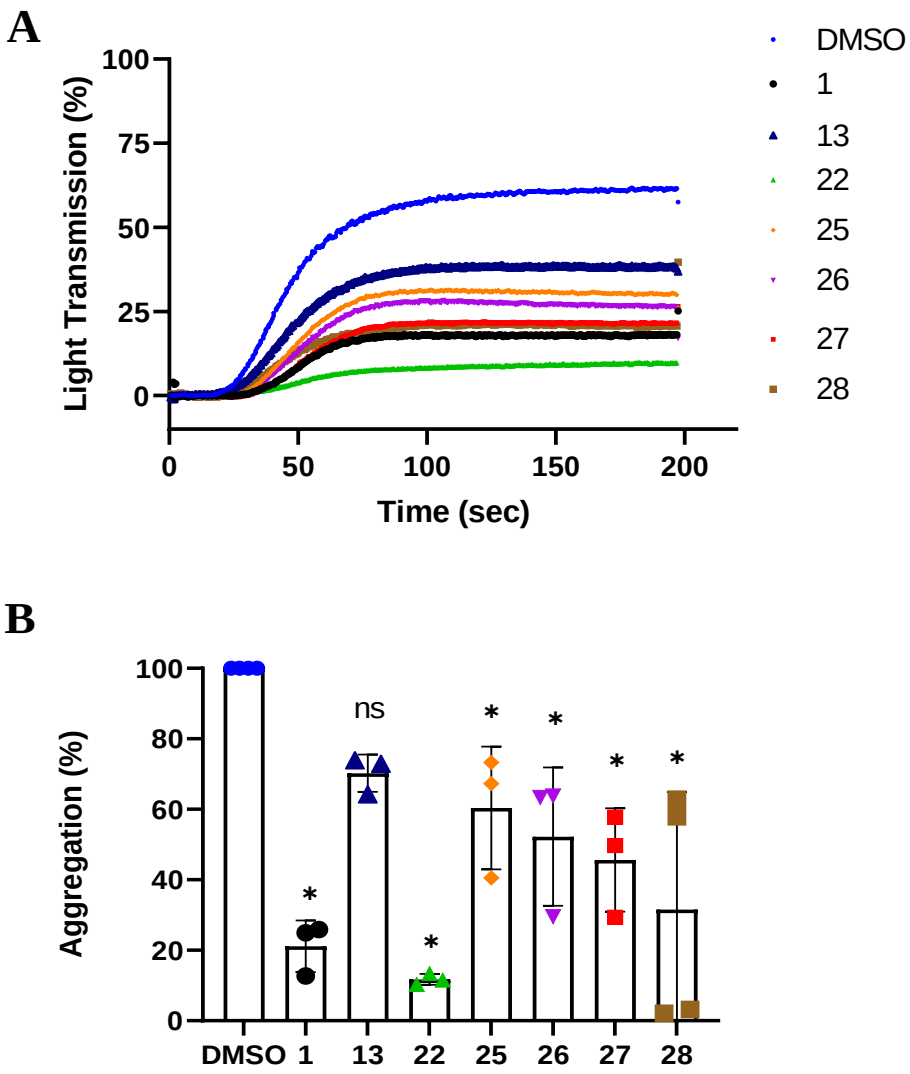


Figure 3.5. Inhibition of collagen-induced platelet aggregation by the 30 compounds selected for screening. *(A) Representative aggregation traces showing the effect of the 30 compounds (10μM) picked up by the virtual compound screening of the MCCC library on collagen-induced platelet aggregation in washed platelets. Compounds either had not effect (Ai) or more than 20% reduction effect (Aii) on light transmission through this assay. (B) The aggregation percentage of the control (DMSO) and each potential inhibitor were measured after addition of 3μg/μL collagen in washed platelets. Aggregation was monitored by light transmission aggregometry at 37°C with constant stirring at 1200 rpm. The percentage of DMSO to washed platelets was 1/300. Data points were normalised to the corresponding agonist control of the donor to represent overall aggregation. A 20% and a 50% threshold are marked in the graph as a dotted and a dashed line respectively. Data presented as maximum signal (n=1).*

From the seven compounds tested (Figure 3.6), only **22** consistently inhibited collagen-induced aggregation by more than 50% when tested in platelets of four more donors and had the lowest of variations between different blood donors. In particular, two out of four donors showed great variation, even though the compounds were tested on different days. Platelets were drawn from one donor per day and hence each n number represents a different day as well. **1**, **27** and **28** inhibition was around 40% for all three of them while a reduction of approximately 30% was seen by **25** and **26**. Inhibition of compound **13** remained around 20%.



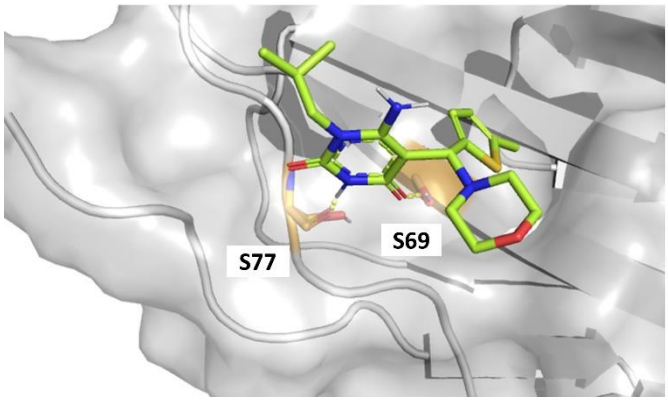
No.	*Inhibition activity (%)
1	49±4
13	17±4
22	55±3
25	34. ±7
26	31±8
27	26±7
28	41±11

Figure 3.6. Structure and aggregation assay of top seven compounds with inhibition properties against collagen-induced aggregation. *(A) Representative aggregation traces showing the effect of the top seven inhibitors from the aggregation assay (n=4) following the addition of 3µg/mL collagen. Compounds were tested at 10µM for their ability to inhibit collagen-induced platelet aggregation in washed platelets. (B) The aggregation percentage of the 3µg/µL collagen with DMSO control (left) and each potential inhibitor were measured after addition of 3µg/µL collagen in washed platelets. Aggregation was monitored by light transmission aggregometry at 37°C with constant stirring at 1200 rpm. The percentage of DMSO to washed platelets was 1/300. Individual data points are presented in this graph to emphasise on donor variability. Data points were normalised to the corresponding agonist control of each donor to represent overall aggregation. *Inhibition activity is measured as the difference between the maximum light transmission DMSO control of each donor (n=4) and the light output of each molecule. The error of the difference is represented as the standard error of difference. Significance was measured using one-way ANOVA with a Dunnett post-hoc test where: P≤0.05. 0.1234 (ns), 0.0332 (*), 0.0021 (**), 0.0002 (***), <0.0001 (****). Data presented as mean±SD (n=4).*

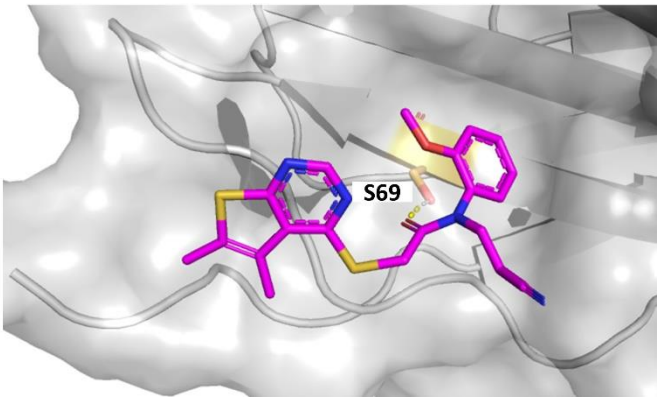
When looking at the docking poses of the seven inhibitors with the highest inhibition activity against GPVI (Figure 3.7), it seems that the molecules binding in the CRP pocket all bind GPVI residue S69 through a hydrogen bond donor and therefore this must be a key interacting residue for small molecule tethering. In fact, this was the only polar interaction that **22** formed. Other moieties within these molecules formed hydrogen bonds with GPVI residues R38, S77 and Q82 through hydrogen bond donors, as seen in molecules, **25** and **26**, while hydrogen bond acceptors formed interactions with moieties E40, S77 and Q82, as seen by molecules **1**, **25** and **27**. In addition, π-π stacking interactions, which are non-covalent interactions between the π bonds of aromatic rings, were also observed in molecules **1** and **26** with residue Trp76.

For the molecules that bind the collagen pocket, no common GPVI amino acids that bind both molecules were found. **13** shows hydrogen bonding through an amide moiety with residues V52 and F54 but was located outside the deepest part of the pocket cavity. On the other hand, **28** formed polar interactions with GPVI residues S61 and Y66 through a hydrogen bond acceptor and donor respectively (Figure 3.7).

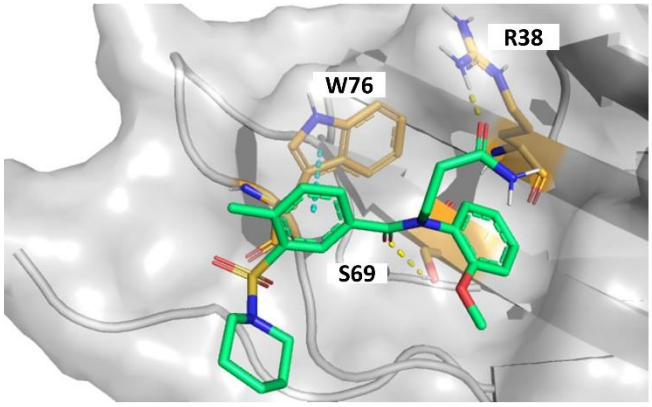
27



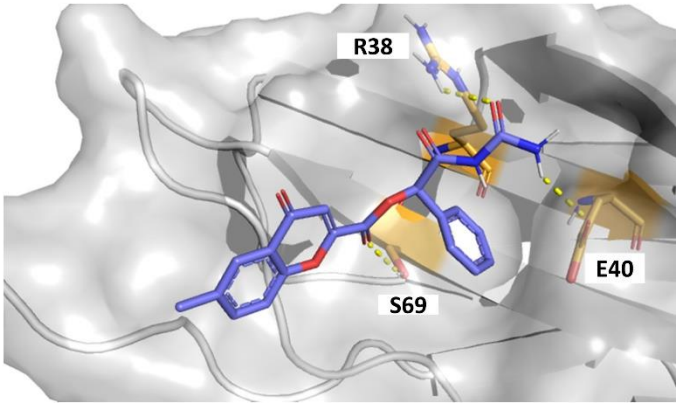
22



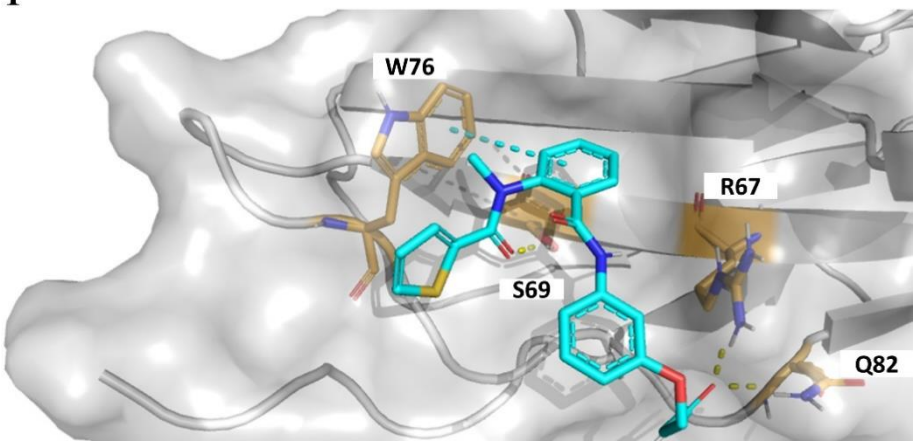
26



25



1



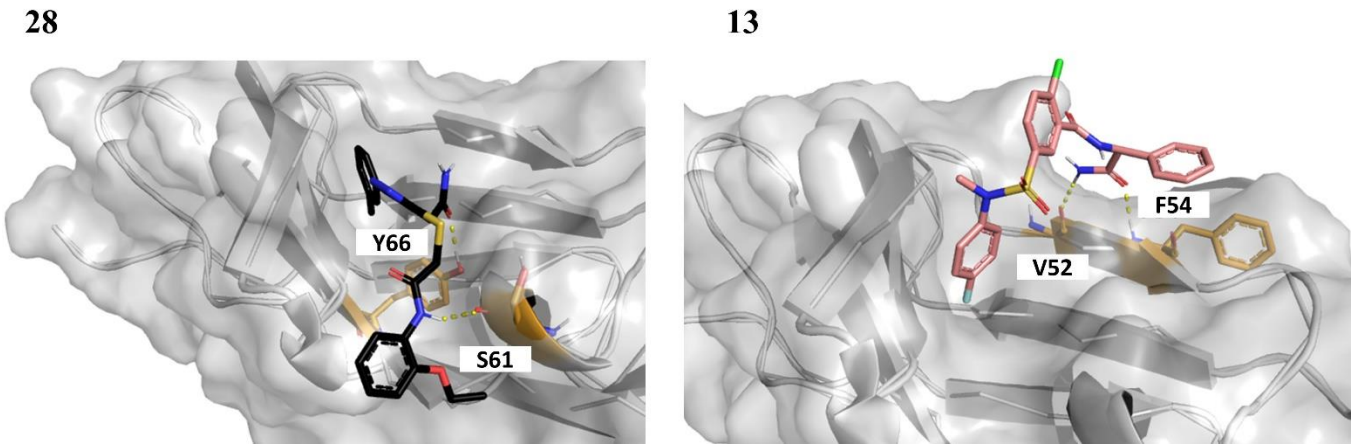


Figure 3.7. Top docking poses of the inhibitors within their corresponding binding pockets. *The chemical structures of the top seven selected hit compounds obtained following Glide function docking (Schrödinger Release 2018-1) using default settings and no docking restrictions. Docking pose visualisation of ligands in the receptor cavities and picture generation was conducted using PyMOL 2.2.0. Hydrogen bonds are coloured yellow and π-π stacking interactions are coloured cyan. The interacting amino acids for the CRP (**1**, **22**, **25**, **26**, **27**) and collagen (**13**, **28**) pocket are shown with the ones involved in polar interactions with each molecule highlighted and labelled. PDB: 2GI7.*

Two compounds (Figure 3.8) recently discovered in a combined virtual screening were found to inhibit collagen-induced platelet aggregation (Olğaç *et al.*, 2022). This study employed a similar workflow to the present study, including the grid coordinates, based on Sitemap results, and the use of a structure-based E-pharmacophore function. However, in the Olğaç et al. study, more than 6 million compounds from the MolPort 2016-10 database were screened for pharmacophore fitting. These compounds were tested in this study as alternative controls for GPVI inhibition by small molecules.

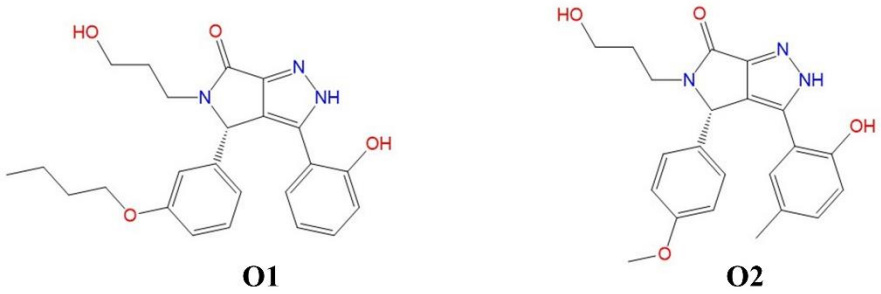


Figure 3.8. Chemical structures of compounds O1 and O1. *Compounds were outsourced from Otava Chemicals Ltd and correspond to the Olğac et al. (2022) study compounds* ***1*** *(O1) and* ***2*** *(O2).*

The next step was to distinguish whether the mode of action of these inhibitors is specific to GPVI or works synergistically with other receptors, such as PAR1, a major thrombin receptor that induces rapid and powerful platelet activation and aggregation, and CLEC-2, another major platelet ITAM receptor. For this purpose, the hits that showed an inhibition of collagen-induced platelet aggregation of over 40% (**1**, **22** and **28**) were chosen. The ones found in the Olğac *et al.* (2022) study, **O1** and **O2**, were also tested (Figure 3.). These compounds were tested for inhibition of platelet aggregation induced by thrombin receptor activating peptide (TRAP), a powerful platelet and PAR1 agonist, and rhodocytin, an agonist for ITAM platelet receptor, CLEC-2. A higher collagen concentration was also used to check if a dose-dependent relationship could be observed for any of the aforementioned inhibitors (Figure 3.9).

When all compounds were tested, all compounds fully inhibited aggregation at a collagen concentration of 3μg/mL (Figure 3.1A). At a higher collagen concentration of 10μg/mL, all compounds, except **28**, did not inhibit aggregation ($p \leq 0.05$) (Figure 3.1B). After addition of rhodocytin, it seems that **28**, **O1** and **O2** greatly affected rhodocytin-induced aggregation ($p \leq 0.05$) (Figure 3.1C). Similarly to rhodocytin, TRAP-induced platelet aggregation was not inhibited in a significant manner ($p \leq 0.05$) by **1** and **28** but not **22**, **O1** or **O2** (Figure 3.1D). **28** significantly inhibited all platelet agonists while **1** had an effect TRAP-induced platelet aggregation, and hence these two compounds do not operate through selective inhibition. Hence, significant inhibition effects of **22**, **O1** and **O2** were only shown following the addition of collagen at 3μg/mL, while other agonists were not significantly inhibited. Amongst the former, **22** had the most selective inhibition profile between the different platelet agonists. **22** was further tested alongside **O1** and **O2** to investigate their mechanism of action.

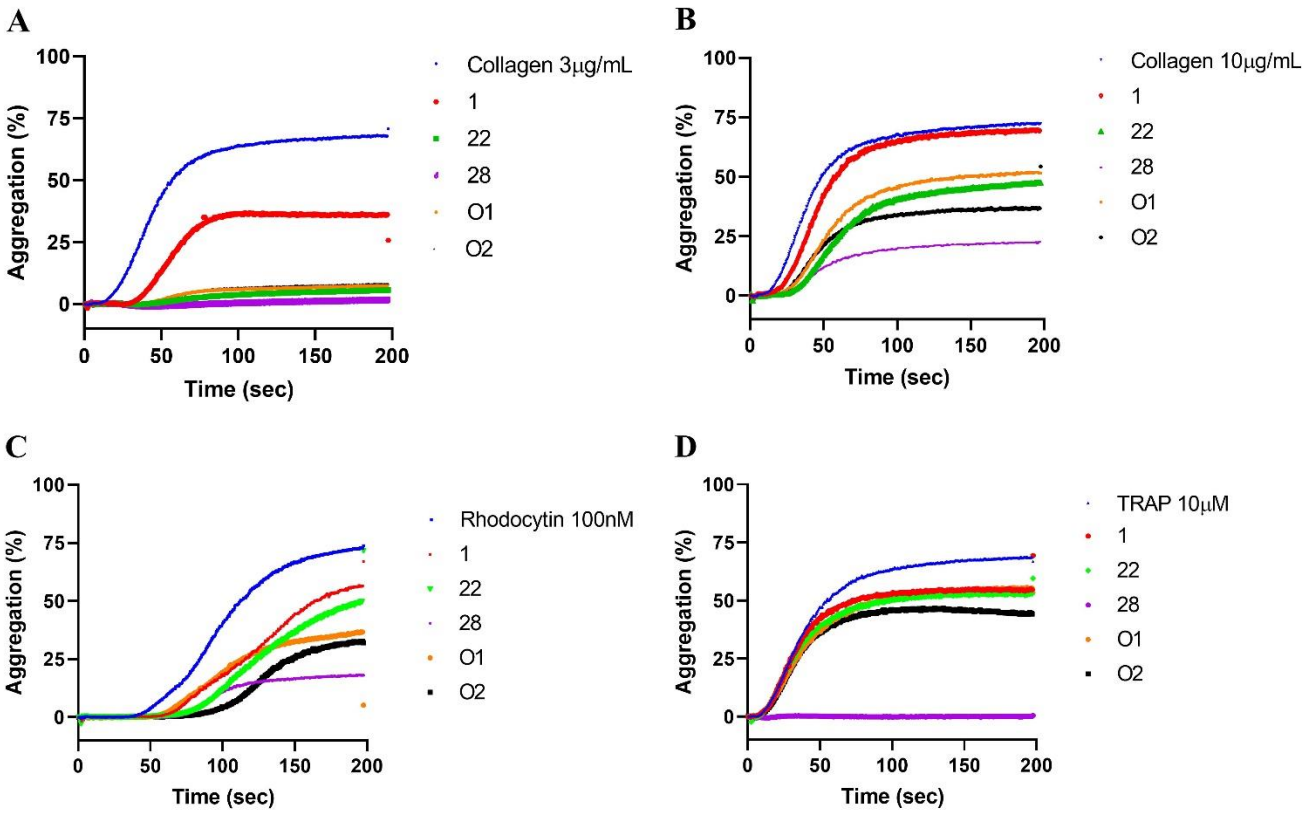


Figure 3.9. Summary data of light transition aggregation assays. *Representative traces of aggregation results (n=3). Each control includes 1:300 DMSO solvent to platelets and the corresponding platelet agonist concentration. All compounds were added at a final concentration of 10µM while the colouring of all compounds is constant in all graphs (Blue: Agonist control, Red:* ***1****, Green:* ***22****, Purple:* ***28****, Orange:* ***O1****, Black:* ***O2****). Aggregation results of pre-incubated platelets with an inhibitor followed by stimulation with (A) 3µg/mL and (B) 10µg/mL of collagen (GPVI receptor agonist), (C) 10µM of TRAP (PAR-1 receptor agonist) and (D) 100nM of rhodocytin (CLEC-2 receptor agonist).*

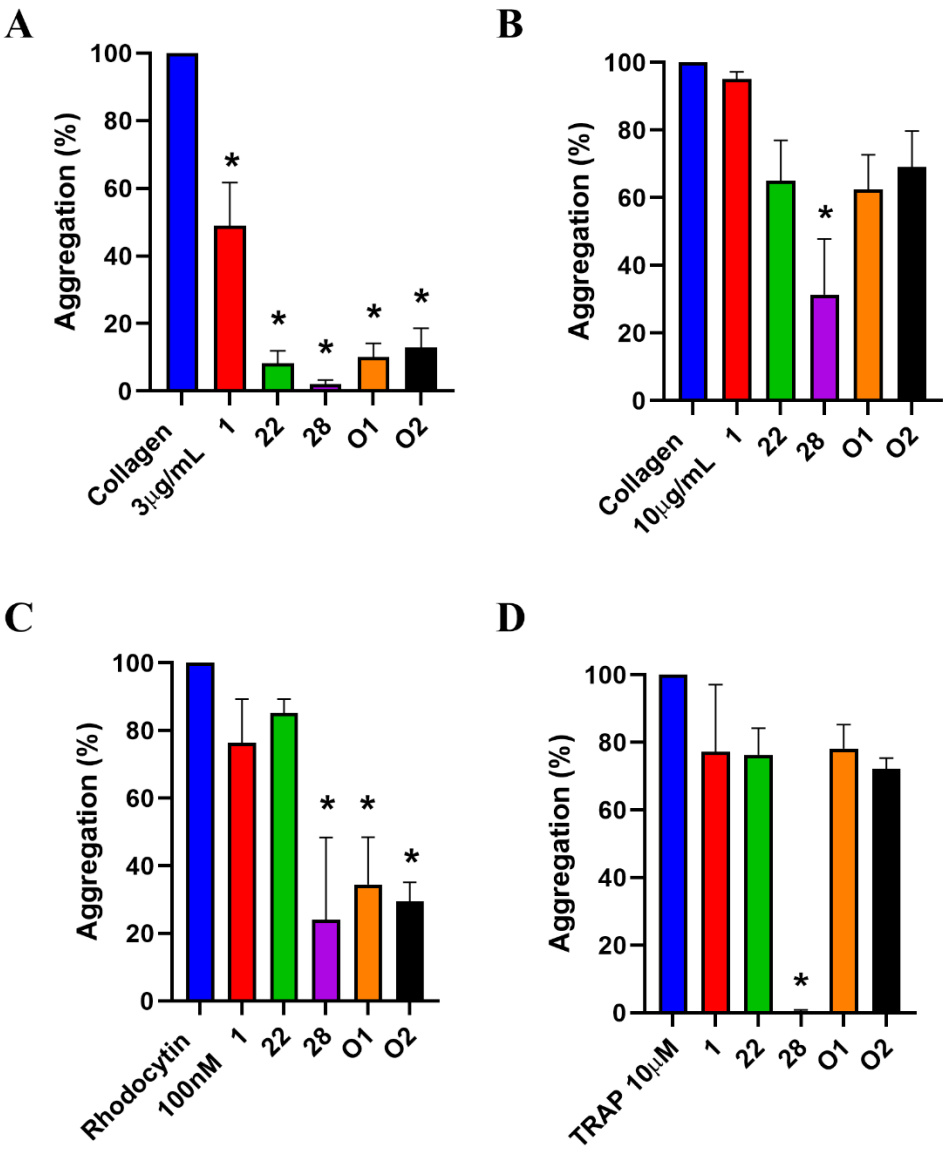


Figure 3.10. Average aggregation data and standard deviation values corresponding to the platelet aggregation experiments using 22, O1 & O2. *Agonist control,* ***22****,* ***O1*** *or* ***O2*** *were added in a platelet sample before the addition of (A) 3µg/mL of collagen, (B) 10µg/mL of collagen, (C) 100nM of rhodocytin or (D) 10µM of TRAP. (Blue: Agonist control, Red:* ***1****, Green:* ***22****, Purple:* ***28****, Orange:* ***O1****, Black:* ***O2****). The present values correspond to the average values in the plateau phase of the curve. In the case of rhodocytin the highest values, instead of the plateau average were used, where applicable. The increased standard deviation is derived from sample variation. The responses on rhodocytin correspond to the recorded time of experimentation (200 sec). Data points were normalised to the corresponding agonist control of each donor to represent overall aggregation. Significance was measured using one-way ANOVA with a Dunnett post-hoc test where: P≤0.05. Data presented as mean±SD (n=3). One extra independent experiment was conducted for rhodocytin for all compounds (n=4).*

3.3.5 Competition enzyme-linked immunosorbent assay (ELISA): 22, O1 and O2 binding to monomeric or dimeric recombinant GPVI

After identifying three candidate antagonists for GPVI, the next step was to confirm whether compounds are inhibiting collagen binding through a competitive or non-competitive manner. Since increasing the concentration of collagen to 10μg/mL was able to overcome the inhibition seen on a lower collagen concentration, 3μg/mL, it is expected to observe a competitive inhibition of GPVI tethering to collagen. Concurrently, we wanted to explore whether they can selectively inhibit collagen binding in the monomeric or the dimeric form of GPVI. A competition enzyme-linked immunosorbent assay (ELISA) was employed for this task and a potent nanobody inhibitor raised against human GPVI, Nb2 (Slater *et al.*, 2021), was used as positive control.

The 96-well ELISA plates were coated 100μL of collagen (4μg/mL) and inhibition was tested in a mixture of a constant GPVI construct concentration of 100nM with increasing compound concentrations (Figure 3.14). None of the compounds inhibited collagen binding in concentrations up to 100μM, unlike Nb2 that completely inhibited the interaction of collagen to GPVI with both constructs at a concentration 1000 times lower.

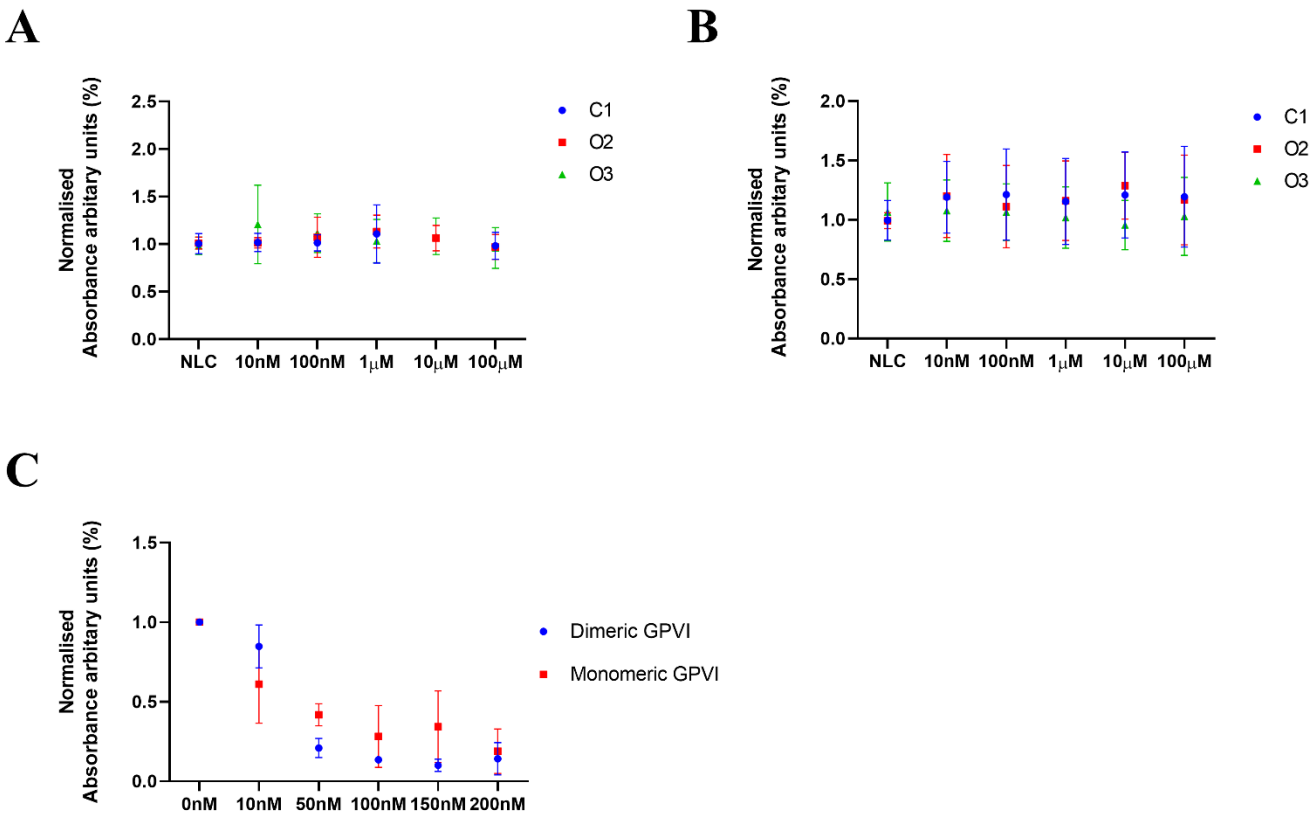


Figure 3.14. Competition ELISA of dimeric and monomeric GPVI binding to GPVI with collagen and 22, O1 & O2. *ELISA 96-well plate layout of competition ELISA between compounds* ***22***, ***O1*** *and* ***O2*** *and GPVI-Fc (dimeric GPVI) or GPVI (monomeric GPVI). The plates were coated for 15-18 h with Horm collagen (4μg/mL). Each GPVI construct concentration, dimeric (A) or monomeric (B), per well was 100nM was added simultaneously with of 10nM, 100nM, 1μM, 10μM and 100 μM of* ***22***, ***O1*** *or* ***O2*** *concentrations.. Anti 6 His-HRP or anti-IgG-Fc-HRP, for monomeric and dimeric GPVI, respectively, were used for selective GPVI form detection. (C) Positive inhibition control Nb2 was added simultaneously with 100nM of wither monomeric or dimeric GPVI of 10nM, 50nM, 100nM, 150μM and 200 μM. Mean fluorescence intensity (MFI) values were normalised to No-Ligand Control (NLC, 1% DMSO) cell values. Data represented as mean±SEM from three different experiments (n=3).*

3.3.6 Effect of 22, O1 & O2 on NFAT signalling

Following the results from aggregation and ELISA experiments, the next step was to investigate the effect of these molecules on GPVI signalling. This would clarify whether the compounds are still able to inhibit GPVI signalling through non-competitive binding to an allosteric site or that the effect of these molecules is mostly non-specific. For this purpose, an NFAT-luciferase reporter assay in a DT40 cell line was utilized. An NFAT assay format for sustained GPVI signalling in DT40 cells has been previously described (Tomlinso*n et al*., 2007).

The NFAT-luciferase assay involves the insertion of an NFAT reporter gene conjugated to a luciferase enzyme. NFAT expression is driven by activation of protein kinase and elevation of Ca^{2+}, with a combination of PMA and Ca^{2+} ionophore serving as a positive NFAT signalling control. DT40 cells were chosen based on the fact that it is a haematopoietic cell line and that it shares signalling proteins with the ones found in the GPVI signalling cascade.

Despite their ability to inhibit collagen at low-mid micromolar levels, as demonstrated in the aggregation assay, the tested molecules only inhibited wild-type (WT) GPVI signalling at concentrations greater than 100μM (Figure 3.15). 125μM of 22, O1 and O2 reduced collagen-induced signalling while the presence of a higher concentration, 200μM, resulted in signal levels which were lower than the basal ones. Positive control Nb2 brought inhibition to basal levels at a concentration 100 times lower (1μM). The transfection efficacy for this set of experiments was approximately 50% (Figure 3.16).

Since none of the compounds tested display significant inhibition or selectivity at concentrations of 25μM, these agents were not further investigated and hence are not mentioned in following chapters.

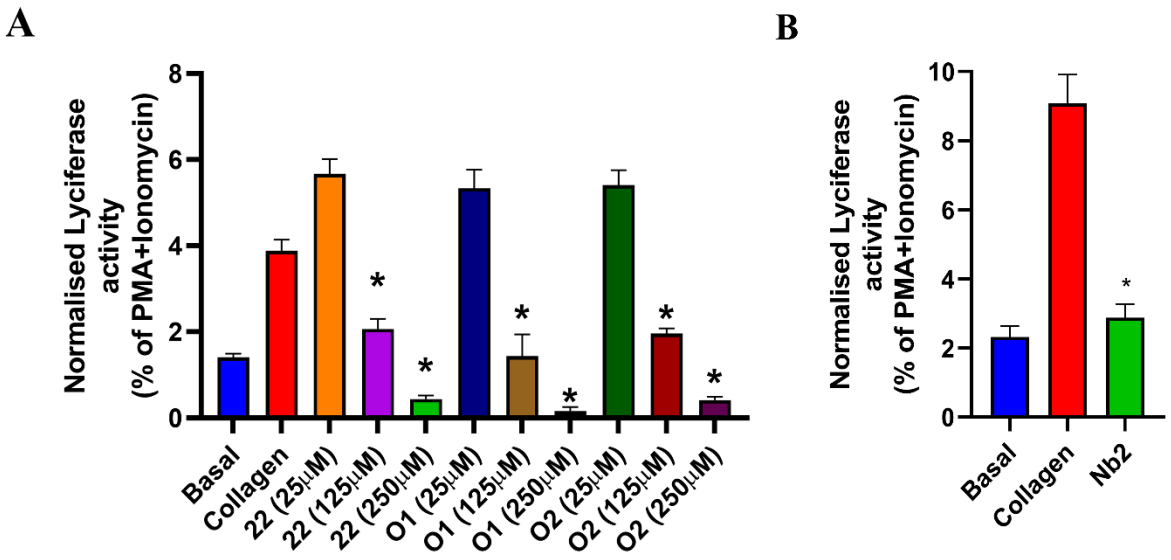


Figure 3.15. Effect of 22, O1 & O2 on collagen signalling. *The DT40 cell line was transfected with a nuclear factor of activated T-cells (NFAT)–luciferase reporter construct 2µg of plasmid each of GPVI and FcRγ expression constructs or empty vector controls. The NFAT-luciferase DNA quantity was 15µg. Sixteen hours post-transfection, expression of GPVI was confirmed by flow cytometry. Cells were either left unstimulated (DT40 control), or were stimulated with collagen (10µg/mL) after addition of (A) 25, 125 or 250µM of* ***22****,* ***O1*** *or* ***O2*** *or (B) 1µM of Nb2, or phorbol 12-myristate 13-acetate (PMA) (50ng/mL) plus ionomycin (1µM). Six hours later, cells were lyzed and assayed for luciferase. Raw data of luciferase activity are shown here as arbitrary units (AU). Luciferase data were normalized for PMA plus ionomycin values and are presented as a percentage of the positive control PMA plus ionomycin response. The DT40 control values have been subtracted from the test data sets before normalization. Significance was measured using one-way ANOVA with a Dunnet post-hoc test where: P≤0.05. Statistical significance was compared to collagen while error bars represented as mean±SEM from three different experiments performed in triplicate (n=3).*

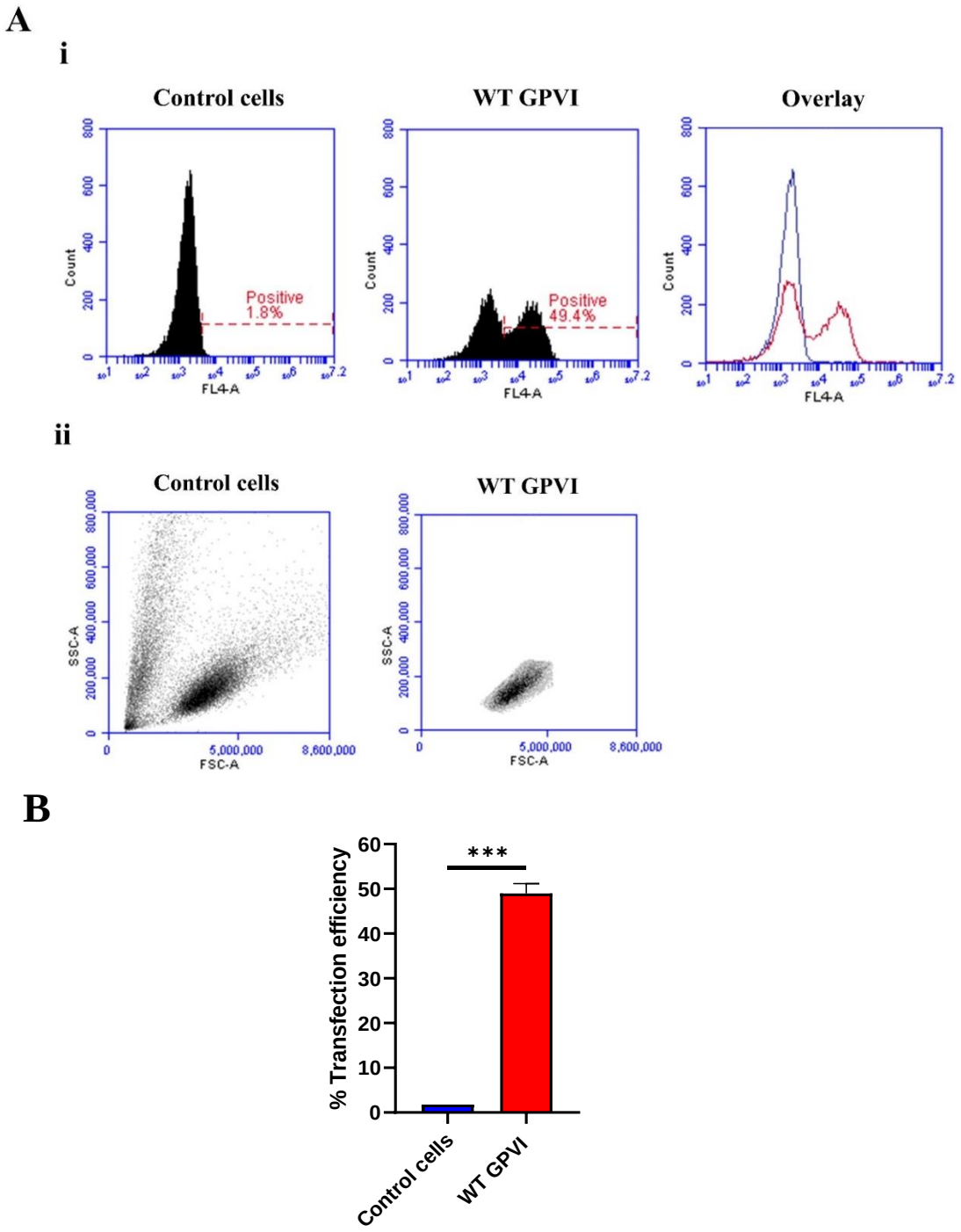


Figure 3.16. Expression of different GPVI DNA quantities in DT40 cells. *GPVI expression was detected by flow cytometry to detect transfection efficacy. DT40 cells were transfected using electroporation with 2µg wild-type (WT) GPVI, 2µg human FcRγ chain and 15µg of NFAT luciferase reporter construct DNA. (Ai) Representative histogram of geometric mean fluorescence intensities of GPVI-positive in DT40 chicken B cells were detected using an anti-GPVI HY101 antibody (1:400) and an anti-mouse Alexa Fluor-647 secondary antibody for staining (1:400). (Aii) Flow cytometry data displayed as dot plots of fluorescence versus forward scatter. Gating was applied to exclude any counts outside the gating range. (B) Flow cytometry data are presented as the transfection efficiency of WT GPVI showing percentage of cells positive for indicated GPVI receptor. Significance was measured using a Student's t test where: P≤0.05. Statistical significance was compared to basal while error bars represented as mean±SEM from a single experiment performed in quadruplet (n=1).*

3.4 Discussion

The goal of this Chapter was the development of small molecule ligands through *in silico* modelling techniques to be used as a tool for the identification of more selective and potent ligands for GPVI, due to the low number and selectivity of small compound inhibitors for GPVI. Studies on the development compound GPVI inhibitors mostly utilise a defined site within this region backed by virtual screening findings (Taylor *et al.*, 2014; Bhunia *et al.*, 2017; Olğaç *et al.*, 2022) or the use of GPVI ligands losartan and pep-10L in structure-based approaches using NMR (Kato-Takagaki *et al.*, 2009; Ono *et al.*, 2014). However, a limitation of these approaches is the lack of crystallography data available to pinpoint the location of the collagen binding site and the use of low potency precursors for inhibitor design (Damaskinaki *et al.*, 2021). The literature related to the GPVI binding site of collagen mostly comprises mutation studies (Lecut *et al*., 2004; Smethurst *et al*., 2004, 2007; O'Connor *et al*., 2006; Arthur *et al*., 2007; Kato-Takagaki *et al*., 2009; Loyau *et al*., 2012) that place the binding site as spanning through a linear-like area, formed in the D1 region of the Ig immunoglobulin (Chapter 1). According to recent crystallographic data, the CRP binding site (Feitsma *et al*., 2022) is proximal to the suggested collagen one (Lecut *et al*., 2004; Smethurst *et al*., 2004; O'Connor *et al*., 2006).

During *in silico* investigations, a challenge during the design of the virtual screening is that there in not a pocket in D1 domain, according to the crystal structures available for GPVI (PDB: 2GI7, 5OU7-9), that is deep and hydrophobic enough for tethered molecules to generate high docking scores. This was confirmed by the low docking scores, represented as changes in Gibb's free energy (ΔG) of bound molecules to GPVI. For this purpose, SiteMap was used to identify a binding site with the highest druggability. The final decision was made based on literature findings, crystallography data of the CRP binding site, SiteMap score, and proximity to amino acids important for collagen, CRP or ligand binding. The resulting pockets were the collagen pocket and the CRP pocket, each referring to the small molecule binding region within the collagen binding site and the CRP binding site respectively.

Each of the pockets in all PDB files that corresponded to the selected pockets was used to generate an E-model pharmacophore from the receptor cavity. The structures that had the best pharmacophore alignment were then chosen for virtual docking experiments. The structure-based pharmacophore generated in this study was not biased towards the docking of losartan or **5** within the GPVI binding site, unlike previous virtual screening attempts. This was applied

so that there was no restriction in the chemical space available for this screen and the potential for identification of new receptor-ligand interactions and higher affinity ligands. The generated pharmacophore was, therefore, different yet the elements of both pharmacophores generated by Olğac *et al*. (2022) were all present in the pharmacophore generated in this study for the collagen pocket. This includes two hydrogen bond acceptors, a hydrogen bond donor and a negative charge with their coordinates being in close alignment (Figure 3.). This indicates that these common elements are indeed predicted to be critical for strong ligand binding. The CRP pocket was not previously explored for docking studies of small molecules and hence had not any reported reference. This is not surprising due to the shallow, wide and predominantly hydrophilic nature of this binding surface which might be more suited for docking natural compounds, peptides or larger ligands in general.

Compounds **5** and **4** were tested against a platelet aggregation assay in washed platelets as a positive and negative control. Although **4** indeed did not show any inhibition of collagen-induced platelet aggregation, **5** also showed no significant inhibition activity in washed platelets. The original study tested **5** in PRP, instead of washed platelets, and it showed a 20% inhibition when tested at 10μM and a collagen concentration of 2 μg/mL. In combination with a higher collagen concentration used in this study (3 μg/mL), the heterogeneity of PRP or PRP-specific elements might be participating in the inhibition process and hence more studies need to be conducted for these compounds, including direct binding to GPVI.

The 15 compounds with the highest docking score (30 compounds in total) from each pocket were selected for screening. Using light transmission as a physical screening tool, the results indicated that only seven compounds were able to significantly inhibit collagen-induced platelet aggregation with **1**, **22** and **28** in a consistent manner and having an inhibition effect of over 40%. All molecules comprised three rings, most of them aromatic, linked with short polar linkers. Five were from the CRP pocket docking group while two were from the collagen pocket docking pocket. The ones from the CRP docking pocket seems to comprise multiple aromatic and aliphatic rings linked with short polar linkers which includes polar atoms in one of its aromatic rings. All of the compounds from this group formed hydrogen bonds with Ser69 through hydrogen bond acceptors within the polar linker group. The only exception **27**, which elucidated hydrogen bonding with the GPVI residues, including Ser69, through its pyrimidine-2,4(1*H*,3*H*)-dione ring. From the collagen group, the molecules also had multiple aromatic rings, but no aliphatic rings, linked with short and highly polar linkers. Both molecules formed

hydrogen bonds with the GPVI residues. It has to be noted that CRP was not implemented as an agonist in this assay and therefore the effect that the inhibitors picked from the CRP pocket virtual screening is not tested.

When investigating the biological activity of these inhibitors, the most effective inhibitor was **22** and was further compared to two outsourced small molecule inhibitors as positive controls, **O1** and **O2** (*Olğaç et al*., 2022). Collagen-induced aggregation was while was minimally affected while TRAP or rhodocytin-induced aggregation was minimally affected. The effect seen in rhodocytin was time-depend as it was fully overcome when letting the experiment occur for a longer period (>3 min). None of the compounds tested were able to compete with Horm collagen in a competition ELISA set-up of immobilised dimeric or monomeric GPVI. In contrast, Nb2 inhibited GPVI tethering to collagen which inhibited this interaction. This effect was more profound from 50 nM onwards with the 10nM having a big variability to give confidence to these results, though it seems to affect monomeric GPVI in a greater extent. This effect is most likely attributed to the lower number of GPVI binding sites in this construct. The inhibition effect on platelet aggregation could have been mediated by non-competitive binding. Through NFAT-luciferase assay it was confirmed that **22**, **O1** or **O2** could not inhibit collagen-induced GPVI signalling at 25 μM. A significant reduction was seen at 125 μM and 250 μM. However, these concentrations are too high and the signal reduction in luminescence could be attributed to luciferase off-target inhibition rather than selective GPVI inhibition. Compounds were not added in the PMA + ionomycin positive controls to see if they had an effect on the relevant biological cascade as well. A firefly luciferase-related counter screen needs to be implemented and concentrations lower than 125 μM need to be implemented to make a definitive conclusion on this assay.

Unlike the small molecules inhibitors that have been reported for GPVI, the endogenous ligands and antibodies use avidity and a complex multi-interaction network to create a high affinity binding to GPVI (Clar*k et al*., 2021; Xu *et al*., 2021; Feitsma *et al*., 2022). The size and interaction potential, that proteins are inherited with, are two properties that complement each other and are hard to balance in a small molecule. Given the challenging receptor shape, it would be more appropriate for virtual screens to utilise large and diverse structures, such as natural compound libraries, rather than libraries with compounds of Lipinski's drug-like properties. Natural compound libraries are abundant in chemotypes with higher flexibility and complexity than conventional drug libraries, properties that increase the chance of identifying

a multi-interaction or high complexity ligand through screening. Another approach would be to employ a screening of the full MCCC library, without a pharmacophore screening step, to include more potential compounds.

In conclusion, a virtual screen using a structure-based pharmacophore was developed for both the known small molecules' binding pocket within the collagen binding region and the previously non-explored CRP pocket. A selective effect on collagen-induced aggregation was observed over rhodocytin or TRAP-induced aggregation for compound **22**. However, competition ELISA did not show any competition of GPVI with collagen while it failed to inhibit GPVI-mediated NFAT signalling up to 25 μM. Hence, the hits generated in this study are not likely to exert inhibition through a GPVI-selective mechanism. Co-crystallization with potent ligands, such as literature described nanobodies (Slater *et al.*, 2021), is needed to give a clear insight on the binding mode of strong binding ligands. Mapping the binding sites of these ligands will open up the field for further investigation of GPVI inhibitors. Chapter 4 explores the information gained by Nb2 and another nanobody crystallised in the present study, Nb35, which could potentially be exploited for the effective design of future virtual screens for GPVI ligands.

Chapter 4

Mapping the binding sites of nanobodies on GPVI

4.1 Introduction

The majority of current targeting strategies to block GPVI include protein ligands that compete for collagen binding, with two anti-GPVI agents having entered clinical trials. The first, Revacept, is a soluble recombinant dimeric fusion protein (GPVI-Fc) comprising two ectodomain copies of GPVI, which competes with platelet GPVI for binding to collagen (Goebel *et al.*, 2013; Harbi *et al.*, 2021). It has completed phase II trials for its use in symptomatic carotid stenosis (NCT01645306) and stable coronary artery disease (NCT03312855). Only the latter has been reported, with no reported side effect (Mayer *et al.*, 2021), possibly due to the trial design which focussed on stable disease. The second is a blocking monoclonal antibody fragment, ACT017, renamed as glenzocimab (Voors-Pette *et al.*, 2019), which completed a phase II clinical trial (NCT05070260) as an add-on therapy for thrombolysis/thrombectomy treatment during the acute phase of ischaemic stroke. The primary endpoint of the trial was safety, but there was a clear trend to efficacy and a decrease in bleeding (ACTICOR BIOTECH, 2022).

Several other monoclonal antibodies and antibody fragments have been raised against GPVI, including 9O12, JAQ1, 1G5 and 12A5, that bind GPVI with high affinity and block activation by collagen (Nieswandt, Schult*e, et al*., 2001; Lecut *et al*., 2003; Al-Tamimi *et al*., 2009). Glenzocimab is a humanised form of 9O12.2 (Voors-Pette *et al.*, 2019). Attempts to identify the epitopes of certain antibodies have been described, as is the case for 9O12 (Lecut *et al.*, 2004) and 10B12 (Smethurst *et al.*, 2004). Using molecular and homology modelling to generate the ectodomain of GPVI, the binding sites of 9012 and 10B12 were mapped to the D1 domain, which was also supported by binding assays, with 9O12 residing in an adjacent but not identical site to that of 10B12. However, it has been reported that structural characterisation of the co-crystal glenzocimab in complex with extracellular monomeric GPVI shows that the site of interaction of glenzocimab is to the D2 domain of GPVI (Jandrot-Perrus, 2022). Glenzocimab binding induces both allosteric modulation of the CRP binding site, through a shift within the βC strand and consequently the position of Arg38, an important residue for CRP binding, and steric hindrance, through the light variable chain, to inhibit CRP and collagen binding. Removal of GPVI residues in the D2 domain, 129-136, that comprise multiple CRP contact points, blocked glenzocimab binding, supporting the aforementioned findings (Jandrot-

Perrus, 2022). It is therefore essential that structural characterisation and visualisation is implemented to address the limitations of mutagenesis studies and modelling.

Recently, 54 nanobodies (Nb) were raised against the recombinant Ig domains of GPVI (Slater *et al.*, 2021), from which three, Nb2, Nb21 and Nb35, were selected as the most potent inhibitors of platelet aggregation to collagen and CRP (IC_{50} values of 172, 85, and 115nM for Horm collagen (5 μg/ml) and 1, 22, and 1nM for CRP (10 μg/ml), respectively). Also the same nanobodies blocked GPVI-Fc (100nM) binding to a Horm collagen surface in a solid-phase binding assay with IC_{50} values for Nb2, Nb21 and Nb35 of 18, 61, and 39nM, respectively (Slater *et al.*, 2021).

One of the main challenges in developing small-molecule inhibitors for GPVI is the lack of knowledge of the ligand binding sites, as well as an absence of potent small molecule inhibitors to serve as lead compounds. The former has changed with the co-crystallisation of CRP and GPVI (Feitsma *et al.*, 2022) (PDB: 5OU8,9) and the demonstration of multiple sites of contact as discussed in Chapter 1. In addition, a recombinant GPVI N72-glycosylation mutant (GPVI NQ), in which the N-glycosylation site in D1 domain (N72) had been mutated to a glutamine residue was successfully co-crystallized with Nb2 and the binding site mapped by X-ray crystallography (PDB: 7NMU). The binding site of Nb2 is adjacent to that of CRP in the D1 domain suggesting that the inhibitory effect of Nb2 is due to steric hindrance, as shown in Figure 4.1A, based on the data from recent studies (Slater *et al.*, 2021; Feitsma *et al.*, 2022).

As discussed in section 1.4.3., the structure of the Nb2-GPVI complex also revealed a novel domain swap, where two D2 domain from GPVI monomer exchange structural elements and fold into a dimer (Slater *et al.*, 2021),facilitated by the presence of an extended loop that forms a domain swap hinge. The authors showed that deletion of this hinge did not affect Nb2 binding but collagen-induced GPVI signalling was abolished. Although the evidence suggest that this domain swap may be a functional dimeric GPVI conformation, this may be a conformation induced by the crystallization conditions or stabilisation by Nb2 of this conformation in the crystal. Binding of the CDR3 loop to the top of the CRP binding groove in D1 and the C` β-sheet causes a shift of around 1.5Å and subsequently a small distortion of the groove in addition to steric hindrance which may impair CRP and collagen binding (Figure 4.17B). The amino acids involved in the polar interaction with GPVI include the residues: Glu21, Ser45-Gln48, Pro56, Ala57 and Ser61 (Figure 4.17C). The majority of these interact with residues from the Nb2 CDR3 loop, while Ser45, Arg46 and Tyr47 are directly adjacent with the binding site for

CRP. One residue from the CDR1 region, Tyr31, also forms a hydrogen bond with residue Gln48. The binding site of Nb2 appears to be in close proximity to residues Lys59 and Arg60, which greatly reduce collagen and CRP binding affinity when mutated (Smethurst *et al.*, 2004; Horii *et al.*, 2006; O'Connor *et al.*, 2006), and are proposed to distort the binding site for collagen or CRP. The amino acids involved in CRP binding are described in more detail in Chapter 1.

These findings, alongside the progress made in structural characterization of GPVI-ligand complexes, have now opened up the field to further explore the binding site of potent GPVI ligands, such as nanobodies, and determine their mode of binding. This knowledge may also help identify potent small molecule inhibitors.

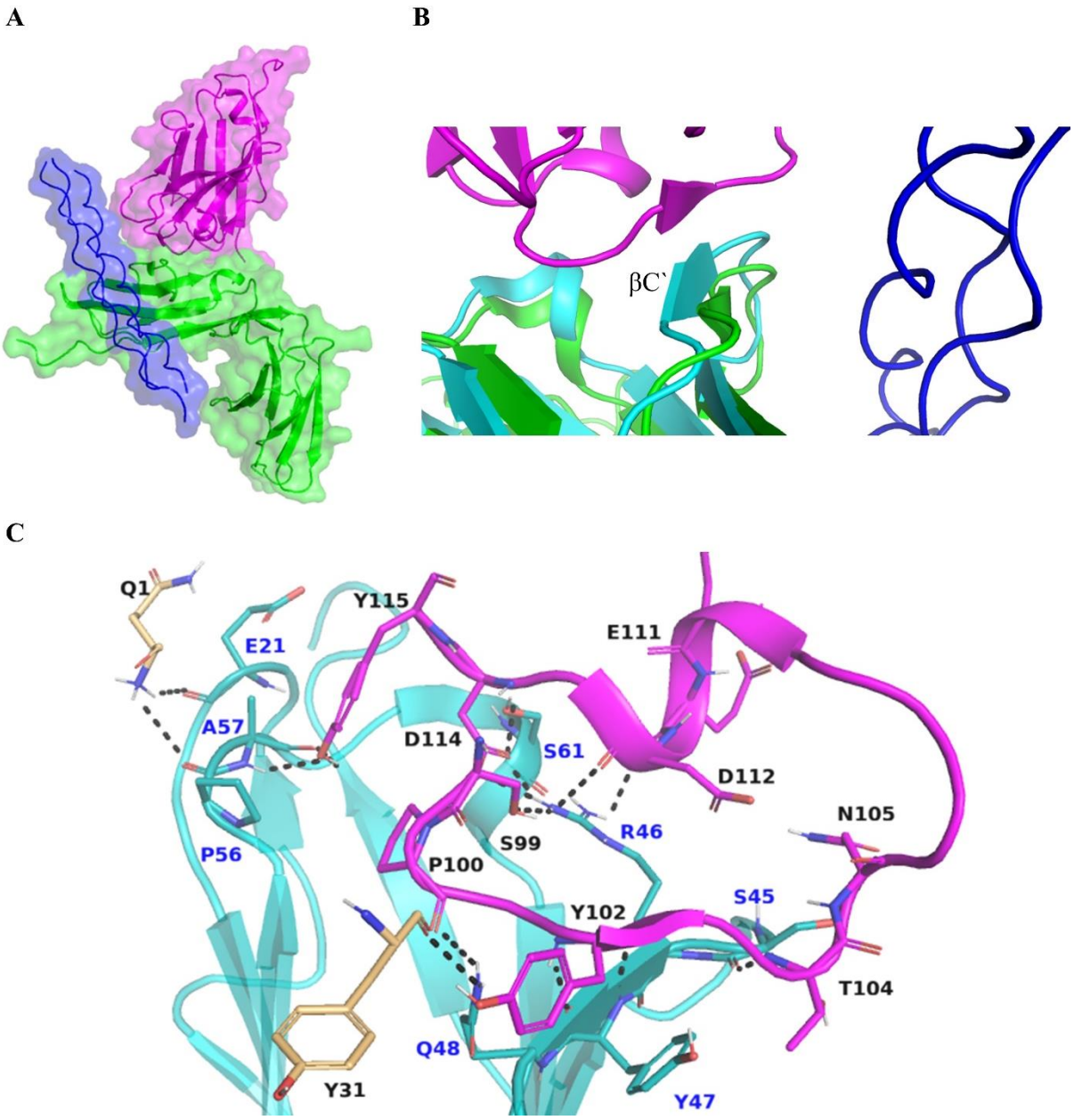


Figure 4.17. Binding interface of Nb2 to the surface of GPVI. *(A) The binding sites of Nb2 and CRP are shown in a surface and cartoon representation of Nb2 (magenta) modelled onto the GPVI structure (green) bound on CRP (blue). (Nb2, PDB: 7NMU; CRP/GPVI, PDB: 5OU8). (B) Cartoon view of the CRP binding groove within GPVI before (green) and after Nb2 binding (cyan) with the βC` labelled, showing a 1.5Å shift between the two conformations. CRP is shown in blue and Nb2 in magenta. (C) Zoomed view of the amino acids involved in polar interaction of the GPVI D1 domain (cyan) with the Nb2 CDR3 loop amino acids Glu21, Ser45-Gln48, Pro56, Ala57 and Ser61 (E21, S45-Q48, P56, A57 and S61), and those interacting with the CDR1 loop (E21 and P56). The GPVI amino acids are shown as green sticks with blue labels. The Nb2 residues involved in polar interactions with GPVI from the CDR3 loop coloured in magenta Tyr31, Ser99, Pro100, Ty102, Thr104, Asn105, Glu111, Asp112 and Asp114 (Y31, S99, P100, Y102, T104, N105, E111, D112 and D114) and non-CDR3 residues in orange Gln1 and Tyr115 (Q1 and Y115) and their corresponding labels are coloured in black. The CDR3 loop is shown in a cartoon representation while the amino acids that make polar interactions with GPVI are shown in sticks. Black dashes indicate hydrogen bond interactions between Nb2 and GPVI. Images adapted from Slater et al., (2021).*

4.2 Aims

Uncovering the interactions between potent inhibitors and GPVI will further aid the design of novel anti-GPVI therapeutic agents. Hence, the focus of this chapter lies in using X-ray crystallography to map the binding site of newly developed GPVI-specific nanobodies to the surface of the receptor and to support this using directed mutagenesis and binding displacement studies. This information will identify key interactions that characterize high-affinity GPVI ligands. The lack of sequence overlap within the CDR3 loops between Nb2, Nb21 and Nb35, the three most potent inhibitory nanobodies, suggests that there may be unique and shared amino acids on GPVI.

4.3 Results

4.3.1 Crystallisation of GPVI in complex with nanobodies 21 and 35

In addition to Nb2, Nb21 and Nb35 were potent inhibitors of CRP and collagen induced GPVI signalling and platelet aggregation (Slater et al., 2021). Combined with the low sequence overlap with Nb2, especially the CDR3 region which is the major Nb2 binding region, with an alignment score of 21.1% for the CDR3 region of Nb21 and 31.6% for the one Nb35 (generated with ClustalW 2.1 Mutliple Sequence Alignment) (Figure 4.2), these nanobodies were candidates for crystallisation. The low sequence overlap indicates that these nanobodies may bind to distinct sites on GPVI to that Nb2 and could therefore be used to identify novel binding pockets

```
Nb2       QVQLQESGGGLVQPGGSLRLSCAAAGFTFDYYAIAWFRQAPGKEREGVSCISSS-DGTTY  59
Nb21      QVQLQESGGGLVQPGGSLRLSCAASGRTFTRSIMGWFHQAPGKEREFLAGISWS-GANTY  59
Nb35      QVQLQESGGGLVQAGGSLRLSCAASGVTFDSAAMAWFRQVPGKEREFVAVISTESGGRTD  60
          ************* **********:* **    :.**:*.****** :: ** . .. *

Nb2       YADSVKGRFTISKDNAKNTMYLQMNSLKPEDTAVYYCATSPLYSTNDRCIS--EDYDYWG  117
Nb21      YADSVRGRFTISRDNAKNTVSLQMNSLNPEDTAVYYCAADPSHPG-SLISTRRSDYDSWG  118
Nb35      HADSVKGRFLISRDNARHMVYLQMNSLNPEDTAVYYCASSLLYCSASGCYANRDSYDYWG  120
          :****:*** **:***:: : ******:**********:.  :   .   :  ..** **

Nb2       QGTQVTVSSAAAYPYDVPDYGS    139
Nb21      RGTQVTVSSAAAYPYDVPDYGS    140
Nb35      QGTQVTVSSAAAYPYDVPDYGS    142
          :*********************
```

Figure 4.2. Sequence alignment between the inhibitory nanobodies Nb2, Nb21 & Nb35. *The different CDR regions of each nanobody are coloured as follows; CDR1: red, CDR2: yellow, CDR3: green. The Nb2 residues involved in polar contacts with GPVI are shown in bold and highlighted in pink. The positions with a single, fully conserved residue are indicated with * below the sequence rows,* **:** *shows a conservation between groups of strongly similar properties in the Nb2, Nb21 and Nb35 sequence, respectively, and* **.** *represents a conservation between groups of weakly similar properties. The nanobody alignments were generated using CLUSTAL O (1.2.4) multiple sequence alignment.*

Nb21 and Nb35 were engineered by Dr Alexandre Slater to include a thrombin cleavage site before the His-tag, in order to generate His-tag free nanobodies for crystallisation. For the generation of the GPVI/Nb complexes, a GPVI construct consisting of the D1 and D2 domains with the N72 glycosylation site mutated to a glutamine (N72Q) was used (GPVI NQ). Each protein (Nb21, Nb35 or GPVI-NQ) was purified with gel filtration in a Tris 20mM, NaCl 140mM, pH=7.4 buffer and then mixed in a 1:1 molar ratio of 135μM and added to the gel filtration column (Figure 4.3A). The individual filtration fractions were checked with a Bolt™ 4 to 12%, Bis-Tris, 1.0 mm gel (Figure 4.3B). Proteins were concentrated to 10 mg/mL, with the final crystallisation concentration being 6 mg/mL.

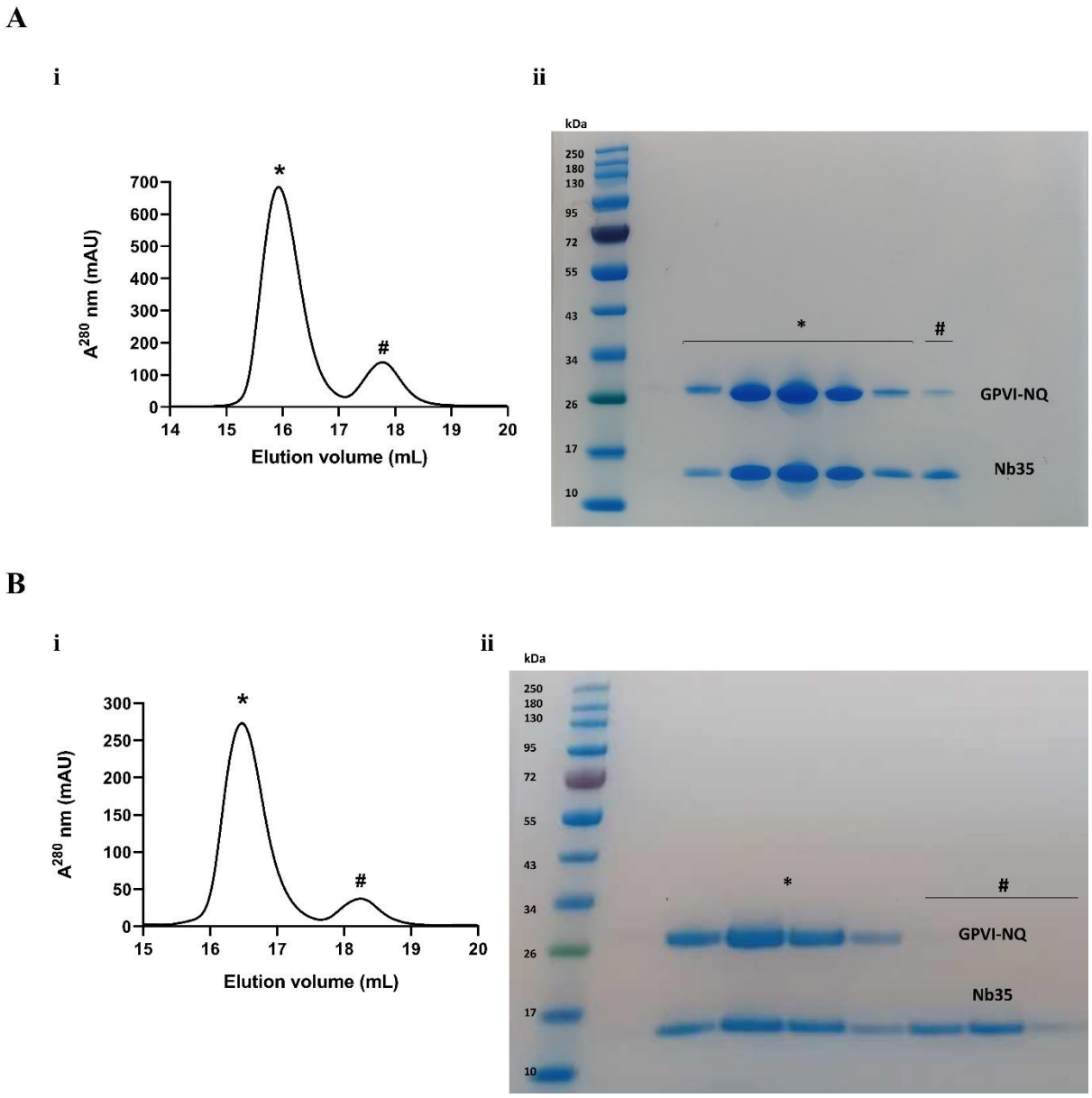


Figure 4.3. Gel filtration of nanobody complexes for crystallisation studies. *(A) Gel filtration was conducted in an ÄKTA Pure™ apparatus Superdex ® 200 Increase 10/300 GL and a column and 0.5mL fractions were collected. The Asn72 glycosylation site mutant (N72Q) of the D1 and D2 domains of GPVI was used for crystallisation (GPVI NQ). The major peak (16 mL) represents the (Ai) Nb35-GPVI NQ complex and (Bi) Nb21 while the following peak (18 mL) corresponds to unbound Nb35 and Nb21 respectively. (B) Representative gel of filtration fractions run. Protein bands were visualised with Coomassie brilliant blue staining. Fractions from the major peak (*) for (Aii) Nb35 or (Bii) Nb21 were collected for crystallisation while the smaller peaks (#) for each nanobody were excluded.*

The crystallisation and x-ray diffraction studies were performed with Prof. Jonas Emsley, based in the in the University of Nottingham, Biodiscovery Institute. A protein crystal was obtained for Nb35-GPVI NQ complex using 6mg/mL of the protein complex concentration in a buffer of 1.6M magnesium sulfate heptahydrate 0.1M MES monohydrate, pH=6.5. (Figure 4.4). The diffraction data were generated by the Diamond Light Source i24 Beamline (see Chapter 2).

The same procedure was then followed for the generation of Nb21 and GPVI NQ complex. Crystals of this complex were obtained (Figure 4.) using 5mg/mL of the protein complex in a buffer of 0.1M sodium cacodylate, 15% w/v PEG 4000 and pH=6.0. However, optimisation did not yield any crystals suitable for analysis of the x-ray crystallography diffraction, due to the presence of multiple crystals in one cluster, and this complex was not further investigated.

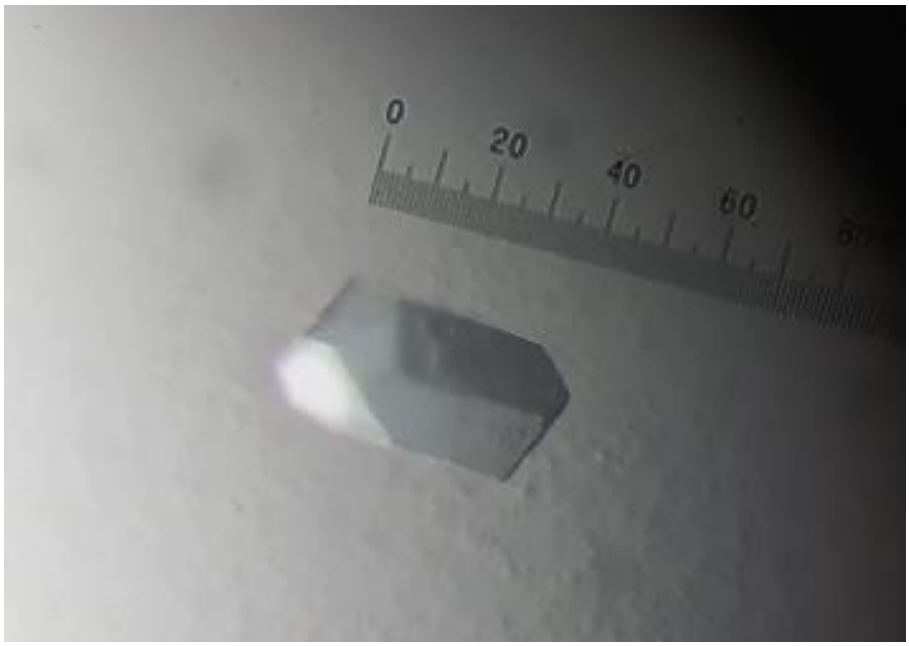


Figure 4.4. Protein crystal of Nb35-GPVI NQ complex used for x-ray diffraction. *The Asn72 glycosylation site mutant (N72Q) of the D1 and D2 domains of GPVI was used for crystallisation (GPVI NQ). The screening conditions that yielded a protein crystal of 6mg/mL Nb35-GPVI NQ complex was 1.6M magnesium sulfate heptahydrate 0.1M 2-(N-morpholino)ethanesulfonic acid (MES) monohydrate, pH=6.5.*

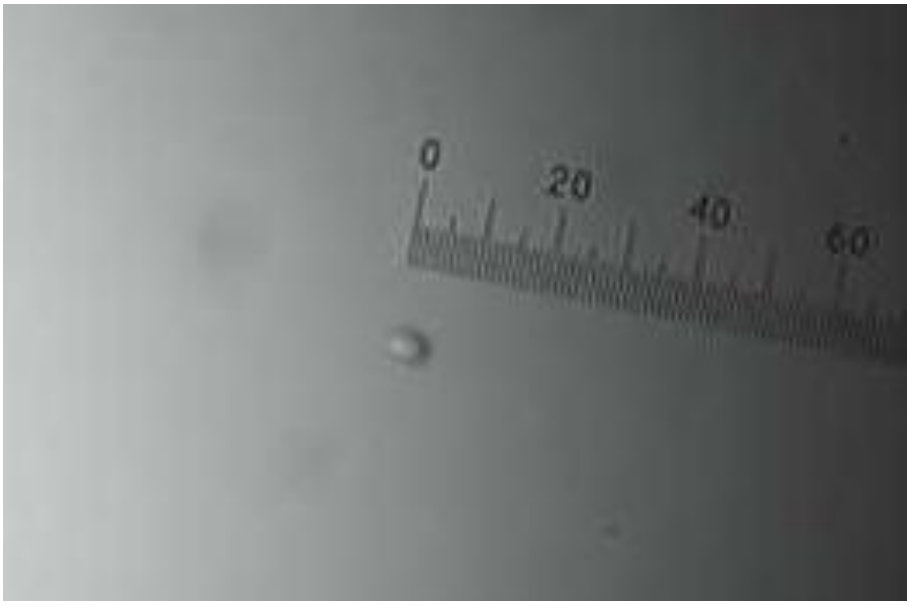


Figure 4.5. Protein crystal of Nb21-GPVI NQ complex. *The Asn72 glycosylation site mutant (N72Q) of the D1 and D2 domains of GPVI was used for crystallisation (GPVI NQ). The screening conditions that yielded a protein crystal of 5mg/mL NB21-GPVI NQ complex was 0.1M sodium cacodylate, 15% w/v polyethylene glycol (PEG) 4000 and pH=6.0.*

For the structure analysis of Nb35-GPVI complex, CCP4 software suite was used with molecular replacement using the first crystal structure of extracellular human platelet GPVI (PDB: 2GI7) and a homology model for Nb35 as templates for crystal structure refinement (see Chapter 2). Although 5OU7 has a higher resolution, 2GI7 includes extra amino acids in the D2 domain, including ones in the A-B loop, P102-S105, and the C-C` loop, Pro131-Asn136, which are included in the construct used in this study.

The final crystal structure solved had a resolution of 3.78Å and Rwork and Rfree values of 0.235 and 0.314, respectively. The resolution of the Nb35-GPVI NQ complex was lower when compared to the structure of Nb2 bound to GPVI and some residues within GPVI and Nb35 could not be modelled. Non-modelled residues in GPVI were found in the A-B loop in the D2 domain, Pro100-Gly107, and the C-C` loop of the D2 domain, Lys127-Arg139 (labelling in accordance with Horii *et al.*, 2006). Some residues from Nb35, including residues from the CDR3 loop, Tyr103-Ser107, and the VIB nanobody core and few amino acids away from the CDR2 region, Ser64-Gly67, were also not modelled.

Despite the lack of some structural information within the crystal data, the Nb35 binding site was elucidated and mapped within the D1 domain of GPVI, adjacent to the CRP binding site (Figure 4.A). The main polar interactions between GPVI and Nb35 were mainly found between the C-C` strands and the 3_{10} helix, the loop between E-F β-strands in D1. Polar interactions were found between nanobody residues from the CDR3 loop Leu101 and Tyr118 with GPVI residues Arg46 and Ala57, respectively. Residue Glu54 from the CDR2 region of Nb35 also interacts with GPVI residue Tyr47. Nb35 residues from the CDR1 region do not seem to participate in polar interactions with GPVI (Figure 4.B). When modelling Nb35 to the GPVI/CRP complex structure, it seems that the CDR2 and CDR3 loops are docked toward the CRP binding site in the C strand of the D1 domain. Residues Arg46 and Tyr47 are also part of the CRP binding groove and could contribute in steric clashes between the two ligands.

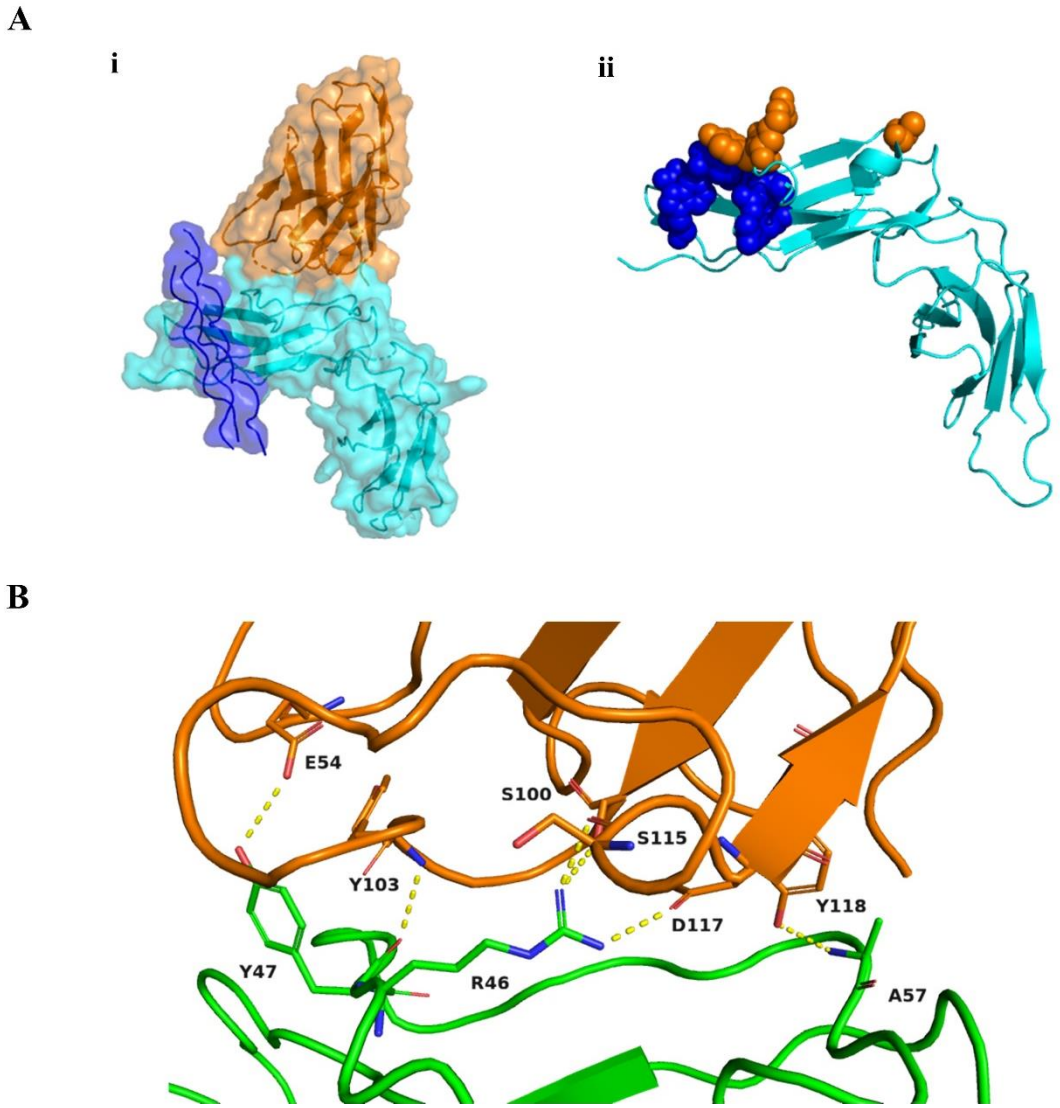


Figure 4.6. Binding interface of Nb35 to the surface of GPVI. *(A) Relative locations of the Nb35 and CRP binding sites within GPVI. (i) Surface representation of Nb35 (orange) modelled to the previously described GPVI–CRP crystal structure (PDB: 5OU8), with GPVI coloured in cyan and CRP in blue. (ii) GPVI residues that form polar interactions with Nb35 and CRP binding residues, shown as orange and blue spheres, respectively, onto GPVI (cyan). (B) Zoomed view of the GPVI D1 domain (cyan) bound to Nb35 (orange). The Nb35 amino acids (orange) involved in polar interaction with the GPVI D1 domain (cyan) are shown in a stick representation Arg46, Tyr47 and Ala57 (R46, Y47 & A57). Yellow dashes indicate hydrogen bond interactions between Nb35 and GPVI. Amino acids from the Nb35 Glu54, Ser100, Leu101, Tyr101, Ser115, Asp117 and Tyr118 (E54, S100, L101, Y103, S115, D117 & Y118). Residues Arg46 and Tyr47 are shared with the surface for CRP binding.*

The structure shows that the binding epitope of Nb35 is overlapping with the one for Nb2 (Figure 4.A). But unlike Nb2, binding of Nb35 to GPVI did not induce a domain swap or a significant conformational change. Further, GPVI was monomeric unlike in all other reported crystal structures of GPVI, other than that for the co-crystal of GPVI and glenzocimab, as mentioned above. However, in this case a dimer could not be formed as this is the site of binding of glenzocimab.

Looking at the binding interactions between the two nanobodies and GPVI, Leu101 from Nb35 and Ser99 from Nb2 act as hydrogen bond donors through their carbonyl group with GPVI residue Arg46. Tyr118 from Nb35 and Tyr115 from Nb2 interact with backbone carbonyl group of GPVI residue Ala57 (Figure 4.B). However, the binding residues of Nb2 that form polar interactions seem to be higher in number (11 amino acids in Nb2 over 3 in Nb35) and more widespread within the binding surface onto GPVI. This difference though could be attributed to the low resolution and absence of electron density within amino acids of the CDR3, which may result in a different Nb35 tertiary structure or lack of binding residues, i.e. in the CDR3 region. Interestingly, there are three amino acids in GPVI that are shared between Nb2 and Nb35 when bound to GPVI, with Arg46 and Tyr47 being more distant to Ala57.

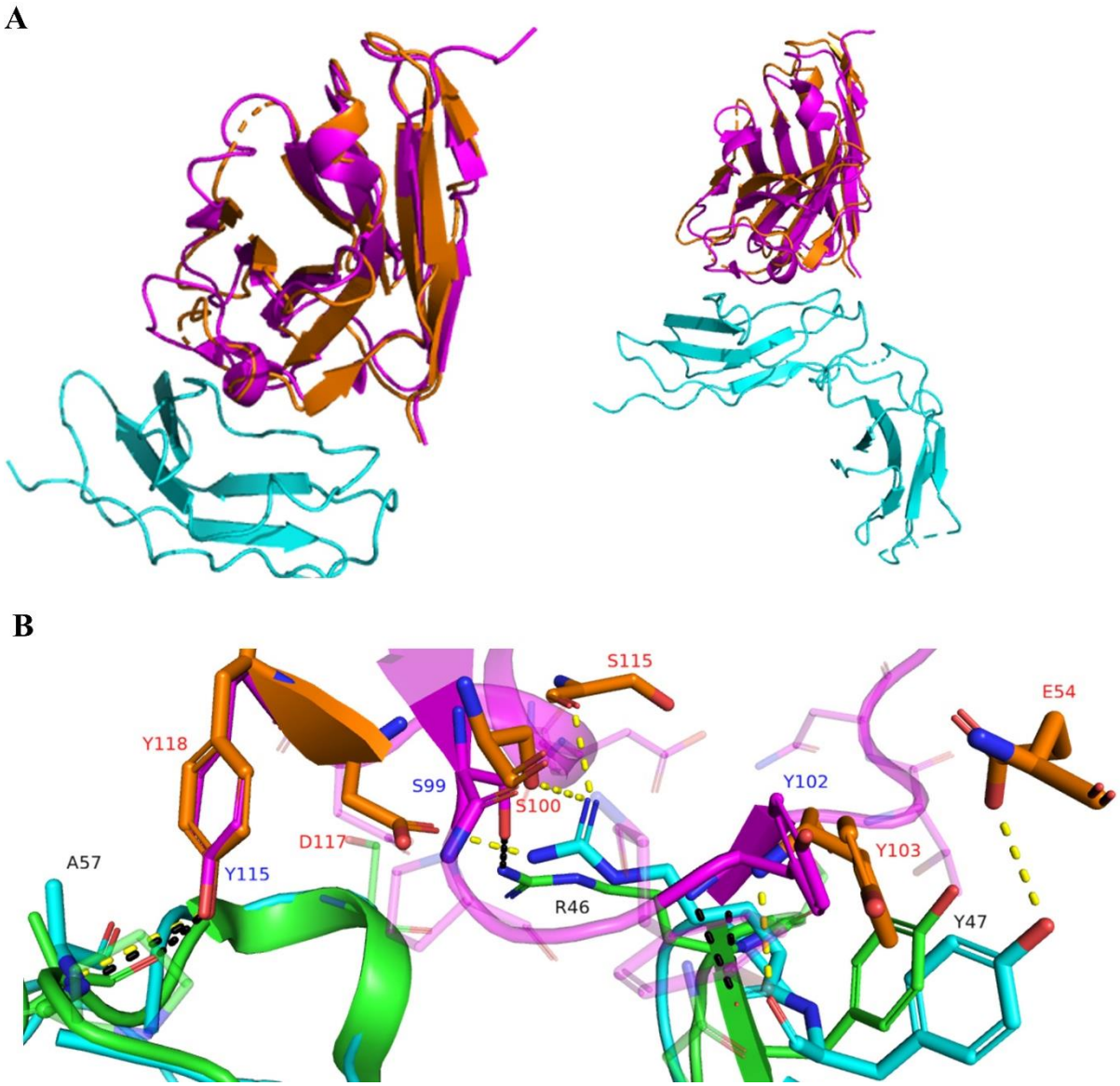


Figure 4.7. Comparison between the Nb2 and Nb35 binding site. *(A) Cartoon representation of the overlap between the binding sites of Nb2 (magenta) and Nb35 (orange). Nb2 (PDB: 7NMU) was modelled onto the GPVI monomer bound to Nb35 structure, generated in this study. (B) Zoomed view of nanobody residues responsible for binding of GPVI residues Arg46, Tyr47 and Ala57 (R46, Y47 and A57) of both Nb2 (magenta) and Nb35 (orange) shown in sticks. The Nb2-bound (green) and Nb35-bound GPVI (cyan) structures were aligned using PyMOL (Nb2/GPVI, PDB: 7NMU). The hydrogen bonds formed between GPVI and Nb2 are shown in black and the ones formed between GPVI and Nb35 are shown in yellow. The nanobody residues responsible for binding of the three GPVI residues (black labels) are labelled in red for the Nb35 residues and blue for the Nb2 ones. The rest of the Nb2 cartoon and other interactions are set in a lower transparency.*

Interestingly, the binding site that has been previously targeted for the development of small molecule inhibitors for GPVI through *in silico* studies (Bhunia *et al.*, 2017; Olğaç *et al.*, 2022) and structure-based approaches (Ono *et al.*, 2014), comprises most of the amino acids that both Nb2 and Nb35 are binding, including Arg46 and Tyr47, and in the same binding region. The pocket also includes some of the amino acids that Nb2 binds, such as Gln48 and Pro56, and other amino acids encompassed by the Nb2 and Nb35 binding region as well (Figure 4.).

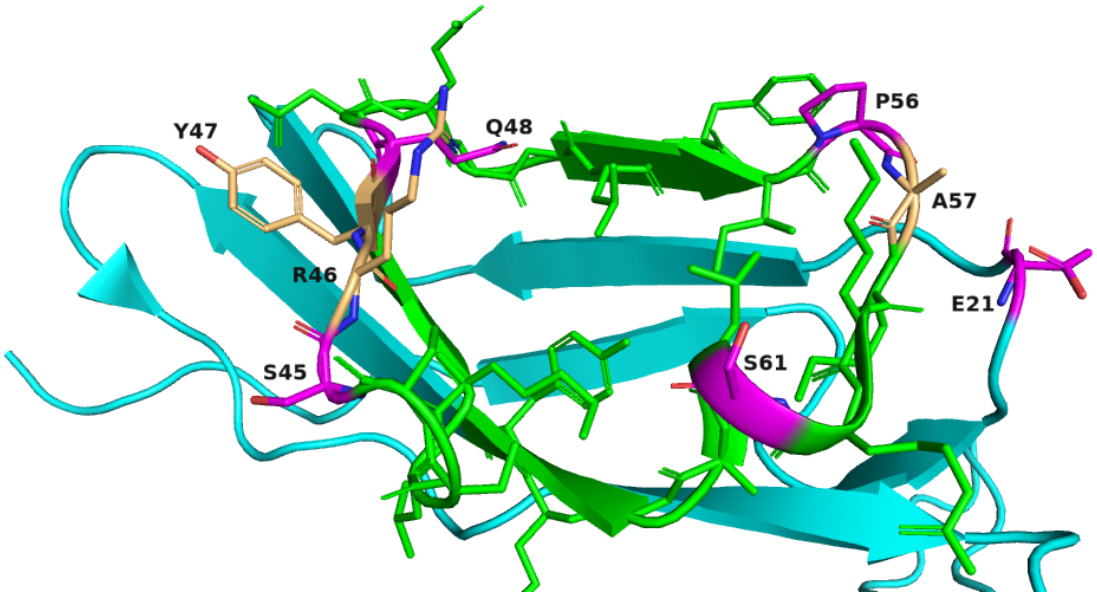


Figure 4.8. Overlay of the GPVI amino acids that are included in nanobody binding and the ones included in the small molecule binding site. *Zoomed view of the binding residues of GPVI (PDB: 2GI7) D1 domain that both nanobodies bind. The amino acids of GPVI (cyan) that bind Nb2 are coloured in magenta while the residues responsible for both Nb2 and Nb35 binding are coloured in light orange. The ones that comprise the small ligand binding pocket, generated by SiteMap, are shown in sticks and are coloured in green.*

4.3.2 Probing the Nb21 binding site through mutations studies

Since the Nb21-GPVI complex structure was not obtained, the next step was to target potentially key amino acids for the inhibitory properties of Nb35 and Nb2 or other residues important for GPVI ligand binding to determine the role of these in Nb21 binding. The focus was turned to arginine residues due to the contribution of certain GPVI arginines in the binding affinity of CRP, collagen and Nb2 (Horii *et al.*, 2006; Slater *et al.*, 2021; Feitsma *et al.*, 2022) and Nb35, determined through crystal structure analysis and mutation studies. It has also been suggested that, considering the structural diversity of GPVI ligands, these agents are more likely to mediate activation through polar interactions with charged ligand moieties, leading to receptor clustering or altered protein-protein interactions rather than a "close-fitting" binding mechanism (Montague *et al.*, 2021). Hence arginine residues present an opportunity to investigate the interactions between these polar residues and the selected nanobodies.

In particular, GPVI residue Arg46 forms multiple polar interactions with both Nb2 and Nb35 and is expected to greatly affect Nb21 binding, if the binding site between the three is the same. On the other hand, Arg38 and Arg67 both form direct polar interactions with CRP (Feitsma *et al*., 2022) and should indicate whether Nb21 binds to this site. Arg60 has been previously reported in the literature to reduce collagen binding to GPVI when mutated (Horii *et al.*, 2006) while being in close proximity to the binding site of Nb2 and Nb35, without forming polar interactions with them. Mutating this residue would help to clarify whether the Nb21 binding site is located near the D1-D2 interface.

Following these hypotheses, protein mutants R38A, R46A, R60A and R67A were generated through site-directed mutagenesis (Figure 4.9). Alanine was used as the replacement amino acid due to its non-bulky and chemically inert structure and its common use in alanine-scanning mutagenesis.

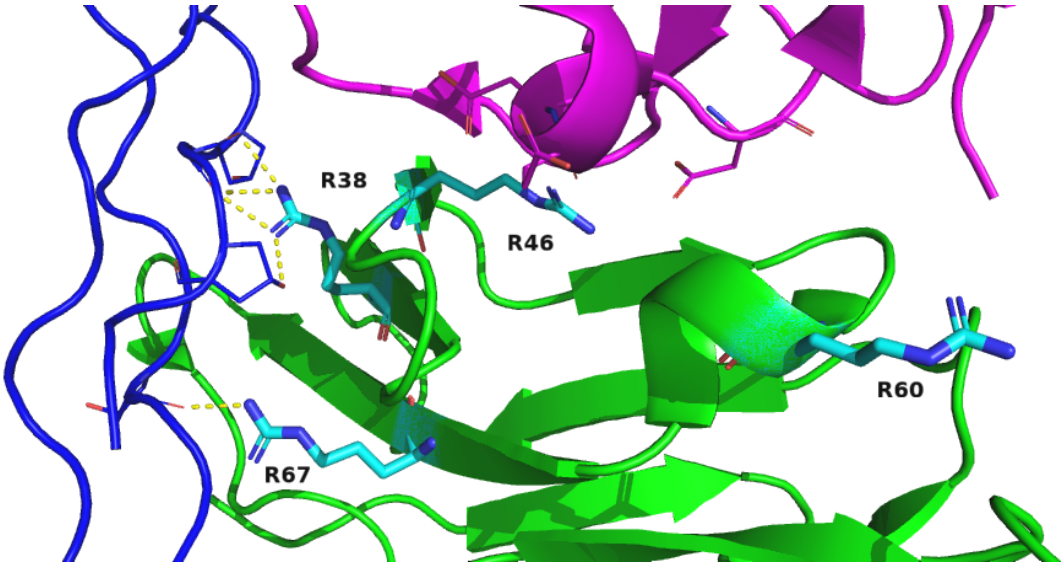


Figure 4.9. Residue R38, R46, R60 & R67 location within the D1 GPVI domain*. The residues used in mutation studies (cyan) are shown in stick representation in the GPVI D1 domain (green) after Nb2 (magenta) binding. Nb2 was modelled using PyMOL onto the CRP/GPVI complex (Nb2, PDB: 7NMU; CRP/GPVI, PDB: 5OU8). Yellow dashes are showing hydrogen bonds between CRP and GPVI while the Nb2 residues Ser99, Glu111, Asp112 and Asp114 interacting with R46 are also shown (S99, E111, D112 & D114).*

A NFAT-luciferase assay that monitors sustained GPVI signalling in DT40 cells was used to test the mutant receptors. This technique has been previously described before to establish a cell line NFAT assay to investigate GPVI signalling (Tomlinson *et al.*, 2007). Initially, we used different amounts of DNA and agonist concentrations to optimise the signal ratio between unstimulated and stimulated samples. Firstly, DT40 cells were transfected using 0.3, 1, 3 or 10µg of wild type (WT) GPVI with an equal quantity of FcRγ-chain vector and 15µg NFAT-luciferase. Mock transfected DT40 cells and PMA plus ionomycin served as controls (not shown). A significant difference between the luciferase signal of unstimulated and collagen-stimulated GPVI transfected cells (Figure 4.) was achieved using concentrations equal to or higher than 1µg of DNA for transfection but increasing the amounts for transfection led to a marginal change in response (1µg: 3.3±0.9, 3µg: 3.3±0.9, 10µg: 2.5±0.4 fold). Hence, 1µg was selected for assay optimisation based on the lowest DNA quantity needed to achieve a transfection efficacy of a minimum of 50% and a robust response to collagen (Figure 4.11).

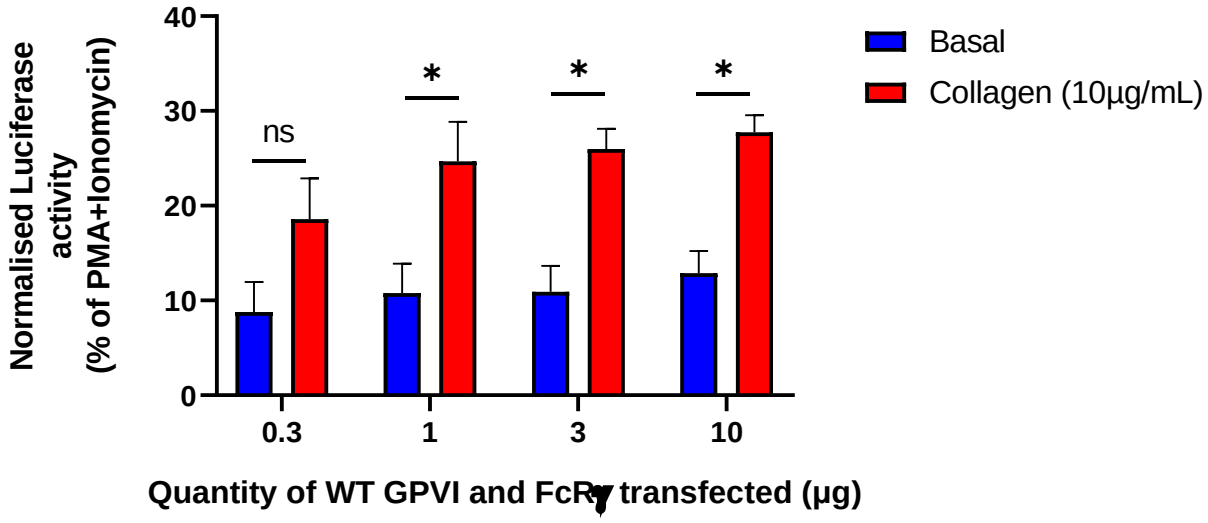


Figure 4.10. NFAT signal optimization based on DNA transfection efficiency. *The DT40 cell line was transfected with 15µg nuclear factor of activated T-cells (NFAT)–luciferase reporter construct, 0.3, 1, 3 or 10µg of each plasmid wild type (WT) GPVI and FcRγ expression constructs. Cells were either left unstimulated (DT40 control, data not shown) or were stimulated with collagen (10µg/mL) or phorbol 12-myristate 13-acetate (PMA) (50ng/mL) plus ionomycin (1µM). Luciferase data were normalised for PMA plus ionomycin values. The DT40 control values have been subtracted from the test data sets before normalisation. Significance was measured using multiple t tests for basal vs collagen or CRP with a Holm-Sidak post-hoc test; * = p≤0.05, ns = p>0.05. Data presented as mean±SEM from two experiment each performed in triplet (n=2).*

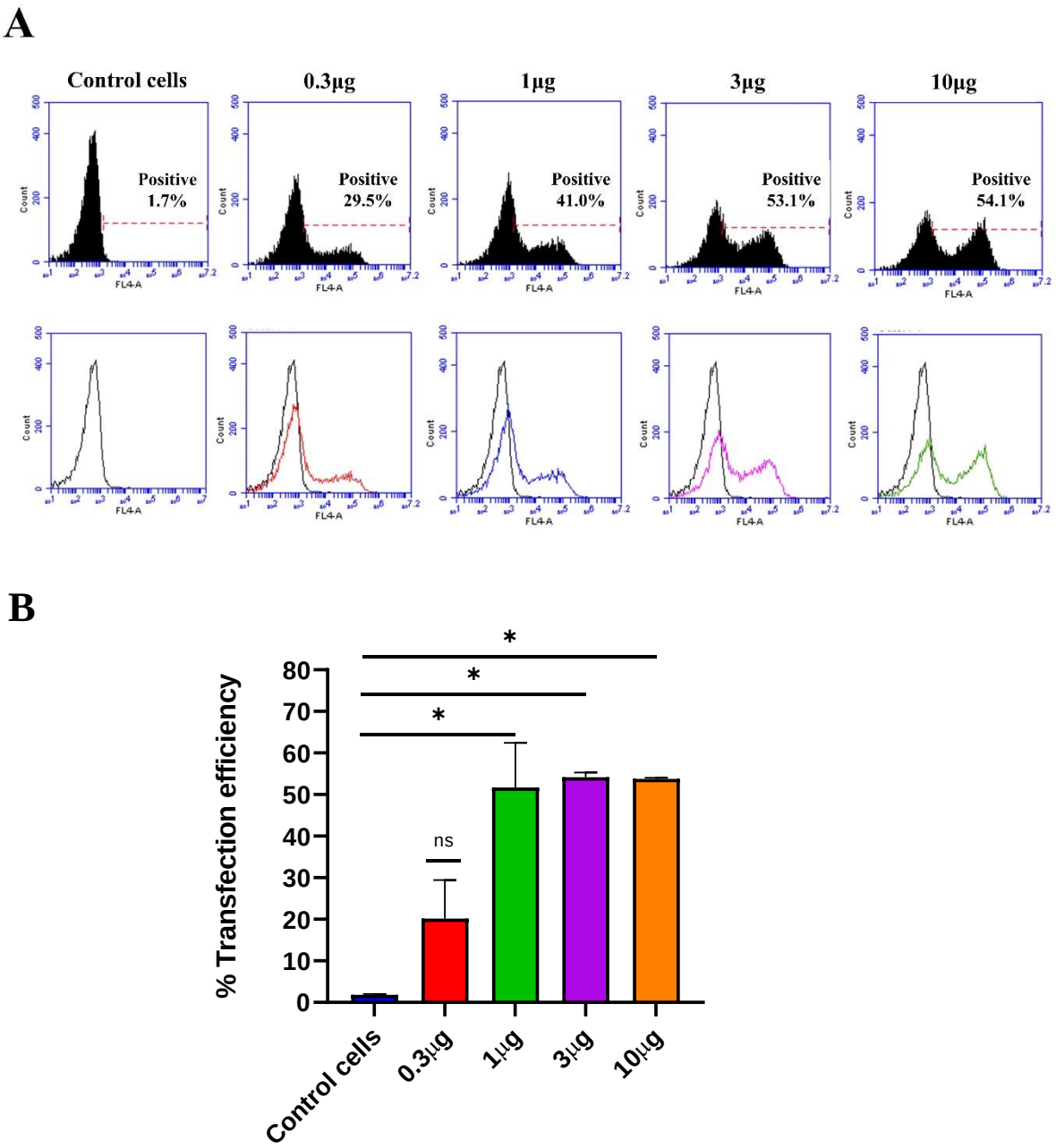


Figure 4.11. Expression of WT GPVI from different DNA quantities in DT40 cells. *GPVI expression was detected by flow cytometry to determine transfection efficacy of different DNA quantities to optimize transfection of WT GPVI. DT40 cells were transfected using electroporation with 0.3, 1, 3 and 10µg of wild-type (WT) GPVI, an equal amount of human FcRγ chain and 15µg of NFAT luciferase reporter construct DNA. (A) Top row: Representative histograms of geometric mean fluorescence intensities of GPVI-positive in the different DT40 chicken B cell lines (0.3, 1, 3 and 10µg) were detected using an anti-GPVI HY101 antibody (1:400) and an anti-mouse Alexa Fluor-647 secondary antibody for staining (1:400). The control cell line represents primary and secondary antibody-tagged DT40 cells. Bottom row: Overlay between control cells and each transfected cell line. (B) Flow cytometry data are presented as the transfection efficiency of WT GPVI showing percentage of cells positive for indicated GPVI receptor. Significance was measured using one-way ANOVA analysis with a Dunnett post-hoc test where: * = p≤0.05, ns = p>0.05. Statistical significance was compared to control cell*

values while error bars represented as mean±SEM from two experiments each performed in triplet (n=2).

In a preliminary experiment, collagen stimulated a dose dependent increase in NFAT-luciferase activity signal in GPVI-transfected cells with the greatest response induced by 10µg/mL of collagen (2.7-fold±0.16) (Figure 4.12). Therefore, this concentration of collagen was used for the following NFAT assays.

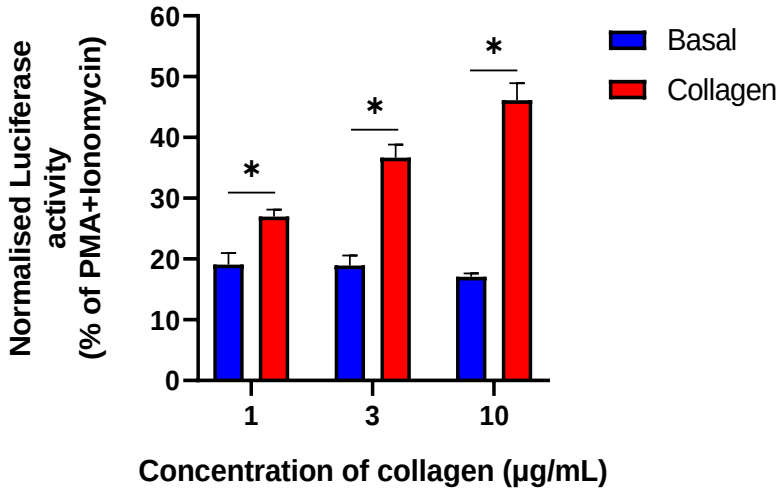


Figure 4.12. NFAT signal optimization based on agonist concentration. *The DT40 cell line was transfected with 15µg nuclear factor of activated T-cells (NFAT)–luciferase reporter construct, 1µg of plasmid each of WT GPVI and FcRγ expression constructs. Cells were either left unstimulated (basal), or were stimulated with collagen (1, 3 or 10µg/mL) or collagen-related peptide, CRP (1, 3 or 10µg/mL), or phorbol 12-myristate 13-acetate (PMA) (50ng/mL) plus ionomycin (1µM). Luciferase data were normalised for PMA plus ionomycin values and are presented as a percentage of the positive control PMA plus ionomycin response. The DT40 control values have been subtracted from the test data sets before normalisation. Significance was measured using multiple t-test with a Bonferroni and Dunn post-hoc test where* * = $p \leq 0.05$, ns = $p > 0.05$. *Data presented as mean±SEM performed in triplet (n=1).*

Following optimisation of the NFAT assay conditions, four new cell lines were generated, one for each GPVI mutation of interest. These mutated lines will be referred to as R38A, R46A, R60A and R67A. Collagen (10µg/mL) increased the NFAT-luciferase activity significantly ($p \leq 0.05$) of WT GPVI, R46A and R60A by 3.5±0.73, 2.8±0.59, and 4.6±0.91 fold respectively (Figure 4.13). However, R38A and R67A failed to support collagen-induced signalling (Figure 4.13). For this reason, only R46A and R60A mutations were used in further studies. There was no significant difference in the transfection efficacy observed between the different mutant WT transfected cell lines (Figure 4.14), suggesting that the transfection efficiency is not affected by the presence of these point mutations, as expected.

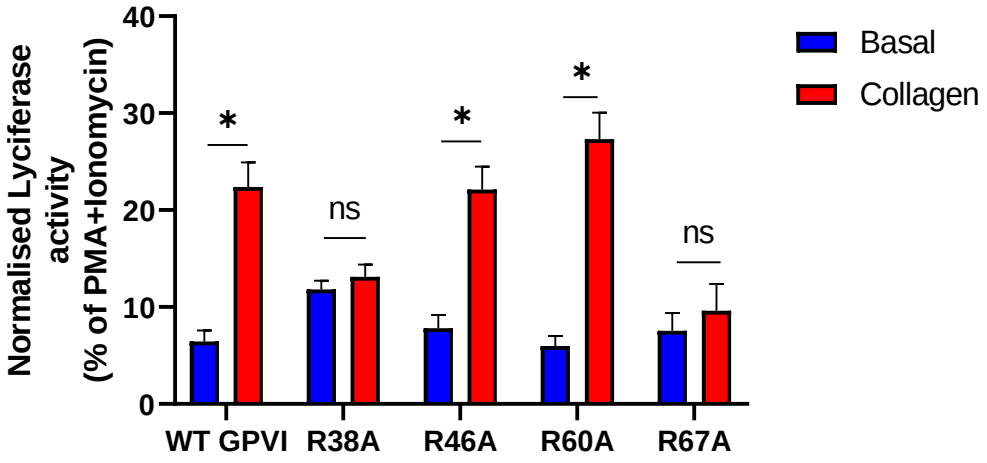


Figure 4.13. Effect of R38A, R46A, R60A & R67A GPVI mutations to GPVI signalling. *The DT40 cell line was transfected with a nuclear factor of activated T-cells (NFAT)–luciferase reporter construct, 1µg of plasmid each of GPVI and FcRγ expression constructs (WT or mutated GPVI) or empty vector controls. The NFAT-luciferase DNA quantity was 15µg. Sixteen hours post-transfection, expression of GPVI was confirmed by flow cytometry. Cells were either left unstimulated (DT40 control), or were stimulated with collagen (10µg/mL) or phorbol 12-myristate 13-acetate (PMA) (50ng/mL) plus ionomycin (1µM). Luciferase data were normalised for PMA plus ionomycin values and are presented as a percentage of the positive control PMA plus ionomycin response. The DT40 control values have been subtracted from the test data sets before normalisation. Significance was measured using multiple t-test with a Bonferroni and Dunn post-hoc test where* * = $p \leq 0.05$, ns = $p > 0.05$. Data presented as mean±SEM performed in triplet (n=6).*

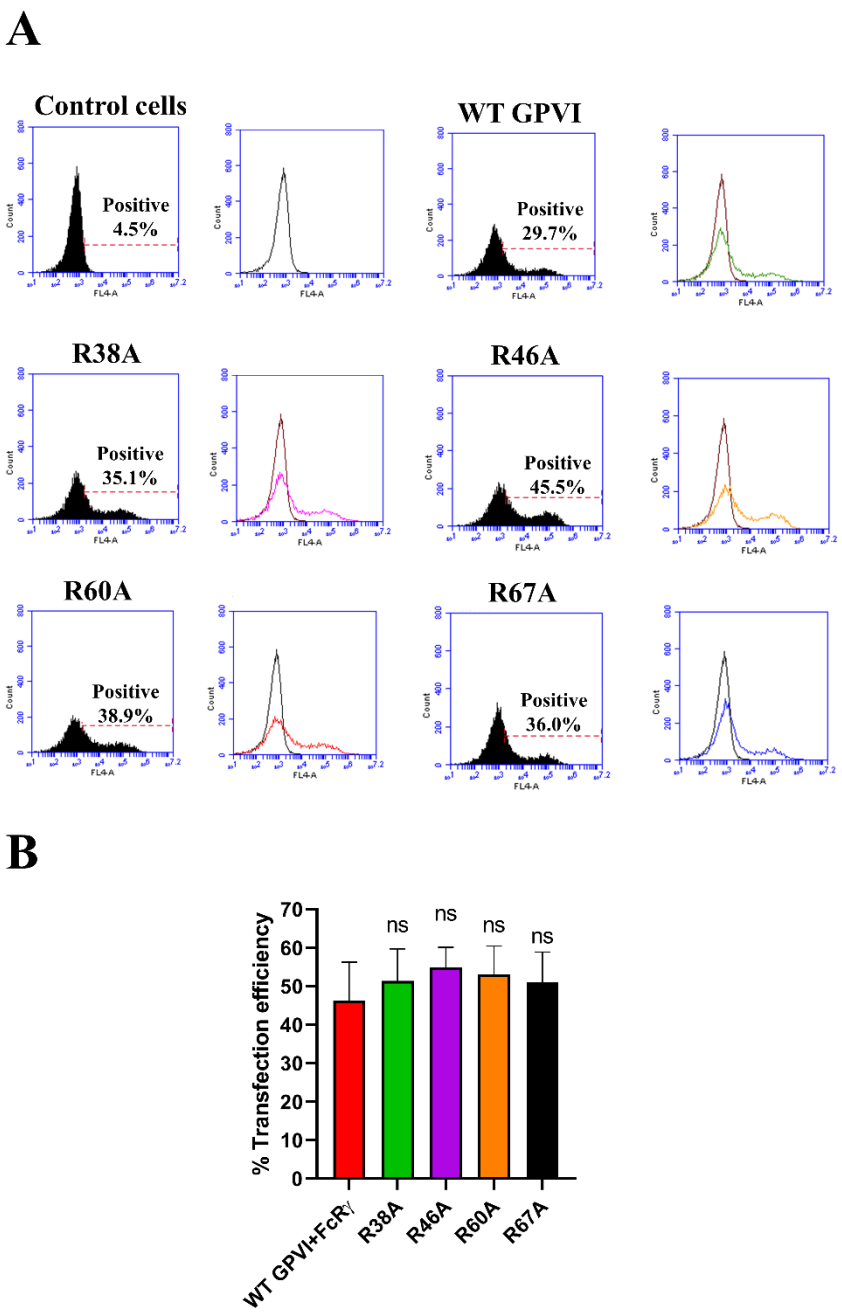


Figure 4.14. Expression of GPVI mutant constructs in DT40 cells. *GPVI expression was detected by flow cytometry to determine transfection efficacy of different GPVI mutants (R38A, R46A, R60A, R67A) and WT GPVI as a control. DT40 cells were transfected using electroporation with 1µg of wild-type (WT) GPVI or a GPVI mutants (R38A, R46A, R60A, R67A), an equal amount of human FcRγ chain and 15µg of NFAT luciferase reporter construct DNA. The control cell line represents primary and secondary antibody-tagged DT40 cells. (A) Left row: Representative histograms of geometric mean fluorescence intensities of GPVI-positive in DT40 chicken B cells were detected using an anti-GPVI HY101 antibody (1:400) and an anti-mouse Alexa Fluor-647 secondary antibody for staining (1:400). Right row: Overlay between control cells and each transfected cell line. (B) Flow cytometry data are presented as the transfection efficiency of WT GPVI showing percentage of cells positive for indicated GPVI receptor. Significance was measured using One-way ANOVA with a Dunnet post-hoc test where* = p≤0.05, ns = p>0.05. Data presented as mean±SEM performed in triplet (n=2).*

The R46A and R60A mutated GPVI constructs were transfected into cell lines and incubated with 100nM of Nb2, Nb21 and Nb35 to investigate the effect of these mutations on the ability of the selected nanobodies to inhibit collagen signalling (Figure 4.15). In this set of experiments, the collagen-stimulated to basal signal ratio was greater compared to the previous experiments. The response in the WT GPVI, R46A and R60A cell lines were 10.6±2.0, 12.6±2.0 and 20.5±3.6-fold, respectively (Figure 4.15). All three nanobodies significantly reduced collagen signalling ($p<0.05$) in the WT GPVI cell lines, as seen by a decrease in the luciferase activity after the addition of Nb2, Nb21 and Nb35 to 1.6±0.4, 3.6±1.0 and 2.2±0.49-fold, respectively (Figure 4.15). The inhibitory effect of the nanobodies was completely abolished in the R46A mutant but not altered in the R60A mutant line other than for Nb21 where the response was reduced by approximately 50%. This value was significant compared to both the basal and collagen-induced response ($p\leq0.05$) and suggests that Nb21 may have an overlapping but distinct binding site to Nb2 and Nb35.

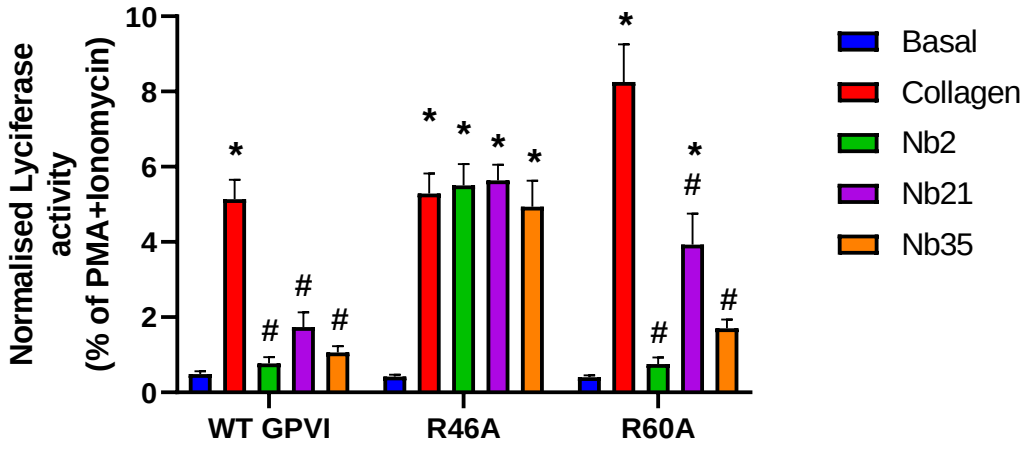
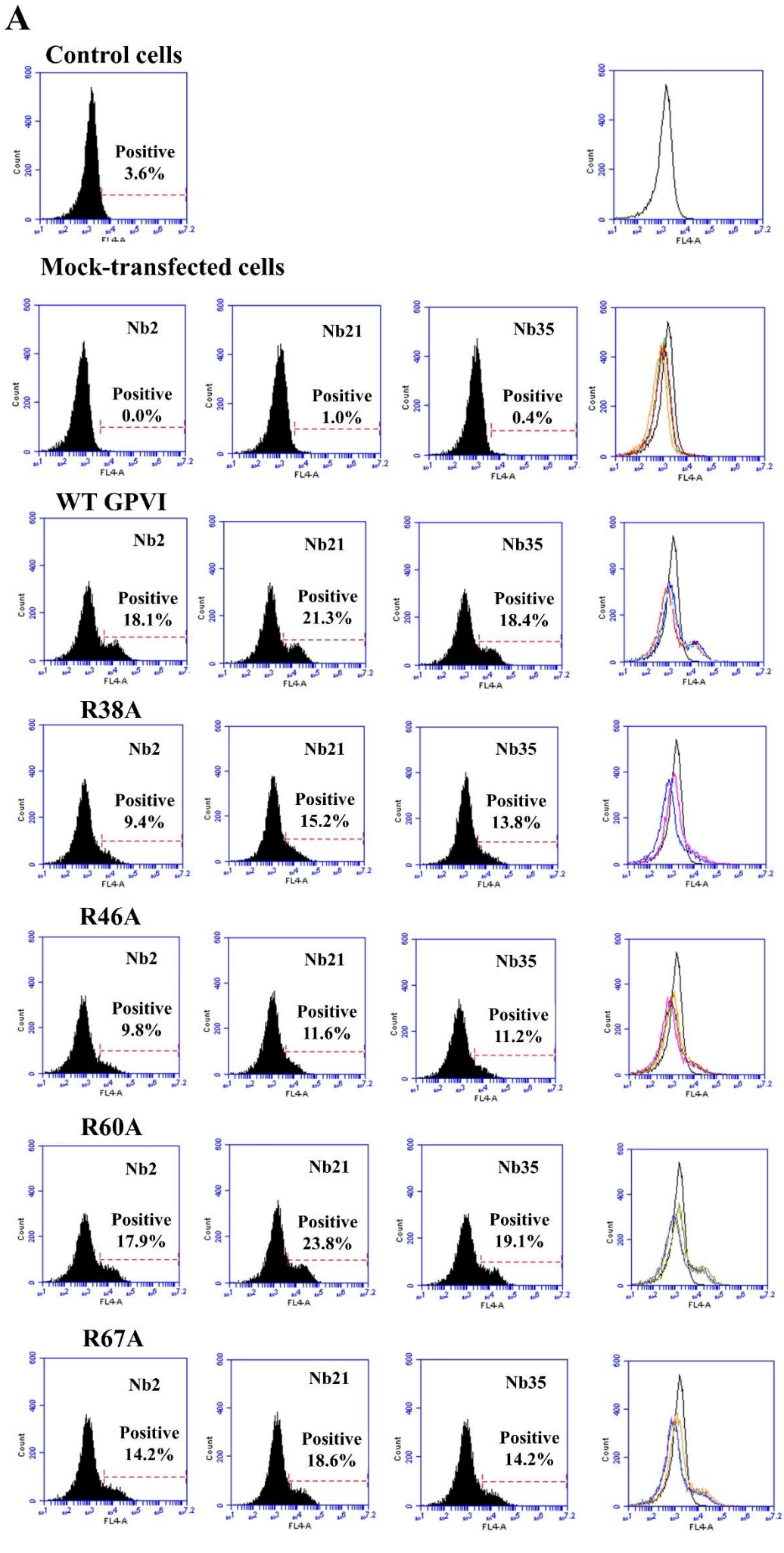


Figure 4.15. Effect of R46A & R60A GPVI mutations to inhibition efficacy of Nb2, Nb21 & Nb35 towards GPVI signalling. *A DT40 cell line was transfected with a nuclear factor of activated T-cells (NFAT)–luciferase reporter construct, 1µg of plasmid each of GPVI and FcRγ expression constructs or empty vector controls. Cells were either left unstimulated (basal) incubated with 100nM of Nb2, Nb21 or Nb35, or stimulated with 10µg/mL of collagen) or 50ng/mL of PMA plus 1µM of ionomycin. Luciferase data were normalised for PMA plus ionomycin. The DT40 plus 100nM of Nb2, Nb21 or Nb35 control values have been subtracted from the data before normalisation. Significance was measured using a two-way ANOVA test with a Tukey post-hoc test where: *= p≤0.05 (basal), # = p≤0.05 (collagen), ns = p>0.05. Data presented as mean±SEM performed in triplet (n=3).*

4.3.3 Flow cytometry for nanobody binding

Following the NFAT signalling studies, flow cytometry experiments were implemented to investigate whether the loss / reduction in the ability of the three inhibitory nanobodies to inhibit collagen-induced signalling seen in GPVI mutants R46A and R60A was due to reduced binding compared to the WT GPVI. 100nM of the three His-tagged nanobodies were pre-incubated in transfected DT40 cell lines with empty vector, WT GPVI or the generated GPVI mutants (R38A, R46A, R60A and R67A). Although R38A and R67A were not tested alongside the nanobodies in NFAT assays, we still wanted to test the ability of these nanobodies to bind these mutants to further map the binding site. An anti-His Alexa-647 antibody was used to detect the presence of bound nanobodies to the tested GPVI constructs. None of the nanobodies showed any significant background fluorescence ($p<0.05$) when tested in the mock-transfected cell lines (Figure 4.16A).

A significant reduction ($p<0.05$) in the binding of all three nanobodies to the R46A mutant of more than 50 %, while an increased binding of more than 100% on R60A was observed (Figure 4.16B). Binding of all nanobodies to the R38A was reduced by approximately 30% and was increased by approximately 20% in the presence of R67A. However the binding difference between WT GPVI and R38A and R67A were not significant ($p<0.05$). The reduction in binding to the R46A mutant is consistent with the abolition of the inhibitory effect of the three nanobodies.


A
Control cells
Positive
3.6%
Mock-transfected cells
Nb2
Positive
0.0%
Nb21
Positive
1.0%
Nb35
Positive
0.4%
WT GPVI
Nb2
Positive
18.1%
Nb21
Positive
21.3%
Nb35
Positive
18.4%
R38A
Nb2
Positive
9.4%
Nb21
Positive
15.2%
Nb35
Positive
13.8%
R46A
Nb2
Positive
9.8%
Nb21
Positive
11.6%
Nb35
Positive
11.2%
R60A
Nb2
Positive
17.9%
Nb21
Positive
23.8%
Nb35
Positive
19.1%
R67A
Nb2
Positive
14.2%
Nb21
Positive
18.6%
Nb35
Positive
14.2%
Count
FL4-A

B

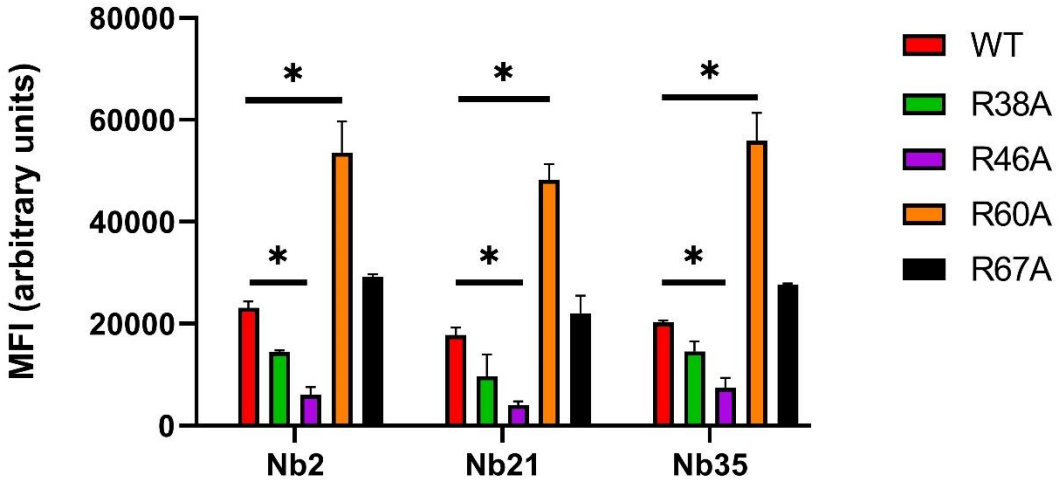


Figure 4.16. Effect of R38A, R46A, R60A and R67A GPVI mutations to the binding of His-tagged Nb2, Nb21 and Nb35. *DT40 cells were transfected using electroporation with 1µg of wild-type (WT) GPVI or a GPVI mutants (R38A, R46A, R60A, R67A), an equal amount of human FcRγ chain and 15µg of NFAT luciferase reporter construct DNA. A stained DT40 cell line with an anti-His Alexa-647 secondary antibody was used as a control (control cells) while cells were also transfected with 1µg of an empty pcDNA3.1 vector (mock-transfected cells). 100nM of His-tagged Nb2, Nb21 or Nb35 were used for detection of nanobody binding. An anti-His Alexa-647 antibody (1:400) was used to detect the His-tagged nanobodies bound to each GPVI construct. (A) Left rows: Representative histograms of geometric mean fluorescence intensities of nanobody bound to GPVI positive cells in DT40 chicken B cell lines. Right row: Overlay between control cells and each transfected cell line. (B) Flow cytometry data are presented as binding efficiency of each nanobody to the different GPVI constructs showing percentage of cells positive for indicated Nb2, Nb21 & Nb35 bound to GPVI. Fluorescence from the control cells was removed from each measurement. Significance was measured using two-way ANOVA analysis with a Dunnet post-hoc test for each nanobody group compared to WT GPVI expression values where: * = p≤0.05, ns = p>0.05. Data presented as mean±SEM performed in triplet (n=3).*

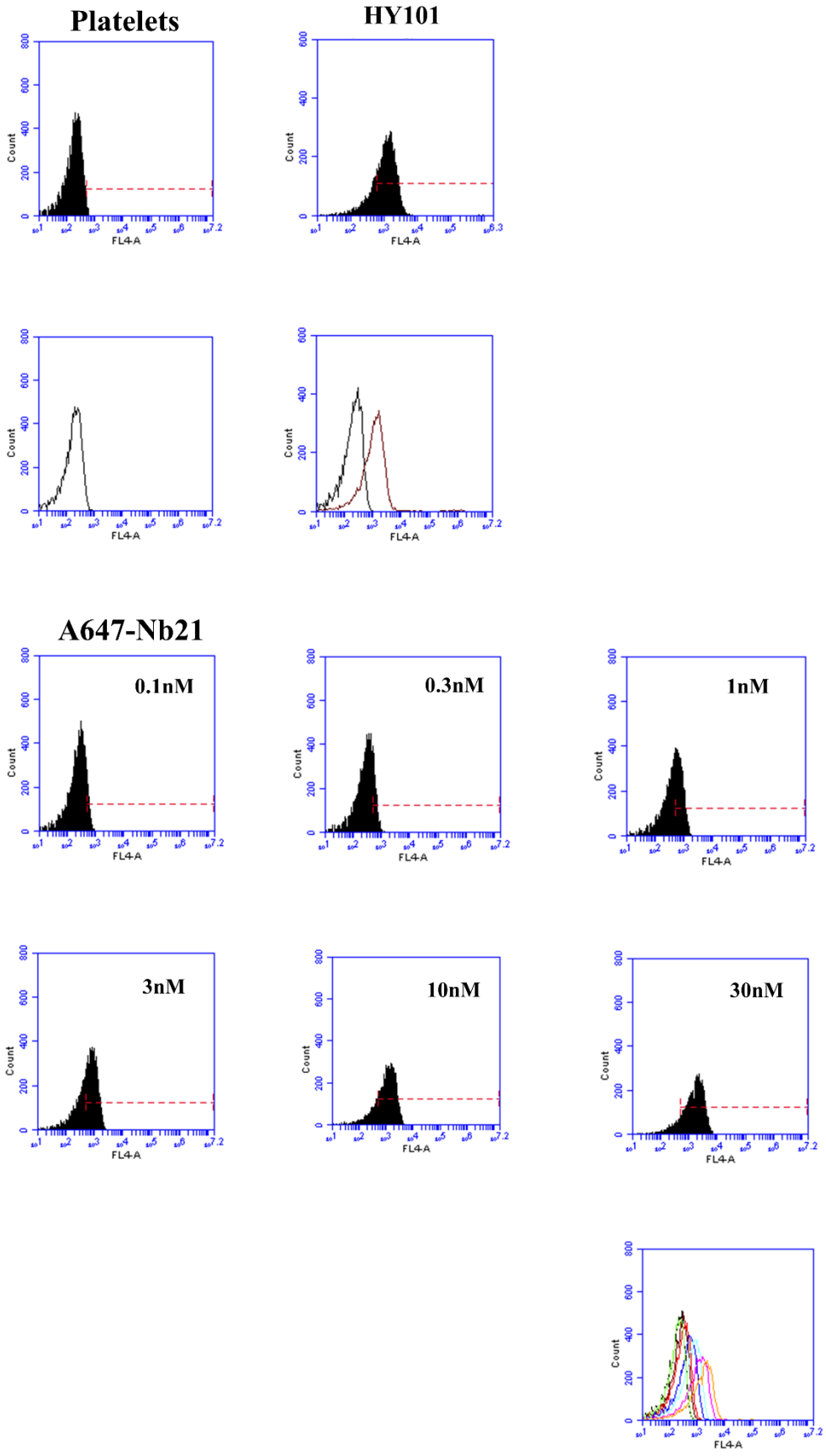
4.3.4 Flow cytometry for nanobody displacement in human platelets

Flow cytometry experiments were performed to investigate whether Nb21 displacement is seen for the corresponding binding site by Nb2 and Nb35. This was attempted by the use of directly labelled versions of each nanobody with Alexa Fluor™ 647 succinimidyl ester and measurements of the reduction of fluorescence between the labelled nanobodies and their non-labelled equivalents. For this work, the chosen cell line was washed human platelets, due to the high number of GPVI copies and direct physiological relevance.

The first step was to generate the labelled version of Nb21 by a direct labelling with Alexa Fluor™ 647 succinimidyl carboxylic acid succinimidyl ester in an adjusted pH=7.8 for 1 h. The free dye was removed with dialysis in PBS and the final concentrations and degree of labelling (DOL) were calculated (see Chapter 2 for more details). The generated labelled version of His-tagged Nb21 (A647-Nb21) had an average DOL of 0.4±0.1.

A saturation curve using A647-Nb21 was generated and the % transfection and MFI measured. Antibody HY101 raised in mice and an anti-mouse IgG Alexa Fluor 647 were used to detect GPVI levels on platelet. A647-Nb21 was used in increasing concentrations (0.1-30nM). Platelet positivity is not shown for these experiments, since transfection is not needed for it and human platelets naturally express GPVI. A marker was used to subtract platelet fluorescence. There was a concentration-dependent increase in MFI (Figure 4.17). Concentration of 100 nM and 300 nM had great variations between the different experiments and were excluded from final data analysis. Saturation was not achieved in this set-up and hence no reference to the potency of Nb21, and compared to the one potency to Nb2 can be made.. The latter has been reported to bind to GPVI with a K_D of 1nM (Slater *et al.*, 2021).

A


Platelets
HY101
A647-Nb21
0.1nM
0.3nM
1nM
3nM
10nM
30nM
Count
FL4-A

B

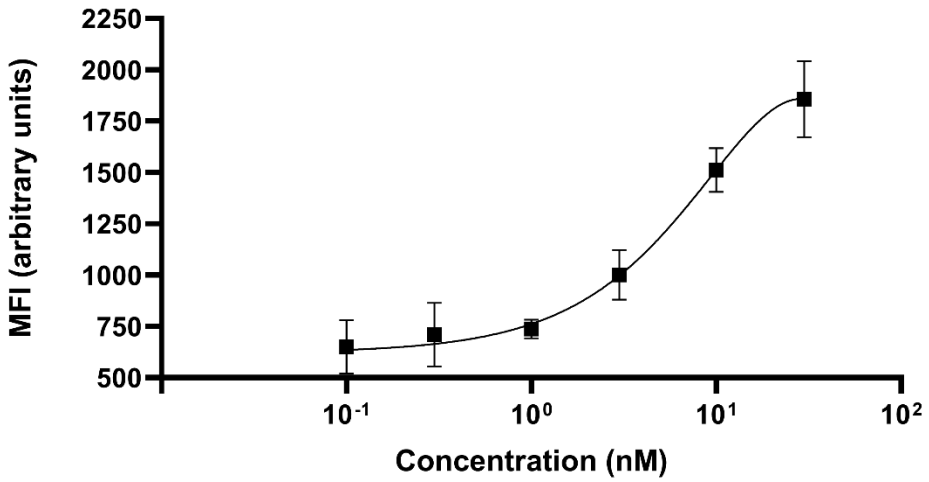
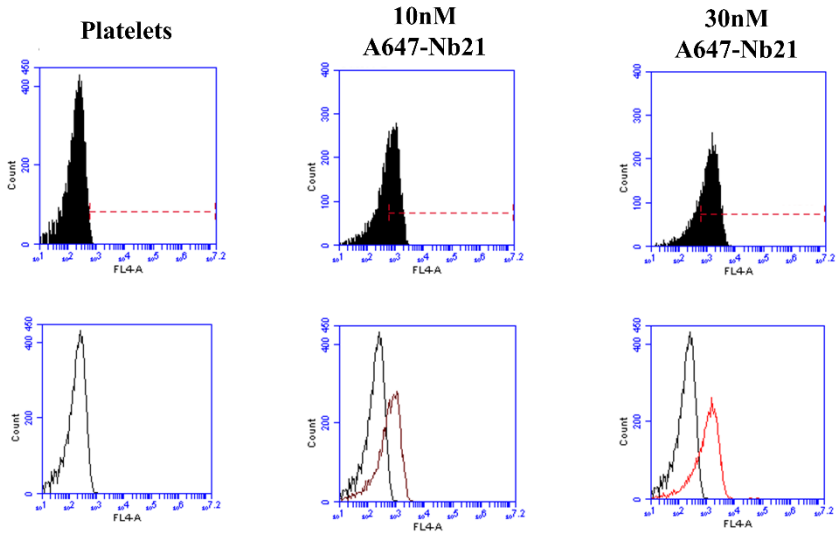


Figure 4.17. Saturation assay of A647-Nb21 in washed platelets*. 10,000 events/sample in washed platelets (PBS) were incubated with His-tagged Nb21 labelled with Alexa Fluor™ 647 succinimidyl ester in increasing concentrations of 0.1 0.3, 1, 3, 10 and 30nM to generate a saturation curve of binding. (A) Black-filled figures: Representative histograms of geometric mean fluorescence intensities of different nanobody concentrations bound to washed platelets. Platelets were also incubated with an anti-human GPVI targeting antibody (HY101, 1:400) raised in mice and an anti-mouse IgG Alexa Fluor™ 647 (1:400) to detect platelet GPVI levels. White-filled figures: Overlay between control cells and His-tagged incubated samples. (B) Flow cytometry data represented as MFI (arbitrary units) after non-linear regression fit. Data presented as mean±SEM performed in triplet (n=3).*

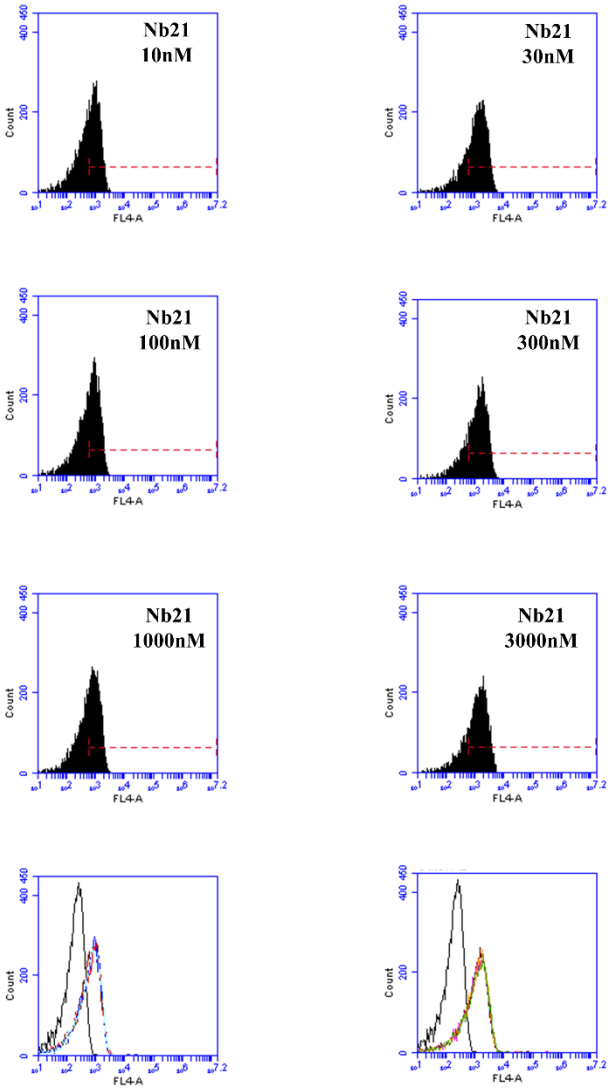
The non-labelled Nb21 nanobody version (Nb21) was then used to determine the nanobody concentration needed for A647-Nb21 displacement (Figure 4.18). Since saturation was not observed, both 10 nM and 30 nM were tested for displacement. There was no displacement of A647-Nb21 (10 or 30nM), even with the use of concentrations up to 100-fold higher for each concentration suggesting that the binding was non-specific.

A



Displacement of 10nM A647-Nb21

Displacement of 30nM A647-Nb21



B

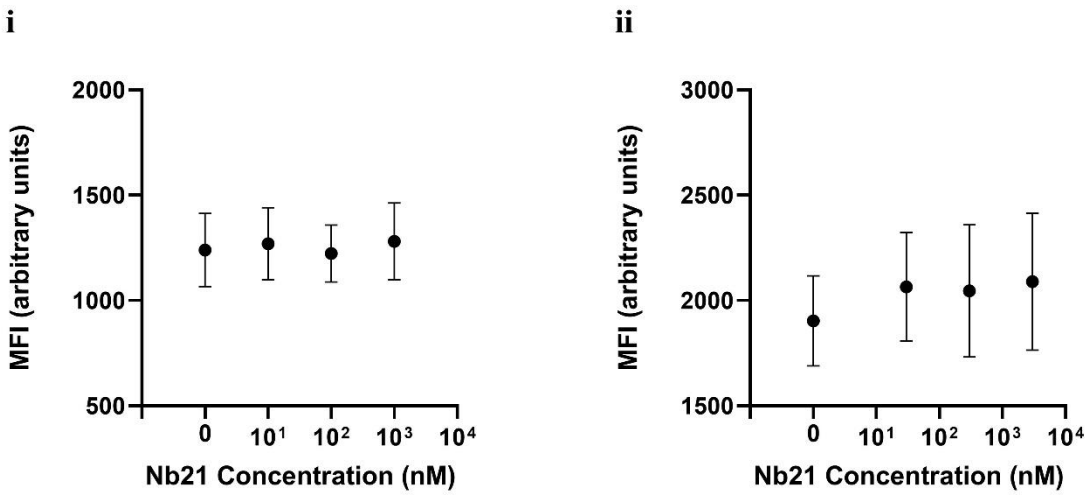


Figure 4.18. Displacement assay of A647-Nb21 in washed platelets by Nb21. *10,000 events/sample in washed platelets (PBS) were incubated with were incubated with A647-Nb21 at a constant concentration of 10nM or 30nM followed by the addition of increasing concentration of Nb21 of 10, 100 and 1000nM or 30, 300, 3000nM respectively for displacement assays with Nb21. (A) Black-filled traces: Representative histograms of geometric mean fluorescence intensities of different nanobody concentrations bound to washed platelets. Transparent traces: Overlay between control cells and each and His-tagged Nb21 incubated samples. (B) Flow cytometry data represented as MFI (arbitrary units). Data presented as mean±SEM performed in triplet (n=2).*

As displacement was not observed by the unlabelled equivalent of Nb21, Nb2 and Nb35, Nb2 and Nb35 (A647-Nb2 and A647-Nb35) were labelled and saturation curves were generated using the same workflow. The DOL was 0.5±0.2 for both A647-Nb2 and A647-Nb35. However, a similar behaviour was observed with the saturation curves generated by Nb2 and Nb35 (Figure 4.19). A pilot run of unlabelled versions of Nb2 and Nb35 against 10nM A647-Nb21 was then employed to see if any displacement by these nanobodies would be observed but this also did not show displacement (Figure 4.20).

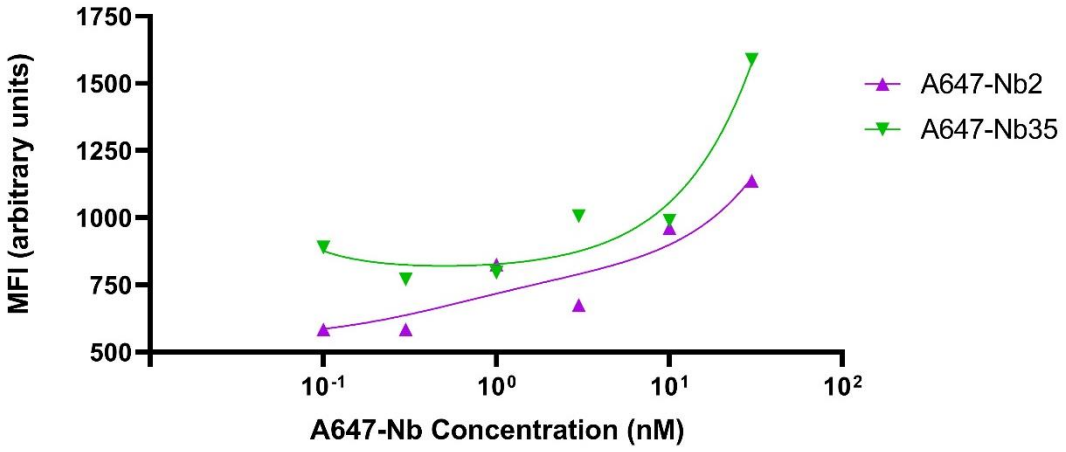
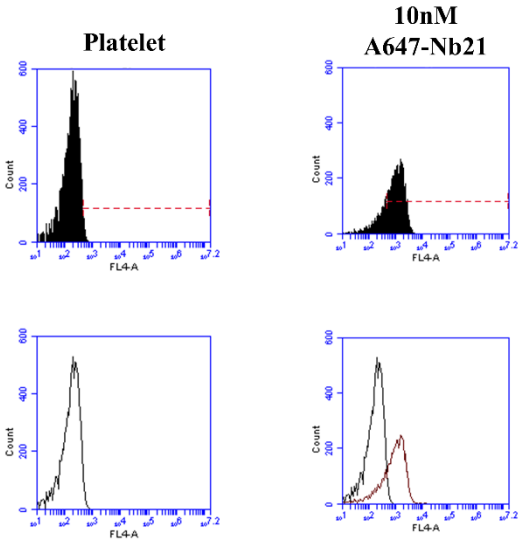
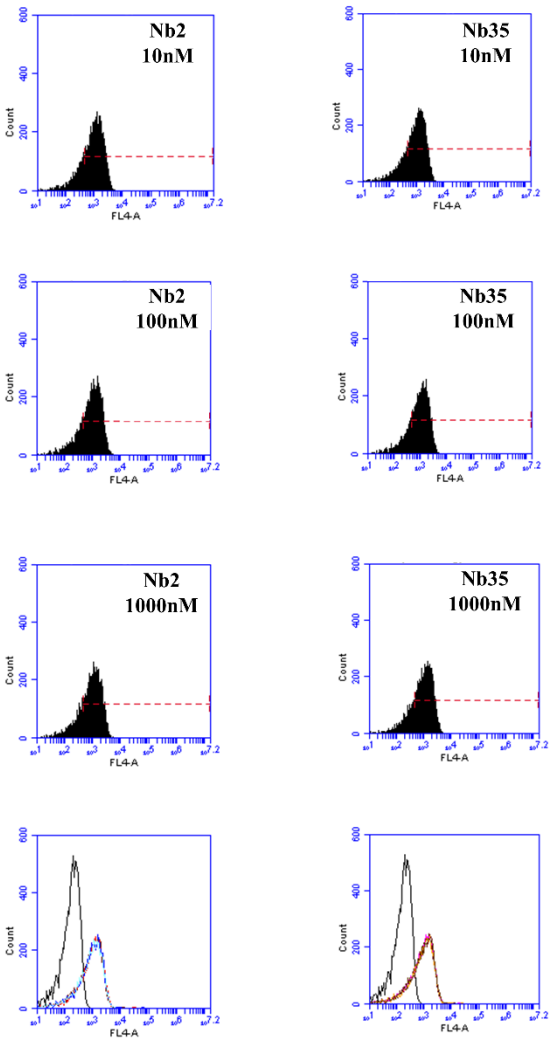


Figure 4.19. Saturation curve of A-647 Nb2 and A647-Nb35 in washed platelets. *10,000 events/sample in washed platelets (PBS) were incubated with His-tagged Nb2 or His-tagged Nb35 labelled with Alexa Fluor™ 647 succinimidyl ester in increasing concentrations of 0.1 0.3, 1, 3, 10 and 30nM to generate a saturation curve of binding. Flow cytometry data represented as MFI (arbitrary units) for Nb2 (purple) and Nb35 (green). Data presented as mean±SEM performed in triplet (n=3).*

A



Displacement of 10nM A647-Nb21



B

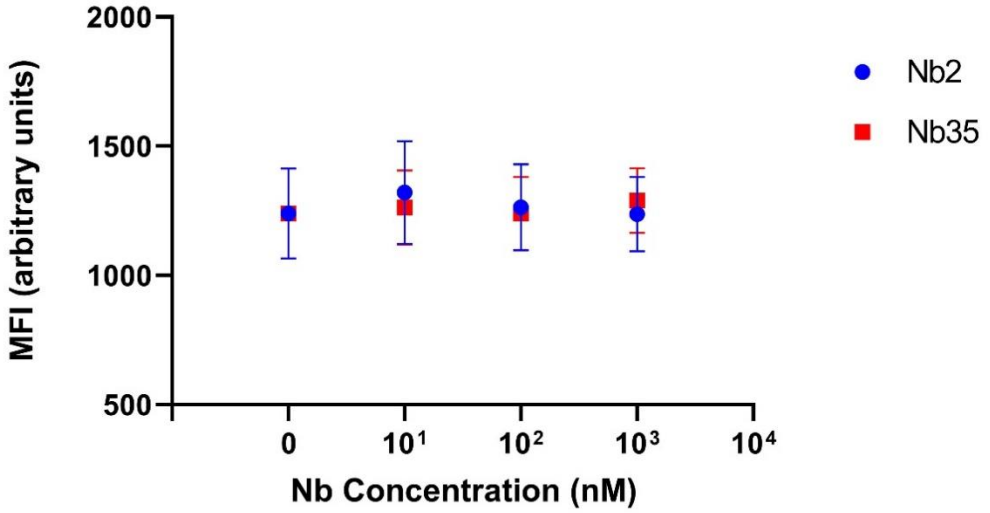
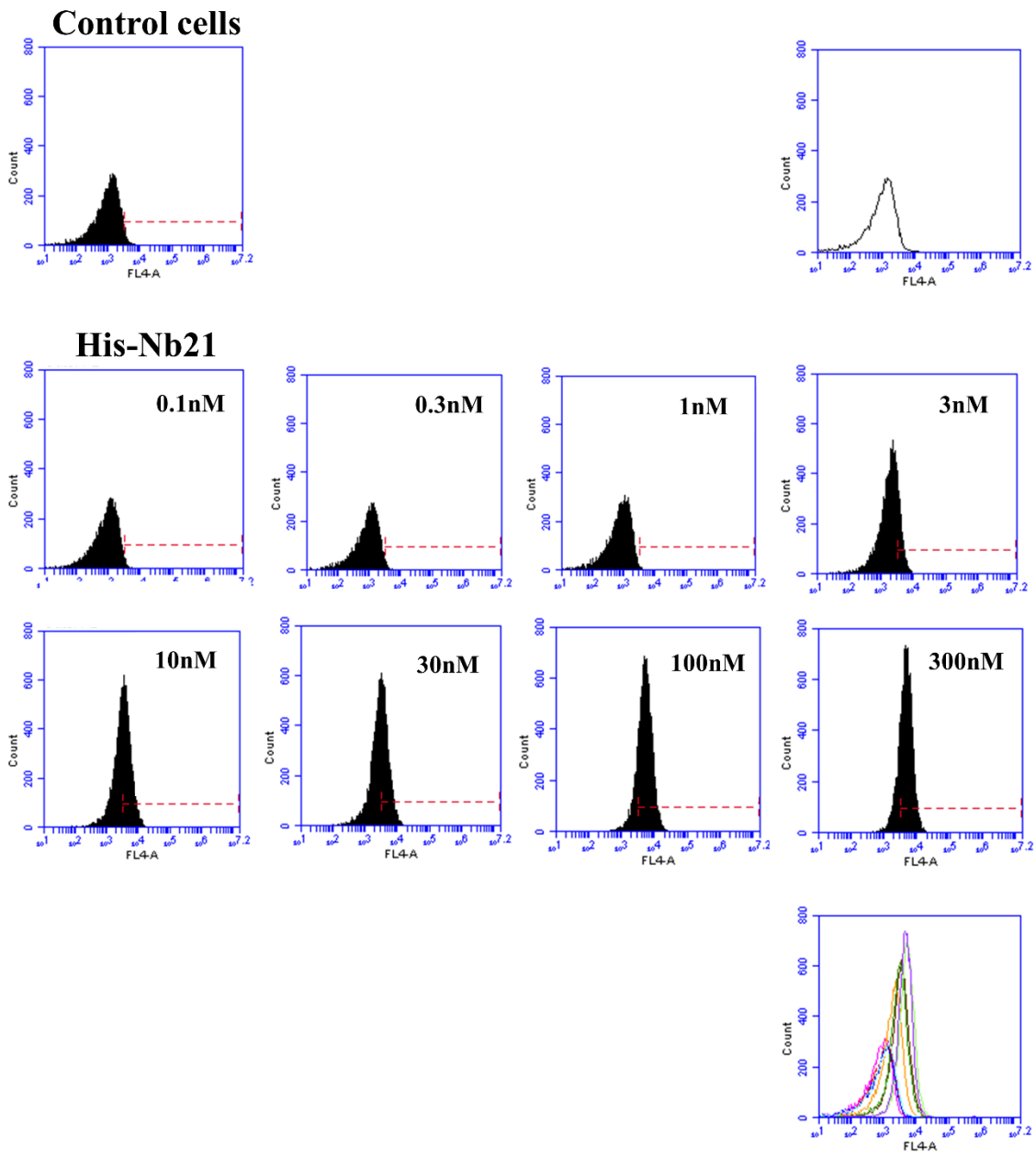


Figure 4.20. Displacement assay of His-tagged Nb21 in washed platelets by Nb2 and Nb35. *10,000 events/sample in washed platelets (PBS) were incubated were incubated with A647-Nb21 at a constant concentration of 10nM or 30nM followed by the addition of increasing concentration of Nb2 or Nb35 of 1, 10, 100 and 1000nM for displacement assays with Nb21. (A) Black-filled graphs: Representative histograms of geometric mean fluorescence intensities of different nanobody concentrations bound to washed platelets. White-filled graph: Overlay between control cells and each sample. (B) Flow cytometry data represented as MFI (arbitrary units). Data presented as mean±range performed twice (n=2).*

Since labelling nanobodies with Alexa Fluor 647 was not optimal for displacement assays, the His-tag nanobody versions were used in combination with an anti-His Alexa 647 secondary antibody to generate new saturation curves for Nb21 (Figure 4.21), in an attempt to use a fluorescent agent that binds nanobodies with higher specificity and incubate reagents for longer periods. The concentration for displacement chosen for this experimental series was 100 nM, instead of 10 or 30 nM, as full occupancy might have not been achieved in previous experiments. 100 nM and 300 nM of Nb21 had a less variable effect of fluorescence reduction while saturation is more likely achieved, compared to previous attempts. However, notable variability was still observed at 10 nM, 100 nM and 300 nM, making it hard to conclude the true mean fluorescence seen on these concentrations.

A


Control cells
His-Nb21
0.1nM
0.3nM
1nM
3nM
10nM
30nM
100nM
300nM
Count
FL4-A

B

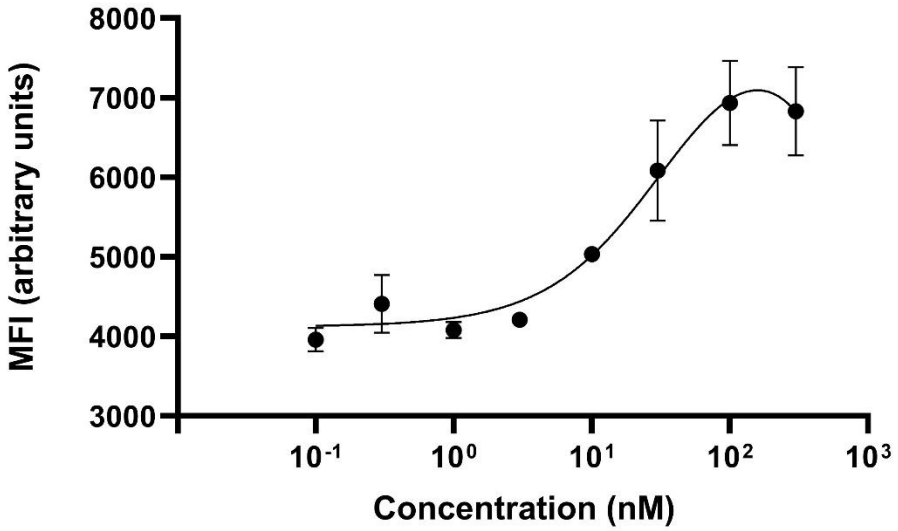
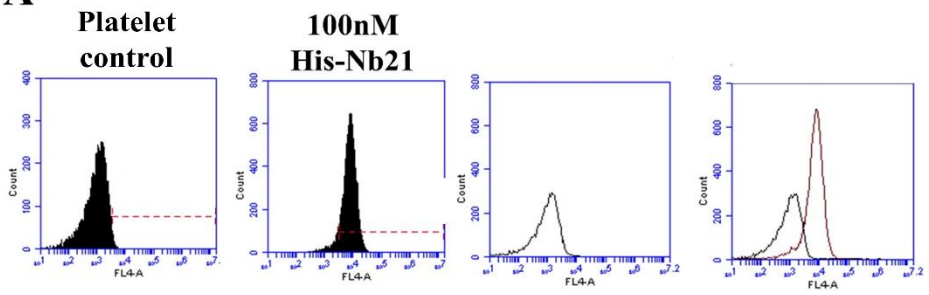


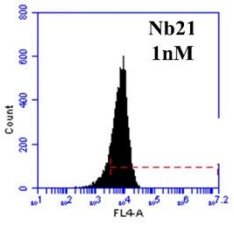
Figure 4.21. Saturation assay of His-tagged Nb21 in washed platelets. *10,000 events/sample in washed platelets (PBS) were incubated with His-tagged Nb21 in increasing concentrations of 0.1 0.3, 1, 3, 10, 30, 100 and 300nM to generate a saturation curve of binding. His-tagged Nb21 was detected with an anti-His Alexa Fluor 647 secondary antibody. (A) Representative histograms of geometric mean fluorescence intensities of different nanobody concentrations bound to washed platelets. White-filled graphs: Overlay between control cells and His-tagged incubated samples. (B) Flow cytometry data represented as MFI (arbitrary units) after non-linear regression fit (GraphPad Prism 8.4.3). Data presented as mean±SEM performed in triplet (n=3).*

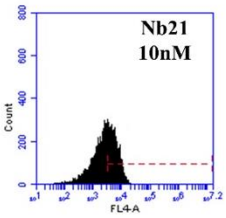
Then, the non-His-tag Nb21 nanobody version (Nb21) was used to determine the nanobody concentration needed for His-Nb21 displacement and vice versa (Figure 4.22). In this case, the His-tagged version was first incubated with washed platelets followed by incubation with the non-His tagged Nb21 and a final incubation with the anti-His Alexa Fluor 647 to detect binding levels of the His-tagged nanobody. A marked concentration-dependent reduction was observed this time with a concentration of 100nM completely displacing His-tagged Nb21. A displacement with non-His-tag Nb2 and Nb35 was not explored.

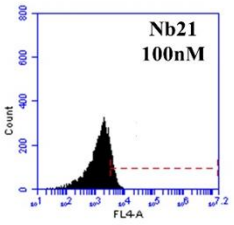
A

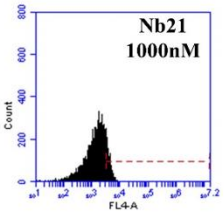


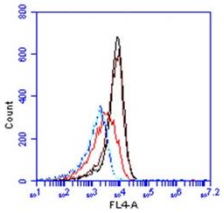
Displacement of His-Nb21 by Nb21











B

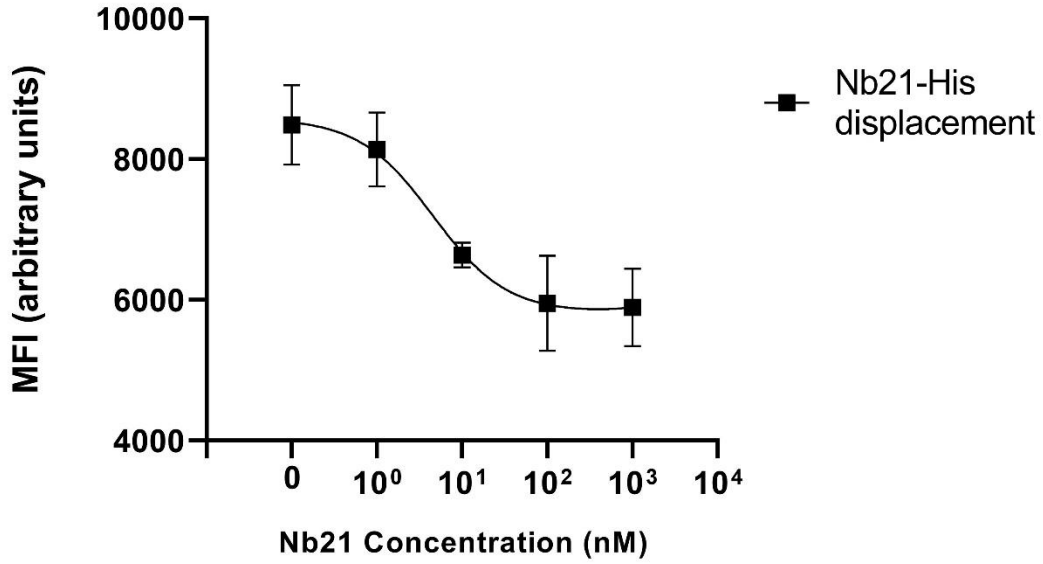


Figure 4.22. Displacement assay of His-Nb21 and Nb21 in washed platelets*. 10,000 events/sample in washed platelets (PBS) were incubated with a constant concentration of 100nM of His-tagged Nb21 and then increasing concentrations of Nb21 at 1, 10, 100 and 1000nM for displacement assays. An anti-His Alexa Fluor 647 secondary antibody (1:400) was used as a staining control and to detect the presence of His-Nb21 bound to platelets (platelet control). (A) Black-filled graphs: Representative histograms of geometric mean fluorescence intensities of different nanobody concentrations bound to washed platelets. White-filled graphs Overlay between control cells and each and His-tagged or Nb21 incubated samples. (B) Flow cytometry data represented as MFI (arbitrary units). An MFI of 6666±693 is observed for platelets alone. Non-linear regression fit was used to generate the Nb21 displacement curve. Data presented as mean±SEM performed in triplet (n=3).*

4.3.5 Outsourced data for the binding of Nb21 and Nb35 on GPVI

It has been mentioned in Slater *et al*. (2021), that Nb21 and Nb35 were displaced by Nb2 but the data were not shown. After personal communication with post-doctoral fellow, Alexandre Slater (University of Birmingham, UK), the data were supplied for discussion purposes for this Thesis. The experiment he conducted included the use of a competition ELISA assay, where ELISA plates were coated with GPVI-Fc and then His-tagged Nb21 and Nb35 were added to the coated plate. After GPVI-Fc binding was achieved, non-His-tagged Nb2 was added in increasing concentrations. The results from the competition ELISA showed that binding of both Nb21 and Nb35 to GPVI-Fc was displaced by untagged Nb2, in a concentration-dependent manner (Figure 4.23).

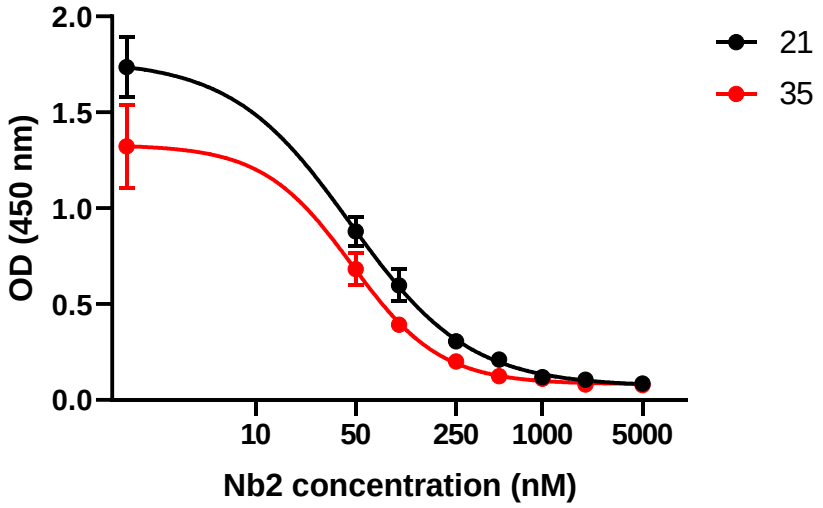


Figure 4.23. Results of competition ELISA for Nb21 and Nb35 displacement by Nb2. *Slater A., personal communication for data not shown in Slater et al. 2021. 96-well ELISA adhesive polystyrene plates were coated with GPVI-Fc (5 nM) overnight. His-tagged Nb21 and Nb35 (50 nM each) were added to the coated plates. After GPVI-Fc binding by the His-tagged nanobody constructs was achieved, non-His-tagged Nb2 was added in increasing concentrations of 50, 100, 250, 500, 1000, 2000 and 5000nM. His-tagged nanobody binding was detected with anti His-HRP and fluorescence at 450nm was detected using a plate reader. Non-linearregression fit (GraphPad Prism 8.4.3) was used for the generation of the displacement curve. (Slater A., personal communication, 30 May 2022).*

Regarding Nb35, post-doctoral fellow Eleyna Slater (University of Birmingham, UK) has also shared her data from surface plasmon resonance (SPR) experiments for Nb35 binding on monomeric and dimeric GPVI (Figure 4.24). These data were also supplied for discussion purposes for this Thesis. Her experiment included coating of CM5 chips of a Biocore T200 instrument with either extracellular monomeric GPVI or dimeric GPVI-Fc by amine-coupling, the addition of an Nb35 solution throw flow conditions and ligand tethering to the GPVI-coated surface was measured. Nb35 bound dimeric GPVI extracellular GPVI with a comparable K_D of 0.89±0.04 nM to the one for monomeric GPVI, with the latter being only slightly lower, (K_D=0.65±0.09 nM).

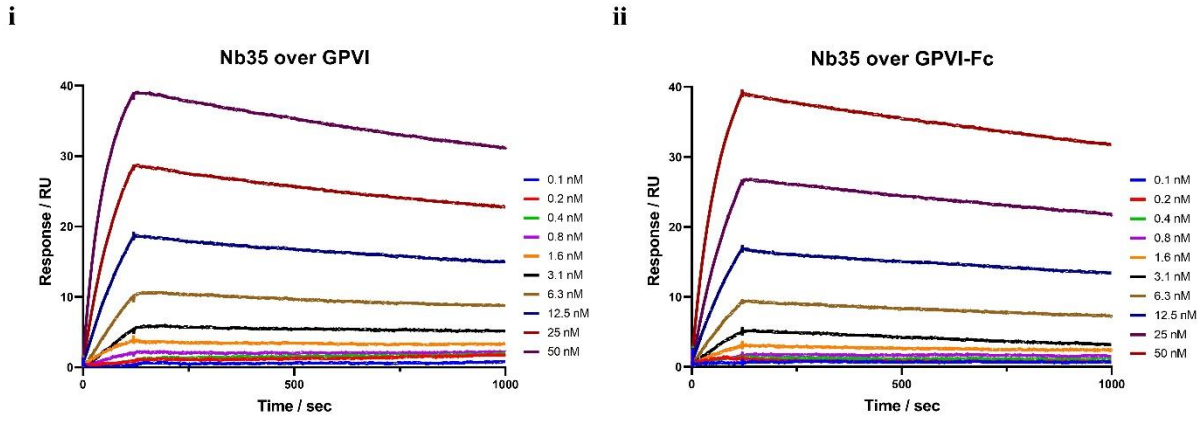


Figure 4.24. SPR analysis for Nb35 binding on monomeric and dimeric extracellular GPVI. *In a Biacore T200 apparatus (Cytiva), extracellular region monomeric GPVI or GPVI-Fc was directly immobilised on the CM5 chip by amine-coupling to the carboxylmethylated dextran-coated surface. Reference surfaces were blocked using 1M ethanolamine, pH=8. All sensograms shown are double reference subtracted and at least two replicates were injected per cycle (n=3). Experiments were conducted at 25°C with a flow rate of 30 µL/min in HBS-EP running buffer (0.01 M HEPES pH 7.4, 0.15 M NaCl, 3 mM EDTA, 0.005% v/v surfactant P20). Multi-cycle kinetic assays were used with at least 5 concentration points between 0.1x and 10x of the K_D. Each concentration of Nb35 was run by 120 sec injection, 900 sec dissociation, 30 sec regeneration with 10 mM glycine pH=1.5 followed by a 300 sec stabilisation period. Kinetic analysis was performed using the Biacore T200 Evaluation software with a global fitting to a 1:1 binding model. (Slater E., personal communication, 31 May 2022).*

4.4 Discussion

A focus of this study was to use potent, inhibitory nanobodies with low sequence overlap to Nb2 in the CDR regions that potentially bind novel binding sites on GPVI or compete for the same binding site as Nb2. The lack of sequence overlap between Nb2, Nb21 and Nb35 in their CDR3 domain made the latter two interesting for further investigation of their GPVI binding site.

Nb35 was successfully co-crystallized with the GPVI NQ ectodomain enabling the key residues and interactions for GPVI to be mapped. Interestingly, the generated structure showed that Nb35 binds to the same surface as Nb2, which was mapped within the D1 domain, adjacent to the CRP binding site, as previously described (Slater *et al.*, 2021). However, Nb35 binding did not induce a domain swap and a GPVI dimer was not formed. Instead the resulting GPVI structure was in a monomeric conformation. Although GPVI has been shown to be present in the membrane both as monomers and dimers (Berlanga *et al.*, 2007; Jung *et al.*, 2012; Poulter *et al.*, 2017; Clark *et al.*, 2021), dimerisation of recombinant GPVI ectodomain has not been observed in solution (Horii *et al.*, 2006). It is then possible that the monomeric conformation present in the Nb35 complex structure was indeed induced by the difference in the crystallisation conditions while the main mechanism behind Nb35 inhibition of collagen-induced signalling is most likely attributed in the reduction of avidity-based interactions through steric hindrance and regional distortion upon Nb35 tethering adjacent to the CRP binding site. This is in line with recent results suggesting that increased affinities of ligands to dimeric constructs are promoted by avidity rather than a unique dimer conformation (*Xu et al*., 2021). In addition, data supplied by post-doctoral fellow Eleyna Slater on Nb35 binding to coated monomeric and dimeric extracellular GPVI through SPR, supports that Nb35 bind the two conformations with a similar K_D and hence does not recognise a distinct binding epitope, with only a slightly higher affinity for monomeric GPVI. However, with the resolution of this crystal structure being on the low side and the lack of some modelled residues, especially in the D2 domain, potential conformations and shifts could have been concealed. Therefore, although the possibility of Nb35 stabilising a unique GPVI conformation that prevents GPVI dimerisation cannot be entirely disregarded, it is the least likely mechanism of action.

Although some interactions might be missing, it is apparent that GPVI residues Arg46, Tyr47 and Ala57 are essential for both Nb35 and Nb2 binding. This suggests that this docking triad is important for Nb2 and Nb35 tethering to GPVI. Interestingly, it is the conserved

residues in the two nanobodies that bind the same GPVI residues with overlapping or proximal coordinates. In particular, residues Ser99 from Nb2 and Ser100 from Nb35 form hydrogen bonds with GPVI residue Arg46 through the hydroxymethyl group, acting as hydrogen bond donors. Tyr115 from Nb2 and Tyr118 from Nb35 also act as hydrogen bond donors through their phenyl side chains to form a hydrogen bond with GPVI residue Ala57. On the other hand, Tyr102 from Nb2 and Tyr103 from Nb35 utilise their backbone nitrogen as hydrogen bond acceptors to form hydrogen bonds with Tyr47. Therefore, both nanobodies use the same type of amino acids to form polar bonds with the GPVI residues comprising the docking triad.

When comparing the binding site of Nb35 to the small molecule binding site used in previous *in silico* screening attempts (Bhunia *et al.*, 2017; Olğaç *et al.*, 2022), the coordinates of the two are overlapping with GPVI residues that bind Nb35 or Nb2 being located on the C` sheet and the 3_{10} helix of D1. Arg46 has been one of the key amino acids to target in these attempts while forming crucial polar interactions with small molecule GPVI inhibitors (Bhunia *et al.*, 2017; Olğaç *et al.*, 2022), including O1 and O2 (see Chapter 3). Lys41, Lys59 and Ser61 have also been reported to form hydrogen bonds with these ligands while losartan to interact with Tyr47 and Met58 (Ono *et al.*, 2014). These findings also strengthen the selection originally made for this pocket to be targeted for virtual screening of small molecule ligands while Arg46, Tyr47 and Ala57 could be vital target residues for future virtual screenings or SAR studies, especially Ala57 that has not been reported to form polar interactions with any of these ligands.

In addition, most small molecule inhibitors and those identified from other virtual screenings (Bhunia *et al.*, 2017; Olğaç *et al.*, 2022) form hydrogen bonds with Arg46. All these findings confirm that Arg46 is an effective residue for a strong inhibition effect towards GPVI with no effect on collagen binding. This residue could then be targeted for the development of ligands that work with an allosteric mechanism. Although other compound inhibitors show inhibition of collagen-induced GPVI signalling, as seen by virtual docking, platelet aggregation and platelet adhesion of the resulted compound inhibitors, these agents were not tested through binding assays with GPVI, such as ITC or SPR and therefore the exact mechanism of action is not fully elucidated and is less likely to involve steric hindrance on collagen binding. This is even more prevalent by the use of the racemic mixture in both studies rather than the individual enantiomers (Bhunia *et al.*, 2017; Olğaç *et al.*, 2022). As a high affinity is needed to achieve effective inhibition of collagen-related signalling on GPVI, a potential strategy would be

targeting Arg46, in combination with Tyr47 and Ala57. This could also be aided by the use of libraries that include natural compounds, peptides or ones that don't adhere to Lipinski's rules to increase the chance of finding a ligand that can achieve nanomolar-level affinity. Although R38 and R67 could be appealing targets for the design of small molecule inhibitors, as mutating these residues abolishes collagen signalling, the swallow nature of the CRP binding region makes virtual screening challenging. Even employing compounds or ligands from the aforementioned libraries, strong tethering and sufficient CRP competition must be achieved to surpass the multivalency challenge presented by GPVI agonists and ensure effective inhibition. The drug design could turn towards bigger ligands with to combat this challenge.

Mutating Arg60A was not previously reported to affect CRP binding but greatly affected collagen binding (Horii *et al.*, 2006). In the present study, mutating Arg60 did not affect collagen-induced GPVI signalling in the NFAT assay or the inhibitory effect of Nb2 and Nb35, but partially reduced that of Nb21. The partial effect on the inhibitory activation Nb21 suggests that this nanobody could be binding to an overlapping but distinct site to Nb35 and Nb2. This is consistent with Nb21 being displaced by Nb2 in a competition ELISA (Slater *et al*., 2021, Slater A., personal communication, 30 May 2022), as discussed above, and the reduction in inhibition in the presence of R46A mutation. Considering that Nb21 lacks the preserved residues that Nb2 and Nb35 require for binding to Arg46, it could be that Nb21 is binding in a proximal site and adapts a different docking pose to the former two by utilizing an interaction with Arg60. Optimisation of the crystallisation conditions for Nb21-GPVI complex or molecular modelling studies could answer this and pinpoint the coordinates this binding interface. In addition, the effect that nanobodies have upon CRP binding and CRP-induced activation was not characterised in this study.

The results from the binding studies using flow cytometry showed that mutating R60A and R67A increases the binding to all nanobodies while R46A and R38A reduce Nb21 and Nb35 binding to similar levels as Nb2, with the differences in binding found between the WT GPVI and R46A and R60A, were found to be significant. Therefore the importance of mutating R46 and Arg60 in GPVI signalling could be linked to the effect of these mutants have in nanobody binding, with R46A inhibiting collagen signalling by a reduction in binding of all nanobodies, while R60A directly or allosterically affecting Nb21 binding.

It has been previously reported that Nb21 was displaced by Nb2 in an ELISA set-up (Slater *et al*., 2021, Slater A. personal communication, 30 May 2022). The fact that Nb21 could not

compete with itself following Alexa Fluor™ 647 labelling could be attributed to either the A647 tag reacting with the basic amino acids within the binding domain in Nb21, reducing the specificity of the labelled nanobody, or due to the slow off rate of these nanobodies. . This was also seen by the labelled Nb2 and Nb35 when generating saturation curves. In contrast, using non-His tagged nanobody first and then displacing with the His-tagged version showed that displacement can be achieved, which come in hand with the longer incubation times (1 h overall incubation times compared to the 15 min ones in the previous set-up). An experimental set-up where a His-tagged Nb21 is used to fully bind GPVI on platelets and the addition of a non-His Nb21 with a final detection of His-tag levels through a secondary fluorescent antibody might be more appropriate.. Unfortunately, due to time limitations of this project, this was not possible.

In conclusion, a new nanobody was co-crystallised with the extracellular domain of GPVI, and revealed an overlapping binding site with previously described Nb2 with conserved residues of Nb2 and Nb35 binding the same GPVI residues and a similar binding pose. In addition, it was demonstrated that Arg46 is a crucial residue for the elucidation of the full inhibitory effects of Nb2, Nb21 and Nb35. Mutating this residue significantly reduced their inhibitory effects on collagen signalling. On the other hand, Arg60 seems to play an important role on the inhibition of collagen signalling of Nb21 but not Nb2 and Nb35. These results are highly relevant for the design of high-affinity GPVI targeting agents, including small molecule inhibitors.

Chapter 5

General Discussion

5.1 Drug discovery and development: from small molecules to new medicines

The current COVID-19 pandemic has imposed a grievous toll on human lives throughout the globe and almost every aspect of human life has been greatly affected. However, despite its devastating effects, the tremendous mobilization and global unity of the drug discovery and development community proved that when collective human resolve is employed, progress for therapies can skyrocket. While it usually takes 10–15 years to develop a vaccine, by 2020 results from phase III clinical trials of the Pfizer/BioNTech vaccine in adults (Polack *et al.*, 2020) and by 2021 for adolescents (Frenck *et al.*, 2021) were announced, with the results of trials by other pharmaceutical companies following soon after. This offers enormous encouragement for the promotion of future therapeutic strategies and the development of novel therapeutic agents (Villoutreix, 2021).

There is a wide variety of therapeutic agents to choose from for future medicinal strategies. Even the traditional usage of small molecules offers a plethora of options including synthetic compounds, natural products, carbohydrates, nucleic acids, peptides and stapled peptides. “Biologics” are gaining more and more popularity in drug discovery, especially for targeting PPIs which in many cases are undruggable by small molecules (Lu *et al.*, 2020). Biologics can vary from antibodies, antibody fragments and nanobodies, recombinant and fusion proteins, to other smaller biological molecules such as siRNAs, mRNA, miRNA, whole cells or genes (Andrews *et al.*, 2015).

Antibodies and small molecules can also be combined with a small molecule (antibody-drug conjugates) through the design of heterobifunctional small molecules, composed of two active domains and a linker. These can be lysosome targeting chimeras (LYTACs), macroautophagy degradation targeting chimeras (MADTACs) or proteolysis targeting chimera (PROTACs) that

can target proteins for degradation. The latter have been developed for targeting ubiquitination-related pathological diseases, such as the neurodegenerative disease Alzheimer's, and cancer, by degradation of pathogenic proteins (Khan *et al.*, 2020; Alabi and Crews, 2021).

89 biologics compared to 289 small molecule drugs have been approved between 2010 and 2019 (Brown and Wobst, 2021). This is attributed to the difficulty in developing biologics for oral administration, as well as a high cost of development and in some cases production, although progress is being made in this area (Homayun *et al.*, 2019). Gene editing technologies, including CRISPR/Cas9 and cell-based therapies also have enormous potential, as demonstrated by the recent advances in the treatment of cystic fibrosis (Allan *et al.*, 2021) and blood-specific diseases (Staal *et al.*, 2019), but there are also many issues to overcome.

5.2 Summary of results

The overall project goal was to characterize the mode of action and to map the binding site of anti-GPVI ligands in order to understand the mechanisms behind GPVI inhibition and identify novel binding grooves that can be used for future design of inhibitors. My approach was through a combination of structural-based virtual screening and testing, fluorescence-based assays, mutation studies and protein crystallography of GPVI in complex with potent nanobody ligands.

The main finding of Chapter 3 is the development of a virtual screening based on a structured-based pharmacophore for identifying potential GPVI small molecule inhibitors. Although compound **22** showed a selective effect on collagen-induced aggregation, competition ELISA and NFAT-luciferase showed that it most likely does not inhibit GPVI through a selective mechanism. Chapter 4 explored the co-crystallization of nanobodies Nb21 and Nb35, with the crystal complex of Nb35 and the extracellular domain of GPVI being resolved. The binding site overlaps with that of Nb2 with conserved residues within the two

nanobodies binding the same GPVI residues. The GPVI residue Arg46 was identified as a crucial residue for the inhibitory effects of Nb2, Nb21 and Nb35 on collagen signalling and verified by mutation studies. Arg60 also plays an important role in the interaction with Nb21 but not Nb2 and Nb35.

5.3 *In silico* investigation for small molecule ligands for GPVI

Small-molecule GPVI inhibitors have been previously reported, with the most thoroughly studied being losartan (Taylor *et al.*, 2014). A number of other synthetic compounds (Anil Kumar *et al.*, 2014; Bhunia *et al.*, 2017; Misra *et al.*, 2018) and natural bioactive compounds (Hsiao *et al.*, 2007; Lin *et al.*, 2013; Chang *et al.*, 2017; Lee *et al.*, 2017) have been investigated. However, all of the former have IC_{50} values in the micromolar range on platelet aggregation assays (Chapter 3, Table 1) and display off-target effects on other platelet receptors suggesting that the majority act through a generalized effect on luciferase off-target inhibition or shared signalling cascade rather than a competitive or allosteric binding site interaction.

The purpose of the studies in Chapter 3 was to develop a screening strategy for the identification of selective and potent hits for the development of small molecule GPVI inhibitors. A virtual structure-based pharmacophore screening based on the previously identified binding pocket within GPVI for collagen (Kato-Takagaki *et al.*, 2009; Ono *et al.*, 2010; Taylor *et al.*, 2014; Bhunia *et al.*, 2017; Olğaç *et al.*, 2022) and the recently characterised pocket for CRP (Feitsma *et al.*, 2022) were used. More than 84,000 compounds were screened from the MCCC library, with 30 being tested for inhibition of collagen-induced aggregation on washed platelets. Compound **22** selectively inhibited collagen-induced aggregation over rhodocytin and TRAP-induced aggregation. However, when **22** was tested in an ELISA there was no competition with collagen for binding to monomeric or dimeric GPVI. Since CRP was not used as an agonist in the light transmission assay or ELISA, the effect of these inhibitors

on CRP is unknown. It would then be beneficial to test in the future to identify differences in the effects inhibitors might have in collagen and CRP-induced signalling. 22 also failed to inhibit GPVI-mediated NFAT signalling in a GPVI-transfected HEK293T cell line. This was also observed with literature compounds **O1** (1) and **O2** (2) from Olğac *et al.* (2021), while compound **4** from Bhunia *et al.* (2017) did not inhibit collagen-induced platelet aggregation. The present study used a higher collagen concentration (3 μg/mL over 1 μg/mL) used by Bhunia *et al*. (2017) which could explain their inability to inhibit collagen-induced platelet aggregation. But **O1** and **O2** were tested using the aforementioned experimental conditions as well as the same supplier and compound concentration, and therefore the reason for these observations is not as clear. Nb2, used as a control, successfully inhibited both collagen-induced aggregation, GPVI binding to collagen and GPVI signalling which is in line with previous literature findings (Slater *et al.*, 2021). Therefore, the hits found in this study do not inhibit GPVI through a selective mechanism.

5.4 Mapping the binding sites of nanobodies on GPVI

Co-crystallization with known, potent ligands, such as that between GPVI and Nb2 (Slater *et al.*, 2021), is required to provide a clear structural insight on the docking mode and binding site of strong GPVI binders. Mapping the binding sites of these ligands will open up the field for development of more powerful GPVI inhibitors. Chapter 4 explores the information gained from crystallisation of a new nanobody, Nb35, with the extracellular domain of GPVI.

Nanobody Nb35, a potent nanobody raised against GPVI (Slater *et al*. 2021), was successfully co-crystallised with the extracellular domain of GPVI. Crystal analysis revealed an overlapping binding site with previously described Nb2 (Slate*r et al*., 2021). Both Nb2 and Nb35 bind the same GPVI residues, Arg46, Tyr47 and Ala57. These GPVI amino acids were bound by conserved residues of Nb2 (Ser99, Tyr115, Tyr102) and Nb35 (Ser100, Tyr118,

Tyr103), which also bind to Arg46, Tyr47 and Ala57 respectively in a similar binding pose and coordinates. These results provide information on the binding site for the future design of virtual screens for GPVI inhibitors. In particular, a screen design could be based on binding restrictions for docked ligands, including binding to residues Arg46, Tyr47 and Ala57, while positional or hydrogen bond constraints can be implemented for docked molecules to adopt the same binding pose as the ones that Nb2 and Nb35 residues do when bound to the receptor. Other binding interaction, such as docking to residue Tyr66, which lies deeper in this binding pocket, could promote stronger ligand binding. As previously mentioned, natural compound, peptide or larger ligand libraries would be more appropriate for this screening set-up. This is important to increase the chances of identifying a nanomolar affinity inhibitor. However, it is unclear if such an inhibitor would work as Nb2 and Nb35 work through steric hindrance as the site does not overlap with that of CRP and a strategy based on mapping of this site should also be used.

Mutating Arg38 and Arg67, residues crucial for CRP binding to GPVI (Feitsma *et al*., 2022), also abolished collagen signalling. The CRP binding site is some distance away from the previously suggested collagen binding site (Horii *et al*., 2006) and suggests that the binding sites for collagen and CRP overlap. However, the structure of GPVI with fibrillar collagen has not been reported to confirm this. R38A and R67A did not significantly affect the binding of Nb2, Nb21 and Nb35 to GPVI. Arg38 and Arg67 could therefore be targets for the design of small molecule inhibitors, although the shallow nature of the CRP binding region makes virtual screening challenging. Another considerable challenge when developing small molecule inhibitors for GPVI is that they need to be able to compete with the multivalent nature of endogenous GPVI ligands that promote avidity-driven activation of GPVI (R. G. Xu *et al.*, 2021). However, nanomolar-range affinity and slow off-rate kinetics sufficient competition must be achieved to surpass the multivalency challenge presented and ensure effective

inhibition by collagen and other GPVI ligands (Damaskinaki *et al.*, 2021). On the other hand, residue Arg46 is of particular importance for inhibitory effects of Nb2, Nb21 and Nb35. Mutating this residue significantly abolished the inhibitory effects on collagen signalling of all three nanobodies in NFAT-luciferase while binding studies using flow cytometry demonstrated that binding to R46A construct was significantly reduced. On the other hand, Arg60 seems to play an important role on the inhibition of collagen signalling of Nb21, but not Nb2 and Nb35, and also an increase in binding of all nanobodies, suggesting that the binding sites overlap but are not the same. Since the effect that nanobodies have upon CRP binding and CRP-induced activation was not investigated. CRP could be implemented as an agonist in the above NFAT assay set-up to compare the effect of nanobodies on CRP compared to collagen. Using biophysical methods, such as SPR, can show whether this effect is attributed to less binding of the agonist to GPVI in a more robust manner, compared to the aforementioned flow cytometry set-up. The inhibition effect on CRP and collagen induced activation and binding could then be assessed.

Although, alanine scanning site-directed mutagenesis is a widely-used technique to identify protein residues important for function or ligand binding, it can induce a variety of effects on the final receptor tertiary structure and hence implementing structural characterisation through crystallography has a lower risk of error than molecular modelling. The advantage of crystallography have been demonstrated both by the structural characterisation of the binding sites for glenzocimab (Billiald *et al.*, 2022) and CRP to GPVI compared to mutation studies and molecular modelling done for the same ligands in the past (Lecut *et al.*, 2004; Horii *et al.*, 2006). Since the effects of R46A to nanobody binding can be explained by the position of residue Arg46 in the GPVI crystal and its importance in Nb2 and Nb35 tethering, we can be more confident that the reduction in signalling and binding is directly linked to the crystal structure findings. The attempt to see whether Nb21 was displaced by Nb2 in flow cytometry

set up was not completed and therefore more data coyuld be generated if this experiment was performed. However this approach has many limitations, including the low non-His Nb21 yields, limited incubation times due to platelet viability and absence of wash steps to remove unbound reagents in addition to the slow off nanobody kinetics. All the former are affecting the data generated and hence incubation times should be longer. Although this set up could be promising on measuring binding on intact washed human platelets in a flow environment, optimisation is needed or other experimental approaches to be considered. Overall, the increase of nanobody binding on R60A might be linked to an increase in collagen signalling and that the reduction of Nb21 signalling is due to Arg60 being part of the Nb21 binding site, without any crystallography data, a definite conclusion on its role cannot be made.

5.5 Further discussion

When it comes to limitation in screening approaches, the major ones faced are the nature of GPVI available pockets for virtual screening and the physical screening assays. Since both GPVI binding regions are relatively flat and swallow surfaces, especially the CRP binding pocket, it would be more suited for docking larger ligands, such as peptides or natural compounds, rather than libraries with compounds of Lipinski's drug-like properties (Lu *et al.*, 2020; Damaskinaki *et al.*, 2021). It could also be beneficial to avoid a pharmacophore screening in order to increase the chances for identifying an inhibitor.

Alterative screening approaches such as NMR rely on real-time ligand exchange that compete within detection limits. NMR is more beneficial for slower ligand off-rates, low-affinity complexes ($K_D < 10^{-6}$ M) and high flexibility ligands (Ziarek *et al.*, 2011; del Carmen Fernandez-Alonso *et al.*, 2013). ELISA or AlphaScreen (a bead-based, non-radioactive Amplified Luminescent Proximity Homogeneous Assay) could be more helpful as a first test

to identify PPI inhibitors and to directly monitor ligand–receptor interactions and has been previously implemented in that context (Schorpp *et al.*, 2014).

AlphaFold has recently emerged as an artificial intelligence-based protein structure prediction tool for the human proteome and relies on currently available genomic data as a learning approach to predict structures. The training set used for AlphaFold is the Protein Data Bank (PDB) (Senio*r et al*., 2020) to predict the distances β carbons of protein amino acids and then uses more complex calculations (including residue physicochemical properties such as Wan de Waals radii, electrostatic force region, etc) to find the lowest protein energy state. However, it is still unable to predict parameters such as metal ions, cofactors, other ligands and post-translational modifications, such as phosphorylation or glycosylation, while interactions of oligomers, especially the ones not available in the database, and some amino acid side chains are not always placed correctly (Perrakis and Sixma, 2021). Despite the increase in the number of PDB entries and the increase in algorithm training over the past two years, it is still highly dependent on these databases. This means that some limitations include the fact that a PDB entry may not be the natural fold state of a protein or the fact that it can extrapolate information around known points of the protein-structure space and may not accurately predict novel configurations (Marcu *et al*., 2022). Hence, it is necessary to use the prediction confidence as a guide to understand which protein parts are likely to be accurately predicted. Currently, the extracellular domain of GPVI is accurately predicted but the prediction on the transmembrane domain is of low confidence and therefore more structural data is needed to accurately predict this region.

GPVI structural research would benefit from deciphering the structure of full-length GPVI linked with the FcRγ chain in the membrane to visualise the full GPVI conformation in a more biological relevant setting to map the interactions between GPVI and FcRγ. In addition, this information would enable the comparison of currently available crystal structures and provide

an insight on how ligand binding to extracellular GPVI affects intracellular signalling through the FcRγ chain. Cryoelectron microscopy (cryo-EM) is a powerful alternative to X-ray crystallography or NMR spectroscopy for macromolecular structures and bigger protein complexes without the need for crystallization. This technique has already been used to successfully characterise the structure of platelet receptor αIIbβ3 with mAb-based anti-platelet drug, abciximab, (Nešić *et al*., 2020) and could provide a powerful tool for elucidating the full GPVI structure.

When exploring the structure of currently available GPVI-specific agents, one could wonder whether there is a potential for monomeric CRP to be re-engineered into a competitive inhibitor for GPVI and whether it is reasonable to expect a small molecule to effectively block this with adequate affinity could be useful. The GPVI-CRP complex interaction is now mapped and involves multiple interactions between the two proteins while CRP is only highly potent as a platelet agonist only after cross-linking (CRP-XL), with soluble monomeric CRP being a significantly weaker agonist (Smethurst *et al*., 2007). It has also been shown that the smallest effective GPVI recognition motifs comprise two GPO triplets, either adjacent or separated by four GPP triplets agonist (Smethurst *et al*., 2007). Therefore one would argue that extrapolating the core interactions from CRP monomers to develop a competitive inhibitor for collagen interacting to GPVI could be an effective targeting strategy. However, there are many disadvantages to this strategy, including the challenging structural architecture of the targeting receptor, a high cost of production for CRP-based agents and the need for steric hindrance, when investigating competitive inhibition of GPVI interaction with collagen. There is also a likely need for complete inhibition of GPVI function and clustering to elicit a beneficial therapeutic effect, as demonstrated by minimal effect of the *GPVI* c.711_712insA allele on platelet function of heterozygous patients (Matus *et al.*, 2013; Perrella *et al.*, 2021). Hence,

GPVI does not seem currently amenable to small molecule inhibition, can explain the higher success number of biologics as anti-GPVI targeting agents.

5.6 Future of GPVI inhibitors

There are many reasons why GPVI is as an attractive target for manipulating platelet function. GPVI is exclusively found on the surface of platelets, which presents an opportunity for selective targeting with less off-target effects, while it is GPVI there is a plethora of anti-GPVI antibodies and antibody fragments that affect the function or downregulation of receptor surface levels of the molecule. Phenotypically, loss of GPVI has a minimal effect on physiological haemostasis, while pathological thrombus formation is significantly reduced, as shown in both patients and animal models.

However, thrombosis is a complex process modulated by many proteins and gene products in the human system. More clinical studies are needed to evaluate the suitability and efficiency of GPVI inhibitors as a monotherapy, or in combination with the existing antiplatelet and anticoagulant therapies, for the treatment of acute conditions and their potential in chronic treatment. For example, anti-GPVI treatment severely impeded haemostasis in mice lacking α2β1 or mice simultaneously treated with aspirin (Grüner *et al.*, 2004). Currently, the clinical benefit of revacept is limited by its expensive cost of production, as well as intravenous administration, making patient compliance and accessibility difficult. The main mechanism of revacept relies on competition with collagen, and not GPVI, one of the bodies most abundant proteins, which may reveal other adverse implication of this treatment in future clinical trials.

Overall, targeting GPVI may be a stand-alone treatment but there is lots of evidence suggesting that GPVI inhibitors will not only exert powerful antithrombotic benefits but may also prove effective in the treatment of coronary artery disease and possibly inflammatory diseases. Several protein GPVI-targeting agents have been reported, in contrast to fewer and

weaker small-molecule GPVI antagonists, with the latter often lacking evidence for target engagement while their biological efficacy cannot always be replicated within different groups. Recent advances in GPVI research, including structural identification of the collagen binding site, CRP sequence, the binding coordinates and key inhibition residues of two different potent anti-GPVI nanobodies may now support the de novo development of specific small molecule inhibitors for the collagen-GPVI interaction while minimizing drug off-target binding i.e., GPVI and LAIR-1.

5.7 Final conclusions

GPVI has emerged as a promising pharmacological target for the prevention of both arterial thrombosis and thromboinflammatory diseases with a lower bleeding risk compared to current antithrombotic therapies. Protein GPVI ligands occupy a large surface area of the receptor and can utilise avidity to increase their overall effect (Lecut *et al.*, 2003; Li *et al.*, 2007; Voors-Pette *et al.*, 2019), whilst small molecules by their nature interact with a smaller area (Jones and Thornton, 1996). The affinity of the current small-molecule inhibitors for GPVI is in the micro-molar range and does not appear to be due to competition (Rognan, 2015; Damaskinaki *et al.*, 2021).

The lack of structural characterisation, effective design of virtual screenings and the selection of appropriate compound libraries and relevant tool compounds or anti-GPVI agents are important elements for overcoming the targeting challenges on the identification and development of GPVI inhibitors. In the present study, the structure of a new potent nanobody, Nb35, was mapped in complex with GPVI and the effect of different GPVI residues on the binding of potent anti-GPVI nanobodies. These findings are directly applicable in the future design of screening strategies for high-affinity GPVI ligands, including small molecule inhibitors.

References

Achison, M., Joel, C., Hargreaves, P. G., Sage, S. O., Barnes, M. J., & Farndale, R. W. (1996). Signals elicited from human platelets by synthetic, triple helical, collagen-like peptides. *Blood Coagul. Fibrinolysi*s, 7(2), 149–152. doi: 10.1097/00001721-199603000-00009.

ACTICOR BIOTECH. (2022, May 9). Presentation of positive results from the ACTIMIS Phase 1b/2a study in stroke at ESOC 2022 [Press release]. https://uploads-ssl.webflow.com/60ed4d6a6fc45c3a0e3cfb8f/62795d2630c4e7f2cf18aa9d_Acticor_PR_ESOC_EN_090522%20-%202.pdf. (Accessed: 1 July 2022).

Ahmed M. U., Receveur N., Janus-Bell E., Mouriaux C., Gachet C., Jandrot-Perrus M., . . . Mangin P. H. (2021). Respective roles of Glycoprotein VI and FcγRIIA in the regulation of αIIbβ3-mediated platelet activation to fibrinogen, thrombus buildup, and stability. *Res. Pract. Thromb. Haemost.*, 5(5), 1–7. doi:10.1002/rth2.12551.

Al-Tamimi, M., Mu, F. T., Arthur, J. F., Shen, Y., Moroi, M., . . . Gardiner, E. E. (2009). Anti-glycoprotein VI monoclonal antibodies directly aggregate platelets independently of FcgammaRIIa and induce GPVI ectodomain shedding. *Platelets*, 20(2), 75–82. doi:10.1080/09537100802645029.

Alkarithi, G., Duval C., Shi Y., Macrae F. L. & Ariëns R. A. S. (2021). Thrombus structural composition in cardiovascular disease, *Arterioscler. Thromb. Vasc. Biol*. doi: 10.1161/ATVBAHA.120.315754.

Alshehri, O. M., Montague, S., Watson, S., Carter, P., Sarker, N., Manne, B. K., . . . Watson, S. P. (2015). Activation of glycoprotein VI (GPVI) and C-type lectin-like receptor-2 (CLEC-2) underlies platelet activation by diesel exhaust particles and other charged/hydrophobic ligands. *Biochem. J*., 468(3), 459–473. doi:10.1042/BJ20150192.

Alshehri O. M., Hughes, C. E., Montague, S., Watson, S. K., Frampton, J., Bender, M. & Watson, S. P. (2015). Fibrin activates GPVI in human and mouse platelets. *Blood*, 126 (13), 1601–1608. doi: 10.1182/blood-2015-04-641654.

Anania J. C., Chenoweth A. M., Wines B. D. & Hogarth, M. P. (2019). The human FcγRII (CD32) family of leukocyte FcR in health and disease, *Front. Immunol.*, 10(464), 1–17. doi:10.3389/fimmu.2019.00464.

Andrews, L., Ralston, S., Blomme, E., & Barnhart, K. (2015). A snapshot of biologic drug development: Challenges and opportunities. *Hum. Exp. Toxicol.*, 34(12), 1279–1285. doi:10.1177/0960327115603594.

Andrews, R. K., Kamiguti, A. S., Berlanga, O., Leduc, M., Theakston, R. D., & Watson, S. P. (2001). The use of snake venom toxins as tools to study platelet receptors for collagen and von Willebrand factor. *Haemostasis*, 31(3-6), 155–172. doi:10.1159/000048059.

Andrews, R. K., Gardiner, E. E., Shen, Y., & Berndt, M. C. (2003). Structure-activity relationships of snake toxins targeting platelet receptors, glycoprotein Ib-IX-V and glycoprotein VI. Current medicinal chemistry. *Curr. Med. Chem. Cardiovasc. Hematol. Agents*, 1(2), 143–149. doi:10.2174/1568016033477559.

Arthur, J. F., Shen, Y., Kahn, M. L., Berndt, M. C., Andrews, R. K., & Gardiner, E. E. (2007b). Ligand binding rapidly induces disulfide-dependent dimerization of glycoprotein VI on the platelet plasma membrane. *J. Biol. Chem.*, 282(42), 30434–30441. doi:10.1074/jbc.M701330200.

Arthur, J. F., Dunkley, S. & Andrews, R. K. (2007a). Platelet glycoprotein VI-related clinical defects, *Brit. J. Haematol.*, 139(3), 363-372. doi:10.1111/j.1365-2141.2007.06799.x.

Asselin J., Gibbins J. M., Achison M, Lee Y. H., Morton L. F., Farndale R. W., Barnes M. J. & Watson S. P. (1997). A Collagen-Like Peptide Stimulates Tyrosine Phosphorylation of syk and Phospholipase Cγ2 in Platelets Independent of the Integrin α2β1. *Blood*, 89(4), 1235–1242. doi: 10.1182/blood.V89.4.1235.

Association, W. M. (2013). World Medical Association Declaration of Helsinki: Ethical Principles for Medical Research Involving Human Subjects. *JAMA*, 310(20), 2191–2194. doi: 10.1001/jama.2013.281053.

Astarita, J. L., Acton, S. E., & Turley, S. J. (2012). Podoplanin: emerging functions in development, the immune system, and cancer. *Front. Immun.*, 3, 283. doi:10.3389/fimmu.2012.00283.

Barnes, M. J., Knight, C. G., & Farndale, R. W. (1996). The use of collagen-based model peptides to investigate platelet-reactive sequences in collagen. *Biopolymers*, 40(4), 383–397. doi:10.1002/(sici)1097-0282(1996)40:4<383::aid-bip4>3.0.co;2-s.

Batuwangala, T., Leduc, M., Gibbins, J. M., Bon, C., & Jones, E. Y. (2004). Structure of the snake-venom toxin convulxin. *Acta. Crystallogr. D. Biol. Crystallogr.*, 60(Pt 1), 46–53. doi:10.1107/s0907444903021620.

Beghein, E. & Gettemans, J. (2017). Nanobody technology: A versatile toolkit for microscopic imaging, protein-protein interaction analysis, and protein function exploration, *Front. Immunol.*, 8, 1–14. doi: 10.3389/fimmu.2017.00771.

Bender, M., Hofmann S., Stegner D., Chalaris A., Bösl M., Braun A., Scheller J., Rose-John S. & Nieswandt B. (2010). Differentially regulated GPVI ectodomain shedding by multiple platelet-expressed proteinases, *Blood*, 116(17), 3347–3355. doi: 10.1182/blood-2010-06-289108.

Bender, M., Hagedorn, I. & Nieswandt, B. (2011). Genetic and antibody-induced glycoprotein VI deficiency equally protects mice from mechanically and FeCl 3-induced thrombosis, *J. Thromb. Haemost.*, 9(7), 1423–1426. doi: 10.1111/j.1538-7836.2011.04328.x.

Bergmeier, W. and Stefanini, L. (2013). Platelet ITAM signaling, *Cur. Opin. Hematol.*, 20(5). Available at: https://journals.lww.com/co-hematology/Fulltext/2013/09000/Platelet_ITAM_signaling.8.aspx.

Berlanga, O., Bobe, R., Becker, M., Murphy, G., Leduc, M., Bon, C., Barry, F. A., Gibbins, J. M., Garcia, P., Frampton, J., & Watson, S. P., (2000). Expression of the collagen receptor glycoprotein VI during megakaryocyte differentiation, *Blood*, 96(8), 2740–2745. doi: 10.1182/blood.v96.8.2740.

Berlanga, O., Bori-Sanz, T., James, J. R., Frampton, J., Davis, S. J., Tomlinson, M. G., & Watson, S. P. (2007). Glycoprotein VI oligomerization in cell lines and platelets. *J. Thromb. Haemost.*, 5(5), 1026–1033. doi:10.1111/j.1538-7836.2007.02449.x.

Best D., Y. A. Senis, Jarvis G. E., Eagleton H. J., Roberts D. J., Saito T., Jung S. M., Moroi M., Harrison P., Green F. R. & Watson S. P. (2003). GPVI levels in platelets: relationship to platelet function at high shear. *Blood*, 102(8), 2811-2818. doi:10.1182/blood-2003-01-0231

Bhateria, M., Rachumallu, R., Yerrabelli, S., Saxena, A. K., & Bhatta, R. S. (2017). Insight into stereoselective disposition of enantiomers of a potent antithrombotic agent, S002-333 following administration of the racemic compound to mice. *Eur. J. Pharm. Sciences*, 101, 107–114. doi:10.1016/j.ejps.2017.02.012.

Bhunia, S. S., Misra, A., Khan, I. A., Gaur, S., Jain, M., Singh, S., . . . Saxena, A. K. (2017). Novel Glycoprotein VI antagonists as antithrombotics: Synthesis, biological Evaluation, and molecular modeling Studies on 2,3-disubstituted tetrahydropyrido(3,4-b)indoles, *J. Med. Chem.*, 60(1), 322–337. doi: 10.1021/acs.jmedchem.6b01360.

Billiald, P., Slater, A. S., Welin, M., Clark, J. C., Loyau, S., Pugnière, M., . . . Jandrot-Perrus, M. (2022). Targeting platelet GPVI with glenzocimab: a novel mechanism for inhibition. *Blood* Adv, bloodadvances.2022007863. doi.org/10.1182/bloodadvances.2022007863.

Bori-Sanz, T., Inoue, K. S., Berndt, M. C., Watson, S. P., & Tulasne, D. (2003). Delineation of the region in the glycoprotein VI tail required for association with the Fc receptor gamma-chain. *J. Biol. Chem.*, 278(38), 35914–35922. doi:10.1074/jbc.M301826200

Boulaftali, Y., Hess, P. R., Kahn, M. L. & Bergmeier, W. (2014). Platelet ITAM signaling and vascular integrity, *Circ. Res.*, 114(7), 1174–1184. doi:10.1161/CIRCRESAHA.114.301611.Platelet.

Bourne, J. H., Colicchia, M., Di, Y., Martin, E., Slater, A., Roumenina, L. T., Dimitrov, J. D., Watson S. P. & Rayes, J. (2020). Heme induces human and mouse platelet activation through C-type-lectin-like receptor-2. *Haematologica*, 106(2), 626-629; doi:10.3324/haematol.2020.246488.

Bourne, J. H., Beristain-Covarrubias, N., Zuidscherwoude, M., Campos, J., Di, Y., Garlick, E., . . . Rayes, J. (2021). CLEC-2 prevents accumulation and retention of inflammatory macrophages during murine peritonitis. *Front. Immuno.l*, 12, 693974. doi:10.3389/fimmu.2021.693974.

British Heart Foundation (2021). UK Factsheet, British Heart Foundation, Updated July 2021, 1–21, Retrieved 15 December 2021, https://www.bhf.org.uk/what-we-do/our-research/heart-statistics/heart-statistics-publications.

Brondijk, T. H., de Ruiter, T., Ballering, J., Wienk, H., Lebbink, R. J., van Ingen, H., Boelens, . . . Huizinga, E. G. (2010). Crystal structure and collagen-binding site of immune inhibitory receptor LAIR-1: Unexpected implications for collagen binding by platelet receptor GPVI. *Blood*, 115(7), 1364–1373. doi:10.1182/blood-2009-10-246322.

Brown, D. G. & Wobst, H. J. (2021). A Decade of FDA-Approved Drugs (2010 − 2019): Trends and Future Directions. *J. Med. Chem.*, 64(5), 2312–2338. doi: 10.1021/acs.jmedchem.0c01516.

Bültmann, A., Li, Z., Wagner, S., Peluso, M., Schönberger, T., Weis, C., . . . Münch, G. (2010). Impact of glycoprotein VI and platelet adhesion on atherosclerosis--a possible role of fibronectin. *J. Mol. Cell Cardiol.*, 49(3), 532–542. doi:10.1016/j.yjmcc.2010.04.009.

Burkhart, J. M., Vaudel, M., Gambaryan, S., Radau, S., Walter, U., Martens, L., Geiger, J., Sickmann, A. & Zahedi, R. P. (2012). The first comprehensive and quantitative analysis of human platelet protein composition allows the comparative analysis of structural and functional pathways. *Blood*, 120(15), e73–e82. doi:10.1182/blood-2012-04-416594

del Carmen Fernández-Alonso, M., Díaz, D., Berbis, M. Á., Marcelo, F., Cañada, J., & Jiménez-Barbero, J. (2012). Protein-carbohydrate interactions studied by NMR: from molecular recognition to drug design. *Cur. Prot. Pep. Sci.*, 13(8), 816–830. doi: 10.2174/138920312804871175.

Cerletti, C., Tamburrelli, C., Izzi, B., Gianfagna, F., & de Gaetano, G. (2012). Platelet-leukocyte interactions in thrombosis. *Thromb. Res.*, 129(3), 263–266. doi:10.1016/j.thromres.2011.10.010.

Chandasana H., Chhonker Y. S., Prasad Y. D., Laxman T. S., Anil Kumar K.S., Dikshit D.K. & Bhatta R.S. (2015). Pharmacokinetics and tissue distribution study of novel potent antiplatelet agent S007-867 in mice using HPLC-MS/MS, *Xenobiotica*, 45(6), 530–537. doi: 10.3109/00498254.2014.994053.

Chan, N. C., & Weitz, J. I. (2019). Antithrombotic Agents. *Circ. Res.*, 124(3), 426–436. doi.org/10.1161/CIRCRESAHA.118.313155.

Chang, C. H., Chung, C. H., Tu, Y. S., Tsai, C. C., Hsu, C. C., Peng, H. C., Tseng, Y. J., & Huang, T. F. (2017). Trowaglerix venom polypeptides as a novel antithrombotic agent by targeting immunoglobulin-like domains of glycoprotein VI in platelets. *Arterioscler. Thromb. Vasc. Biol.*, 37(7), 1307–1314. doi:10.1161/ATVBAHA.116.308604.

Cheng, J. W., Colucci, V., Howard, P. A., Nappi, J. M., & Spinler, S. A. (2015). Vorapaxar in atherosclerotic disease management. *Ann. Pharmacother.*, 49(5), 599–606. doi:10.1177/1060028015571410.

Clark, J. C., Neagoe, R., Zuidscherwoude, M., Kavanagh, D. M., Slater, A., Martin, E. M., . . . Watson, S. P. (2021). Evidence that GPVI is expressed as a mixture of monomers and dimers, and that the d2 domain is not essential for GPVI activation. Thromb Haemost, 121(11), 1435–1447. doi:10.1055/a-1401-5014.

Clemetson, K. J. (2010). Snaclecs (snake C-type lectins) that inhibit or activate platelets by binding to receptors. *Toxicon.*, 56(7), 1236–1246. doi:10.1016/j.toxicon.2010.03.011.

Clemetson K. J. (2012). Platelets and primary haemostasis. *Thromb. Res.*, 129(3), 220–224. doi:10.1016/j.thromres.2011.11.036.

Clemetson, K. J., & Clemetson, J. M. (2013). Chapter 9 - Platelet Receptors. In A. D. Michelson (Ed.), *Platelets* (Third Edition) (pp. 169-194): Academic Press.

Cohen, Y. C., Djulbegovic, B., Shamai-Lubovitz, O., & Mozes, B. (2000). The bleeding risk and natural history of idiopathic thrombocytopenic purpura in patients with persistent low platelet counts. *Arch. Inter. Med.*, 160(11), 1630–1638. doi:10.1001/archinte.160.11.1630.

Coppinger, J. A., Cagney, G., Toomey, S., Kislinger, T., Belton, O., McRedmond, J. P., . . . Maguire, P. B. (2004). Characterization of the proteins released from activated platelets leads to localization of novel platelet proteins in human atherosclerotic lesions. *Blood*, 103(6), 2096–2104. doi:10.1182/blood-2003-08-2804.

Daly M. E. (2011). Determinants of platelet count in humans. *Haematologica*, 96(1), 10–13. doi:10.3324/haematol.2010.035287

Damaskinaki, F. N., Moran, L. A., Garcia, A., Kellam, B., & Watson, S. P. (2021). Overcoming challenges in developing small molecule inhibitors for GPVI and CLEC-2. *Platelets*, 32(6), 744–752. doi:10.1080/09537104.2020.1863939

Deppermann C. (2018). Platelets and vascular integrity. *Platelets*, 29(6), 549–555. doi:10.1080/09537104.2018.1428739.

Donner, L., Toska, L. M., Krüger, I., Gröniger, S., Barroso, R., Burleigh, A., . . . Elvers, M. (2020). The collagen receptor glycoprotein VI promotes platelet-mediated aggregation of β-amyloid. *Sci. Signal.*, 13(643), eaba9872. doi:10.1126/scisignal.aba9872.

Du X., Magnenat E., T. Wells & Clemetson K.J. (2002a). Alboluxin, a snake C-type lectin from Trimeresurus albolabris venom is a potent platelet agonist acting via GPIb and GPVI, *Thromb. Haemostas.*, 87(04): 692-698. doi: 10.1055/s-0037-1613067.

Du, X. Y., Clemetson, J. M., Navdaev, A., Magnenat, E. M., Wells, T. N., & Clemetson, K. J. (2002b). Ophioluxin, a convulxin-like C-type lectin from Ophiophagus hannah (King cobra) is a powerful platelet activator via glycoprotein VI. *J. Biol. Chem.*, 277(38), 35124–35132. doi:10.1074/jbc.M204372200.

Dütting, S., Bender, M., and Nieswandt, B. (2012). Platelet GPVI: a target for antithrombotic therapy?!. *Trends Pharmacol. Sci.*, 33(11), 583–590. doi:10.1016/j.tips.2012.07.004

Ebrahim, M., Jamasbi, J., Adler, K., Megens, R. T. A., M'Bengue, Y., Blanchet, X., . . . Siess, W. (2018). Dimeric Glycoprotein VI binds to collagen but not to fibrin. *Thromb. Haemost.*, 118(2), 351-361. doi:10.1160/TH17-04-0302.

Eckly, A., Hechler, B., Freund, M., Zerr, M., Cazenave, J. P., Lanza, F., . . . Gachet, C. (2011). Mechanisms underlying FeCl3-induced arterial thrombosis. *J. Thromb. Haemost.*, 9(4), 779–789. doi:10.1111/j.1538-7836.2011.04218.x.

Elaskalani, O., Khan, I., Morici, M., Matthysen, C., Sabale, M., Martins, R. N., Verdile, G., & Metharom, P. (2018). Oligomeric and fibrillar amyloid beta 42 induce platelet aggregation partially through GPVI. *Platelets*, 29(4), 415–420. doi:10.1080/09537104.2017.1401057.

Estevez, B., and Du, X. (2017). New concepts and mechanisms of platelet activation signaling. *Physiology (Bethesda)*, 32(2), 162–177. doi:10.1152/physiol.00020.2016

Feitsma, L. J., Brondijk, H. C., Jarvis, G. E., Hagemans, D., Bihan, D., Jerah, N., . . . Huizinga, E. G. (2022). Structural insights into collagen binding by platelet receptor glycoprotein VI. *Blood*, 139(20), 3087–3098. doi:10.1182/blood.2021013614.

Flierl, U., Nero, T. L., Lim, B., Arthur, J. F., Yao, Y., Jung, S. M., . . . Peter, K. (2015). Phosphorothioate backbone modifications of nucleotide-based drugs are potent platelet activators. *J. Exp. Med.*, 212(2), 129–137. doi:10.1084/jem.20140391.

Frenck, R. W., Jr, Klein, N. P., Kitchin, N., Gurtman, A., Absalon, J., . . . C4591001 Clinical Trial Group (2021). Safety, Immunogenicity, and Efficacy of the BNT162b2 Covid-19 Vaccine in Adolescents. *N. Engl. J. Med.*, 385(3), 239–250. doi:10.1056/NEJMoa2107456.

Friesner, R. A., Banks J. L., Murphy R. B., Halgren, T. A., Klicic, J. J., Mainz, D. T., . . . Shenkin, P. S. (2004). Glide: a new approach for rapid, accurate docking and scoring. 1. Method and assessment of docking accuracy. *J. Med. Chem.*, 47(7), 1739-1749. doi:10.1021/jm0306430.

Friesner, R. A., Murphy, R. B., Repasky, M. P., Frye, L. L., Greenwood, J. R., Halgren, T. A., . . . Mainz, D. T. (2006). Extra precision glide: docking and scoring incorporating a model of hydrophobic enclosure for protein-ligand complexes. *J. Med. Chem.*, 49(21), 6177-6196. doi:10.1021/jm051256o.

Gardiner, E. E., Karunakaran, D., Shen, Y., Arthur, J. F., Andrews, R. K., & Berndt, M. C. (2007). Controlled shedding of platelet glycoprotein (GP)VI and GPIb-IX-V by ADAM family metalloproteinases. *J. Thromb. Haemostas.*, 5(7), 1530–1537. doi:10.1111/j.1538-7836.2007.02590.x.

Gaur, S., Fatima, Z., Dixit, A., Ali, Z., Surin, W. R., Kapoor, K., . . . Saxena, A. K. (2006). 2-alkyl/aryl sulphonyl-1,2,3,4-tetrahydro-9H-pyrido (3,4-B) indole-3-carboxylic acid esters/amides useful as antithrombotic agents. WO2006070385A1, *WIPO*, Available at: https://patentscope.wipo.int/search/en/detail.jsf?docId=WO2006070385.

Garg, A., & Balthasar, J. P. (2007). Physiologically-based pharmacokinetic (PBPK) model to predict IgG tissue kinetics in wild-type and FcRn-knockout mice. *J. Pharmacokinet. Pharmacodyn.*, 34(5), 687–709. doi.org/10.1007/s10928-007-9065-1.

Gelse, K., Pöschl, E., & Aigner, T. (2003). Collagens--structure, function, and biosynthesis. *Adv. Drug Deliv. Rev.*, 55(12), 1531–1546. doi:10.1016/j.addr.2003.08.002.

Goebel, S., Li, Z., Vogelmann, J., Holthoff, H. P., Degen, H., Hermann, D. M., . . . Münch, G. (2013). The GPVI-Fc fusion protein revacept improves cerebral infarct volume and functional outcome in stroke. *PLoS ONE*, 8(7): e66960. doi:10.1371/journal.pone.0066960.

Goerge, T., Ho-Tin-Noe, B., Carbo, C., Benarafa, C., Remold-O'Donnell, E., Zhao, B. Q., . . . Wagner, D. D. (2008). Inflammation induces hemorrhage in thrombocytopenia. *Blood*, 111(10), 4958–4964. doi:10.1182/blood-2007-11-123620.

Golebiewska, E. M., and Poole, A. W. (2015). Platelet secretion: From haemostasis to wound healing and beyond. *Blood reviews*, 29(3), 153–162. doi:10.1016/j.blre.2014.10.003.

Greinacher, A., Thiele, T., Warkentin, T. E., Weisser, K., Kyrle, P. A., & Eichinger, S. (2021). Thrombotic Thrombocytopenia after ChAdOx1 nCov-19 Vaccination. *N. Engl. Med.*, 384(22), 2092–2101. doi:10.1056/NEJMoa2104840.

Greinacher, A., Selleng, K. & Warkentin, T. E. (2017). Autoimmune heparin-induced thrombocytopenia. *J. Thromb. Haemost.*, 15(11), 2099–2114. doi: 10.1111/jth.13813.

Gremmel, T., Frelinger, A. L., 3rd, and Michelson, A. D. (2016). Platelet Physiology. *Semin. Thromb. Hemost.*, 42(3), 191–204. doi:10.1055/s-0035-1564835.

Gros, A., Syvannarath, V., Lamrani, L., Ollivier, V., Loyau, S., Goerge, T., . . . Ho-Tin-Noé, B. (2015). Single platelets seal neutrophil-induced vascular breaches via GPVI during immune-complex-mediated inflammation in mice. *Blood*, 126(8), 1017–1026. doi:10.1182/blood-2014-12-617159.

Grozovsky, R., Giannini, S., Falet, H., and Hoffmeister, K. M. (2015). Regulating billions of blood platelets: glycans and beyond. *Blood*, 126(16), 1877–1884. doi:10.1182/blood-2015-01-569129.

Grüner, S., Prostredna, M., Aktas, B., Moers, A., Schulte, V., Krieg, T., . . . Nieswandt, B. (2004). Anti-glycoprotein VI treatment severely compromises hemostasis in mice with reduced alpha2beta1 levels or concomitant aspirin therapy. *Circulation*, 110(18), 2946-2951. doi:10.1161/01.CIR.0000146341.63677.3C

Guan, K. & Dixon, J. E. (1991). Eukaryotic proteins expressed in Escherichia coli: An improved thrombin cleavage and purification procedure of fusion proteins with glutathione S-transferase. *Anal. Biochem.*, 192(2), 262–267. doi:10.1016/0003-2697(91)90534-Z.

Hakes, D. J. & Dixon, J. E. (1992). New vectors for high level expression of recombinant proteins in bacteria. *Anal. Biochem.*, 202(2), 293–298. doi:10.1016/0003-2697(92)90108-J.

Halgren, T. A. (2007). New method for fast and accurate binding-site identification and analysis. *Chem. Biol. Drug Des*., 69(2), 146–148. doi: 10.1111/j.1747-0285.2007.00483.x.

Halgren, T. A. (2009). Identifying and characterizing binding sites and assessing druggability. *J. Chem. Inf. Model*, 49(2), 377–389. doi: 10.1021/ci800324m.

Halgren, T. A., Murphy, R. B., Friesner, R. A., Beard, H. S., Frye, L. L., Pollard, W. T., & Banks, J. L. (2004). Glide: a new approach for rapid, accurate docking and scoring. 2. Enrichment factors in database screening. *J. Med. Chem.*, 47(7), 1750-1759. doi:10.1021/jm030644s.

Harbi, M. H., Smith, C. W., Nicolson, P., Watson, S. P., & Thomas, M. R. (2021). Novel antiplatelet strategies targeting GPVI, CLEC-2 and tyrosine kinases. *Platelets*, 32(1), 29–41. doi:10.1080/09537104.2020.1849600.

Harmsen, M. M., & De Haard, H. J. (2007). Properties, production, and applications of camelid single-domain antibody fragments. *Appl. Microbiol. Biotechnol.*, 77(1), 13–22. doi:10.1007/s00253-007-1142-2.

Hartwig, J.H. (2013) The Platelet Cytoskeleton. Third Edit, Platelets. *Third Edit. Elsevier Inc*. doi: 10.1016/B978-0-12-387837-3.00008-0.

Hayes, J. S., Lawler, O. A., Walsh, M. T., Kinsella, B. T. (1999). The prostacyclin receptor is isoprenylated. Isoprenylation is required for efficient receptor-effector coupling, *J. Biol. Chem.*, 274(34), 23707-23718. doi: 10.1074/jbc.274.34.23707.

Hechler, B., and Gachet, C. (2011). P2 receptors and platelet function. *Purinergic Signal.*, 7(3), 293–303. doi:10.1007/s11302-011-9247-6

Heuberger, D. M. and Schuepbach, R. A. (2019) Correction to: Protease-activated receptors (PARs): Mechanisms of action and potential therapeutic modulators in PAR-driven inflammatory diseases. *Thromb. J.*, 17(1), 1–24. doi:10.1186/s12959-019-0212-x.

Ho-Tin-Noé, B., Boulaftali, Y., & Camerer, E. (2018). Platelets and vascular integrity: how platelets prevent bleeding in inflammation. *Blood*, 131(3), 277–288. doi:10.1182/blood-2017-06-742676.

Ho-Tin-Noé, B., Demers, M. & Wagner, D. D. (2011). How platelets safeguard vascular integrity. *J. Thromb. Haemost*., Suppl 1(Suppl 1), 56–65.. doi: 10.1111/j.1538-7836.2011.04317.x.

Homayun, B., Lin, X. & Choi, H.-J. (2019). Challenges and Recent Progress in Oral Drug Delivery Systems for Biopharmaceuticals. *Pharmaceutics*, 11(3), 129. doi: 10.3390/pharmaceutics11030129.

Horii, K., Brooks, M. T., & Herr, A. B. (2009). Convulxin forms a dimer in solution and can bind eight copies of glycoprotein VI: implications for platelet activation. *Biochemistry*, 48(13), 2907–2914. doi:10.1021/bi801820q.

Horii, K., Kahn, M. L., & Herr, A. B. (2006). Structural basis for platelet collagen responses by the immune-type receptor glycoprotein VI. *Blood*, 108(3), 936–942. doi:10.1182/blood-2006-01-010215.

Hsiao, G., Lee, J. J., Lin, K. H., Shen, C. H., Fong, T. H., Chou, D. S., & Sheu, J. R. (2007). Characterization of a novel and potent collagen antagonist, caffeic acid phenethyl ester, in human platelets: *in vitro* and *in vivo* studies. *Cardiovasc. Res.*, 75(4), 782–792. doi:10.1016/j.cardiores.2007.05.005.

Hughes, C. E., Auger, J. M., McGlade, J., Eble, J. A., Pearce, A. C., & Watson, S. P. (2008). Differential roles for the adapters Gads and LAT in platelet activation by GPVI and CLEC-2. *J. Thromb. Haemost.*, 6(12), 2152–2159. doi:10.1111/j.1538-7836.2008.03166.x.

Hughes, C. E., Navarro-Núñez, L., Finney, B. A., Mourão-Sá, D., Pollitt, A. Y., & Watson, S. P. (2010) CLEC-2 is not required for platelet aggregation at arteriolar shear, *J. Thromb. Haemostas.*, 8(10), 2328-2332. doi: 10.1111/j.1538-7836.2010.04006.x.

Im, J. H., Jin, Y. R., Lee, J. J., Yu, J. Y., Han, X. H., Im, S. H., . . . Yun, Y. P. (2009). Antiplatelet activity of beta-carboline alkaloids from Perganum harmala: a possible mechanism through inhibiting PLCgamma2 phosphorylation. *Vasc. Pharmacol.*, 50(5-6), 147–152. doi: 10.1016/j.vph.2008.11.008

Induruwa, I., Moroi, M., Bonna, A., Malcor, J. D., Howes, J. M., Warburton, E. A., . . . Jung, S. M. (2018). Platelet collagen receptor Glycoprotein VI-dimer recognizes fibrinogen and fibrin through their D-domains, contributing to platelet adhesion and activation during thrombus formation. *J. Thromb. Haemost.*, 16(2), 389–404. doi:10.1111/jth.13919.

Induruwa, I., McKinney, H., Kempster, C., Thomas, P., Batista, J., Malcor, J. D., . . . Jung, S. (2022). Platelet surface receptor glycoprotein VI-dimer is overexpressed in stroke: The Glycoprotein VI in Stroke (GYPSIE) study results. *PloS ONE*, 17(1), e0262695. doi:10.1371/journal.pone.0262695

Inoue, O., Suzuki-Inoue, K., McCarty, O. J., Moroi, M., Ruggeri, Z. M., Kunicki, T. J., Ozaki, Y., & Watson, S. P. (2006). Laminin stimulates spreading of platelets through integrin alpha6beta1-dependent activation of GPVI. *Blood*, 107(4), 1405–1412. doi:10.1182/blood-2005-06-2406.

Isakov, N. (1997). Immunoreceptor tyrosine-based activation motif (ITAM), a unique module linking antigen and Fc receptors to their signaling cascades. *J, Leukoc, Biol*., John Wiley & Sons, Ltd, 61(1), 6–16. doi: 10.1002/jlb.61.1.6.

Jamasbi, J., Megens, R. T., Bianchini, M., Münch, G., Ungerer, M., Faussner, A., . . . Siess, W. (2015). Differential inhibition of human atherosclerotic plaque-induced platelet activation by dimeric GPVI-Fc and anti-GPVI antibodies: functional and imaging studies. *J, Amer, Coll, Cardiol*,, 65(22), 2404–2415. doi:10.1016/j.jacc.2015.03.573.

Jiang, P., Loyau, S., Tchitchinadze, M., Ropers, J., Jondeau, G., & Jandrot-Perrus, M. (2015). Inhibition of glycoprotein VI clustering by collagen as a mechanism of inhibiting collagen-

induced platelet responses: The example of losartan. *PloS ONE*, 10(6), e0128744. doi:10.1371/journal.pone.0128744.

Jin, J., Quinton, T. M., Zhang, J., Rittenhouse, S. E., and Kunapuli, S. P. (2002). Adenosine diphosphate (ADP)-induced thromboxane A(2) generation in human platelets requires coordinated signaling through integrin alpha(IIb)beta(3) and ADP receptors. *Blood*, 99(1), 193–198. doi:10.1182/blood.v99.1.193.

Jones, S., & Thornton, J. M. (1996). Principles of protein-protein interactions. *Proc. Natl. Acad. Sci.*, U S A., 93(1), 13–20. doi:10.1073/pnas.93.1.13

Jovčevska, I., & Muyldermans, S. (2020). The therapeutic potential of nanobodies. *BioDrugs*, 34(1), 11–26. doi:10.1007/s40259-019-00392-z.

Jung, S. M., Takemura, Y., Imamura, Y., Hayashi, T., Adachi, E., & Moroi, M. (2008). Collagen-type specificity of glycoprotein VI as a determinant of platelet adhesion. Platelets, 19(1), 32–42. doi:10.1080/09537100701609027.

Jung, S. M., Moroi, M., Soejima, K., Nakagaki, T., Miura, Y., Berndt, M. C., . . . Farndale, R. W. (2012). Constitutive dimerization of glycoprotein VI (GPVI) in resting platelets is essential for binding to collagen and activation in flowing blood. *J. Biol. Chem.*, 287(35), 30000–30013. doi:10.1074/jbc.M112.359125.

Jung, S. M., Tsuji, K., & Moroi, M. (2009). Glycoprotein (GP) VI dimer as a major collagen-binding site of native platelets: direct evidence obtained with dimeric GPVI-specific Fabs. *J. Thromb. Haemostas.*, 7(8), 1347–1355. doi:10.1111/j.1538-7836.2009.03496.x.

Kalyanasundaram, A., Lincoff, A. M., & Medscape (2011). Managing adverse effects and drug-drug interactions of antiplatelet agents. *Nat. Rev. Cardiol.*, 8(10), 592–600. doi.org/10.1038/nrcardio.2011.128.

Kanaji, S., Kanaji, T., Furihata, K., Kato, K., Ware, J. L., & Kunicki, T. J. (2003). Convulxin binds to native, human glycoprotein Ib alpha. *J. Biol. Chem.*, 278(41), 39452–39460. doi:10.1074/jbc.M300199200

Kato-Takagaki, K., Mizukoshi, Y., Yoshizawa, Y., Akazawa, D., Torii, Y., Ono, K., . . . Takahashi, H. (2009). Structural and interaction analysis of glycoprotein VI-binding peptide selected from a phage display library. *J. Biol. Chem.*, 284(16), 10720–10727. doi:10.1074/jbc.M808563200.

Kato, K., Kanaji, T., Russell, S., Kunicki, T. J., Furihata, K., Kanaji, S., . . . Ware, J. (2003). The contribution of glycoprotein VI to stable platelet adhesion and thrombus formation illustrated by targeted gene deletion. *Blood*, 102(5), 1701–1707. doi:10.1182/blood-2003-03-0717.

Kauskot, A., & Hoylaerts, M. F. (2012). Platelet receptors. *Handb. Exp. Pharmacol.*, (210), 23–57. doi:10.1007/978-3-642-29423-5_2.

Kojima, H., Moroi, M., Jung, S. M., Goto, S., Tamura, N., Kozuma, Y., . . . Nagasawa, T. (2006). Characterization of a patient with glycoprotein (GP) VI deficiency possessing neither anti-GPVI autoantibody nor genetic aberration. *J. Thromb. Haemost.*, 4(11), 2433–2442. doi:10.1111/j.1538-7836.2006.02173.x.

Koupenova, M., Kehrel, B. E., Corkrey, H. A., & Freedman, J. E. (2017). Thrombosis and platelets: an update. *Eur. Heart. J.*, 38(11), 785–791. doi:10.1093/eurheartj/ehw550.

Koupenova, M., & Ravid, K. (2018). Biology of platelet purinergic receptors and implications for platelet heterogeneity. *Front. Pharmacol.*, 9, 37. doi:10.3389/fphar.2018.00037.

Kramer, R. Z., Bella, J., Mayville, P., Brodsky, B., & Berman, H. M. (1999). Sequence dependent conformational variations of collagen triple-helical structure. Nat Struct Biol, 6(5), 454–457. doi:10.1038/8259.

Anil Kumar, K. S., Misra A., Siddiqi T. I., Srivastava S., Jain M., Bhatta R. S., . . . Dikshit D. K. (2014). Synthesis and Identification of Chiral Aminomethylpiperidine Carboxamides as Inhibitor of Collagen Induced Platelet Activation. *Eur. J. Med. Chem.*, 81, 456-472. doi:10.1016/j.ejmech.2014.05.017.

Labelle, M., & Hynes, R. O. (2012). The initial hours of metastasis: the importance of cooperative host-tumor cell interactions during hematogenous dissemination. *Cancer Discov*., 2(12), 1091–1099. doi:10.1158/2159-8290.CD-12-0329.

Lecut, C., Feeney, L. A., Kingsbury, G., Hopkins, J., Lanza, F., Gachet, C., . . . Jandrot-Perrus, M. (2003). Human platelet glycoprotein VI function is antagonized by monoclonal antibody-derived Fab fragments. *J. Thromb. Haemostas.*, 1(12), 2653–2662. doi:10.1111/j.1538-7836.2003.00495.x.

Lecut, C., Arocas, V., Ulrichts, H., Elbaz, A., Villeval, J. L., Lacapère, J. J., . . . Jandrot-Perrus, M. (2004). Identification of residues within human glycoprotein VI involved in the binding to collagen: evidence for the existence of distinct binding sites. *J. Biol. Chem.*, 279(50), 52293–52299. doi:10.1074/jbc.M406342200

Lee, T. Y., Chang, C. C., Lu, W. J., Yen, T. L., Lin, K. H., Geraldine, P., . . . Sheu, J. R. (2017). Honokiol as a specific collagen receptor glycoprotein VI antagonist on human platelets: Functional ex vivo and *in vivo* studies. *Sci. Rep.*, 7, 40002. doi:10.1038/srep40002.

Lee, W. H., Du, X. Y., Lu, Q. M., Clemetson, K. J., & Zhang, Y. (2003). Stejnulxin, a novel snake C-type lectin-like protein from Trimeresurus stejnegeri venom is a potent platelet agonist acting specifically via GPVI. *Thromb. Haemostas.*, 90(4), 662–671. doi:10.1160/TH03-05-0269.

Levine, G. N., Bates, E. R., Blankenship, J. C., Bailey, S. R., Bittl, J. A., Cercek, B., . . . Ting, H. H. (2011). 2011 ACCF/AHA/SCAI Guideline for Percutaneous Coronary Intervention: executive summary: a report of the American College of Cardiology Foundation/American Heart Association Task Force on Practice Guidelines and the Society for Cardiovascular

Angiography and Interventions. Circulation, 124(23), 2574–2609. doi.org/10.1161/CIR.0b013e31823a5596.

Li, H., Lockyer, S., Concepcion, A., Gong, X., Takizawa, H., Guertin, M., . . . Liu, Y. (2007). The Fab fragment of a novel anti-GPVI monoclonal antibody, OM4, reduces in vivo thrombosis without bleeding risk in rats. *Arterioscler. Thromb. Vasc. Biol.*, 27(5), 1199–1205. doi:10.1161/ATVBAHA.107.140590.

Li, S., Tarlac, V., & Hamilton, J. R. (2019). Using PAR4 Inhibition as an Anti-Thrombotic Approach: Why, How, and When? *Int. J. Mol. Sci*., 20(22), 5629. doi:10.3390/ijms20225629.

Li, Z., Delaney, M. K., O'Brien, K. A., & Du, X. (2010). Signaling during platelet adhesion and activation. *Arterioscler. Thromb. Vasc. Biol.*, 30(12), 2341–2349. doi:10.1161/ATVBAHA.110.207522.

Lin, K. H., Kuo, J. R., Lu, W. J., Chung, C. L., Chou, D. S., Huang, S. Y., . . . Sheu, J. R. (2013). Hinokitiol inhibits platelet activation ex vivo and thrombus formation *in vivo*. *Biochem. Pharmacol.*, 85(10), 1478–1485. doi:10.1016/j.bcp.2013.02.027.

Lipman, N. S., Jackson, L. R., Trudel, L. J., & Weis-Garcia, F. (2005). Monoclonal versus polyclonal antibodies: distinguishing characteristics, applications, and information resources. *ILAR J*, 46(3), 258–268. doi:10.1093/ilar.46.3.258.

Lockyer, S., Okuyama, K., Begum, S., Le, S., Sun, B., Watanabe, T., . . . Tandon, N. N. (2006). GPVI-deficient mice lack collagen responses and are protected against experimentally induced pulmonary thromboembolism. *Thromb. Res.*, 118(3), 371–380. doi:10.1016/j.thromres.2005.08.001.

Loving, K., Salam, N. K. & Sherman, W. (2009). Energetic analysis of fragment docking and application to structure-based pharmacophore hypothesis generation. *J. Comput. Aided Mol. Des.*, 23(8), 541-554. doi:10.1007/s10822-009-9268-1.

Lowe, K. L., Navarro-Núñez, L., Bénézech, C., Nayar, S., Kingston, B. L., Nieswandt, B., . . . Desanti, G. E. (2015). The expression of mouse CLEC-2 on leucocyte subsets varies according to their anatomical location and inflammatory state. *Eur. J. Immunol.*, 45(9), 2484–2493. doi:10.1002/eji.201445314.

Loyau, S., Dumont, B., Ollivier, V., Boulaftali, Y., Feldman, L., Ajzenberg, N., & Jandrot-Perrus, M. (2012). Platelet glycoprotein VI dimerization, an active process inducing receptor competence, is an indicator of platelet reactivity. *Arterioscler. Thromb. Vasc. Biol*., 32(3), 778–785. doi:10.1161/ATVBAHA.111.241067.

Lu, H., Zhou, Q., He, J., Jiang, Z., Peng, C., Tong, R., & Shi, J. (2020). Recent advances in the development of protein-protein interactions modulators: mechanisms and clinical trials. *Signal Transduct. Target. Ther.*, 5(1), 213. doi:10.1038/s41392-020-00315-3.

Machlus, K. R. and Italiano, J. E. (2013). The incredible journey: From megakaryocyte development to platelet formation, *J. Cell Biol*., 201(6), 785–796 doi: 10.1083/jcb.201304054.

Machlus, K. R., and Italiano, J. E. (2019). Megakaryocyte development and platelet formation. *Platelets*, 25–46. Elsevier. doi:10.1016/B978-0-12-813456-6.00002-3.

Makurvet, F. D. (2021). Biologics vs. Small Molecules: Drug Costs and Patient Access. *Med. Drug Disc.*, 9, 100075. doi.org/10.1016/j.medidd.2020.100075.

Mammadova-Bach, E., Ollivier, V., Loyau, S., Schaff, M., Dumont, B., Favier, R., . . . Jandrot-Perrus, M. (2015). Platelet glycoprotein VI binds to polymerized fibrin and promotes thrombin generation. *Blood*, 126(5), 683–691. doi:10.1182/blood-2015-02-629717.

Mangin, P. H., Onselaer, M. B., Receveur, N., Le Lay, N., Hardy, A. T., Wilson, C., . . . Watson, S. P. (2018). Immobilized fibrinogen activates human platelets through glycoprotein VI. *Haematologica*, 103(5), 898–907. doi:10.3324/haematol.2017.182972.

Marcu, S. B., Sabin T., & Tangney M. (2022). An Overview of Alphafold's Breakthrough. *Front. Artif. Intell.*, 5, 875587. doi:10.3389/frai.2022.875587.

Margraf, A., & Zarbock, A. (2019). Platelets in inflammation and resolution. *J. Immunol.*, 203(9), 2357–2367. doi:10.4049/jimmunol.1900899.

Massberg, S., Konrad, I., Bültmann, A., Schulz, C., Münch, G., Peluso, M., . . . Gawaz, M. (2004). Soluble glycoprotein VI dimer inhibits platelet adhesion and aggregation to the injured vessel wall *in vivo*. *FASEB J*, 18(2), 397–399. doi:10.1096/fj.03-0464fje.

Matus, V., Valenzuela, G., Sáez, C. G., Hidalgo, P., Lagos, M., Aranda, E., . . . Mezzano, D. (2013). An adenine insertion in exon 6 of human GP6 generates a truncated protein associated with a bleeding disorder in four Chilean families. *J. Thromb. Haemostas.*, 11(9), 1751–1759. doi:10.1111/jth.12334.

McFadyen, J. D., Schaff, M., and Peter, K. (2018). Current and future antiplatelet therapies: emphasis on preserving haemostasis. *Nat. Rev. Cardiol.*, 15(3), 181–191. doi:10.1038/nrcardio.2017.206.

Mehta, S. R., Yusuf, S., Peters, R. J., Bertrand, M. E., Lewis, B. S., Natarajan, M. K., . . . Clopidogrel in Unstable angina to prevent Recurrent Events trial (CURE) Investigators (2001). Effects of pretreatment with clopidogrel and aspirin followed by long-term therapy in patients undergoing percutaneous coronary intervention: the PCI-CURE study. *Lancet*, 358(9281), 527–533. doi.org/10.1016/s0140-6736(01)05701-4.

Misra, A., Prakash, P., Aggarwal, H., Dhankani, P., Kumar, S., Pandey, C. P., . . . Dikshit, M. (2018). Anti-thrombotic efficacy of S007-867: Pre-clinical evaluation in experimental models of thrombosis *in vivo* and *in vitro*. *Biochem. Pharmacol.*, 148, 288–297. doi:10.1016/j.bcp.2018.01.013.

Mitchell, L. S. and Colwell, L. J. (2018a). Analysis of nanobody paratopes reveals greater diversity than classical antibodies, *Prot. Eng. Des. Sel.*, 31(7-8), 267–275. doi: 10.1093/protein/gzy017.

Mitchell, L. S., & Colwell, L. J. (2018b). Comparative analysis of nanobody sequence and structure data. *Proteins*, 86(7), 697–706. Doi:10.1002/prot.25497.

Miura, Y., Takahashi, T., Jung, S. M., & Moroi, M. (2002). Analysis of the interaction of platelet collagen receptor glycoprotein VI (GPVI) with collagen. A dimeric form of GPVI, but not the monomeric form, shows affinity to fibrous collagen. *J Biol Chem*, 277(48), 46197–46204. doi:10.1074/jbc.M204029200.

Montague, S. J., Patel, P., Martin, E. M., Slater, A., Quintanilla, L. G., Perrella, G., . . . Watson, S. P. (2021). Platelet activation by charged ligands and nanoparticles: platelet glycoprotein receptors as pattern recognition receptors. *Platelets*, 32(8), 1018–1030. doi:10.1080/09537104.2021.1945571.

Moroi, M., Jung, S. M., Okuma, M., & Shinmyozu, K. (1989). A patient with platelets deficient in glycoprotein VI that lack both collagen-induced aggregation and adhesion. *J. Clin. Invest.*, 84(5), 1440–1445. doi:10.1172/JCI114318.

Moroi, M., & Jung, S. M. (2004). Platelet glycoprotein VI: its structure and function. *Thromb. Res.*, 114(4), 221–233. doi:10.1016/j.thromres.2004.06.046.

Morton, L. F., Hargreaves, P. G., Farndale, R. W., Young, R. D., & Barnes, M. J. (1995). Integrin alpha 2 beta 1-independent activation of platelets by simple collagen-like peptides: collagen tertiary (triple-helical) and quaternary (polymeric) structures are sufficient alone for alpha 2 beta 1-independent platelet reactivity. *Biochem. J.*, 306 (Pt 2), 337–344. doi:10.1042/bj3060337.

Morrow, D. A., Braunwald, E., Bonaca, M. P., Ameriso, S. F., Dalby, A. J., Fish, M. P., . . . TRA 2P–TIMI 50 Steering Committee and Investigators (2012). Vorapaxar in the secondary prevention of atherothrombotic events. *N. Engl. J. Med.*, 366(15), 1404–1413. doi:10.1056/NEJMoa1200933.

Murakami, M. T. *et al.* (2003). Crystal structure of the platelet activator convulxin, a disulfide-linked α4β4 cyclic tetramer from the venom of Crotalus durissus terrificus. *Biochem. Biophys. Res. Commun.*, 310(2), 478-482. doi: 10.1016/j.bbrc.2003.09.032.

Muyldermans S. (2013). Nanobodies: natural single-domain antibodies. *An. Rev. Biochem.*, 82, 775–797. doi:10.1146/annurev-biochem-063011-092449.

Nagy, M., Perrella, G., Dalby, A., Becerra, M. F., Garcia Quintanilla, L., Pike, J. A., . . . Watson, S. P. (2020). Flow studies on human GPVI-deficient blood under coagulating and noncoagulating conditions. *Blood Adv.*, 4(13), 2953–2961. doi:10.1182/bloodadvances.2020001761.

Nieswandt, B., Brakebusch, C., Bergmeier, W., Schulte, V., Bouvard, D., Mokhtari-Nejad, R., . . . Fässler, R. (2001a). Glycoprotein VI but not alpha2beta1 integrin is essential for platelet interaction with collagen. *EMBO J*, 20(9), 2120–2130. doi:10.1093/emboj/20.9.2120.

Nieswandt, B., Schulte, V., Bergmeier, W., Mokhtari-Nejad, R., Rackebrandt, K., Cazenave, J. P., . . . Zirngibl, H. (2001b). Long-term antithrombotic protection by *in vivo* depletion of platelet glycoprotein VI in mice. *J. Exp. Me*., 193(4), 459–469. doi:10.1084/jem.193.4.459.

Nieswandt, B., Pleines, I., & Bender, M. (2011). Platelet adhesion and activation mechanisms in arterial thrombosis and ischaemic stroke. *J. Thromb. Haemost*., 9 Suppl 1, 92–104. doi:10.1111/j.1538-7836.2011.04361.x.

Nieswandt, B., & Watson, S. P. (2003) Platelet-collagen interaction: Is GPVI the central receptor? *Blood*, 102(2), 449–461. doi: 10.1182/blood-2002-12-3882.

Nurden, A. T. & Nurden, P. (2014). Congenital platelet disorders and understanding of platelet function, *Br. J. Haematol*., 165(2), 165–178. doi: 10.1111/bjh.12662.

Nurden, P., Jandrot-Perrus, M., Combrié, R., Winckler, J., Arocas, V., Lecut, C., . . . Nurden, A. T. (2004). Severe deficiency of glycoprotein VI in a patient with gray platelet syndrome. *Blood*, 104(1), 107–114. doi:10.1182/blood-2003-11-3842.

O'Connor, M. N., Smethurst, P. A., Farndale, R. W., & Ouwehand, W. H. (2006). Gain- and loss-of-function mutants confirm the importance of apical residues to the primary interaction of human glycoprotein VI with collagen. *J. Thromb. Haemost.*, 4(4), 869–873. doi:10.1111/j.1538-7836.2005.01764.x

Offermanns, S. (2006) Activation of platelet function through G protein-coupled receptors, *Circ. Res*., 99, 1293–1304. doi: 10.1161/01.RES.0000251742.71301.16.

Olafsen, T., & Wu, A. M. (2010). Antibody vectors for imaging. *Semin. Nuc. Med.*, 40(3), 167–181. doi:10.1053/j.semnuclmed.2009.12.005.

Olğaç, S., Olğaç, A., Yenicesu, İ., & Ozkan, Y. (2022). Identification of novel antiplatelet agents by targeting Glycoprotein VI: A combined virtual screening study. *Bioorg. Chem*., 121, 105661. doi:10.1016/j.bioorg.2022.105661.

Ono, K., Ueda, H., Yoshizawa, Y., Akazawa, D., Tanimura, R., Shimada, I., & Takahashi, H. (2010). Structural basis for platelet antiaggregation by angiotensin II type 1 receptor antagonist losartan (DuP-753) via glycoprotein VI. *J. Med. Chem.*, 53(5), 2087–2093. doi:10.1021/jm901534d.

Ono, K., Takeuchi, K., Ueda, H., Morita, Y., Tanimura, R., Shimada, I., & Takahashi, H. (2014). Structure-based approach to improve a small-molecule inhibitor by the use of a competitive peptide ligand. *Angew. Chem. Int. Ed.. Engl*, 53(10), 2597–2601. doi:10.1002/anie.201310749

Onselaer, M. B., Hardy, A. T., Wilson, C., Sanchez, X., Babar, A. K., Miller, J., . . . Watson, S. P. (2017). Fibrin and D-dimer bind to monomeric GPVI. *Blood Adv*., 1(19), 1495–1504. doi:10.1182/bloodadvances.2017007732

Onselaer, M. B., Nagy, M., Pallini, C., Pike, J. A., Perrella, G., Quintanilla, L. G., . . . Watson, S. P. (2020). Comparison of the GPVI inhibitors losartan and honokiol. *Platelets*, 31(2), 187–197. doi:10.1080/09537104.2019.1585526.

Ozaki, Y., Suzuki-Inoue, K., & Inoue, O. (2009). Novel interactions in platelet biology: CLEC-2/podoplanin and laminin/GPVI. *J. Thromb. Haemost.*, 7 Suppl 1, 191–194. doi:10.1111/j.1538-7836.2009.03372.x.

Pan, Y., & Xia, L. (2015). Emerging roles of podoplanin in vascular development and homeostasis. *Front. Med*., 9(4), 421–430. doi:10.1007/s11684-015-0424-9.

Periayah, M. H., Halim, A. S., & Mat Saad, A. Z. (2017). Mechanism action of platelets and crucial blood coagulation pathways in hemostasis. Periayah MH, Halim AS, Mat Saad AZ. Mechanism Action of Platelets and Crucial Blood Coagulation Pathways in Hemostasis. *Int. J. Hematol. Oncol. Stem Cell Res*., 11(4):319-327., 11(4), 319–327.

Perrakis, A., & Sixma, T. K.. (2021). AI Revolutions in Biology. *EMBO Reports* 22(11), e54046. doi:10.15252/embr.202154046.

Perrella, G., Nagy, M., Watson, S. P., & Heemskerk, J. (2021). Platelet GPVI (Glycoprotein VI) and thrombotic complications in the venous system. *Arterioscler. Thromb. Vasc. Biol*., 41(11), 2681–2692. doi:10.1161/ATVBAHA.121.316108.

Plow, E. F., Wang, Y. and Simon, D. I. (2018). The search for new antithrombotic mechanisms and therapies that may spare hemostasis, *Blood*, 131(17), 1899–1902. doi: 10.1182/blood-2017-10-784074.

Pluthero, F. G., and Kahr, W. (2018). Imaging platelets and megakaryocytes by high-resolution laser fluorescence microscopy. *Methods Mol. Biol*. (Clifton, N.J.), 1812, 13–31. doi:10.1007/978-1-4939-8585-2_2.

Polack, F. P., Thomas, S. J., Kitchin, N., Absalon, J., Gurtman, A., Lockhart, S., . . . C4591001 Clinical Trial Group (2020). Safety and Efficacy of the BNT162b2 mRNA Covid-19 Vaccine. *N. Engl. J. Med.*, 383(27), 2603–2615. doi:10.1056/NEJMoa2034577.

Polgár, J., Clemetson, J. M., Kehrel, B. E., Wiedemann, M., Magnenat, E. M., Wells, T. N., & Clemetson, K. J. (1997). Platelet activation and signal transduction by convulxin, a C-type lectin from Crotalus durissus terrificus (tropical rattlesnake) venom via the p62/GPVI collagen receptor. *J. Biol. Chem*., 272(21), 13576–13583. doi:10.1074/jbc.272.21.13576.

Poulter, N. S., Pollitt, A. Y., Owen, D. M., Gardiner, E. E., Andrews, R. K., Shimizu, H., . . . Jung, S. M. (2017). Clustering of glycoprotein VI (GPVI) dimers upon adhesion to collagen as a mechanism to regulate GPVI signaling in platelets. *J. Thromb. Haemost.*, 15(3), 549–564. doi:10.1111/jth.13613.

Qiao, J., Al-Tamimi, M., Baker, R. I., Andrews, R. K., and Gardiner, E. E. (2015). The platelet Fc receptor, FcγRIIa. *Immunolog. Rev*., 268(1), 241–252. doi:10.1111/imr.12370.

Rayes, J., Watson, S. P. and Nieswandt, B. (2019) Functional significance of the platelet immune receptors GPVI and CLEC-2. *J. Clin. Invest.*, 129(1), 12–23. doi: 10.1172/JCI122955.

Ran, X., & Gestwicki, J. E. (2018). Inhibitors of protein-protein interactions (PPIs): an analysis of scaffold choices and buried surface area. *Curr. Opin. Chem. Biol.*, 44, 75–86. doi.org/10.1016/j.cbpa.2018.06.004.

Raynal, N., Hamaia, S. W., Siljander, P. R., Maddox, B., Peachey, A. R., Fernandez, R., . . . Farndale, R. W. (2006). Use of synthetic peptides to locate novel integrin alpha2beta1-binding motifs in human collagen III. *J. Biol. Chem.*, 281(7), 3821–3831. doi:10.1074/jbc.M509818200.

Riba, R., Hughes, C. E., Graham, A., Watson, S. P., & Naseem, K. M. (2008). Globular adiponectin induces platelet activation through the collagen receptor GPVI-Fc receptor gamma chain complex. *J. Thromb. Haemost.*, 6(6), 1012–1020. doi:10.1111/j.1538-7836.2008.02982.x.

Rognan, D. (2015). Rational design of protein-protein interaction inhibitors. *Med. Chem. Comm.*, 6, 51. doi: 10.1039/c4md00328d.

Saboor, M., Ayub, Q., Ilyas, S., and Moinuddin (2013). Platelet receptors; an instrumental of platelet physiology. *Pak. J. Med. Sci.*, 29(3), 891–896. doi:10.12669/pjms.293.3497.

Salam, N. K., Nuti, R. & Sherman, W. (2009). Novel method for generating structure-based pharmacophores using energetic analysis. *J. Chem. Inf. Model*, 49(10), 2356-2368. doi:10.1021/ci900212v.

Sastry, G. M., Adzhigirey, M., Day, T., Annabhimoju, R. & Sherman, W. (2013) Protein and ligand preparation: parameters, protocols, and influence on virtual screening enrichments. *J. Comput. Aided Mol. De.s*, 27(3), 221-234. doi:10.1007/s10822-013-9644-8.

Schönberger, T., Ziegler M, Borst O., Konrad I., Nieswandt B., Massberg S., . . . Gawaz, M. (2012). The Dimeric Platelet Collagen Receptor GPVI-Fc Reduces Platelet Adhesion to Activated Endothelium and Preserves Myocardial Function after Transient Ischemia in Mice. *Am. J. Physiol. Cell Physio.l*, 303(7):C757-C766. doi:10.1152/ajpcell.00060.2012.

Schulte, V., Rabie, T., Prostredna, M., Aktas, B., Grüner, S., and Nieswandt, B. (2003). Targeting of the collagen-binding site on glycoprotein VI is not essential for *in vivo* depletion of the receptor. *Blood*, 101(10), 3948–3952. doi:10.1182/blood-2002-10-3242.

Schultz, N. H., Sørvoll, I. H., Michelsen, A. E., Munthe, L. A., Lund-Johansen, F., Ahlen, M. T., . . . Holme, P. A. (2021). Thrombosis and Thrombocytopenia after ChAdOx1 nCoV-19 Vaccination. *N. Engl. J. Med.*, 384(22), 2124–2130. doi:10.1056/NEJMoa2104882.

Schulz, C., von Brühl, M. L., Barocke, V., Cullen, P., Mayer, K., Okrojek, R., . . . Schmidt, R. (2011). EMMPRIN (CD147/basigin) mediates platelet-monocyte interactions *in vivo* and augments monocyte recruitment to the vascular wall. *J. Thromb. Haemost.*, 9(5), 1007–1019. doi:10.1111/j.1538-7836.2011.04235.x

Sharda, A. & Flaumenhaft, R. (2018). The life cycle of platelet granules. *F1000Research*, 7, 236. doi:10.12688/f1000research.13283.1.

Schorpp, K., Rothenaigner, I., Salmina, E., Reinshagen, J., Low, T., Brenke, J. K., Gopalakrishnan, J., Tetko, I. V., Gul, S., & Hadian, K. (2014). Identification of small-molecule frequent hitters from AlphaScreen high-throughput screens. *J. Biomol. Screen*, 19(5), 715–726. doi:10.1177/1087057113516861.

Schrödinger Release 2018-1: Schrödinger, LLC, 2018, New York, NY, USA.

Scully, M., Cataland, S. R., Peyvandi, F., Coppo, P., Knöbl, P., Kremer Hovinga, J. A., . . . HERCULES Investigators (2019). Caplacizumab Treatment for Acquired Thrombotic Thrombocytopenic Purpura. *N. Engl. J. Med.*, 380(4), 335–346. doi:10.1056/NEJMoa1806311.

Scully, M., Singh, D., Lown, R., Poles, A., Solomon, T., Levi, M., . . . Lester, W. (2021). Pathologic Antibodies to Platelet Factor 4 after ChAdOx1 nCoV-19 Vaccination. *N. Engl. J. Med.*, 384(23), 2202–2211. doi:10.1056/NEJMoa2105385.

Senior, A. W., Evans, R., Jumper, J., Kirkpatrick, J., Sifre, L., Green, . . . Hassabis, D. (2020). Improved protein structure prediction using potentials from deep learning. *Nature*, 577(7792), 706–710. doi:10.1038/s41586-019-1923-7.

Shoulders, M. D., & Raines, R. T. (2009). Collagen structure and stability. *Annu. Rev. Biochem.*, 78, 929–958. doi:10.1146/annurev.biochem.77.032207.120833.

Slater, A., Perrella, G., Onselaer, M. B., Martin, E. M., Gauer, J. S., Xu, R. G., . . . Watson, S. P. (2019). Does fibrin(ogen) bind to monomeric or dimeric GPVI, or not at all?. *Platelets*, 30(3), 281–289. doi:10.1080/09537104.2018.1508649

Slater, A., Di, Y., Clark, J. C., Jooss, N. J., Martin, E. M., Alenazy, F., . . . Watson, S. P. (2021). Structural characterization of a novel GPVI-nanobody complex reveals a biologically active domain-swapped GPVI dimer, *Blood*, 137(24), 3443–3453. doi: 10.1182/blood.2020009440.

Smethurst, P. A., Joutsi-Korhonen, L., O'Connor, M. N., Wilson, E., Jennings, N. S., . . . Ouwehand, W. H. (2004). Identification of the primary collagen-binding surface on human glycoprotein VI by site-directed mutagenesis and by a blocking phage antibody. *Blood*, 103(3), 903–911. doi:10.1182/blood-2003-01-0308.

Smethurst, P. A., Onley, D. J., Jarvis, G. E., O'Connor, M. N., Knight, C. G., Herr, A. B., . . . Farndale, R. W. (2007). Structural basis for the platelet-collagen interaction: the smallest motif within collagen that recognizes and activates platelet Glycoprotein VI contains two glycine-proline-hydroxyproline triplets. *J. Biol. Chem.*, 282(2), 1296–1304. doi:10.1074/jbc.M606479200.

Smyth, S. S., McEver, R. P., Weyrich, A. S., Morrell, C. N., Hoffman, M. R., Arepally, G. M., . . . 2009 Platelet Colloquium Participants (2009). Platelet functions beyond hemostasis. *J. Throm. Haemost.*, 7(11), 1759–1766. doi:10.1111/j.1538-7836.2009.03586.x.

Snell, D. C., Schulte, V., Jarvis, G. E., Arase, K., Sakurai, D., Saito, T., . . . Nieswandt, B. (2002). Differential effects of reduced glycoprotein VI levels on activation of murine platelets by glycoprotein VI ligands. *Biochem. J.*, 368(Pt 1), 293–300. doi:10.1042/BJ20020335.

Sorushanova, A., Delgado, L. M., Wu, Z., Shologu, N., Kshirsagar, A., Raghunath, R., . . . Zeugolis, D. I. (2019). The Collagen Suprafamily: From Biosynthesis to Advanced Biomaterial Development. *Adv. Mater.*, 31(1), e1801651. doi:10.1002/adma.201801651.

Stamboroski, S., Joshi, A., Noeske, P. M., Köppen, S., & Brüggemann, D. (2021). Principles of Fibrinogen Fiber Assembly *In Vitro*. *Macromol. Biosci.*, 21(5), e2000412. doi:10.1002/mabi.202000412.

Steeland, S., Vandenbroucke, R. E., & Libert, C. (2016). Nanobodies as therapeutics: big opportunities for small antibodies. *Drug Discov. Today*, 21(7), 1076–1113. doi:10.1016/j.drudis.2016.04.003.

Stevens, R. F., & Meyer, S. (2002). Fanconi and Glanzmann: the men and their works. *Brit. J. Haematol.*, 119(4), 901–904. doi:10.1046/j.1365-2141.2002.03812.x.

Sugiyama T., Okuma M., Ushikubi F., Sensaki S., Kanaji K. & Uchino H. (1987). A novel platelet aggregating factor found in a patient with defective collagen-induced platelet aggregation and autoimmune thrombocytopenia', *Blood*, 69(6), 1712–1720. doi: 10.1182/blood.v69.6.1712.1712.

Suzuki-Inoue, K., Tulasne, D., Shen, Y., Bori-Sanz, T., Inoue, O., Jung, S. M., . . . Watson, S. P. (2002). Association of Fyn and Lyn with the proline-rich domain of glycoprotein VI regulates intracellular signaling. *J. Biol. Chem.*, 277(24), 21561–21566. doi:10.1074/jbc.M201012200

Suzuki-Inoue, K. *et al.* (2018) Platelet CLEC-2: Roles beyond Hemostasis, *Sem. Thromb. Hemost.*, 44(02), 126-134 doi: 10.1055/s-0037-1604090.

Tang, Q., Owens, R. J., & Naismith, J. H. (2021). Structural biology of nanobodies against the spike protein of SARS-CoV-2. *Viruses*, 13(11), 2214. doi:10.3390/v13112214.

Taylor, L., Vasudevan, S. R., Jones, C. I., Gibbins, J. M., Churchill, G. C., Campbell, R. D., & Coxon, C. H. (2014). Discovery of novel GPVI receptor antagonists by structure-based repurposing. *PloS ONE*, 9(6), e101209. doi:10.1371/journal.pone.0101209.

Thon, J. N., and Italiano, J. E. (2012). Platelets: production, morphology and ultrastructure. *Hand. Exp. Pharmacol.*, (210), 3–22. doi:10.1007/978-3-642-29423-5_1.

Tsoupras, A., Zabetakis, I. and Lordan, R. (2019). Platelet aggregometry assay for evaluating the effects of platelet agonists and antiplatelet compounds on platelet function *in vitro*. *MethodsX*, 6, 63–70. doi:10.1016/j.mex.2018.12.012.

Tomlinson, M. G., Calaminus, S. D., Berlanga, O., Auger, J. M., Bori-Sanz, T., Meyaard, L., & Watson, S. P. (2007). Collagen promotes sustained glycoprotein VI signaling in platelets

and cell lines. *J. Thromb. Haemost.*, 5(11), 2274–2283. doi:10.1111/j.1538-7836.2007.02746.x.

Tsuchiya, H. (2011). Comparative Effects of α -, β -, and γ -Carbolines on Platelet Aggregation and Lipid Membranes. *J. Toxicol.*, 2011, 1–9. doi: 10.1155/2011/151596.

Vargason, A. M., Anselmo, A. C., & Mitragotri, S. (2021). The evolution of commercial drug delivery technologies. *Nat. Biomed. Eng.*, 5(9), 951–967.doi.org/10.1038/s41551-021-00698-w.

Villoutreix, B. O. (2021). Post-pandemic drug discovery and development : facing present and future challenges, *Front. Drug Discov*., 1(July), 1–7. doi: 10.3389/fddsv.2021.728469.

Vogel R. F., Delewi R., Badimon L., Angiolillo D. J. & Vlachojannis G. J. (2022) Current Status and Future Direction of Antithrombotic Therapy for Patients with STEMI Undergoing Primary PCI. Rev. *Cardiovasc. Med.*, 23(9), 297. doi.org/10.31083/j.rcm2309297.

Voors-Pette, C., Lebozec, K., Dogterom, P., Jullien, L., Billiald, P., Ferlan, P., . . . Jandrot-Perrus, M. (2019). Safety and Tolerability, Pharmacokinetics, and Pharmacodynamics of ACT017, an Antiplatelet GPVI (Glycoprotein VI) Fab. *Arterioscler. Thromb. Vasc. Biol*., 39(5), 956–964. doi:10.1161/ATVBAHA.118.312314.

Voss, B., McLaughlin, J. N., Holinstat, M., Zent, R., and Hamm, H. E. (2007). PAR1, but not PAR4, activates human platelets through a Gi/o/phosphoinositide-3 kinase signaling axis. Mol Pharm, 71(5), 1399–1406. doi:10.1124/mol.106.033365.

Ware, J., Corken, A., and Khetpal, R. (2013). Platelet function beyond hemostasis and thrombosis. *Curr. Opin. Hematol.*, 20(5), 451–456. doi:10.1097/MOH.0b013e32836344d3.

Waterhouse, A., Bertoni, M., Bienert, S., Studer, G., Tauriello, G., Gumienny, R., . . . Schwede, T. (2018). SWISS-MODEL: homology modelling of protein structures and complexes. *Nucleic Acids Res*., 46(W1), W296–W303. doi:10.1093/nar/gky427.

Watson, S. P., Herbert, J. M., and Pollitt, A. Y. (2010). GPVI and CLEC-2 in hemostasis and vascular integrity. *J. Thromb. Haemost.*, 8(7), 1456–1467. doi:10.1111/j.1538-7836.2010.03875.x.

Weisel, J. W., & Litvinov, R. I. (2017). Fibrin: Formation, structure and properties. *Subcell Biochem.*, 82, 405–456. doi:10.1007/978-3-319-49674-0_13.

Watson, S. P., Morgan, N. V. & Harrison, P. (2015). The Vascular Function of Platelets. In Postgraduate Haematology (eds A.V. Hoffbrand, D.R. Higgs, D.M. Keeling and A.B. Mehta). doi:10.1002/9781118853771.ch37.

Weisel, J. W., & Litvinov, R. I. (2017). Fibrin Formation, Structure and Properties. *Subcell Biochem.*, 82, 405–456. doi:10.1007/978-3-319-49674-0_13.

WHO (2021) ‘WHO 2021 Fact sheet’, WHO, Updated 11 July 2021, Retrieved 15 December 2021. Available at: https://www.who.int/news-room/fact-sheets/detail/cardiovascular-diseases-(cvds).

Wijten, P., van Holten, T., Woo, L. L., Bleijerveld, O. B., Roest, M., Heck, A. J., & Scholten, A. (2013). High precision platelet releasate definition by quantitative reversed protein profiling--brief report. *Arterioscler. Thromb. Vasc. Biol.*, 33(7), 1635–1638. doi:10.1161/ATVBAHA.113.301147.

Woulfe D. S. (2005). Platelet G protein-coupled receptors in hemostasis and thrombosis. *J. Thromb. Haemost.*, 3(10), 2193–2200. doi:10.1111/j.1538-7836.2005.01338.x.

Xu, J., Xu, K., Jung, S., Conte, A., Lieberman, J., Muecksch, F., . . . Casellas, R. (2021). Nanobodies from camelid mice and llamas neutralize SARS-CoV-2 variants. *Nature*, 595(7866), 278–282. doi:10.1038/s41586-021-03676-z.

Xu, R. G., Gauer, J. S., Baker, S. R., Slater, A., Martin, E. M., McPherson, H. R., . . . Ariëns, R. (2021). GPVI (Glycoprotein VI) interaction with fibrinogen is mediated by avidity and the fibrinogen αC-Region. *Arterioscler. Thromb. Vasc. Biol.*, 41(3), 1092–1104. doi:10.1161/ATVBAHA.120.315030.

Yang, E. Y., & Shah, K. (2020). Nanobodies: Next generation of cancer diagnostics and therapeutics. *Front. Onc.*, 10, 1182. doi:10.3389/fonc.2020.01182.

Yi, W., Li, Q., Shen, J., Ren, L., Liu, X., Wang, Q., . . . Zhu, L. (2014). Modulation of platelet activation and thrombus formation using a pan-PI3K inhibitor S14161. *PloS ONE*, 9(8), e102394. doi:10.1371/journal.pone.0102394.

Zhang, D., Ebrahim, M., Adler, K., Blanchet, X., Jamasbi, J., Megens, R., . . . Siess, W. (2020). Glycoprotein VI is not a Functional Platelet Receptor for Fibrin Formed in Plasma or Blood. *Thromb. Haemost*., 120(6), 977–993. doi:10.1055/s-0040-1710012.

Zhao, M. et al. (2006) Synthesis of new class dipeptide analogues with improved permeability and antithrombotic activity. *Bioorg. Med. Chem.*, 14(14), 4761–4774. doi: 10.1016/j.bmc.2006.03.026.

Zheng, Y. M., Liu, C., Chen, H., Locke, D., Ryan, J. C., & Kahn, M. L. (2001). Expression of the platelet receptor GPVI confers signaling via the Fc receptor gamma -chain in response to the snake venom convulxin but not to collagen. *J. Biolog. Chem.*, 276(16), 12999–13006. doi:10.1074/jbc.M009344200.

Ziarek, J. J., Peterson, F. C., Lytle, B. L., & Volkman, B. F. (2011). Binding site identification and structure determination of protein-ligand complexes by NMR a semiautomated approach. *Methods Enzymol.*, 493, 241–275. doi:10.1016/B978-0-12-381274-2.00010-8.